UNIVERSITY OF LONDON THESIS

Degree PhD Year 2005 Name of Author IOANNIDOU, S.

Structural and functional analysis of vascular permeability

Sofia Ioannidou

Endothelial Cell Biology Laboratory

Cancer Research UK, London

A thesis submitted for the degree of

Doctor of Philosophy at the University of London

November 2004

ProQuest LLC
789 East Eisenhower Parkway
P.O. Box 1346
Ann Arbor, MI 48106-1346

Abstract

Vascular permeability and its regulation are indispensable for normal circulatory function and tissue homeostasis. When unregulated, vascular permeability contributes significantly to blood vessel related pathologies, such as cancer and diabetic retinopathy. Interposed between blood and tissues, endothelial cells become structurally and functionally differentiated, to mediate controlled permeability. The aim of this thesis work was to develop suitable systems to study two different aspects of vascular permeability, endothelial fenestrae formation and tyrosine phophatase-based regulation of paracellular permeability.

Transcellular permeability describes the passage of water and macromolecules across endothelial cells. A route for transcellular permeability is provided by fenestrae, the 60 nm circular pores that span the entire thickness of highly attenuated endothelia encountered in endocrine or filtrating organs. In an attempt to gain insight into the structure and biogenesis of fenestrae I helped set up an *in vitro* culture system where fenestrae could be rapidly induced in cell biological and biochemical quantities. To understand the molecular composition of fenestrae I established a biochemical method for their enrichment. Subtractive proteomic analysis performed on a subcellular fraction enriched in plasma membranes revealed proteins with roles in actin filament disassembly, plasma membrane remodeling, endocytosis, and membrane to cytoskeleton linkage. One particular candidate, the membrane-cytoskeleton linker moesin, was validated as a component of fenestrae by immunocytochemical means.

Paracellular permeability occurs through tight or adherens junctions that join endothelial cells. In order to understand the regulation of paracellular permeability through adherens junctions I focused on Vascular Endothelial Protein Tyrosine Phosphatase (VE-PTP), a demonstrated phosphatase modulator of the junctional protein VE-cadherin. To this end I established transgenic mice with inducible expression of wildtype or mutant VE-PTP in endothelial cells. A correlation between VE-PTP expression at the RNA level and embryonic defects suggests the potential utility of the mice as models of adherens junction dysfunction.

Acknowledgements

There are more than one ways of doing a PhD. This one involved two labs, two continents, two distinctly different research environments, and the privilege of meeting admirable scientists and precious friends along the way. I would like to thank my supervisor Dave Shima, whose ideas, enthusiasm, and great passion for science have been sources of inspiration throughout. My appreciation also goes to Greg Robinson and Eric Ng for the stimulating discussions as well as for critically reading the manuscript; Steve Samuelsson, for his endless patience and willingness to help with all aspects of imaging; Elise Daly for critically reading the manuscript; Donna Stolz for her generous supply of an indispensable reagent; Katrin Deinhardt and Kirsty Roberts for collaborations and contributions to the fenestrae project; Afrodite Bilioni for helping with the logistics of transcontinental binding and submission. Finally, I feel grateful towards the scientific and administrative support teams of both CRUK and Eyetech. I would like to recognise Steve Gschmeissner, Rose Watson, David Frith, Amy Snodgrass, Eunice Cheung, Ruth Caramanica, Qiang Li, Eva Skokanova, and Michael Gee, who through their expertise and competence have made this thesis possible.

This work was financed by Cancer Research UK and Eyetech Pharmaceuticals, Inc.

To my parents

Table of contents

Table of figures

Chapter 1: Introduction

1.1 Historical Perspective

The concept of the circulatory system as a closed circuit was established by the English physician William Harvey (1578-1657). Building on the ideas of Aristotle (384-322 BC) and Galen (129-216), in his famous *Anatomical Disquisition on the Motion of the Heart and Blood in Animals,* Harvey presented evidence of blood flowing outward from the heart, circulating through arteries and veins, and eventually returning to the heart [1]. He firmly believed that nothing in nature exists in vain, and was confident that the circulatory system was responsible for the delivery of nutritive fluid around the body.

The recognition of nutrient supply and waste removal as the ultimate functions of the cardiovascular system prevails to this day. A central question within this concept concerns the process of material passage between blood and tissues, collectively referred to as vascular permeability. In 1953, John Pappenheimer integrated physical laws with measurements of capillary permeability in animals, to explain "the invisible flow" of material through the vessel [2, 3]. He postulated that the capillary wall was rendered permeable to lipid-insoluble molecules through the existence of numerous ultramicroscopic pores, in a hypothesis formally known as the Pore Theory [2, 3]. The first visualisation of structures that could account for Pappenheimer's postulates came with the application of electron microscopy to the study of blood capillaries. Intercellular gaps, attachment belts (interendothelial junctions), fenestrae, and caveolae, were recognised as structural features of the endothelium that could be linked to its permeability properties [4-6], although their size and frequency did not correspond exactly to the pore theory measurements. In an attempt to probe for the true permeability properties of each of the observed structures, subsequent studies made use of particulate or enzymatic tracers that could be visualised by electron

microscopy (reviewed in [7, 8]). On the basis of the ultrastructural localisation of tracers at various time intervals after their intravascular or interstitial administration, size- and charge- restrictive properties were attributed to a variety of structures within capillary walls [8]. Freeze-fracture electron microscopy provided the most detailed descriptions of the intricate architecture of intercellular junctions and fenestrae [9-11], while biochemical isolation studies began identifying the molecular components of junctions and caveolae [12-16]. Finally, in the course of the last decade, advances in genome sequencing and mammalian genetics have culminated in the engineering of transgenic and knockout mice for components or putative modulators of tight junctions, adherens junctions, and caveolae, so as to facilitate assessing their contribution to permeability [17-20].

1.2 Heterogeneity of the endothelium

1.2.1 Endothelial differentiation and organ function

Precise regulation of blood-tissue interchange is indispensable for fluid homeostasis, delivery and uptake of metabolites to and from tissues, and filtration. Accordingly, vascular endothelial cells, the primary barrier to free blood-tissue exchange, adopt highly specialised features and behaviors to mediate and monitor the flux of macromolecules and fluids across the vascular wall. For example, the vascular endothelium of the blood-brain and the blood-retinal barriers is fortified by tight junction components that restrict access of fluid and blood components to sensitive neural tissues [21-23]. To compensate for the need of nutrients, barrier cells are equipped with a multitude of membrane transporters that ensure the provision of

glucose and essential amino acids [24-26]. The other extreme of endothelial barrier differentiation is that of lymphatic vessels, an extremely permeable endothelium whose function is the uptake of extravascular fluid for clearance, transport and return to the circulation [27, 28]. Consistent with this function, lymphatic endothelial cells have thin walls, loose junctions, and are devoid of surrounding support cells or basement membrane [27, 28]. Between the two extremes of hyperpermeable and impermeable endothelia, are endothelia in organs requiring abundant but more regulated vascular permeability. Organs mediating endocrine, absorptive or filtrating functions are supported by a highly specialised vascular endothelium containing numerous plasma membrane pores, the fenestrae [8]. Finally, throughout the vascular tree, the integrity and continuity of endothelial sheets is maintained by the presence of adherens junctions, or a desmosomal-like structure in the case of lymphatics, which hold neighbouring cells attached to one another [29, 30].

1.2.2 An evolutionary perspective on endothelial morphogenesis

Observations on the phylogeny of the vasculature have suggested a progression towards a more closed circulatory system in the course of evolution [31]. In primitive chordates such as *amphioxus*, endothelial cells are separated by large gaps, and often are devoid of basement membranes, ensuring continuous contact between the blood and tissues. In the *hagfish,* which is often regarded as a primitive vertebrate, endothelial cells become more continuous and display intercellular junctions, micropinocytotic vesicles, and fenestrae. In advanced vertebrates, such as teleosts and mammals, such features become more prominent, while a lymphatic system is also in place. It is plausible that increases in the size of organisms demanded a continuous vasculature that would maintain sufficient blood hydrostatic pressure to deliver

nutrients and uptake waste, even from the most distal parts of an animal. Local needs for sustained permeability could be served by the existence of fenestrae, thus avoiding large net losses of fluid. Moreover, the lymphatic system could counteract any fluid losses, by returning extravascular fluid back to the circulation.

Interestingly, freeze-fracture analysis of the capillaries in the kidney of the Atlantic Hagfish, (*Myxine glutinosa*) has revealed sparse fenestrae [32], while no fenestrae have been found in its thyroid or pituitary glands [31]. Fenestrae are however common in the elasmobranchs (subclass encompassing sharks, skates and rays), featuring prominently within their kidneys and intestinal capillaries, and in all higher vertebrates [31]. Whether fenestrae serve a true filtration function in their primitive form, or were adapted to this function through the course of evolution, remains an open question.

1.2.3 Morphological classification of permeability

The recognition of different subendothelial structures that could mediate blood-tissue exchange has led to the classification of vascular permeability according to the pathway followed in traversing the capillary wall. Two modes of permeability have been described: paracellular permeability and transcellular permeability (Figure 1.1). Paracellular permeability refers to the passage of material through orifices existing between cells, or created through opening and closing of tight and adherens junctions. Transcellular permeability describes the passage of material across endothelial cells, through caveolae, transendothelial channels, vesiculo-vacuolar organelles (VVOs), and fenestrae. A brief description of tight junctions, caveolae, VVOs and transendothelial channels and their connection to permeability will directly follow, while fenestrae and adherens junctions will be analysed in detail in the ensuing section.

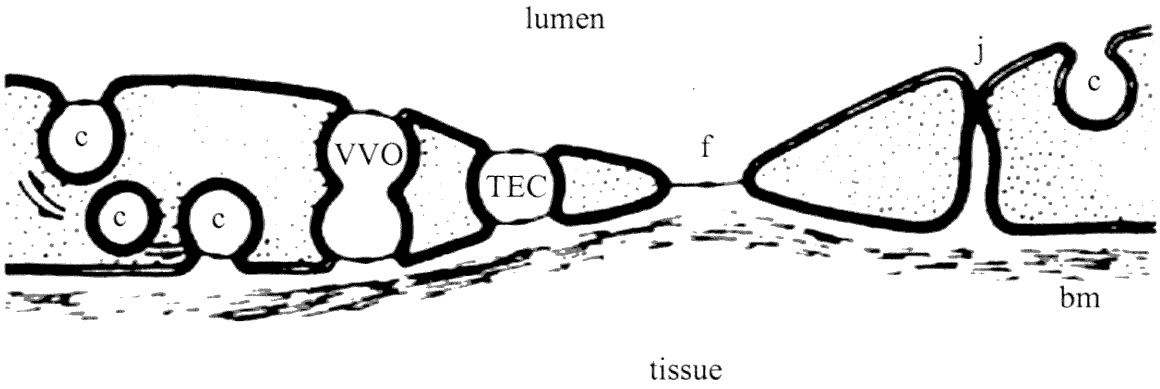

Figure 1.1 Structures mediating transcellular and paracellular permeability. Material passage can occur across the endothelial cell, through caveolae (c), vesiculovacuolar organelles (VVO), transendothelial channels (TEC) or fenestrae (f). Alternatively materials can pass between adjacent endothelial cells through tight or adherens junctions (j). The lumen and tissue fronts of the endothelium and the basement membrane (bm) are denoted. (Schematic adapted from Ref. 8)

1.2.3.1 Tight junctions

Tight junctions are junctional complexes of epithelial and endothelial cells [33]. Unlike their confinement to the most apical region of interepithelial cell contact, in endothelial cells they are found interspersed among adherens junctions (Figure 1.2) [33]. Tight junctions were identified by ultrathin section electron microscopy as so-called kissing points of plasma membranes [9]. Freeze-fracture replica electron microscopy further detailed them as pairs of tight junction strands in apposing plasma membranes, which, when associated, led to the obliteration of the intercellular space [10]. Tight junction strands consist of the transmembrane proteins occludin, junctional adhesion molecule (JAM), and members of the claudin family [33, 34]. Peripheral membrane proteins such as ZO and other PDZ domain-containing proteins participate in the linkage of tight junction strands with the cytoskeleton [33, 34]. Athough initially regarded as completely impermeable barriers, the observation of clefts within tight junctions, that could accomodate 6 Å channels, established their role in paracellular permeability [35-37]. Tight junctions are preferentially developed in arteries versus veins [33], and consistent with their restrictive properties they are a prominent feature of the blood-brain and blood-retinal barriers [21, 23].

1.2.3.2 Caveolae

Caveolae, also referred to as plasmalemmal vesicles, are 60-80 nm-wide flask-shaped invaginations of the plasma membrane, originally identified in endothelial and epithelial cells [4, 38] and subsequently recognised in many cell types [39]. The observation of vesicles at either front of the endothelium, as well as intracellularly, led to the hypothesis of quantal transport of substances across the capillary wall, termed transcytosis [40, 41]. Vesicles loaded with a certain amount of plasma components

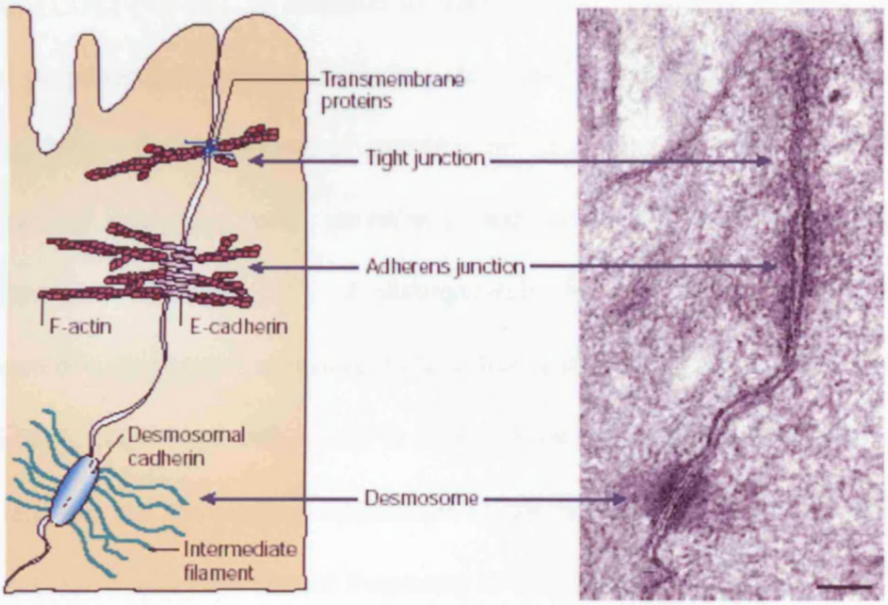

Figure 1.2 Intercellular junctions. Transmission electron micrograph and corresponding schematic of the main types of junctions between skin epithelial cells. Tight junctions are composed of transmembrane proteins that are linked to the actin cytoskeleton, and result in the obliteration of the intercellular space. Adherens junctions are formed by homophilic interactions between proteins of the cadherin family, that are transmembrane and associate with the actin cytoskeleton. An approximately 20 nm space between adjacent cells is permitted by such junctions. Desmosomes consist of transmembrane proteins anchored to intermediate filaments, however are absent from most endothelia. (Reproduced from Ref. 126)

were assumed to bud off one side of the endothelium, shuttle through the cell, and eventually release their cargo at the opposite endothelial front [40, 41]. Transcytosis is thought to take place both in a non-specific fashion, by means of size or charge selectivity, and a receptor-mediated fashion, as in the case of albumin or low density lipoprotein (LDL) [42-44]. In addition to transcytosis, a number of other functions have been proposed for caveolae, including cell signaling, endocytosis, and cholesterol trafficking, [39]. Combinations of caveolin proteins constitute the main structural components of caveolae, with caveolin-1 and caveolin-2 forming oligomers in endothelium and epithelium [45]. A distinguishing feature of endothelial caveolae is the presence of a diaphragm spanning their orifice, a constituent of which is the protein PV-1 [16, 46]. Consistent with a role in transcellular permeability, observed caveolae surface densities are inversely proportional to the endothelial thickness, and among different organs, display the lowest frequency in brain capillaries [8].

1.2.3.3 Vesiculo-vacuolar organelles (VVOs)

Originally identified in tumor blood vessels, VVOs were subsequently observed in the venular endothelium supplying the skin, the skeletal muscle and other tissues [47, 48]. VVOs were described as a bunch of grape-like clusters of membrane-lined vesicles and vacuoles. Over 100 of such vesicles and vacuoles collectively comprise an interconnected structure that traverses the endothelial cytoplasm. Within the structure, open communication is thought to exist between vesicles and vacuoles, albeit in some cases where it is restricted by the presence of a diaphragm. Labelling for caveolin 1 [49], coupled to the feature of the diaphragm are suggestive of a relationship to caveolae. The larger size and greater heterogeneity of most vesicles was deemed representative of multiple fused caveolae [50, 51] . A role for VVOs in transcellular

permeability was inferred from studies showing an accumulation of macromolecular tracers within their compartments in the vasculature of tumors [47, 48]. However, minimal entry of tracers in VVOs was observed for normal endothelium [47, 48].

1.2.3.4 Transendothelial channels

Transendothelial channels, were first identified in muscle capillaries [52], and subsequently observed in many fenestrated endothelia [8]. Frequently referred to as fused vesicles, or fused fenestrae, transendothelial channels contain two diaphragms that are morphologically similar to those identified in fenestrae, caveolae, and VVOs [8, 53]. Moreover, the diaphragms harbour the protein PV-1, a common feature between the diaphragms of fenestrae and caveolae [54]. In light of their sparse distribution, the significance of transendothelial channels is a matter of controversy. Whether they constitute a distinct unit involved in transcellular permeability, or are merely short-lived intermediates in the formation of other diaphragmed structures, remains an open question.

1.3 Fenestrae

1.3.1 Morphology and architecture

Endothelial fenestrae were first observed in 1950 by Gautier, Bernhard, and Oberling, during their ultrastructural studies of glomerular capillaries [55]. Their work was validated by a number of others working in the same system [5, 56, 57], and later generalised to other organs [6, 58]. Named after the latin word for window, fenestrae have been described as transcellular circular pores with an average diameter of ~ 60

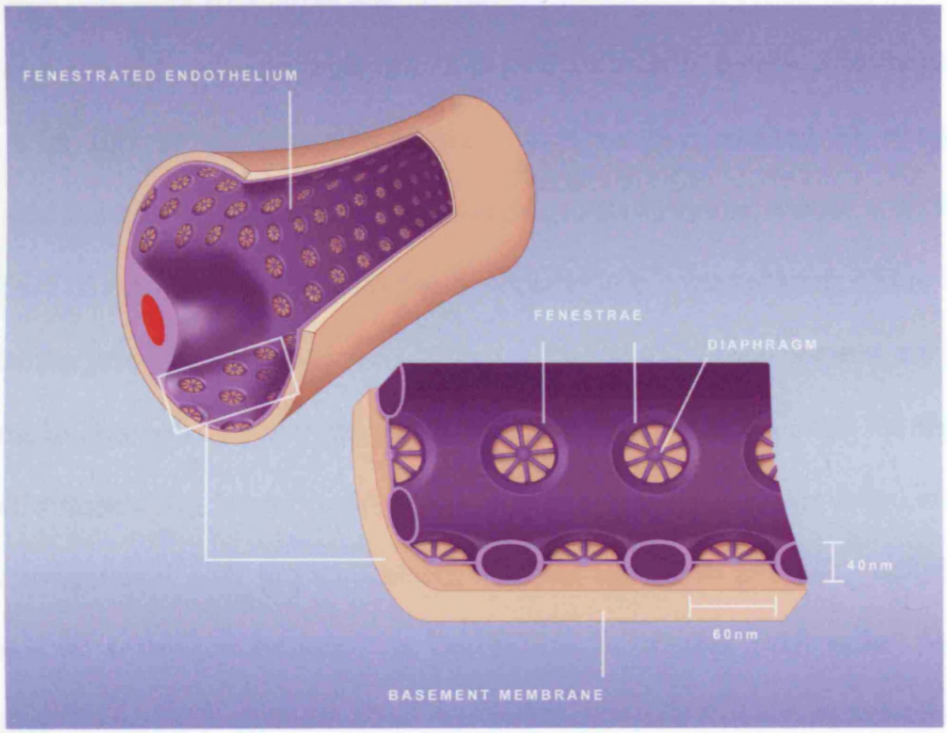

Figure 1.3 Schematic representation of fenestrated endothelium. Fenestrae are found only at the most attenuated regions of endothelial cells where the nucleus and organelles are excluded and the distance from apical to basal plasma membrane is as little as 40 nm. They occur in groups and are arranged in a near-linear fashion with precise spacing between them. Inset shows the fenestral pore to be 60 nm in diameter, with an effective size of 5-6 nm when apertured by a diaphragm. The basement membrane underlying the fenestrated endothelium is indicated. (Schematic adapted from Ref. 59)

nm [6, 59], though they can be as large as ~ 150 nm within the liver sinusoidal endothelium (Figure 1.3) [60]. Fenestrae are encountered in the most attenuated regions of the microvascular endothelium, where the cell profile is as little as 40 nm, and span the entire thickness of the cell without disrupting the continuity of the cell membrane [59]. The substances that traverse the pore never encounter the contents of the cytoplasm, and are transported in a rapid and presumably energy-efficient manner. This is in contrast to transcytosis, which involves the coupling of energy-rich endocytic and exocytic events. In most vascular beds fenestrae contain a diaphragm composed of approximately 8 radial fibrils converging in a central knob, which further dissects the pore into 5-6 nm openings (Figures 1.3 and 1.4) [11]. Fenestrae are known to occur in clusters of approximately 50-100, termed 'sieve plates', that are encircled by a microtubule-rich border [61]. Within a sieve plate, fenestrae are found in a near linear arrangement with precise spacing between each pore [59, 62], implying the presence of a complex intracellular scaffolding to support such order. Whether individual fenestrae, or the sieve plates, are stable structures that persist throughout the lifetime of a differentiated cell or dynamic structures that are rapidly turned-over, is currently unknown.

1.3.2 Chemical and molecular composition

Palade and the Simionescus pioneered the study of fenestrae composition by demonstrating that cationised ferritin (CF) preferentially deposited within a glycocalyx visible on the luminal aspect of the fenestral diaphragm [63, 64]. Capitalizing on this initial observation, they used the CF interaction as a probe for the molecular nature of fenestrae, by monitoring its disappearance following treatment with enzymes of defined specificity. Sensitivity to proteases and certain glycosidases as well as affinity

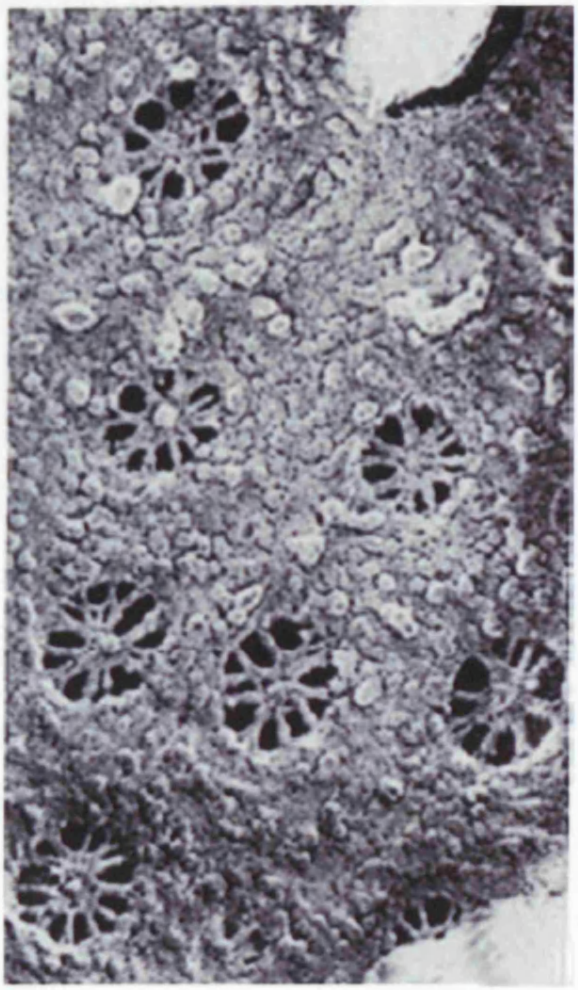

Figure 1.4 Fenestral diaphragms. Quick-freezing and deep-etching of rat kidney peritubular capillaries revealed intertwining fibrils bridging the pore and converging into a central mesh. A luminal view of diaphragms is shown. Magnification: 120,000x. (Reproduced from Ref. 11)

for lectins suggested that acidic glycoproteins and proteoglycans could account for CF-decorated anionic sites on the diaphragms [64, 65]. However, the differential sensitivity to heparinase and heparitinase in the fenestral diaphragms of the intestine and choriocapillaris respectively [64, 66], together with variable results in lectin binding studies in these tissues [65, 67], highlight organ-specific differences in the glycocalyx composition: heparan sulfate proteoglycans presumably form part of the diaphragms in the intestine, while heparin and N-acetylglucosamine-rich glycoproteins are thought to localise on the diaphragms of the choriocapillaris. Moreover, binding of CF to fenestral diaphragms is absent altogether in the bone marrow and the fetal liver [68], while it is highly variable in the fenestrated neovasculature of tumors [69]. Lastly, a differential distribution in the CF labelling was observed between the luminal and abluminal aspects of intestinal and pancreatic fenestrae [70]. CF that was interstitially microinjected following basal lamina digestion with collagenase, failed to label the abluminal aspect of fenestral diaphragms, demonstrating the existence of polarity within each fenestra [70].

Recent studies identified an endothelial cell-specific protein, Plasmalemmal Vesicle 1 Protein (PV-1) as the first known component of the fenestral diaphragm [54]. PV-1 is a 60 kDa Type II transmembrane glycoprotein, believed to form coiled-coil homodimers that constitute the primary structural component of the diaphragm [71]. It should be noted that PV-1, and the diaphragm are not unique to fenestrae but also reside within endothelial cell caveolae and transendothelial channels [16, 54].

Intriguingly, studies on the permeability properties of fenestrae identified a discrepancy between the predicted and the actual passage of water and solutes, even when the area occupied by the diaphragm was taken into account [72]. They further concluded that fenestrae diaphragms may support an overlying glycocalyx, or underlying basal lamina, containing a dense fiber matrix. Scattered information exists

for the presence of sterols [73], furin proteases [74], and Ca^{2+} pumps [75, 76], on or in the vicinity of fenestrae, but awaits validation.

1.3.3. Fenestrae role in transcellular permeability

Attempts to investigate the permeability properties of fenestrae were initiated by Clementi, Palade, Simionescu, and Pino using tracer perfusion studies. Horseradish peroxidase (~ 4 nm in diameter) proved to be readily permeable through diaphragmed fenestrae of the intestinal mucosal capillaries, pancreatic capillaries and the ocular choriocapillaris. Larger tracers such as ferritin (~ 11 nm in diameter), or dextrans and glycogens, were variably permeable, depending on the location of the fenestrated vascular bed in the organism [41, 77-79]. These findings fit remarkably well with data developed by Bearer and Orci, who determined that the presence of a diaphragm transected the 60 nm fenestrae into multiple channels of approximately 5 nm in diameter [11]. Whether permeability through fenestrae is a passive process or is facilitated by specific molecular interactions between components of the pore and traversing substances remains an open question.

Though somewhat speculative, future studies in this area may benefit by examining the structure and function of the nuclear pore, a remarkably analogous structure consisting of two lipid bilayers fused to create a seamless circular opening. Transport of molecules between the cytoplasm and the nucleoplasm is chaperoned by proteins of the nuclear pore that first recognize specific export or import signals on potential cargo molecules, and then act as shuttling factors in a process regulated by the GTPase Ran [80]. So far, selectivity within the fenestrae has only been shown with respect to molecular charge, as inferred from studies demonstrating the particularly high affinity

Figure 1.5 Fenestrated endothelium of the choriocapillaris. The capillary bed supplying supplying nutrients and removing waste from the outer retina is extensively fenestrated. The close association of diaphragmed fenestrae with Bruch's membrane (BM) and microvilli of retinal pigmented epithelium (RPE) is shown. (Courtesy of Eunice Cheung and Steve Samuelsson, Eyetech Research Centre)

of cationic substances for fenestral diaphragms [63, 64], and the strikingly low permeability to negatively charged albumin [81]. Although there is sparse direct evidence of a major physiological role for fenestrae, several functions can be safely attributed to them simply on the basis of their physical properties and their distribution within normal vasculature and during neovascular disease. Fenestrae are postulated to mediate the bi-directional exchange of water, solutes and small macromolecules between blood and tissues. More specifically, fenestrae are believed to function: in the filtration of blood within the choroid plexus that gives rise to cerebrospinal fluid [82]; in the access of endocrine hormones to the bloodstream, such as the release of steroid hormones by the adrenal cortex [83]; in the supply of nutrients to, and removal of waste from, the outer retina by the underlying choriocapillaris (Figure 1.5) [84]; in the ultrafiltration of blood to create primary urine within the kidney glomerulus (Figure 1.6) [85]; in the filtration of potentially hazardous substances in the blood at the liver sinusoids [60].

1.3.4 Biogenesis and regulation

The inability to maintain fenestrated endothelium in tissue culture and the difficulty in quantifying and manipulating the appearance of fenestrae both *in vivo* and *in vitro* have greatly hampered the study of their biogenesis. Up until recently, the induction of fenestrae in cultured endothelial cell lines has been reported to yield numbers that are 3-4 orders of magnitude lower in density than normally observed in vivo. Nevertheless, a small number of key studies published throughout the last 3 decades have highlighted several extracellular and intracellular determinants that may be involved in the differentiation program of a fenestrated endothelial cell.

Figure 1.6 Scanning electron micrograph from a freeze-fractured glomerulus. A view through the lumen of a fenestrated glomerular capillary is shown. The endothelium appears to have a colander-like structure that permits passage of materials from the blood to the glomerular capsule. (Courtesy of Steve Gschmeissner, Cancer Research UK)

1.3.4.1 Endothelial cell micro-environment

Fenestrated microvessels are in constant contact with extracellular matrix, both in the form of routine basal lamina or, in some cases, elaborate, thickened matrix such as the basement membrane of the kidney glomerulus or the multi-lamellate Bruch's membrane, which separates pigmented retinal epithelium from the choriocapillaris. Extracellular matrix could simply provide a structural scaffold to facilitate the extreme shape changes and cell attenuation that accompanies the fenestrated phenotype. However, a more active, instructive role for the extracellular matrix has been proposed to explain, for example, the presence of fenestrae only in the regions of the choriocapillaris that are immediately adjacent to Bruch's membrane [78]. *In vitro* experiments examining the effects of a variety of extracellular matrices suggest that fenestrae formation is supported by specific matrix components, which mimic the situation observed *in vivo* [86, 87].

1.3.4.2 Signal transduction pathways

The first attempts to reprogram the fenestrae differentiation program in cultured endothelial cells relied upon the use of potent and relatively non-specific initiators of intracellular signaling cascades on isolated bovine adrenal cortex endothelial cells. Phorbol myristate acetate (PMA), an activator of Protein Kinase C isoforms and a potent differentiation agent for some cell types, promoted a change in the shape of endothelial cells accompanied by a 5-fold increase in the frequency of diaphragmed fenestrae (~ 6 fenestrae/100μm^2) [88, 89]. Similarly, treatment of cultures with retinoic acid led to a 3-fold increase in the surface density of fenestrae, while transforming growth factor β led to a 7-fold decrease in their density [90]. The physiological relevance of these signaling pathways remains to be established.

The angiogenic growth factor, Vascular Endothelial Growth Factor (VEGF) is the strongest candidate for a signaling protein that induces fenestrae formation [91]. VEGF is an endothelial specific mitogen and motogen, and was originally identified as a vascular permeability factor, approximately 50,000 times more potent than histamine [53]. Although VEGF is greatly down regulated after the completion of embryonic vasculogenesis and angiogenesis, it is continuously and highly expressed in epithelial cells adjacent to fenestrated endothelium [92]. Moreover, fenestrae have been observed in the neovasculature of tumors and in the normally continuous endothelium of the retina during diabetic microangiopathy, both pathological situations that are functionally linked to the local upregulation of VEGF [51, 93]. In fact, *in vivo* studies have demonstrated that VEGF can induce fenestrae within 10 minutes in the continuous endothelium of skeletal muscle and skin, when applied topically or injected intradermally [69], and *in vitro* studies using capillary endothelial cells showed a modest but significant ability of VEGF to promote fenestrae biogenesis [94].

1.3.4.3 Cytoskeleton

The importance of cytoskeletal remodeling in fenestrae biogenesis has been suggested from *in vitro* studies examining the effect of agents that disrupt actin microfilament assembly on highly fenestrated liver sinusoidal endothelial cells [95, 96]. Using a variety of microfilament disruption agents, a 2 to 3 - fold increase in fenestrae numbers was achieved within 30-60 minutes. The physiological relevance of this data was indirectly supported by experiments showing that a dominant negative version of the small GTP-binding protein Rac could block VEGF-driven fenestrae formation during corneal angiogenesis [97]. The authors postulated that inhibition of fenestrae formation was a result of interfering with the actin cytoskeleton, without however

presenting evidence of microfilament reorganisation. The multitude of signalling cascades affected by both VEGF and Rac, demand a cautious interpretation of such results, as a cytoskeleton-independent mechanism would be equally plausible [97].

The cytoskeleton may also be playing a role in short-term fenestrae dynamics. A number of studies have reported an alteration in liver fenestrae diameter in response to hormones or drugs (reviewed in [60]). One mechanism proposed to explain these observations implicated the presence of an actomyosin contractile apparatus surrounding and regulating each fenestra [98].

1.3.4.4 Concepts for fenestrae formation

The limited amount of experimental data can be accommodated in several conceptual models (not mutually exclusive) for fenestrae biogenesis:

1.3.4.4.1 Caveolae give rise to fenestrae

Fenestrae and caveolae share structural features, common tissue distribution, a relationship to the VEGF signaling cascade, and a common putative role in the regulation of vascular permeability. In one of the earliest hypotheses for fenestrae formation, investigators postulated that caveolae may give rise to fenestrae in a process involving fusion of a budding caveolar vesicle with the adjacent plasmalemma [7]. The discovery that PV-1 was common to the diaphragms that reside in both fenestrae and caveolae of endothelial cells further supported this model [54]. Current evidence, however, emphasises more differences than similarities in the nature of the two organelles. General compositional differences between the two organelles were first highlighted in tracer perfusion studies showing that caveolar diaphragms (also referred to as stomatal diaphragms) lacked anionic sites amongst other molecular determinants

that were present within the fenestral diaphragm [63, 64]. Furthermore, exclusion of the main structural component of caveolae, caveolin-1, from fenestrae *in vivo* and *in vitro* [94], and the recent finding that knockout mice completely lacking caveolae still have fenestrae [99], provide compelling evidence for distinct origins of caveolae and fenestrae. However, the existence of a common structural precursor that differentiates to give rise independently to fenestrae and caveolae still remains a valid point for consideration.

1.3.4.4.2 The role of the diaphragm in fenestrae formation

The presence of a diaphragm in fenestrae is variable; it is found in the fenestrated capillaries of the intestine, the choriocapillaris, the choroid plexus and endocrine organs, while it is absent from the more permeable microvessels of the kidney glomerulus and the liver sinusoids [8, 60, 100]. Diaphragmed fenestrae, however, do initially appear within the vessels of developing fetal glomerulus and liver [85, 101], which has raised speculation on a role for the diaphragm in fenestrae biogenesis, in addition to its putative role in gating the pore. Achieving a precise circular opening and facilitating the extreme membrane curvature at the rim of fenestrae, where apical and basal plasma membranes come together, could be functions of the protein-rich diaphragm.

1.3.4.4.3 Apical-basal plasma membrane fusion following actin displacement

Data demonstrating that actin microfilament disassembly triggers fenestrae biogenesis have spawned a model whereby removal of the actin-rich cortex beneath the plasma membrane is required to allow close apposition and fusion of apical and basal plasma membranes [95]. Cortical actin removal has been shown to be an important

prerequisite to membrane fusion during exocytosis, while removal of organelle-bound actin has been suggested to accelerate yeast vacuole membrane fusion [102, 103]. Whether the cytoskeleton also plays an instructive role in fenestrae formation remains to be established.

1.4 Adherens Junctions

1.4.1 Morphology and architecture

The distinction between the various types of intercellular junctions was first made by Farquhar and Palade through their work on intestinal epithelial cells [9]. In contrast to tight junctions (*zonula occludens*) where the intercellular space appeared completely obliterated, adherens junctions (*zonula adherens* or *intermediary junction*) allowed a 200Å-wide space between adjacent epithelial cells (Figure 1.2). Electron dense cytoplasmic material and a fibrillar network were observed along the depth of adherens junctions, which varied in length between 0.2 and 0.5 μm. The same structure, albeit less well-defined, was subsequently observed in endothelial cells [104]. Moreover, in contrast to the orderly succession of the different types of intercellular junctions in epithelial cells, a mosaic pattern of adherens and tight junctions is present along the length of the interendothelial area of contact [33].

1.4.2 Molecular Composition

The main molecular constituents in all adherens junctions are transmembrane proteins of the cadherin family (Figure 1.7) [105]. The extracellular regions of the proteins can

A

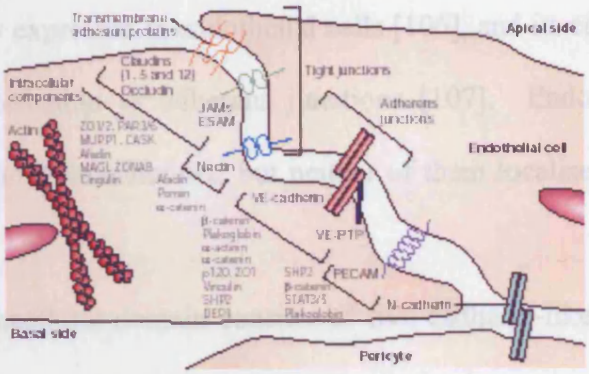

B

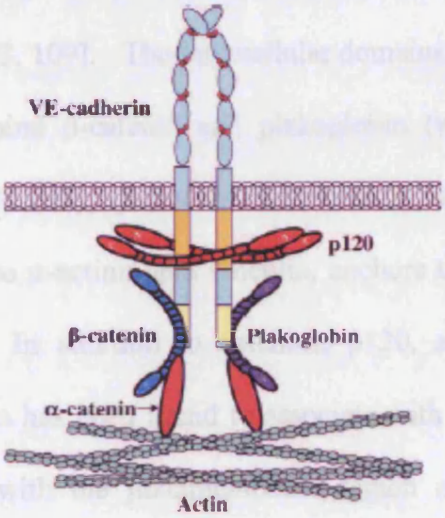

Figure 1.7 Molecular organisation of endothelial cell-cell junctions. (A) Overview of the main types of junctions between endothelial cells, along with their transmembrane and membrane-associated components. VE-PTP, an endothelial specific-phosphatase that associates with VE-cadherin through the extracellular domains and catalyses its tyrosine dephosphorylation, is indicated. (Reproduced from Ref. 121) (B) Detailed view of the composition of endothelial adherens junctions. VE-Cadherin molecules associate through their extracellular domains in *cis* or in *trans*. The intracellular domain of VE-cadherin is linked to proteins of the catenin family, p120, and others. Catenins link the complex to the actin cytoskeleton. (Reproduced from Ref. 109)

mediate calcium-dependent homophilic adhesion, while the cytoplasmic tails associate with the actin cytoskeleton, resulting in the formation of stable junctions [105]. VE-cadherin is specifically expressed in endothelial cells [106], and its correct localisation is essential for the formation of adherens junctions [107]. Endothelial cells also express N-cadherin, and VE-cadherin-2, but neither of them localises to the adherens junction [33].

The VE-cadherin extracellular domain consists of five cadherin-like repeats arranged in a rigid, rod-like structure (Figure 1.7, B) [108]. Cadherins are thought to associate through their extracellular domains both in *cis*, within the same cell, and in *trans*, between adjacent cells, though the precise regions responsible for each arrangement have not been elucidated [33, 109]. The intracellular domains of classic cadherins are highly homologous, and bind β-catenin and plakoglobin (γ-catenin) through their carboxy-terminal region [33, 109]. β-catenin and γ-catenin, in turn bind to α-catenin, which through its binding to α-actinin and vinculin, anchors the complex to the actin cytoskeleton [33, 109]. In addition to catenins, p120, another member of the armadillo family of proteins has been found to associate with VE-cadherin [33, 109]. p120 appears to interact with the juxtamembrane region of VE-cadherin, and in contrast to catenin proteins does not participate in the linkage with the cytoskeleton. ZO-1, nestin, and afadin have been variably found to associate with adherens junctions, though their relevance to the complex is not as clear [33].

VE-cadherin is also present in lymphatics, linked to plakoglobin and p0071, and through them to desmoplakin, and vimentin, in a desmosomal-like structure termed *complexus adhaerentes* [33, 110].

1.4.3 Contribution to paracellular permeability

Adherens junctions are ubiquitous components of the vascular endothelium [33]. VE-cadherin is expressed early on during embryonic development and persists through adulthood [106, 111]. An essential role for VE-cadherin in vascular development was highlighted by the inability of mice with targeted disruption of the VE-cadherin gene to remodel their immature vascular plexi [112]. Embryonic lethality at 9.5 days of gestation precluded any analysis of the effects of VE-cadherin inactivation in vascular permeability.

Evidence from *in vivo* and *in vitro* studies has underlined a clear role for VE-cadherin in paracellular permeability. A key study demonstrated the breakdown of the endothelial barrier upon intravenous administration of a monoclonal antibody against VE-cadherin in a mouse [107]. Physical gaps within the vasculature, interstitial edema, and a number of inflammatory cells in the heart and lungs were evident upon ultrastructural examination. The effect was deemed specific for adherens junctions as the antibody induced the redistribution of VE-cadherin in cultured cells, without affecting tight junctions. *In vitro* evidence suggests that VE-cadherin is the end-target for a number of known permeability mediators: VEGF, thrombin, and histamine lead to a modulation of VE-cadherin with a concomitant increase in paracellular permeability [113-116].

The precise morphological changes accompanying the increase in permeability through junctions are unknown. Nevertheless, it appears that even subtle effects that strengthen or weaken the interactions between the molecular components of the complex can be sufficient in perturbing the endothelial barrier integrity. Such changes are not necessarily mirrored in the distribution of VE-cadherin itself, as evidenced by the increased paracellular permeability in β-catenin null endothelial cells, which

otherwise display correct localisation of VE-cadherin and only altered distribution of α-catenin [17].

A more vigorous mechanism of junctional disorganisation may be in place during leukocyte extravasation in the course of an immune response [117]. Despite not being classified under paracellular permeability, the extent of leukocyte permeation through the capillary wall is a measure of endothelial integrity. In a pathway triggered by the leukocyte adhesion to intercellular adhesion molecule-1 (ICAM-1) [118], VE-cadherin is transiently removed from endothelial junctions, presumably to facilitate the passage of invading leukocytes, after which the adherens junction reassembles [119].

In addition to its role in paracellular permeability, VE-cadherin is implicated in a variety of cellular functions through interactions with intracellular signaling pathways [33, 120, 121]. Its effect in contact inhibition of cell-growth can be attributed to the sequestering of β-catenin at the plasma membrane, the recruitment of the phosphatase DEP-1/CD148 at sites of VEGFR-2, or the prevention of Src-homology-2(SH2)-domain-containing protein from activating the mitogenic RAS signaling pathway. Its role in apoptosis is thought to occur via the activation of the phosphatidylinositol 3-kinase (PI3K) pathway, while its role in the reorganisation of the actin cytoskeleton is attributed to its interaction with Tiam, a guanosine exhange factor for the small GTPase Rac. These and other roles for VE-cadherin have been extensively reviewed [33, 120, 121], and will not be analysed further in this section. Given the multitude of biological roles proposed for adherens junction components, it is not inconceivable that their effects on permeability are also exerted indirectly, through a modulation of transcription or signaling cascades. Along these lines, the conditional inactivation of the β-catenin gene in endothelial cells, leads to an increased number of fenestrae *in vivo* [17].

1.4.4 Regulation

The regulation of VE-cadherin function can occur at many different levels [122]. Control at the stage of gene expression [123-125] will not be discussed, and instead this section will focus on regulation at the post-translational level that is likely to play a role in the dynamic and rapid changes taking place during a permeability response.

1.4.4.1 Linkage to cytoskeleton

VE-cadherin is intimately linked to the cytoskeleton through a number of different ways. α-catenin is a key player in this interaction, as it can associate with microfilaments directly, or indirectly through its binding to vinculin, α-actinin, or afadin, that in turn contain binding sites for actin [33, 126, 127]. The importance of F-actin binding was highlighted in experiments with E-cadherin, revealing that a crucial step in the biogenesis of adherens junctions was the cytoskeletal anchoring, and subsequent stabilisation of the cadherin-catenin complex, appearing as a distinct punctum of fluorescence by light microscopy [127, 128]. Conversely, junction formation and eventual sealing of neighbouring cells were both absent in cells lacking the cytoskeletal adaptor α -catenin [128]. A role for small GTPases in this process has been suggested through evidence for the ability of the Rac effector IQGAP to disrupt the β-catenin/ α-catenin interaction, unless prevented by associating with Rac [129]. Dissociation of VE-cadherin from the actin cytoskeleton has indeed been observed under some conditions that increase junctional phosphorylation and permeability, as inferred from its partition into the Triton X-100-soluble fraction [116, 130].

1.4.4.2 Intracellular trafficking

Newly synthesised cadherins are thought to be transported from the Golgi apparatus to the plasma membrane through a pathway that requires an association with β-catenin [131]. Once they have reached the membrane, endocytosis is regarded as the mechanism regulating their local availability [132, 133]. VE-cadherin internalisation has been observed in response to a variety of stimuli including conditions leading to endothelial barrier dysfunction [109, 134-136].

Experiments on the prototype member of the family, E-cadherin, were the first to highlight a role for p120 in regulating cadherin levels and cell-adhesion [137]. A role for p120 in retaining VE-cadherin at the plasma membrane, and maintaining barrier function, was subsequently suggested through experiments that altered its levels *in vitro* [108, 138, 139]. In the absence of p120, VE-cadherin internalises and co-localises with early endosomes, while the process can be inhibited altogether by the addition of lysosomal inhibitors [140], or rescued by replenishing the levels of p120 [108, 139]. Interestingly, Hakai, an E3 ubiquitin ligase was found to bind E-cadherin and enhance its endocytosis after displacing p120 [141]. In addition, p120 was found to bind the motor protein kinesin and facilitate the delivery of adhesion complexes from vesicular pools to the plasma membrane [142]. Two different mechanisms were proposed to explain the role of p120 in the regulation of VE-cadherin: protection from endocytosis, and promotion of cell-surface trafficking [109, 143].

Finally, a role for the actin cytoskeleton in the internalisation of cadherins has been suggested through studies with the small GTPases Rac and ARF6 [144, 145], while both clathrin-dependent [145] and clathrin-independent [146] endocytosis have been implicated.

1.4.4.3 Cleavage by proteases

Proteolytic cleavage is yet another mechanism recognised in the regulation of adherens junction levels [33]. Shedding of the extracellular domain of E-cadherin can occur through cleavage by metalloproteases [147], while the release of its intracellular domain has been shown for presenilin/gamma-secretase cleavage [148]. Proteolytic digestion of VE-cadherin has been observed, though so far only in the context of endothelial apoptosis and leukocyte extravasation [149, 150].

1.4.4.4 The role of phosphorylation

Tyrosine phosphorylation is a well recognised mechanism for the regulation of cell-cell contacts. A correlation between enhanced tyrosine phosphorylation of the cadherin-catenin complex and junctional destabilisation has been established [151], while confluent endothelial cells in culture are accompanied by a decrease in the tyrosine phosphorylation of their junctional components [130]. Serine/threonine phosphorylation has been reported for E-cadherin [152], and p120 [153], however given the lack of experimental evidence for its significance in VE-cadherin function, this section will focus on the more extensively studied tyrosine phosphorylation.

1.4.4.4.1 Protein tyrosine kinases

A variety of inflammatory and permeability mediators, including histamine, thrombin, and VEGF, lead to an increase in paracellular permeability through their stimulatory actions on receptor protein tyrosine kinases (RPTKs) or G-protein-coupled receptors [113, 114, 116]. Following receptor activation, the VEGF-signaling cascade that leads to an increase in permeability is thought to involve Src tyrosine kinases [154, 155],

which are known to concentrate at adherens junctions [156]. Thrombin, on the other hand, is postulated to exert its effects by displacing the protein tyrosine phosphatase SHP2 from the cadherin-catenin complex [157].

It is noteworthy that VEGF-, histamine-, or thrombin-driven tyrosine phosphorylation and endothelial barrier disruption, could each be manifested in a separate way. A discrepancy exists between the observations on the effects of histamine on adherens junctions, and those of thrombin: the former cause an increase in the phosphorylation of VE-cadherins and catenins, with a concomitant decreased association between the complex and the cytoskeleton [116], akin to a situation of low cell density [130]; the latter also results in an increased tyrosine phosphorylation of junctional components, but this time with a decrease in the interaction within the VE-cadherin-catenin complex, and also a marked change in the cell-surface pattern of VE-cadherin [113]. The effect of VEGF is less clear, as two different studies of junctional perturbation, report both disruption and preservation of the adherens complex association with the cytoskeleton [114, 158].

VE-cadherin, catenins, and p120 can all be modified by phosphorylation, while VE-cadherin itself harbors nine tyrosine residues in its intracellular domain [14]. It appears that a complex mechanism is in place, and each response most likely reflects a combination of different phosphorylation changes that are possible within the realm of permutations available for each molecule and for each cell type. The different patterns of phosphorylation could in turn reflect different regulatory mechanisms, as discussed above.

1.4.4.4.2 Protein tyrosine phosphatases

The continuous changes accompanying protein tyrosine phosphorylation, demand the presence of phosphatases to balance out the actions of kinases. Indeed, a number of protein tyrosine phosphatases (PTPs) have been found to associate with the cadherin-catenin complex, including SHP-2, RPTPκ, RPTPβ/ζ, LAR, SHP-1, RPTPμ, PTP1B [33]. Vascular Endothelial protein tyrosine phosphatase (VE-PTP) is a recently characterised phosphatase present specifically in endothelial cells (Figure 1.7, A) [159]. It is the homologue of human protein tyrosine phosphatase β (HPTPβ), and a member of subclass III of receptor-type PTPs, bearing seventeen fibronectin III (FN III) repeats on its extracellular portion, and a single catalytic domain in the cytoplasmic tail [159, 160]. In contrast to other known phosphatase-substrate interactions, VE-PTP was found to associate with VE-cadherin via the membrane-proximal extracellular domains, while no interaction was detected between VE-PTP and β-catenin [161]. Through triple transfection experiments, VE-PTP was shown to reverse the VEGF-mediated tyrosine phosphorylation of VE-cadherin, and to increase the endothelial barrier function [161]. Mutations in the catalytic domain of VE-PTP abolish its ability to reverse the effects of VEGF on VE-cadherin phosphorylation and on the endothelial barrier function (personal communication; Professor Dietmar Vestweber, Max-Planck-Institute for Molecular Biomedicine, Munster, Germany), suggesting a direct role of phosphatase activity in the regulation of permeability through VE-cadherin. Akin to the function of its mouse homologue, HPTPβ expression is upregulated in a parallel fashion to an increase in membrane PTPase activity in Human Umbilical Vein Endothelial Cells (HUVECs) displaying contact inhibition of cell growth [162]. A substrate for HPTPβ remains unidentified at present. Phosphatase recruitment on cadherin-catenin complexes could mediate additional functions besides simply the dephosphorylation of junctional components. DEP-

1/CD148 is another member of the Type III family of receptor protein tyrosine phosphatases [160], also expressed in endothelial cells, albeit non-exclusively [163]. It has been found to codistribute with VE-cadherin at interendothelial junctions [163], and recently also to dephosphorylate VEGFR-2, when the latter is in complex with VE-cadherin [164]. Dephosphorylation was dependent on the presence of both VE-cadherin and β-catenin, but not p120 [164], and could represent part of a feedback mechanism whereby VE-cadherin mediates attenuation of VEGF signaling, its own activator.

The importance of maintaining a balance between kinases and phosphatases within a cell was underlined in a mouse model with targeted inactivation of the gene encoding DEP-1 [165]. Mice died before embryonic day 11.5, with defects in vascular development characterised by enlarged primitive vessels, impaired vascular remodeling, and increased endothelial proliferation. Loss of function of VE-PTP has not been reported to this day.

1.5 Permeability in disease

Pathological vascular permeability refers to the unregulated extravasation of fluid, plasma proteins, and in extreme situations, also cells, from the blood to the tissues. Such permeability accompanies conditions of acute or chronic inflammation, and neovascular disease. At the cellular level, breakdown of the endothelial barrier is manifested as an induction or a modulation of pre-existing structures mediating physiological permeability.

Tumors exhibit high vascular permeability, in association with angiogenesis [53]. Unusually large intercellular gaps [166], VVOs [47], and fenestrae [167, 168] have all

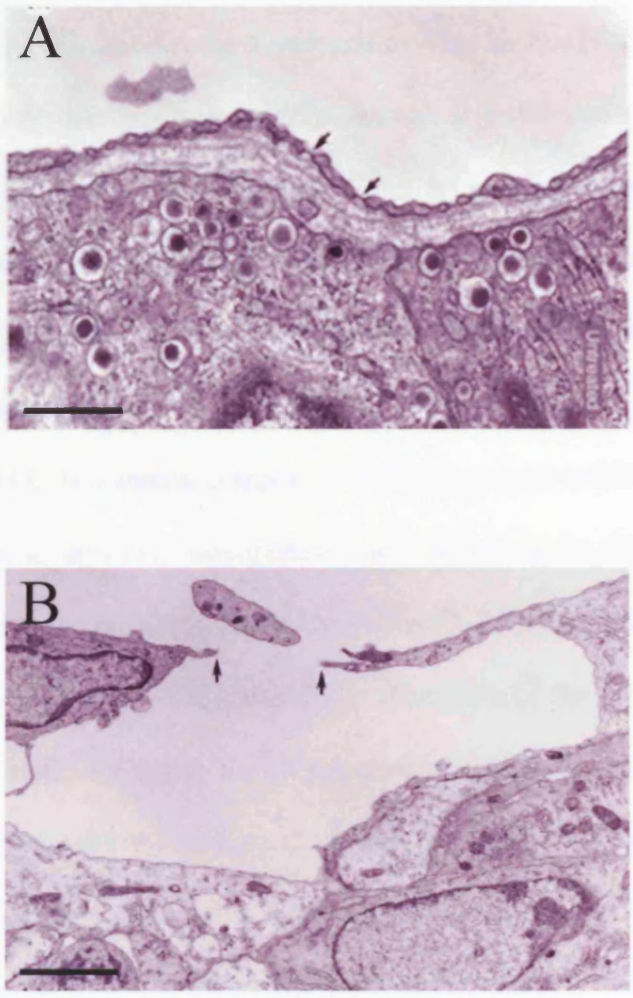

Figure 1.8 Pathological vascular permeability. Abundant endothelial fenestrae are in a tumor vessel as seen by TEM (A) (Reproduced from Ref. 174). Intercellular opening (between arrows) in lining of a tumor vessel viewed by TEM (B) (Reproduced from Ref.166) (Bar = 1 μm)

been observed in the neovasculature of tumors (Figure 1.8), and consistent with their permeability properties can account for the extravasation of plasma proteins and interstitial edema. Intercellular gaps are also the sites of entry of tumor cells into the vasculature, providing the gateway for metastasis to other tissues [155].

Chronic inflammatory diseases such as rheumatoid arthritis and psoriasis are also associated with increased neovascularisation and hyperpermeability. [169, 170]. Leukocyte infiltration is a common element of both diseases, and presumably occurs through disrupted junctions. In addition, psoriatic lesions have been shown to be extensively fenestrated [171].

Upregulation of VEGF is a central component in the hyperpermeability manifestations in tumors, rheumatoid arthritis, retinopathies, and inflammatory skin disorders [53]. Since VEGF is a potent modulator of tight junctions [172], adherens junctions [155], VVOs [51], and fenestrae [69, 173], while a combination of the different endothelial specialisations is usually involved in the hyperpermeability response, distinguishing among their individual contributions is a challenge. Moreover, the actions of VEGF as an endothelial mitogen and motogen, are difficult to isolate from its effects on leakage, as angiogenesis and permeability appear to occur in conjunction. As often happens in diseases that affect the differentiation program of cells, neovascular disease shares many common features with the early vascular system of the brain, prior to the establishement of the blood-brain barrier [22]. Nonetheless, VEGF is capable of inducing rapid changes in permeability, as demonstrated by the formation of fenestrae in normally non-fenestrated vascular beds within minutes of application [173].

Since VEGF is downregulated in most adult tissues [92], with the exception of sites undergoing angiogenic remodeling, it presents an attractive therapeutic target. A recent study showed that an inhibitor of VEGF was able to suppress the presence of tumor endothelial fenestrae and lead to the regression of tumor vessels [174]. More

focused therapeutic targeting on specific VEGF isoforms [175] or specific attributes of endothelial substructures, could potentially enhance the efficacy of treatments.

1.7 Convergence of pathways and outline of thesis

The focus of this thesis is divided among two components of the endothelial barrier, fenestrae and adherens junctions. Despite the obvious morphological and functional differences between the two membrane specialisations, a number of common elements can be recognised.

First of all, VEGF acts as a common denominator between fenestrae, adherens junctions, and also a number of other structures involved in physiological and pathological vascular permeability. Acknowledged as a potent permeability factor, VEGF can regulate the gating properties of junctions, and is most likely involved in both the biogenesis and the maintenance of fenestrae. Binding to different receptors, activation of different intracellular pathways, and interaction with separate signaling cascades could all contribute to the expression of unique phenotypes, starting with a single growth factor. Secondly, the actin cytoskeleton appears to have a central role in establishing both types of endothelial specialisations. Well-accepted determinants of cell shape, actin microfilaments can promote the formation of adherens junctions and, as I will argue in this thesis, inhibit the formation of fenestrae. Regulatory functions, in addition to structural scaffolding, have been attributed to cytoskeletal components of adherens junctions. Equivalent roles for microfilaments in fenestrae are not unlikely, though at the moment remain speculative in absence of substantial experimental evidence.

The studies presented in this thesis were aimed at providing insight into areas of knowledge deficit, in the fields of fenestrae and adherens junction biology. With information almost exclusively at the morphological and ultrastructural level the development of novel tools to enable biochemical and cell biological investigations of fenestrae was deemed critical. On the other hand, the extensively characterised properties of adherens junctions *in vitro* seemed best complemented by *in vivo* studies assessing the consequences of junction modulation on the endothelial barrier. Thus, a structural and functional analysis of vascular permeability was undertaken, the ultimate goals of which were to drive the molecular characterisation of fenestrae, and the creation of an *in vivo* model to study paracellular permeability modulation by phosphatases. The ensuing chapters present the systematic approach pursued in establishing an *in vitro* model for fenestrae formation and devising biochemical methods for the isolation of fenestrated plasma membranes, which resulted in the identification of fenestrae protein candidates through subcellular proteomics, and the characterisation of a novel fenestrae sieve plate component. The last chapter describes the creation of a transgenic mouse model for the study of endothelial barrier dysfunction, through conditional overexpression of wildtype or mutant versions of the adherens junction phosphatase VE-PTP.

Chapter 2: Materials and methods

2.1 Reagents

All chemicals were purchased from Sigma-Aldrich and Fluka, unless otherwise indicated. All culture media and related products were obtained from Invitrogen, unless otherwise stated. All restriction endonucleases were purchased from New England Biolabs. Phosphate Buffered Saline without calcium or magnesium (PBS), Luria-Bertani (LB) medium, LB-agar, Ethylene Diamine Tetraacetic Acid (EDTA), trypsin/versene, and Leibovitz L-15 medium were provided by CRUK or Eyetech Research Center central services. L-glutamate and penicillin/streptomycin were provided by CRUK central services or purchased from Invitrogen. Oligonucleotides were provided by CRUK oligonucleotide synthesis service or purchased from Proligo, unless otherwise indicated.

2.2 Bacterial culture

2.2.1 Preparation of electrocompetent cells

5 ml from an overnight culture of XL-1 blue bacteria (Stratagene), were added to 800 ml of LB medium and grown at 37°C with shaking to an OD_{595} of 0.6. The culture was incubated for 30 minutes on ice and centrifuged at 5,000rpm for 20 minutes at 4°C using a JA-10 rotor of an Avanti J-E centrifuge (Beckman Coulter). The pellet was washed twice with 800 ml ice-cold water, once with 400 ml ice-cold 10% glycerol, and was finally resuspended in 1 volume ice-cold 10% glycerol. Aliquots of the preparation were stored at -80°C.

2.2.2 Transformation

50-500 pg DNA was added to 80 µl of electrocompetent cells in a 1 mm electroporation cuvette (Bio-Rad). Mixtures were incubated on ice for 10 minutes and transformations were performed at 200Ω, 25µF, and 1.8kV. Bacteria were incubated with 400 µl SOC medium at 37°C for 1hour, and then centrifuged at full speed in a microcentrifuge. Pellets were resuspended in 100 µl LB medium, plated on agar plates containing Ampicillin (75 µg/ml) and incubated overnight at 37°C.

2.2.3 Cryopreservation

Bacterial cultures were stored as 50% glycerol stocks at -80°C

2.3 Mammalian tissue culture

2.3.1 Isolation of mouse embryonic fibroblasts

14.5 day old embryos were dissected from the extraembryonic membranes in Dulbecco's Modified Eagle's Medium (DMEM; Invitrogen). The liver was discarded, the head was removed for genotyping and the remainder of the embryo was incubated with 1 ml of trypsin/versene for 45 minutes on a shaker set at 37°C. The embryo was dissociated by pipetting up and down five times, using a plastic Pasteur pipette, and then split between two 60 mm dishes.

2.3.2 Maintenance of mammalian cell lines

Cell Line	Species	Origin	Passage No	Culture conditions
bEND5	mouse	brain endothelioma	13-25	DMEM high glucose with sodium pyruvate, 10%FBS, 4mM L-glutamate, penicillin/streptomycin, 5μM β-mercaptoethanol, non-essential amino acids. 37°C incubator with
Py4.1	mouse	ear and tail hemangiomas		DMEM high glucose with sodium pyruvate, 2%FBS, penicillin/streptomycin. 37°C incubator with 10%CO2
NIH 3T3 (ATCC)	mouse	embryo		DMEM high glucose with sodium pyruvate, 10% FBS, 4mM L-glutamate, penicillin/streptomycin, 1.5g/L sodium bicarbonate. 37°C incubator with 5%CO2
HUVEC (Cascade Biologics)	human	umbilical vein	3-5	M200, low supplement growth serum, penicillin/streptomycin (Cascade Biologics). 37°C incubator with 5%CO2
SVEC4-10 (ATCC)	mouse	lymph node	3-5	DMEM high glucose with sodium pyruvate, 10% FBS, 4mM L-glutamate, penicillin/streptomycin, 1.5g/L sodium bicarbonate. 37°C incubator with 10%CO2
TetO-VE-PTP MEF	mouse	embryo	2-3	DMEM high glucose with sodium pyruvate, 10% FBS Tet system approved (Clontech), 4mM L-glutamate, 2 x penicillin/streptomycin, 1.25 μg/ml Fungizone. 37°C incubator with 10%CO2
MEF 3T3 Tet-Off cell line (Clontech)	mouse	embryo	3	DMEM high glucose with sodium pyruvate, 10% FBS Tet system approved (Clontech), 4mM L-glutamate, penicillin/streptomycin. 37°C incubator with 10%CO2

All cell lines were trypsinised using trypsin/versene solution. Alternatively cell lines were trypsinised using 1x Trypsin EDTA solution (Invitrogen), apart from bEND5 and Py4.1 cells which required 10x Trypsin EDTA solution (Invitrogen), diluted 1:1 with DMEM.

Cells were thawed by diluting the contents of an ampule in 9 volumes of medium, sedimenting the cells at 300g and resuspending the pellet in the appropriate volume of complete medium. Cells were frozen in 10% DMSO, 20% Fetal Bovine Serum (FBS), and 70% of complete medium, and were stored in liquid nitrogen.

2.3.3 Transient transfection of mammalian cell lines

Mouse embryonic fibroblasts (MEFs), isolated from 14.5 day embryos were transfected using either Superfect (Qiagen) or Fugene (Roche). For transfections with Superfect, cells were seeded onto glass coverslips on the day before transfection at a density equivalent to $1x10^5$ cells per well of a 24-well plate. The next day the cells were transfected in serum free DMEM without antibiotics. 1 μg DNA and 5 μl Superfect were incubated with the cells for 3 hours, after which complexes were replaced with normal medium. Cells were fixed 24 hours post transfection. For transfections with Fugene, the same density of cells was seeded and grown overnight, and then transfected in DMEM without antibiotics. 0.2 μg DNA and 0.6 μl Fugene were incubated with the cells, and without replacing the medium, cells were fixed 24 hours post transfection. MEF 3T3 Tet-Off cells were transfected using Superfect (Qiagen) as described above. In all experiments, an expression plasmid encoding Green Fluorescent Protein (GFP) was transfected in parallel as a control for transfection efficiency.

2.3.4 Suppression of Tet-Off constructs by doxycycline

MEF 3T3 Tet-Off cells transfected with Tet-VE-PTP responder constructs, or MEF cells from TetO-VE-PTP transgenic animals (TetO-VE-PTP MEF) transfected with pTetOn (Clontech), were incubated in medium containing 2 μg/ml Doxycycline (Sigma) in order to suppress the expression of the VE-PTP transgene.

2.3.5 Fenestrae induction in endothelial cells

Coverslips and dishes were coated with 1% gelatin (Sigma) solution in PBS for 30 minutes at room temperature. Endothelial cells were seeded on the day before induction at a density equivalent to $1.5x10^6$ cells per 100 mm dish. The next day, cultures were induced at 60-70% confluency, using Cytochalasin B (Sigma) at 10 μM for 2 hours, Latrunculin A (Molecular Probes) at 2.5 μM for 3 hours, or a combination of recombinant mouse VEGF (R&D systems) at 75 ng/ml for 6-72 hours and 10 μM Cytochalasin B for 2 hours. Cells were processed for biochemistry or morphology immediately after the end of the induction.

To inhibit protein synthesis during fenestrae formation, cells were incubated with 10 μg/ml Cycloheximide (Sigma) for 30 minutes, and then induced with VEGF (75 ng/ml) for 6 hours and Cytochalasin B (10 μM) for the last 2 hours.

2.4 DNA techniques

2.4.1 Preparation of genomic DNA

Mammalian tissues were digested in 0.5 ml of lysis buffer (100 mM Tris HCl pH 8.5, 5 mM EDTA, 0.2% SDS, 200 mM NaCl, 0.5 mg/ml proteinase K), shaking at 55°C overnight. Digested tissues were centrifuged to remove any undigested parts, mixed with 0.5 ml isopropanol, and DNA was sedimented by centrifuging at 21,000g for 8 minutes at 4°C. After one wash with 70% Ethanol, DNA was allowed to dry and was finally resuspended in 100 μl of 0.2 x TE buffer (10 mM Tris pH8.0, 1 mM EDTA).

2.4.2 Preparation of plasmid DNA

Plasmid DNA was purified from overnight cultures, grown at 37°C in LB containing Ampicillin (75 µg/ml), using Qiagen plasmid mini kits, QIAfilter plasmid midi, or maxi kits according to the manufacturer's instructions.

2.4.3 Ethanol precipitation of DNA

DNA solutions were mixed with 0.1 volumes 8M LiCl and 3 volumes cold Ethanol. Glycogen was often added to facilitate visualisation of the precipitate. The mixture was placed at -20°C for 20 minutes; DNA was centrifuged at 21,000g for 20 minutes, washed twice with 70% Ethanol, air-dried and resuspended in TE buffer.

2.4.4 Quantitation of DNA

DNA solutions were placed in a quartz cuvette (1 cm path length) and the absorbance of the mixture was read at 260 nm and 280 nm using a Spectrophotometer. The OD_{260} of 1, corresponding to 50 µg/ml double stranded or 33 µg/ml single stranded DNA, was used as a reference for DNA concentration calculations. The $OD_{260/280}$ ratio was used as an estimate for purity of the preparation. A ratio of 1.6-1.9 was considered acceptable.

2.4.5 Restriction enzyme digestion

For small scale diagnostic digests, 0.5 µg of DNA was incubated in the appropriate buffer with 5-10 U of restriction endonuclease in a total volume of 20 µl. The reaction was incubated at the appropriate temperature (25°C or 37°C) for 1-2 hours.

For large scale digests, 5 μg of DNA was incubated in the appropriate buffer with 20-30 U of restriction endonuclease in a total volume of 70 μl. The reaction was incubated for 2-3 hours at 25°C or 37°C. Following digestion, enzymes were inactivated by incubating at 80°C for 20 minutes.

2.4.6 Polymerase chain reaction (PCR)

Primers were 20-22 nucleotides in length, usually with two GC-basepairs at the 3'-end, and annealing temperatures of approximately 55°C. The annealing temperature specific to each primer was calculated using the following formula: Tm = 3 x (sum of GC-basepairs) + 2 x (sum of AT-basepairs). Reactions were carried in a Peltier thermal cycler (MJ Research PCR Machine).

To genotype the TetO-VE-PTP strain, a combination of 3 primers were used in each reaction: TG primer recognised a sequence only present in the transgene, GE primer recognised a sequence only present in the endogenous copy of the gene, and CO primer recognised a region common to both the transgene and the endogenous versions of VE-PTP.

GE: 5'-CTGCCACGGCCCTTGAGCATCG-3'

TG: 5'-CTCGGTACCCGGGTCGAGTAGGC-3'

CO: 5'-ACGCTCAGTGTTATCCACAAGGCCG-3'

2 μl of genomic DNA preparation from mouse tail were mixed with 40 pmols GE primer, 40 pmols TG primer, 80 pmols CO primer, and 15 μl Mega Mix Blue (Helena Biosciences). The reaction conditions were as follows:

Segment 1	1 cycle	94°C for 4 minutes
Segment 2	35 cycles	94°C for 40 seconds
		64°C for 1 minute
		72°C for 1.5 minute
Segment 3	1 cycle	72°C for 3 minutes

Tie2-tTa mice were genotyped using the following PCR primers (provided by Dr. Urban Deutsch, Theodor Kocher Institute, Bern, Switzerland):

HHFW1: 5'-CGATACCATACATAGGTGGAGG-3'

rtTAREV1: 5'-AATGGCTAAGGCGTCGAGCAAAG-3'

10 pmol of each primer were mixed with 2 µl tail DNA and 15 µl Mega Mix Blue (Helena Biosciences), and run according to the following PCR scheme:

Segment 1	1 cycle	94°C for 5 minutes
Segment 2	35 cycles	94°C for 30 seconds
		63°C for 45 seconds
		72°C for 1 minute
Segment 3	1 cycle	72°C for 8 minutes

TetO-LacZ responder strains (nZL2 and TRE-LacZ 2717) were genotyped using the following PCR primers (provided by Dr. Urban Deutsch):

LacZFW4: 5'-CCGTCACGAGCATCATCCTC-3'

LacZREV4: 5'-GACGAAACGCCTGCCAGTATTTAG-3'

13 pmol of each primer were mixed with 2 µl tail DNA and 15 µl Mega Mix Blue, and run using the same reaction conditions as in the Tie2-tTA PCR, only with an annealing temperature of 60°C.

2.4.7 DNA sequencing

Primers of about 18 nucleotides were designed to amplify a region within the gene of interest or the vector sequence surrounding the gene. Reactions were carried out using 500 ng of a given plasmid, 3-4 pmol of primer, and 8 µl of fluorochrome labelling mix (CRUK), in a total volume of 20 µl. PCR conditions were the following:

Segment 1	25 cycles	Denaturation at 96°C for 10 seconds
		Annealing at 50°C for 5 seconds
		Extension at 60°C for 4 minutes

Following amplification, DNA was ethanol precipitated, electrophoresed and visualised. SDS-PAGE electrophoresis and visualisation were performed by CRUK Sequencing Service. Sequence analysis and alignment was performed using the software programs MacVector (Accelrys) and Sequencher (Gene Codes Corporation). The following oligonucleotides were used to sequence TetO-VE-PTP plasmids:

Bluescript T3: 5'-AATTAACCCTCACTAAAGGG-3'

Bluescript T7: 5'-GTAATACGACTCACTATAGGGC-3'

Bluescript M13Fwd: 5'-GTAAAACGACGGCCAGT-3'

VEP-A5: 5'-ACCTTCAGATTTGAGACTTCCATG-3'

VEP-S3: 5'-CAGTGATACCAGCAGATACAGC-3'

VEP-S4: 5'-GTGTCTGCATTCAGACAGGACG-3'

VEP-S5: 5'-CTGTATGTGGTGACTCACAGTG-3'

VEP-FW2: 5'-GGTTCAGCGACACCAACGGAG-3'

VEP-FW4: 5'-CCTCTTGCCTGAGAATCGAGG-3

FWD-R/A: 5'-CATCCGTCACTTTCACTACAC-3'

Oligo(+):

5'-CGCGGCCGCTCTAGAGTTTAAACGGCGCGCCTTAATTAAAGATCTG-3'

All VEP primers were provided by Dr. Urban Deutsch.

2.4.8 DNA agarose gel electrophoresis

Agarose gels were prepared by dissolving 0.6-2% agarose in TAE buffer (40 mM Tris Base pH8.0, 20 mM glacial acetic acid, 1 mM EDTA). Ethidium bromide was added to a final concentration of 0.5 μg/ml. DNA was mixed with 10x BlueJuice™ gel loading buffer (Invitrogen) and electrophoresed at 5-20 V/cm in TAE buffer. A 100 bp or 1 kb DNA ladder (Invitrogen) was loaded in an adjacent well for comparison.

2.4.9 Gel purification of DNA fragments

Gel slices containing relevant DNA fragments were excised and stripped of agarose and contaminants using a gel extraction and nucleotide removal kit (Qiagen).

2.4.10 Cloning

2.4.10.1 Cohesive-end ligation

Restriction digests for the insert and vector were performed. The vector fragment was also dephosphorylated with 0.5 U/μg DNA of alkaline phosphatase (CIP, New England Biolabs), for 1 hour at 37°C, to prevent recircularisation in the case of compatible ends. Following purification, vector and insert were ligated using 200-300 ng total DNA with a 2-4 fold molar excess of insert, and 400 U T4 DNA ligase (New England Biolabs) in 15 μl total volume. The reaction was carried out overnight at 15°C. 1μl of the ligation reaction was used to transform *E.coli* as described above.

2.4.10.2 Blunt-end ligation

Restriction digests of vector and insert were performed as above. Fragments were incubated with T4 DNA polymerase (New England Biolabs) at 1-2 U/μg DNA, 200μM dNTP mix (Ultrapure, Pharmacia), and 0.1 mg/ml BSA, at 12°C for 20 minutes so as to form blunt ends. The polymerase was inactivated by incubating at 75°C for 10 minutes, and the vector was dephosphorylated with alkaline phosphatase as above. Following purification, vector and insert were ligated as described above, only using 2-fold molar excess of vector.

2.5 RNA techniques

2.5.1 RNA isolation

Total RNA was isolated from cells or tissues using the RNeasy mini kit (Qiagen). 3-5x10^6 MEF cells were lysed in 350 µl RLT buffer (Qiagen) by pipetting, and the contents loaded on to 1 RNeasy mini column. 11.5 day old embryos were snap-frozen and immediately homogenised in 800 µl RLT buffer using a mortar and pestle. The lysate was passed through a QIAshredder spin column (Qiagen) and split between two RNeasy mini columns. RNA purification was carried out according to the manufacturer's instructions, with the additional step of on-column DNA digestion performed using the RNase-Free DNase Set (Qiagen). RNA was eluted in water and any remaining DNA was removed from the samples by treating 5 µg RNA with 1U of rDNase I (DNA-*free*, Ambion) in a total volume of 50 µl for 1 hour at 37°C. rDNase I was inactivated by supplementing the reaction with DNase Inactivation reagent, and RNA was snap-frozen and stored at -80°C.

2.5.2 RNA quantitation

RNA solutions were placed in a quartz cuvette (1 cm path length) and the absorbance of the mixture was read at 260 nm and 280 nm using a Spectrophotometer. The OD_{260} of 1, corresponding to 40 µg/ml RNA, was used as a reference for calculations. To obtain an accurate $OD_{260/280}$ ratio, RNA was diluted in 10 mM TrisHCl pH 7.5. A ratio of 1.9-2.1 was expected for a pure preparation.

2.5.3 RNA agarose gel electrophoresis

1.2% agarose gels were prepared in TBE buffer (45 mM Tris-borate pH 8.0, 1 mM EDTA) containing ethidium bromide at a final concentration of 0.5 μg/ml. RNA was mixed with 10x BlueJuice™ gel loading buffer (Invitrogen) and electrophoresed at 5-20 V/cm in TBE buffer. Sharp and distinct ribosomal RNA bands, with the 28S ribosomal RNA band of double intensity to the 18S RNA band, were an indication of intact RNA.

2.5.4 RT-PCR

Reverse transcription of RNA was performed using 1 μg RNA and a two-step reaction using Superscript™ RNase H⁻ Reverse Transcriptase (Invitrogen): RNA, 1 μl Oligo $(dT)_{12-18}$ (Invitrogen), 1 μl 10 mM dNTP (Invitrogen), in a total volume of 12 μl, were heated to 65°C for 5 minutes in a thermal cycler. After cooling on ice, the reaction was supplemented with 4 μl 5x First-Strand buffer, 2 μl 0.1 M DTT, 1 μl RNaseOUT™ (Invitrogen), and heated to 42°C for 2 minutes. Finally, 1 μl SuperScript™ II was added, and the reaction was incubated at 42°C for 50 minutes. The enzyme was inactivated by heating for 15 minutes at 70°C.

To specifically look at TetO-VE-PTP transgene, primers were designed to amplify a region extending to the transcribed exogenous promoter sequence which was also absent from the endogenous copy of the gene:

rt-tg3: 5'-ATGCACTAGTGGCGCCTGTCG-3'

rt-rev1: 5'-ACTTGCTCTGCCACTCCAGTCTGC-3'

The housekeeping gene p97 was selected as an internal control, and was amplified with primers that spanned an intron, so as to distinguish between cDNA and any genomic DNA contaminant:

p97.RT.1859S: 5'-ACGGCAAGCTGCCCCCTGTG-3'

p97.RT.2321A: 5'-CATAGCCGATGGATTTGTCTGC -3'

For each PCR reaction, 2 µl cDNA was mixed with 15 µl Mega Mix Blue (Helena Biosciences), 40 pmol of each TetO-VE-PTP primer, and 1 pmol of each p97 primer. The reaction conditions were the same as for genotyping TetO-VE-PTP mice.

2.5.5 Real time quantitative PCR (Taqman)

Reverse transcription of RNA was performed using 300 ng RNA and the following reaction mix (ABI): 1 x RT buffer, 5.5 mM $MgCl_2$, 500 µM of each dNTP, 2.5 µM random primers, 0.4 U/µl RNase Inhibitor, 1.25 U/µl Multiscribe Reverse Transcriptase, supplemented with Nuclease-Free water (Ambion) to a total volume of 60 µl. cDNA synthesis was carried out in a thermal cycler according to the following scheme:

Segment 1	1 cycle	25°C for 10 minutes
Segment 2	1 cycle	42°C for 60 minutes
Segment 3	1 cycle	95°C for 5 minutes

Taqman cocktails were prepared using 1x PCR master mix (ABI), 5 µl cDNA, 250 nM of each primer, and 500 nM of probe, in a total volume of 25 µl. The following primer/probe sets (ABI) were used:

Endogenous VE_PTP Fwd: 5'- CCA CCG GCC CTT GAG CAT-3'

Endogenous VE_PTP Rev: 5'- CCA GCC AGG GCA CTT CTG-3'

Endogenous VE_PTP Probe: 5'- CGC TCA ACA AGT GGT AC-3'

Transgene VE_PTP Fwd: 5'- GCA TGC AAG CTT CAC ATA TGC-3'

Transgene VE_PTP Rev: 5'- CCA GCC AGG GCA CTT CTG-3'

Transgene VE_PTP Probe: 5'- CGC TCA ACA AGT GGT AC-3'

Total VE_PTP Fwd: 5'- TAA CAC TGA GCG TCG TGC AGA-3'

Total VE_PTP Rev: 5'- CTA GAG ACC CTG GAC TCC AAC AG-3'

Total VE_PTP Probe: 5'- CAG AGC AAG TGA AAT GTA-3'

Tie2-tTA Fwd: 5'- ACG GCG CTC TGG ATA TGG-3'

Tie2-tTA Rev: 5'- TTC CAA GGG CAT CGG TAA AC-3'

Tie2-tTA Probe: 5'- CGA CTT CGA GTT TGA GCA-3'

For VE-PTP, endogenous primer/probe sets were designed to only amplify the endogenous VE-PTP copy, transgene primer/probe sets to only amplify the transgene copy, while total VE-PTP primer/probe sets were non-discriminatory between the two versions.

GAPDH served as the internal control in all reactions, and was amplified with rodent GAPDH primers and probe (ABI).

Reactions were loaded on Prism Optical tubes (ABI) and run in the ABI Prism 7700 Sequence Detection System using the following cycling conditions:

Segment 1	1 cycle	50°C for 2 minutes
Segment 2	1 cycle	95°C for 10 minutes
Segment 3	40 cycles	95°C for 15 seconds
		60°C for 1 minute

Results were analysed using the SDS 7900HT Software 2.2 (ABI).

2.6 Protein techniques

2.6.1 Protein concentration determination

Protein concentrations were determined using the Bio-Rad Protein Assay (Bio-Rad) in microtiter plates. Samples diluted in water, and bovine serum albumin (BSA) standards diluted in water and sample diluent, were incubated with Bio-Rad Protein Assay reagent for 5 minutes at room temperature and the absorbance was measured in a Spectrophotometer at OD_{595}. Standard curves were created based on the absorbance of BSA standards and were used to assign protein concentrations to samples. The Detergent Compatible Bio-Rad Protein Assay was used for proteins in buffers containing high concentrations of detergent, and was carried out in a similar fashion, with sample or standard absorbance measured at OD_{795}.

2.6.2 Protein precipitation

Proteins were precipitated overnight in 80% acetone (v/v) at -80°C and subsequently centrifuged for 30 minutes at 21,000g at 4°C. The pellet was resuspended in the desired volume of buffer.

2.6.3 Plasma membrane isolation using cationic colloidal silica

All steps in the procedure were performed on ice or in centrifuges pre-cooled to 4°C. Cells grown on 150 mm dishes were washed twice with PBS containing calcium and magnesium (Invitrogen), and once with coating buffer (20 mM MES, 135 mM NaCl, 0.5 mM $CaCl_2$, 1 mM $MgCl_2$, pH 5.5). Cells were then coated with 8 ml of a 1% cationic colloidal silica solution (kind gift of Professor Donna Stolz, University of Pittsburg) in coating buffer for 2 minutes. After one wash with coating buffer, cells were coated again, for 1 minute, with 8 ml of 1 mg/ml polyacrylic acid (Aldrich) solution in coating buffer, adjusted to pH 6.0-6.5. Cells were washed once with coating buffer and once with lysis buffer (2.5 mM Imidazole pH 7.0, supplemented with Complete EDTA-free protease inhibitor tablets, Roche), prior to incubation in lysis buffer for 15 minutes. The lysis buffer of induced cells was supplemented with 2.5 μM latrunculin A, to maintain the fenestrated phenotype during the incubation period. Cells were scraped in a total of 2 ml lysis buffer and lysed by 20 strokes in a 7 ml Dounce tissue grinder with a tight pestle (Wheaton). Lysis was ensured by examining the cells by Phase-Contrast Microscopy. Silica-coated plasma membranes and nuclei were sedimented at 900g for 10 minutes. To obtain internal membranes, the supernatant was centrifuged at 100,000g for 30 minutes in a TLA 100.3 rotor of an Optima TLX Ultracentrifuge (Beckman Coulter). The pellet of plasma membrane and nuclei was resuspended in 1 ml of lysis buffer, supplemented with 20 μl of Benzonase

grade II (Merck BDH), and homogenised with 1 ml of 100% Nycodenz in lysis buffer in a dounce tissue grinder. The homogenate was layered onto a 0.5 ml cushion of 70% Nycodenz in lysis buffer, and was supplemented with another layer of 2 ml lysis buffer, prior to sedimenting at 60,000g for 30 minutes in a SW55 Ti rotor of an Optima L-80 Ultracentrifuge (Beckman Coulter). The pellet containing silica-coated plasma membranes was washed 3 times with lysis buffer and proteins were solubilised by boiling silica-coated membranes in silica lysis buffer (3.4% SDS, 120 mM Tris pH 6.8) for 15 minutes. Residual silica was sedimented at 21,000g, and the supernatant containing solubilised plasma membranes was snap-frozen and stored at -80°C.

For quality control purposes, samples were removed from various fractions during the course of the purification and were solubilised in silica lysis buffer. Whole cell lysates were prepared by washing a 150 mm dish twice with PBS, scraping and sedimenting the cells at 300g, and finally lysing the pellet in 300 µl silica lysis buffer. Equal amounts of solubilised cellular fractions were supplemented with DTT and glycerol (EM Science), to a final concentration of 0.1 M and 5%, respectively. They were then separated by SDS-PAGE gel electrophoresis.

2.6.4 Differential extraction of cells

Cells grown on 60 mm dishes were briefly washed with PBS and were then incubated for 30 minutes on ice with 0.5 ml of extraction buffer (10 mM Tris pH 8.0, 150 mM NaCl, 2 mM EDTA, Complete EDTA-free Protease inhibitor tablets, Roche, and 0.1%, 0.2%, 0.5%, or 1% Triton X-100, EM Science). Cells were scraped, and insoluble material was pelleted by centrifugation for 30 minutes at 21,000g at 4°C. Detergent soluble material was acetone precipitated, and pellets recovered from either

the precipitated soluble material, or from the insoluble material were resuspended in the same volumes of 1x SDS sample buffer, to be separated by SDS-PAGE gel electrophoresis.

Alternatively, to visualise insoluble material by immunofluorescence, cells grown on 60 mm dishes were incubated for 3 minutes on ice with 3 ml of extraction buffer. Detergent soluble material was removed; cells were washed twice in PBS, and fixed for immunofluorescence

2.6.5 Immunoprecipitation

Cells grown on 100 mm dishes were briefly washed with PBS and were then incubated for 30 minutes on ice with 1 ml of immunoprecipitation buffer. The following immunoprecipitation buffers were used:

IP buffer 1: 20 mM Tris HCl pH 7.5, 0.1% Triton X-100 (EM Science), 10% glycerol (EM Science), Complete EDTA-free Protease inhibitor tablets (Roche)

IP buffer 2: 10 mM HEPES pH 7.5, 150 mM NaCl, 0.1% NP-40, 1 mM DTT, Complete EDTA-free Protease inhibitor tablets (Roche)

RIPA buffer: 10 mM Tris pH 7.5, 150 mM NaCl, 1% Triton X-100 (EM Science), 0.5% SDS, 5% sodium deoxycholate, Complete EDTA-free Protease inhibitor tablets (Roche)

Differential extraction buffer: 10 mM Tris pH 8.0, 150 mM NaCl, 2 mM EDTA, Complete EDTA-free Protease inhibitor tablets (Roche), 0.1% Triton X-100(EM Science).

Cells were scraped, and insoluble material was pelleted by centrifugation for 30 minutes at 21,000g at 4°C. Protein concentration of the supernatant was measured and 500 μg of the lysate was incubated overnight at 4°C with 5 μg of antibody.

Protein G sepharose™ 4 Fast Flow (Amersham Biosciences) beads were washed 3 times with immunoprecipitation buffer and incubated with the lysate, at a dilution of 1:20 for 1h at 4°C. Immunocomplexes and beads were separated by centrifugation at 16,000g for 5 minutes at 4°C. The beads were washed 3 times with immunoprecipitation buffer and immunocomplexes were eluted by boiling for 10 minutes with 40 µl of 2x SDS sample buffer, to be separated by SDS-PAGE gel electrophoresis.

2.6.6 One-dimensional SDS-Polyacrylamide gel electrophoresis

Gels were poured at a thickness of 1 to 1.5 mm using the Bio-Rad Mini gel assembly kit and acrylamide solutions from National Diagnostics. The separating gel was prepared as follows:

final acrylamide concentration	ProtoGel (ml)	Resolving buffer (ml)	deionised H_2O (ml)
6%	2	2.5	5.39
8%	2.67	2.5	4.72
10%	3.33	2.5	4.06
12%	4	2.5	3.39
15%	5	2.5	2.39

100 µl of 10% APS (Sigma) and 10 µl TEMED (Sigma) were added per 10 ml of gel solution to enhance polymerisation.

The stacking gel was prepared by mixing 1.3 ml ProtoGel, 2.5 ml ProtoGel Stacking Buffer, 6.1 ml deionised H_2O, and the same amounts of APS and TEMED as above.

SDS sample buffer was prepared as a 6x stock solution, containing 0.35 M Tris HCl pH 6.8, 10% SDS, 0.6 M DTT, 30% glycerol, and 0.012% bromphenol blue. Samples were boiled in 1x or 2x sample buffer at 95°C for 5 minutes prior to loading on the gel.

Gels were run in Tris-glycine buffer (25 mM Tris, 250 mM glycine pH 8.3, 0.1% SDS) at 70-180 V.

2.6.7 Western Blotting

Following electrophoretic separation, proteins were blotted onto Hybond™ (Amersham Biosciences) nitrocellulose membranes using a semi-dry blotter (Bio-Rad). Membranes and pieces of Whatman paper were pre-soaked in transfer buffer (80 ml methanol, 32 ml Tris-glycine buffer, 0.4 ml of 10% SDS solution, in a total volume of 400 ml) for 20 minutes. After a brief incubation of the gel in transfer buffer, gel and membrane were sandwiched between six pieces of Whatman paper, with the membrane facing the anode of the electroblotting apparatus. Transfer was carried out at 120 mA per gel for 1 hour (1 mm thick gels) or 1.5 hour (1.5 mm thick gels). Blots were incubated with blocking buffer (5% non-fat dry milk in PBS) for 2 hours at room temperature or overnight at 4°C. The primary antibody was diluted in blocking buffer and applied for 1-2 hours at room temperature or overnight at 4°C. The following primary antibodies were used: mouse anti-GS28 (1:100; BD Biosciences), rabbit anti-PV1 (1:1000; CRUK), rat anti-MECA-32 (1:500; Developmental Studies Hybridoma Bank), mouse anti-tubulin (1:5000; Sigma), mouse anti-actin (1:2000; clone AC-74; Sigma), mouse anti-caveolin 1 (1:1000; BD Biosciences), goat anti-moesin (1:1000; Santa-Cruz), mouse anti-moesin (1:1000; BD Biosciences), goat anti-radixin (1:1000; Santa-Cruz), mouse anti-ezrin (1:1000;

Sigma), rabbit anti-p-Moesin (1:1000; Santa-Cruz), rabbit anti-cofilin (1:1000; Cytoskeleton), mouse anti-annexin II (1:1000; BD Biosciences), goat anti-enolase alpha (1:100; Santa-Cruz), goat anti-hnRNP K (1:100; Santa-Cruz), rabbit anti-merlin (1:1000; gift of Dr. Wallace Ip, University of Cincinnati), mouse anti-GM130 (1:250; BD Biosciences), rat anti-VE-cadherin (1:1000; BD Biosciences). After 3 five-minute washes in blocking buffer, Horseradish peroxidase (HRP) conjugated secondary antibodies were diluted in a similar fashion and applied for 1 hour at room temperature: sheep anti-mouse IgG (1:1000; Amersham Biosciences), donkey anti-rabbit Ig (1:1000; Amersham Biosciences), goat anti-rat (1:1000; Amersham Biosciences), rabbit anti-goat (1:2000; Jackson Immunoresearch). Blots were washed 2 times in blocking buffer and finally once in PBS. The product of the HRP reaction was detected by enhanced chemiluminescence (Amersham Biosciences). Quantitation of the density of bands was performed using Scion Image for Windows (Scion Corporation).

2.6.8 Proteomics

2.6.8.1 Isoelectric focusing and two-dimensional SDS-PAGE electrophoresis (CRUK)

Proteins eluted from silica-coated plasma membranes were TCA/acetone precipitated using the 2-D Clean-Up Kit (Amersham Biosciences) and then resuspended in 8M Urea, 2% CHAPS, 5% Glycerol, 65 mM DTT, 0.5% IPG buffer pH 3-10 (Amersham Biosciences), by shaking for 60 minutes at room temperature. 50 μg of protein was subjected to isoelectric focusing (IEF) on 13 cm Immobiline^{TM} Dry Strip gels pH 3-11 (Amersham Biosciences) using an IPGphor^{TM} Isoelectric Focusing System (Amersham Biosciences). Following IEF, IPG strips were incubated in SDS-PAGE

equilibration buffer containing 50 mM Tris-Cl pH 8.8, 6M Urea, 30% glycerol, 2% SDS, bromophenol blue. Strips were first incubated in reducing equilibration buffer containing 65 mM DTT for 15 minutes, and then in alkylating equilibration buffer containing 25 mg/ml iodoacetamide for another 15 minutes. Following equilibration, SDS-PAGE electrophoresis was performed on 1.5 mm thick 10% polyacrylamide gels, using a Hoefer^{TM} SE 600 standard vertical system (Amersham Biosciences). Gels were fixed for silver staining in a solution of 5% acetic acid and 30% ethanol for 1 hour. Following rinsing, sensitisation for 1 minute in 1.3 mM sodium thiosulphate (STS), and another round of rinsing, gels were incubated in 12 mM $AgNO_3$ for 2 hours at 4°C, in a light-protected environment. Gels were rinsed, and the staining developed by incubation in a solution of 0.3 M K_2CO_3, 0.25 ml/l formalin, and 1.6 mM STS for 10 to 20 minutes. The reaction was stopped by incubating for 30 minutes in 33 mM Tris pH8.0 and 2% acetic acid.

2.6.8.2 Isoelectric focusing and two-dimensional SDS-PAGE electrophoresis (Charles River Proteomics)

Proteins eluted from silica-coated plasma membranes were acetone precipitated and solubilised in 40 mM Tris pH 10.4, 7M Urea, 2M Thiourea, and 1% proprietary detergent (Cellular and Organelle Membrane Solubilising Reagent; Sigma), reduced with tri-butylphosphine, and alkylated with 10 mM acrylamide for 90 minutes at room temperature. Following a second round of acetone precipitation, the pellet was solubilised in 7M Urea, 2M Thiourea, and 2% CHAPS, and 40 µg of protein was subjected to IEF on 11 cm pH 3-10 immobilised pH gradient (IPG) strips (Proteome Systems, Sydney, NSW, Australia). Following IEF, IPG strips were equilibrated in 6M urea, 2% SDS, 50 mM Tris-acetate buffer (pH 7), 0.01% bromophenol blue and

subjected to SDS polyacrylamide gel electrophoresis on 6-15% Gel Chips™ (Proteome Systems). All gels were stained in Sypro® Ruby (Molecular Probes) and imaged by CCD camera on a fluorescent imager (Alpha Innotech)

2.6.8.3 Protein digestion, MALDI analysis, and Bioinformatic database search (Charles River Proteomics)

Protein spots were automatically detected and excised using the Xcise apparatus (Shimadzu Biotech). Gel pieces were washed twice with 150 µl 25 mM ammonium bicarbonate pH 8.2, 50% acetonitrile, then dehydrated by the addition of 100% acetonitrile and air dried. Trypsin (Promega) in 2 mM of 20 µg/mol ammonium bicarbonate was added to each gel piece and incubated at 30°C for 16 hours. The peptides were extracted by sonication. The solution was automatically desalted and concentrated using Zip Tips (Millipore) on the Xcise apparatus, and spotted onto the Axima (Kratos) MALDI target plate. Peptide mass fingerprints of tryptic peptides were generated by matrix assisted laser desorption/ionisation time-of-flight mass spectrometry (MALDI-TOF-MS) using an AximaCFR (Kratos).

Spectra were automatically analysed by the BioinformatIQ integrated suite of bioinformatics tools (Proteome Systems). Protein identifications were assigned by comparing peak lists to a database containing theoretical tryptic digests of NCBI and Swiss Prot sequence databases. Protein identification was evaluated based on percent coverage, MOWSE score, number of peptide matches, peak intensity, and match of isoelectric point (pI) and molecular weight with the location of the protein on the 2D gel.

2.7 Morphology

2.7.1 Histology

Mouse eyes dissected in PBS, were either directly embedded in Tissue-Tek ™ OCT compound (Sakura) on dry ice, or embedded after a 5 minute fixation step at room temperature in 4% paraformaldehyde (PFA) in PBS. 10 μm thick sections were cut along the PO (pupil to optic nerve) horizontal plane, mounted on slides and stored at -80°C.

2.7.2 Immunolabelling

2.7.2.1 Immunohistochemistry on fixed or unfixed mouse sections

Slides were permeabilised in -20°C methanol for 10 minutes, and blocked for 30 minutes in blocking solution (10% Donkey or Goat Serum (Sigma), 0.5% Triton X-100, 1% BSA (Sigma), PBS) in a humidity chamber. The following primary antibodies were used: goat anti-moesin (1:25; Santa-Cruz), rabbit anti-ezrin (1:100; Upstate), rat anti-MECA-32 (1:100; Developmental Studies Hybridoma Bank), rat anti-mouse CD31 (1:300; clone MEC 13.3; BD Biosciences). 80 μl of primary antibody solution was applied to each slide for 1 hour at room temperature in a humidity chamber. The slides were washed 3 times, for five minutes each time, in blocking solution lacking serum. The same procedure was followed for secondary antibodies Alexa488-conjugated goat anti-rabbit or anti-rat IgG (1:1000; Molecular Probes), Alexa633-conjugated goat anti-rat IgG (1:500; Molecular Probes), and Cy3-conjugated donkey anti-goat IgG (1 μg/ml, Jackson Immunoresearch). As negative controls, the primary antibodies were omitted with secondary antibody incubations

performed in the usual way. After three washes, the slides were mounted using Vectashield with DAPI (Vector Laboratories Inc.)

2.7.2.2 Immunofluorescence on coverslips

Cells on coverslips were fixed either in -20°C methanol for 8 minutes or in room temperature 4% PFA for 15 minutes. For PFA fixed cells, fixation was followed by 5 washes in PBS and a 3 minute permeabilisation step in PBT (0.1% Triton X-100, PBS). Coverslips were blocked for 15 minutes in blocking solution (10% Goat or Donkey Serum (Sigma), 0.2% Fish Skin Gelatin (Sigma), PBS). Primary antibodies used on PFA fixed cells were diluted in blocking solution as follows: rat anti-MECA-32 (1:100; Developmental Studies Hybridoma Bank), mouse anti-tubulin (1:500; Sigma), mouse anti-actin (1:200; clone AC-74; Sigma), mouse anti-caveolin 1 (1:100; BD Biosciences), rabbit anti-caveolin (1:100; BD Biosciences), goat anti-moesin (1:50; Santa-Cruz), mouse anti-moesin (1:100; BD Biosciences), goat anti-radixin (1:25; Santa-Cruz), rabbit anti-ezrin (1:100; Upstate), mouse anti-ezrin (1:100; Sigma), rabbit anti-p-Moesin (1:100; Santa-Cruz), rabbit anti-cofilin (1:100; Cytoskeleton), mouse anti-annexin II (1:100; BD Biosciences), goat anti-enolase alpha (1:100; Santa-Cruz), goat anti-hnRNP K (1:100; Santa-Cruz), goat anti-nm23 H2 (1:100; Santa-Cruz), rabbit anti-merlin (1:100; gift of Dr. Wallace Ip, University of Cincinnati). Primary antibodies used on methanol fixed cells were diluted in blocking solution as follows: rabbit anti-PV-1 (1:100; Cancer Research UK), rabbit anti-VE-PTP (1:300; Cancer Research UK), mouse anti-GM130 (1:100; BD Biosciences) Following 15 minutes in blocking solution, coverslips were inverted over 50 µl of primary antibody solution on a piece of parafilm, incubated for 30 minutes at room temperature, and finally washed 3 times, for five minutes each time,

in blocking solution lacking serum. The same procedure was pursued for the following secondary antibodies: Alexa488-conjugated goat anti-rat, anti-mouse, or anti-rabbit IgG (1:1000; Molecular Probes), Alexa633-conjugated goat anti-rat or anti-mouse IgG (1:500; Molecular Probes), Alexa 546-conjugated goat anti-rabbit IgG (1:500; Molecular Probes), Cy3-conjugated donkey anti-goat IgG (1 μg/ml; Jackson Immunoresearch), Cy3-conjugated donkey anti-rat IgG (0.5 μg/ml; Jackson Immunoresearch). To visualise F-actin, Alexa 546-, Alexa 488-, or Alexa 633-conjugated phalloidin (1:50; Molecular Probes) was included in secondary antibody preparations of methanol or PFA fixed cells. Alexa 488-conjugated DNase I (1:500; Molecular Probes) was employed to detect G-actin on PFA fixed cells. As negative controls, primary antibodies were omitted with secondary antibody incubations performed in the usual way. After 3 five-minute washes in blocking solution lacking serum, coverslips were mounted on slides using MOWIOL (Calbiochem) with DABCO (Sigma).

2.7.2.3 Peptide Competition

Peptide competition of the mouse anti-moesin antibody was performed by incubating the antibody with the peptide against which it was raised (moesin peptide; BD Biosciences) or an irrelevant peptide (SNAP-25; BD Biosciences) at a 10,000 : 1 molar ratio of peptide to antibody. Complexes were incubated for 4-5 hours at room temperature with gentle rotation, and centrifuged at 100,000g for 1 h at 16°C in a TLA 100.3 rotor of an Optima TLX Ultracentrifuge (Beckman Coulter). The supernatant was used for immunofluorescence as described above.

2.7.2.4 Live cell labelling for Scanning Electron Microscopy

Cells on coverslips were immediately transferred to ice, and were incubated for 30 minutes with blocking solution (Leibovitz L-15 medium, 0.2% glycine, 1.5% FBS) prior to immunolabelling with primary antibody in antibody diluent (L-15 medium, 1% BSA, 0.25% Fish Skin Gelatin) for 30 minutes. The following primary antibodies were used: rabbit anti-PV1 (1:400; CRUK), rat anti-mouse PECAM (1:100; clone MEC 13.3; BD Biosciences). The cells were washed three times in L-15 medium and incubated for 45 minutes with secondary antibodies diluted in antibody diluent as follows: EM goat anti-rabbit IgG 10 nm Gold (1:40; BBInternational), EM goat anti-rat IgG 5 nm Gold (1:40; BBInternational). Following three washes in L-15 medium, cells were fixed for 2 hours in 3% glutaraldehyde and 1% PFA in 0.08 M sodium cacodylate buffer (pH 7.4).

2.7.2.5 Immunolabelling for wholemount TEM

Cells grown on glass coverslips containing grids (see section 2.7.5.2) were fixed with 0.5% glutaraldehyde for 15 minutes at room temperature, then washed twice with PBS for 10 minutes. Aldehydes were quenched with 50 mM glycine for 5 minutes. Cells were permeabilised with 0.05% Triton X-100 in PBS for 5 minutes and incubated in block (10% Donkey serum, 1% BSA, PBS) for 45 minutes). Primary, secondary, and tertiary antibodies were diluted in block as follows: rat anti-MECA-32 (1:10; Developmental Studies Hybridoma bank), biotin-conjugated donkey anti-rat (1:200; Jackson ImmunoResearch), FluoroNanogold-streptavidin Alexa Fluor®* 488 (1:20; Nanoprobes). Cells were incubated with the primary antibody for 45 minutes, then washed 3 times with PBS, for 10 minutes each time. The same procedure was followed for the secondary and tertiary antibodies. Cells were fixed overnight with

2.5% glutaraldehyde and processed using HQ silver enhancement solutions (Nanoprobes) according to the manufacturer's instructures. Following enhancement, cells were processed for visualisation by wholemount TEM.

2.7.3 β-galactosidase staining of tissues

Embryos were dissected in ice-cold PBS, and fixed with a solution of 2% formaldehyde, 0.2% glutaraldehyde, in PBS (In Situ β-galactosidase staining kit, Stratagene). 10.5 and 11.5 day old embryos were fixed for 1 and 1.5 hours, respectively, at room temperature with gentle rocking. After 5 washes in PBS, embryos were stained in X-Gal solution (In Situ β -galactosidase staining kit, Stratagene) overnight, at 37°C. Embryos were washed 5 times in PBS, postfixed 1 hour at room temperature with 4% PFA, washed 3 times with PBS and mounted.

2.7.4 Light Microscopy

Images were captured using the following instruments and software packages:

1) LSM510 laser scanning confocal microscope (Zeiss); LSM 510 Software (Zeiss)

2) TCS SP2 spectral confocal microscope (Leica); Leica confocal software version 2.5

3) Widefield DMRA4 microscope (Leica); orca ER2 camera (Hamamatsu); Metamorph Software (Universal Imaging Corporation)

4) MZFL III Fluorescence Stereomicroscope (Leica); Retiga Camera (Q-Imaging); OpenLab 3.1.7 (Improvision, Inc.)

Digital images were processed using Adobe Photoshop 7.0 (Adobe Systems Inc.)

2.7.5 Electron Microscopy

2.7.5.1 Scanning Electron Microscopy (SEM)

Cells on coverslips were fixed in 2% PFA (EM grade; Electron Microscopy Sciences), 2.5% glutaraldehyde (Sigma), 0.1 M Sodium Cacodylate for 1 hour at room temperature, and maintained in 2% PFA, 0.1 M Sodium Cacodylate (pH 7.4) thereafter. When ready for processing they were washed twice in 0.1 M Sodium Cacodylate, and post-fixed in 1% Osmium tetroxide (Agar Scientific Ltd.) in cacodylate buffer. After two washes in distilled water, they were dehydrated through a series of ethanol solutions, 5 minutes in each: 50%, 60%, 70%, 80%, 90%, 100%, 100%. Drying was achieved by immersing in Hexamethyldisalazane (HMDS; Sigma) for 5 minutes, twice, and placing on Whatman paper.

Cells fixed after live cell labelling were postfixed with 1% aqueous Osmium tetroxide for 1 hour, washed once in water, and dehydrated through an ascending ethanol series, 5 minutes in each: 50%, 70%, 90%, 100%, 100%, 100%. Drying was achieved using HMDS as above.

Coverslips were mounted on 10 mm stubs (Agar Scientific Ltd.) using carbon adhesive mounts (Agar Scientific Ltd.) and silver dag (Agar Scientific Ltd.) was added to one edge. The specimens were coated with gold in a Polaron SC7640 High Resolution Sputter Coater, or carbon in a Gattan 681 Ion Beam Coater, and examined under a JEOL JSM-6700 Field Emmission Scanning EM.

2.7.5.2 Wholemount Transmission Electron Microscopy (TEM)

Formvar grids for wholemount TEM were prepared by coating 400 mesh nickel grids (Gilder; Electron Microscopy Sciences) using 0.5% Formvar (Ted Pella, Inc.) in

ethylene dichloride (Electron Microscopy Sciences). Grids were placed on coverslips, then carbon coated in a BAF 400 D High Vacuum Freeze-Etching System (Balzers) and UV-sterilised prior to their use in cell culture.

Cells were fixed in 1.25% glutaraldehyde (Electron Microscopy Sciences) and 2.5% PFA (Electron Microscopy Sciences) in 0.1 M Sodium Cacodylate buffer, for 1 hour at room temperature, or overnight at 4°C. Following three five-minute washes in 0.2 M sodium cacodylate, cells were postfixed in 1% Osmium tetroxide (Electron Microscopy Sciences) in cacodylate buffer for 30 minutes. After another 2 washes in 0.2 M sodium cacodylate, and 2 washes in distilled water, cells were dehydrated in an ascending ethanol series. This consisted of one five-minute incubation in 50%, 70% and 85%, ethanol, and two five-minute incubations in 95% and 100% ethanol. Coverslips were immersed in HMDS for 3 minutes and air-dried. Grids were examined under a JEOL 1010 TEM equipped with an AMT digital capture system.

2.7.5.3 TEM of thin sections

Intact monolayers, scraped monolayers, or cellular fractions from the silica isolation protocol were fixed in 2.5% glutaraldehyde, 2% PFA in 0.1 M Sodium Cacodylate buffer for 20 minutes, and stored in 2% PFA, 0.1 M Sodium Cacodylate buffer until processed. For silica-isolated material, agar tubes were prepared by dipping 5µl glass pipettes into agar (Electron Microscopy Sciences) pre-warmed to 65°C, and cooling them down over ice. Silica isolated fractions were placed into the agar tubes and sealed with warm agar. Scraped or intact monolayers, and tubes containing cellular fractions were washed with 0.2 M Sodium Cacodylate for 10 minutes and postfixed with 1% Osmium tetroxide in 0.1 M Sodium Cacodylate for 1 hour. After two 10-minute washes with 0.2 M Sodium Cacodylate, and one wash with distilled water,

specimens were dehydrated through an ascending acetone series of 50%, 70%, 85%, 95%, and 100%. Incubations lasted 7 minutes, while 95% and 100% acetone steps were performed twice. Specimens were infiltrated for 45 minutes with a mixture of 2 parts acetone and 1 part frozen spurs resin, and then for 60 minutes with a mixture of 1 part acetone and 2 parts frozen spurs resin. Finally, they were infiltrated with 100% fresh spurs resin overnight at room temperature. Resin was polymerised by incubating overnight at 60°C. 70-100 nm thick sections, cut using an Ultracut UCT (Leica), were placed onto 200 or 300 mesh copper grids (Gilder; Electron Microscopy Sciences). Grids were stained with uranyl acetate (Ted Pella, Inc.) for 20 minutes and Reynolds stain (made with Lead Nitrate, Ted Pella, Inc. and Sodium Citrate, Sigma) for 2 minutes prior to examination under the TEM.

2.7.5.4 Stereology for Electron Microscopy

20 to 30 SEM images were captured at a magnification of 10,000. Starting from an arbitrary position on the coverslip and systematically random sampling along one direction, an image was captured every 200 μm. Images in which cellular structures occupied less than 50% were dismissed. A grid (2 cm x 2 cm squares with 150 points of intsersection) was overlaid on each image, and the number of grid points falling on any cellular structure, versus the number of grid points falling on sieve plates (more than 10 fenestrae in a group), were counted. Fenestrae abundance was estimated as follows: fraction of plasma membrane covered with fenestrae =

$$\frac{\text{number of grid points falling on sieve plates}}{\text{number of grid points falling on any cell structure}}$$

To measure the density of fenestrae, the number of fenestrae per μm^2 among 10 random sieve plates was calculated; this multiplied by the fraction of plasma

membrane covered with fenestrae yielded an estimate of the density of fenestrae per μm^2 plasma membrane.

For fenestrae quantitation using wholemount TEM, images were captured at a magnification of 25,000. 12 images were obtained per nickel grid, and 3 nickel grids were examined per experiment. Images were opened in Adobe Photoshop 7.0, and a 15 mm grid with 169 points was overlaid on each image. The abundance of fenestrae was calculated as in the stereological approach for SEM.

2.8 Generation of transgenic mice

2.8.1 Construction of transgene cassettes for TetO-VE-PTP

The following steps were taken to generate the vector that would harbour the responder transgene cassettes:

1) plasmid pRL-null (Promega) was digested with NheI and NotI to remove the luciferase gene, blunted and religated to produce pSI1.
2) An XhoI/BamHI fragment of pSI1, containing a multiple cloning site, an artificial intron, and an SV40 late poly (A) signal, was cloned into XhoI/BamHI-digested pBluescript® II KS (Stratagene) to produce pSI2.
3) The operator sequences from pUHC 13-3 [176] were removed by an XhoI/SalI double digest and cloned into Xho/SalI-digested pSI2 to produce pSI3.
4) An oligo containing a series of rare restriction sites (GGGCCCGCGGCCGCTCTAGAGTTTAAACGGCGCGCCTTAATTAAA GATCTGTCGAC) was digested with Apa/SalI and cloned into ApaI/XhoI-digested pSI3 to produce pSI4.

Full-length VE-PTP was excised from pCMV6-XL4 (Genebank AF067196) using Not I, and cloned into the multiple cloning site of pSE420 (Invitrogen), in reverse orientation with respect to the vector's open reading frame. VE-PTP cDNA was released from the resulting vector by a BssHII digest, and cloned into MluI-digested pSI4, to yield pSI5, a plasmid harbouring the cDNA of VE-PTP under the control of the tetracycline response element.

To construct a plasmid with only the extracellular domain of VE-PTP expressed as a soluble protein under the control of the tetracycline response element, the following steps were taken: A 300 bp fragment from an AccI/XbaI digest of pFLAG-CMV-1-V-sol FN17 (provided by Dr. Urban Deutsch, Theodor Kocher Institute, Bern, Switzerland) was ligated to the 8 kb fragment from an AccI/XbaI digest of pCMV6-XL4 VE-PTP FN17Fc (provided by Dr. Urban Deutsch). The resulting plasmid was cut with PmlI and NheI, and the 3.2 kb fragment was ligated to the 5.5 kb fragment of pSI5, digested with PmlI and XbaI, to yield pSI9.

To construct a plasmid with the phosphatase trapping mutant of VE-PTP under the control of the tetracycline response element, pCMV-FLAG1 VE-PTP R/A [159] (provided by Dr. Urban Deutsch) was digested with NheI/Xba I and the resulting 1.3 kb fragment was ligated to the 9kb fragment of the NheI-digested pSI5 to yield pSI10.

2.8.2 Injection of TetO-VE-PTP transgenes into mouse oocytes

Transgenes TetO-VE-PTP, TetO-VE-PTP EC, and TetO-VE-PTP R/A were linearised by digesting 50 μg of the respective plasmids pSI5, pSI9, and pSI10, with BssHII. The 6-7 kb transgenes were separated from the vector on a 1% Agarose Gel in TBE without ethidium bromide. The marker lane and part of the lane containing the digestion products were cut and stained in a solution of 0.5 μg/ml Ethidium Bromide

in TBE for 30 minutes, to avoid exposure of the DNA to UV light. Using the position of the transgene in the stained gel as a landmark, the relevant portion of the unstained gel was excised and gel-purified. Eluates were ethanol precipitated and resuspended in EB buffer (10 mM TrisHCl pH 8.5). A further round of purification was achieved by diluting the DNA in 2.4 ml of 10 mM TrisHCl pH 8.0, 1 mM EDTA, adding 3.0 g of ultrapure CsCl, and ultracentrifuging in a SW50.1 rotor at 20°C for 48 hours at 40,000 rpm. Fractions containing the DNA were pooled and dialysed over 48 hours at 4°C, against a large volume of injection buffer. The solution was filtered through a 0.2 μm filter, and adjusted to a concentration of 1 ng/μl.

0.5 day old mouse embryos were collected from the oviducts of superovulated, mated C57BL/6 or (C57BL/6 x CBA) female mice. Using a glass holding pipette between 80 and 120 μm in diameter, 1-2 pl of the DNA solution was microinjected into the pronuclei of the one-cell embryos prior to the 1st division. Once microinjected, healthy eggs were transferred into the oviducts of 0.5 day pseudopregnant surrogate female mice. Approximately 20-30 microinjected eggs were transferred into each pseudopregnant recipient.

2.8.3 Breeding and maintenance of mouse colony

TetO-VE-PTP transgenic mice were maintained in C57BL/6 or mixed (C57BL/6 x CBA) background. Experimental crosses were performed using driver Tie-2tTA, and TetO-LacZ responder nZL2, TRE-LacZ 2717 strains, all provided by Dr. Urban Deutsch.

For timed-matings, the morning of vaginal plug formation was counted as 0.5 dpc. Tails were removed for genotyping pups and adult mice, and yolksacs were used to genotype embryos as described above.

Chapter 3: *In vitro* model for fenestrae formation

3.1 Background

Endothelial fenestrae were first described in 1950 [55], but their composition, function, and biogenesis remain mostly unknown. Their small size coupled to the lack of specific markers renders their study dependent on ultrastructural methods. *In vitro* studies which normally provide ease of manipulation and characterisation, have historically not been an option, as cells that have fenestrae *in vivo* become dedifferentiated and lose the fenestrated phenotype when placed in culture [87, 94]. As a result, the study of fenestrae has been restricted primarily to *in vivo* and *ex vivo* descriptive and morphological analyses, which not only are complex to conduct, but also provide limited information.

In the course of the past three decades, fenestrae have been observed in tissue culture, through attempts to create more physiological culture conditions for endothelial cells. The first observation of fenestrae in vitro came from cloned endothelial cells that mimicked the three-dimensional appearance of capillaries *in vivo*, when grown in tumor-conditioned medium [177]. Subsequently, low levels of fenestrae induction have been achieved by culturing endothelial cells on epithelial cell – secreted extracellular matrix [86, 87, 94] or treating them with Vascular Endothelial Growth factor (VEGF) [94], a potent permeability mediator implicated in fenestrae formation *in vivo* [69, 92]. Fenestrae formation has also been stimulated by factors of less evident physiological relevance such as phorbol myristate acetate (PMA) [88, 89], retinoic acid [90], and the microfilament disruption agents cytochalasin B and latrunculin A [61, 95, 96, 178]. The maximum number of fenestrae attained in cloned endothelial cells was between 0.05 and 0.2 fenestrae per μm^2 [86, 88-90, 94], which is orders of magnitude lower than what has been documented for fenestrated capillary beds *in vivo,* and insufficient for cell biological or biochemical studies. The greatest

numbers of fenestrae seen to date were in fenestrated primary liver sinusoid endothelial cells which could be made to expand their number of fenestrae by 2-3 fold [61, 95, 178]. Such cells, however, can only be maintained in culture for a few days, and attempts to immortalise them have failed to preserve fenestrae [179].

The limited scientific observations on fenestrae to date, have highlighted the need for a systematic approach to dissect and sequentially analyse these organelles. In a screen of numerous endothelial cell lines, using a combination of several published induction protocols, our laboratory identified an endothelial cell line that was susceptible to fenestrae induction in large quantities. My aim was to explore the optimal conditions for induction that would empower the molecular characterisation of fenestrae. This chapter describes the optimisation of this *in vitro* culture system for fenestrae biogenesis and the development of quantitative ultrastructural methods, with a focus on the modulation of the cytoskeleton.

3.2 Results

3.2.1 In vitro model for fenestrae formation

Following systematic screening through a panel of cloned endothelial cell lines cultured on a gelatin extracellular matrix and induced with PMA, VEGF-A, Cytochalasin B, and Latrunculin A, in various combinations or on their own, the bEND5 brain endothelioma cell line [180] was identified as competent for the formation of fenestrae. The presence of fenestrae was assessed using Scanning electron microscopy (SEM) (Figure 3.1), or wholemount Transmission Electron Microscopy (TEM) (Figure 3.2). Under basal conditions, no or very few fenestrae were observed on the plasma membrane of bEND5 cells (Figures 3.1, A and 3.2, A). After induction, the majority of the peripheral plasma membrane was perforated by numerous fenestrae that occured in sieve plates and were highly ordered: they displayed remarkably consistent pore diameters, linear arrangement and equidistant spacing (Figures 3.1, B, and 3.2, B-C).

To obtain a quantitative assessment of fenestrae numbers, a stereological approach was developed (Figure 3.3). The first step in this method involved the acquisition of SEM or TEM images by means of systematic random sampling. Next, all areas within each image were given the same opportunity to be sampled by randomly overlaying a grid lattice of about 150 points (intersection of gridlines). Counting the number of points falling on fenestrated areas of the plasma membrane (sieve plates), and dividing the value by the number of points falling on any area of the cell, gave an estimation of the fraction of plasma membrane that was fenestrated. Finally, to compare these numbers with measurements in previous *in vivo* or *in vitro* studies, the density of individual fenestrae within fenestrated areas was calculated by counting the

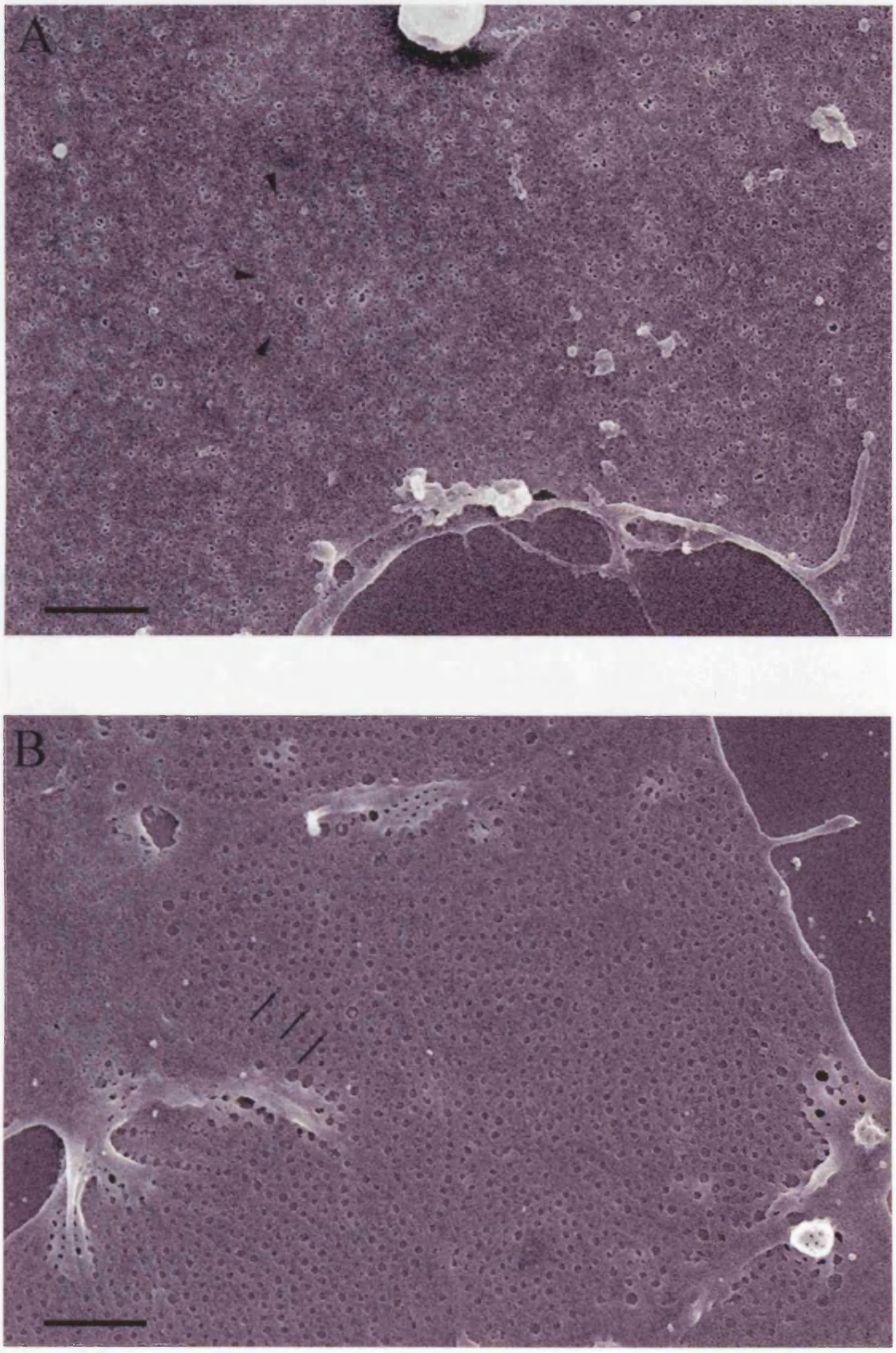

Figure 3.1 *In vitro* fenestrae under SEM. bEND5 cells untreated (A) or induced with 75 ng/ml VEGF for 24 hours and 10 μM Cytochalasin B for 2 hours (B). A large number of vesicles (arrowheads) are present on the continuous plasma membrane of untreated cells (A). The plasma membrane of induced cells is perforated by numerous fenestrae that appear as regularly arranged discontinuities with a diameter of 70 nm (arrows) (B). (Bar = 1 μm)

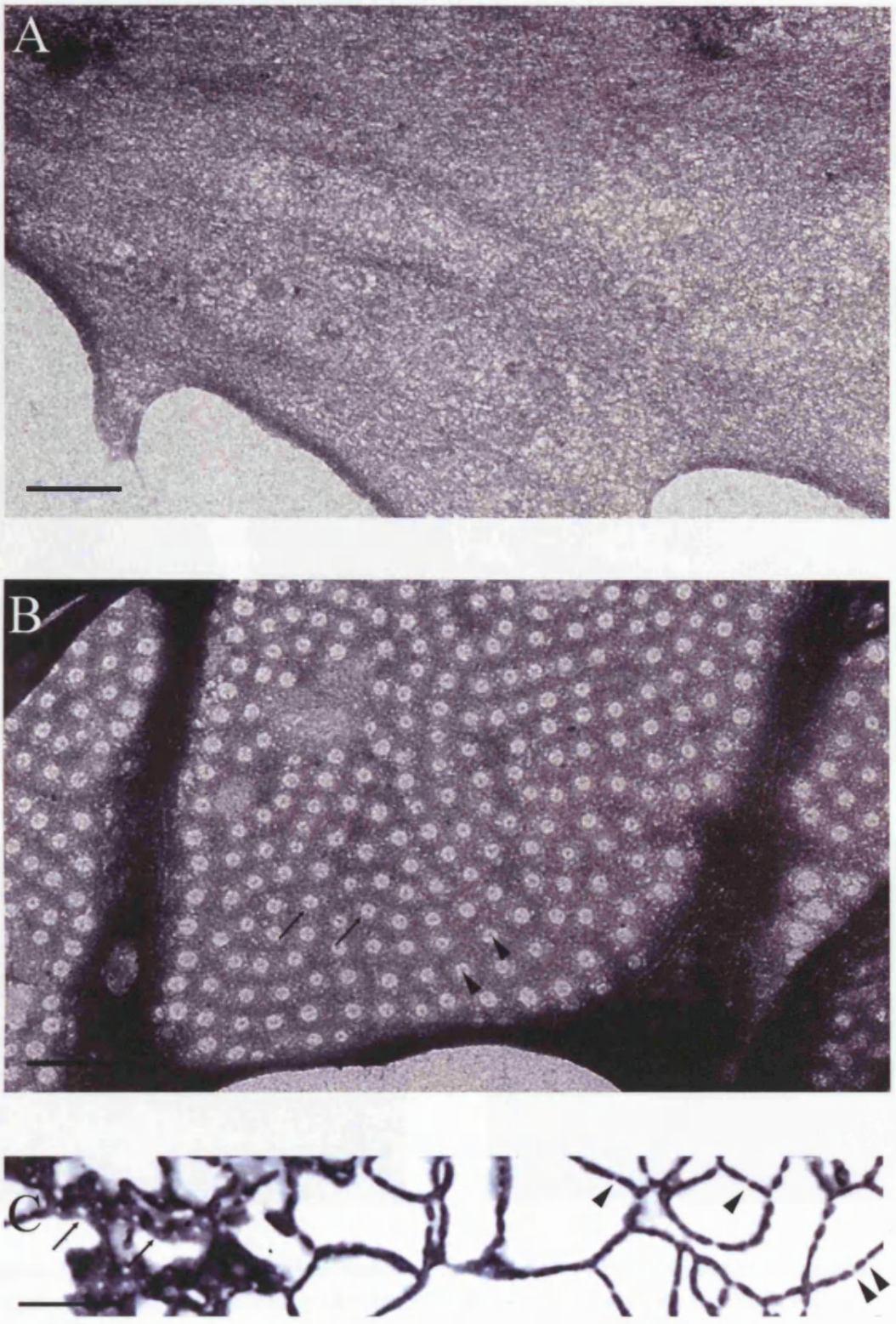

Figure 3.2 *In vitro* fenestrae under TEM. bEND5 cells untreated (A) and induced for 3 hours with 2.5 μM Latrunculin A (B) examined using the wholemount TEM method. A continuous plasma membrane in untreated cells (A) is replaced by numerous well-ordered fenestrae upon induction (B). A trace of the diaphragm spanning each fenestra (arrows) can be seen (arrowhead). Sections through induced cells, cut along the plane of the monolayer, and examined under TEM, reveal the abundance of fenestrae (C). Fenestrae can be seen 'en face' (arrows) and in cross-section (arrowheads). (Bar = 500 nm)

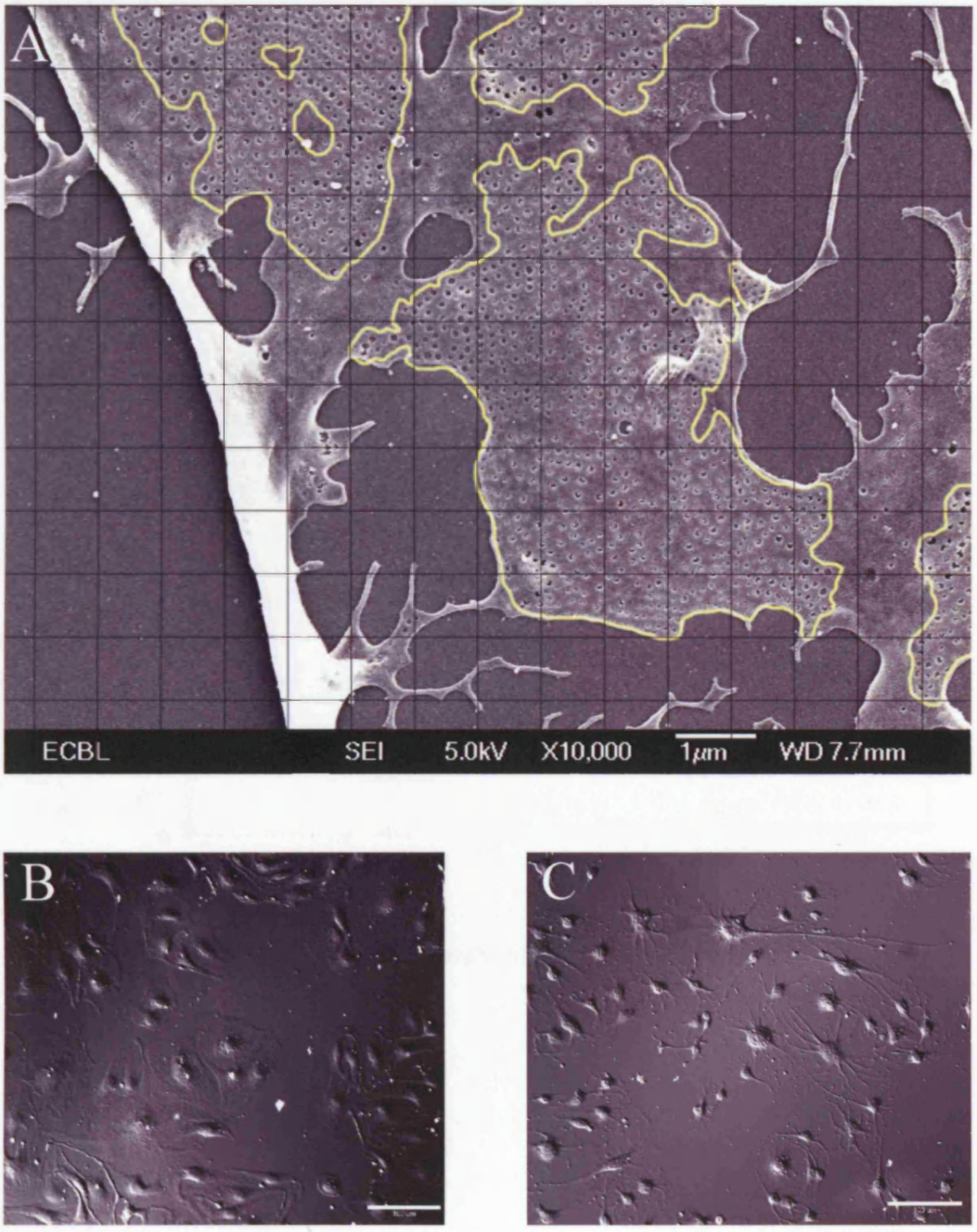

Figure 3.3 Stereology applied to fenestrae quantitation. (A) SEM images were acquired by systematic random sampling, then printed, and sieve plates were marked (yellow line). A grid lattice was randomly overlaid on each image and the number of grid points falling on sieve plates, versus those falling on any cellular structure, were counted. The abundance of fenestrae was estimated based on the following calculation: Fraction of the plasma membrane occupied by fenestrae = grid points falling on sieve plates / grid points falling on any cell area. The number of fenestrae per area of plasma membrane, was calculated as follows: no. of fenestrae per μm^2 of plasma membrane = no. of fenestrae per μm^2 of sieve plate area x fraction of plasma membrane occupied by sieve plates. (B, C) Differential interference contrast (DIC) images of bEND5 cells untreated (B), or induced with 2.5 μM Latrunculin A for 3 hours (C), reflect the cell density during random sampling for stereology. (Bar = 100 μm)

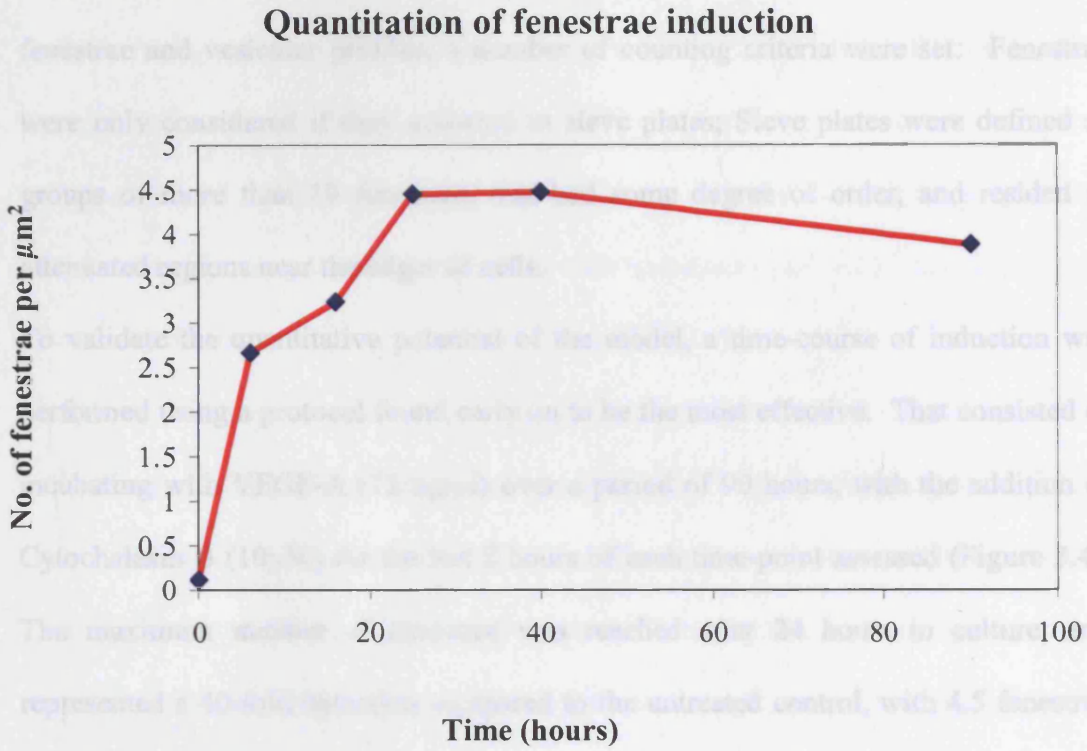

Figure 3.4 Quantitation of fenestrae induction. bEND5 cells were grown on gelatin and treated with VEGF (75 ng/ml) for 6, 16, 25, 40, or 90 hours, with the addition of Cytochalasin B (10 µM) for the last 2 hours of each time point. The number of fenestrae was assessed by SEM. Data points represent the average of 30 images captured per time point.

number of fenestrae occuring in an area of known dimensions, such as a square of the grid lattice that fell within a sieve plate. Multiplying the number of fenestrae per μm^2 of sieve plate area by the fraction of plasma membrane coverage, gave an estimation of the number of fenestrae per μm^2 of total cell plasma membrane. In order to minimise ambiguities in the quantitation, due to similarities between sparse single fenestrae and vesicular profiles, a number of counting criteria were set: Fenestrae were only considered if they occurred in sieve plates; Sieve plates were defined as groups of more than 10 fenestrae, that had some degree of order, and resided in attenuated regions near the edges of cells.

To validate the quantitative potential of the model, a time-course of induction was performed using a protocol found early on to be the most effective. That consisted of incubating with VEGF-A (75 ng/μl) over a period of 90 hours, with the addition of Cytochalasin B (10μM) for the last 2 hours of each time-point assessed (Figure 3.4). The maximum number of fenestrae was reached after 24 hours in culture, and represented a 40-fold induction compared to the untreated control, with 4.5 fenestrae per μm^2, analogous to hundreds or thousands of fenestrae per cell. A number of variations to the original protocol were attempted, including the omission of either VEGF-A or Cytochalasin B from the induction cocktail. Cells treated only with VEGF showed low induction over background, whereas cells treated only with Cytochalasin B for 2 hours attained similar induction levels to cells that had received the combined treatment (data not shown).

3.2.2 Identifying the optimal parameters for induction

3.2.2.1 The effect of cytoskeletal disruption

The dissection of the relative contributions of VEGF-A and Cytochalasin B in a

preliminary analysis of fenestrae formation prompted more in depth studies on the effect of cytoskeletal disruption in our system. Two separate actin filament disruption agents, Cytochalasin B (10 μM) and Latrunculin A (2.5 μM), were assessed in terms of their fenestrae-promoting potentials by SEM. Cytochalasin B belongs to a family of mold metabolites that inhibit the elongation of actin filaments by binding to their barbed, fast growing end with high affinity (Kd ~ 10^{-7}-10^{-8} M) [181, 182]. It is thought to prevent monomer addition without decreasing the concentration of polymerised actin [183]. Latrunculin A belongs to a family of marine sponge toxins which act by forming 1:1 complexes with actin monomers (Kd ~ 10^{-7} M), and thereby decreasing the concentration of actin filaments [184-186].

To isolate primary from secondary events in fenestrae formation, the focus was on the early events, using a short induction protocol (Figure 3.5). Both agents were able to stimulate induction on the order of 100-fold compared to the untreated control, attaining levels of 3.5 to 5 fenestrae per μm^2. Fenestrae started forming as early as after 20 or 30 minutes of treatment with Cytochalasin B, reached a maximum at 2 hours, and declined in number at 3 hours of treatment. Latrunculin A led to a higher maximum number of fenestrae after 3 hours of treatment when compared to Cytochalasin B. The initial slope of the induction curve resembled that of Cytochalasin B, however comparatively more fenestrae started to form with incubations over 30 minutes. Incubations longer than 3 hours didn't lead to any further increase in the number of fenestrae, but the viability of the cells was considerably reduced. As expected, given the biological variation inherent in the system, numbers of fenestrae were not reproduced exactly between different experiments (Figure 3.5). However, induction of fenestrae between treated and untreated cells was always statistically significant, and therefore, albeit not being absolute measurements, numbers of fenestrae per μm^2 are useful for comparative

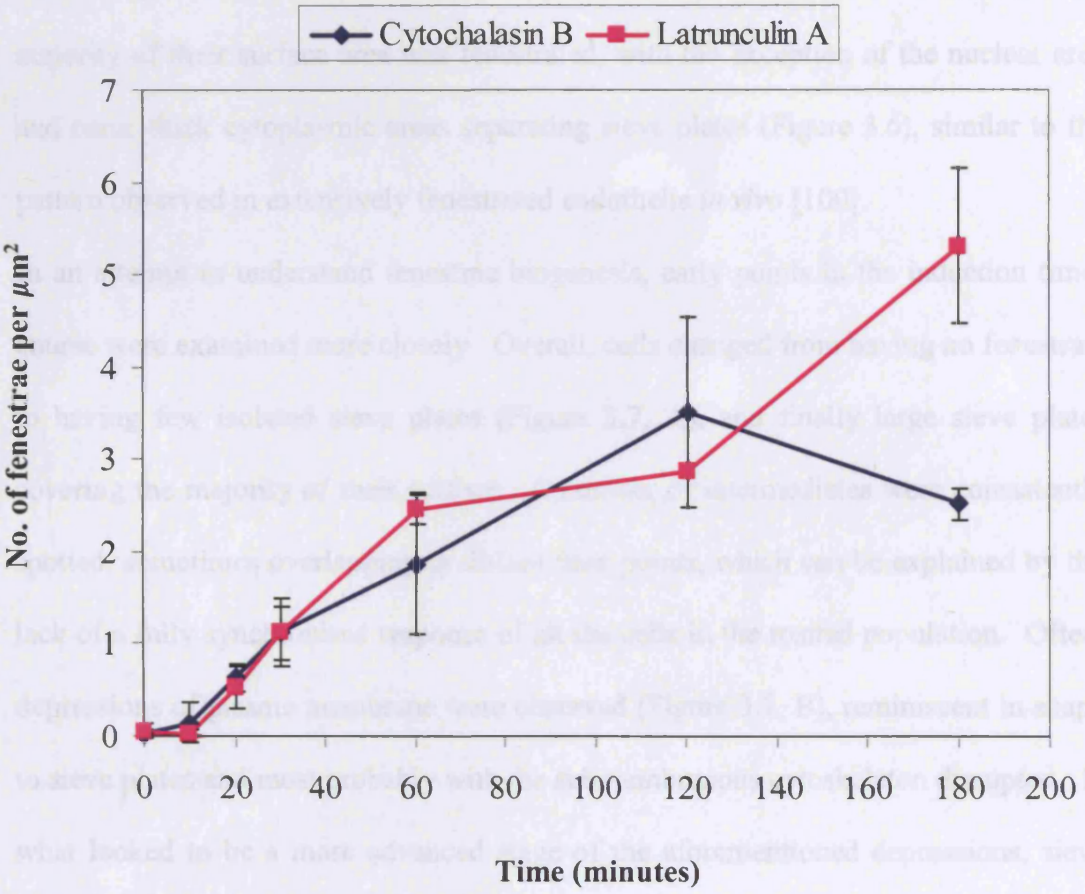

Figure 3.5 Short time course of fenestrae induction by microfilament disruption agents. bEND5 cells were grown on gelatin, treated with Cytochalasin B (10 μM) or Latrunculin A (2.5 μM) for a variety of time points, and the number of fenestrae quantified by SEM. Data points represent averages of two experiments, with 20 images taken per time point in each experiment. Error bars represent the standard deviation between the two experiments. For the 120 minute time point of the Latrunculin A treatment, data was available from only one experiment, therefore the standard deviation could not be calculated.

purposes.

Assessing the morphology of whole cells by SEM at a lower magnification suggested that Latrunculin A led to a more extreme phenotype. A greater proportion of the total cells in the population were responsive to Latrunculin A treatment than to Cytochalasin B, with over 80-90% of cells forming fenestrae. Within those, the majority of their surface area was fenestrated, with the exception of the nuclear area and some thick cytoplasmic areas separating sieve plates (Figure 3.6), similar to the pattern observed in extensively fenestrated endothelia *in vivo* [100].

In an attempt to understand fenestrae biogenesis, early points in the induction time-course were examined more closely. Overall, cells changed from having no fenestrae, to having few isolated sieve plates (Figure 3.7, A), and finally large sieve plates covering the majority of their surface. A number of intermediates were consistently spotted, sometimes overlapping in distant time points, which can be explained by the lack of a fully synchronised response of all the cells in the treated population. Often, depressions of plasma membrane were observed (Figure 3.7, B), reminiscent in shape to sieve plates and most probably with the submembranous cytoskeleton disrupted. In what looked to be a more advanced stage of the aforementioned depressions, sieve plates with fenestrae-like structures that did not span the cytoplasm of the cell were identified (Figure 3.7, C). Finally, fenestrae were often observed near unidentified membrane invaginations (Figure 3.7, D). Whether this close geographical proximity was due to a causal relationship between those structures and fenestrae, or was merely a chance event, was difficult to interpret.

3.2.2.2 The effect of endothelial cell subtypes

Following the identification of Latrunculin A as the most efficient inducer of

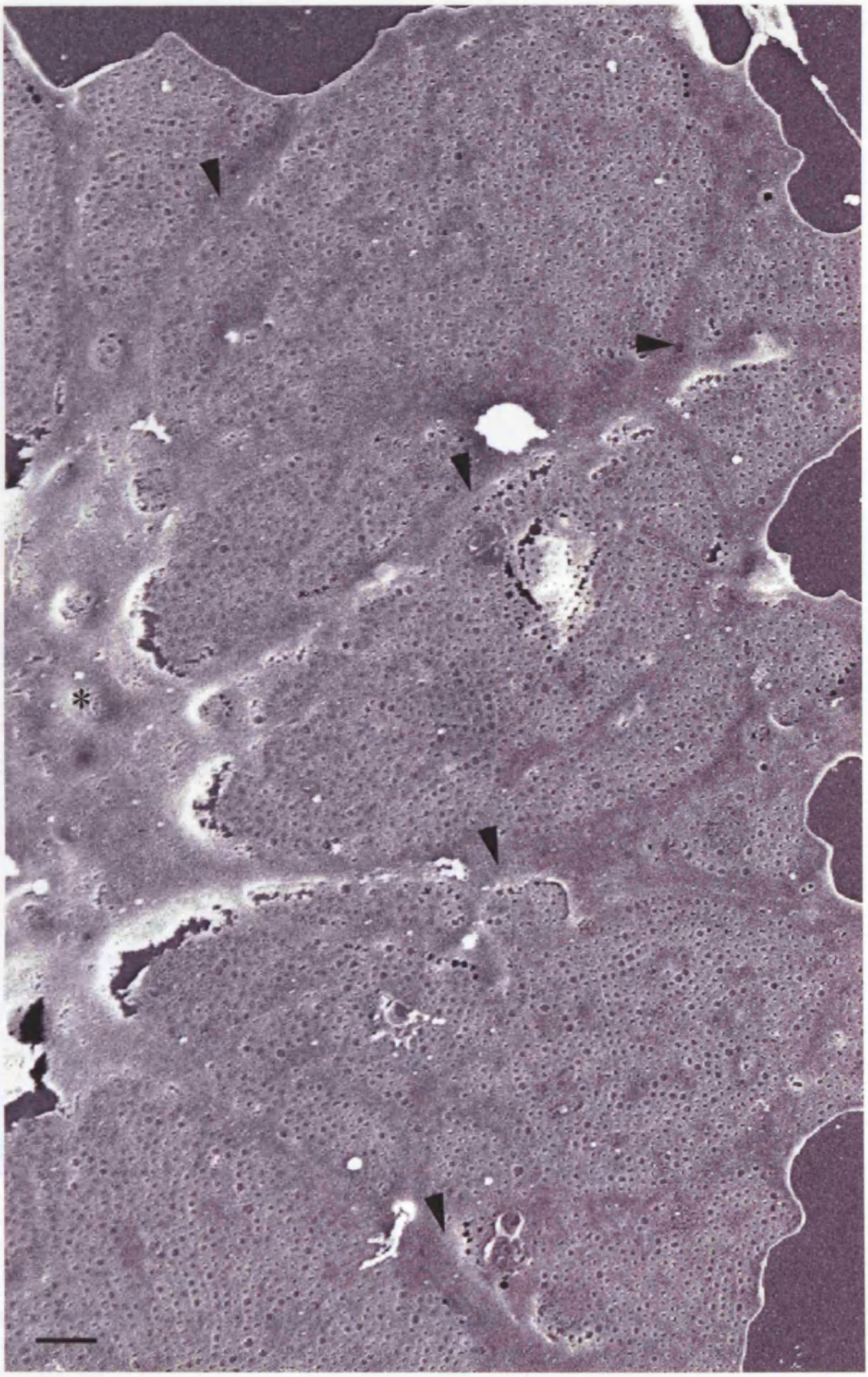

Figure 3.6 Fenestrae under low power SEM. The entire plasma membrane of a bEND5 cell induced with 2.5 μM Latrunculin A for 3 hours is fenestrated, apart from the nucleus (star) and cytoplasmic spacers (arrowheads) between sieve plates. (Bar = 1 μm)

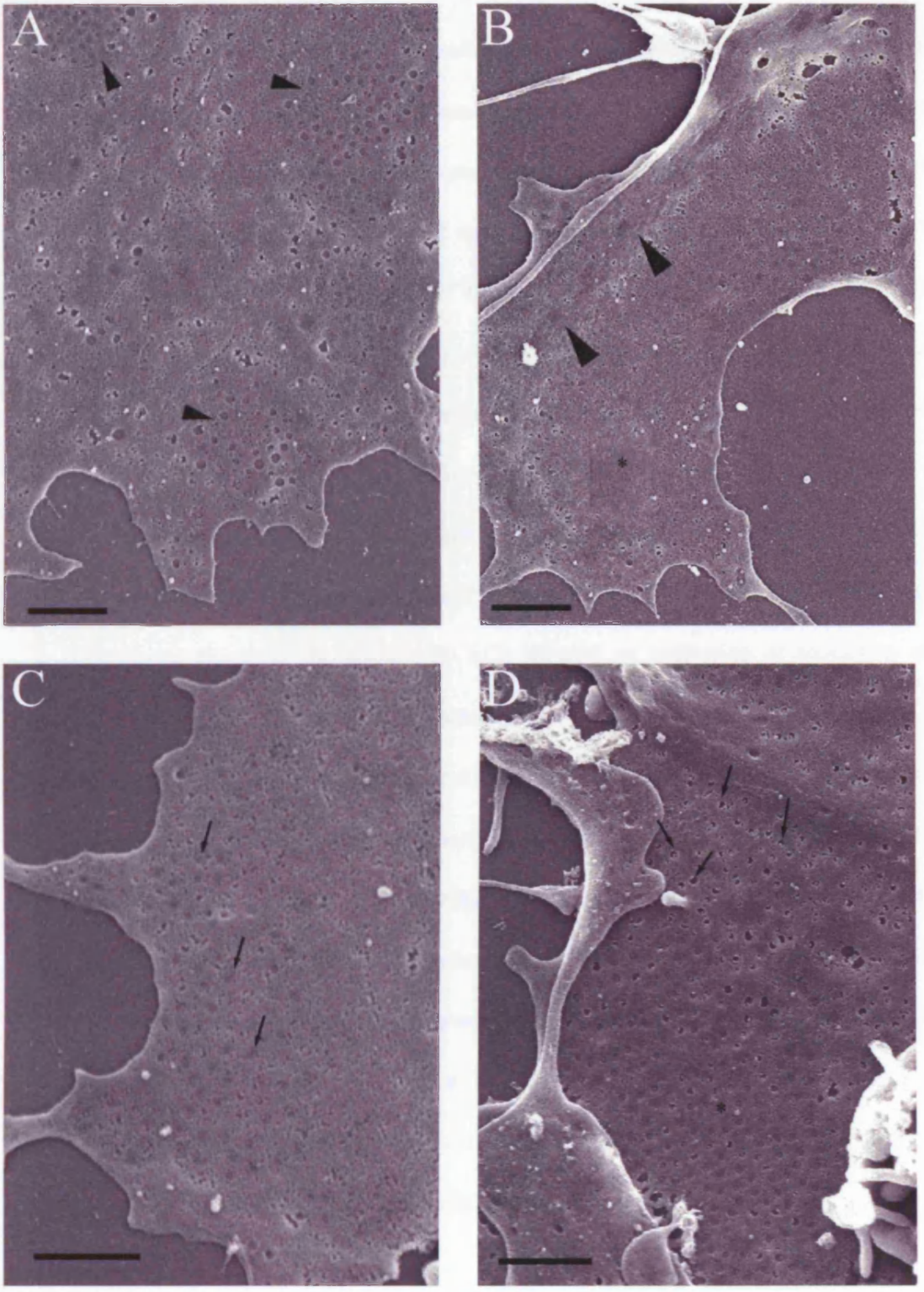

Figure 3.7 Intermediates observed by SEM in early time points of a time-course of fenestrae induction with 2.5 μM Latrunculin A: Small sieve plates (arrowheads) (A), depressions of large patches of the plasma membrane (star) adjacent to thick areas of the cell (arrowheads) (B), fenestrae with apparent incomplete perforation (arrows) (C), diaphragmed vesicles (arrows) clustered near flat fenestrated areas (star) (D). (Bar = 1 μm)

fenestrae, a panel of endothelial cell subtypes was revisited and assessed for their fenestrae-forming potentials under optimal conditions. Three mouse endothelial lines (bEND5, Py4.1, SVEC4-10) and one human primary endothelial line (HUVEC) were cultured on gelatin-coated grids, treated with Latrunculin A for 3 hours, and examined by wholemount TEM (Figure 3.8). bEND5 [180] and Py4.1 [187] cells are endotheliomas, originating from Polyoma middle T transformed brain endothelial cultures and Polyoma middle T transgenic mice, respectively. SVECs are lymph node endothelial cells infected with SV40 virus [188]. HUVECs were selected because of their widespread use as a primary cell strain. Quantitation of the response in each cell line showed that only Polyoma middle T – containing bEND5 and Py4.1 cells were susceptible to fenestrae formation. SVECs showed no indication of fenestrae, and HUVECs produced only very few (Figure 3.9).

Interestingly the response of bEND5 and Py4.1 cells differed both in the magnitude of induction, and in the levels of fenestrae observed in the uninduced state. bEND5 cells harboured greater numbers of fenestrae overall, but contained some background fenestrae even in the absence of induction. Py4.1 cells formed lower absolute numbers of fenestrae, but showed a greater relative induction than bEND5 cells, due to the complete absence of fenestrae in the uninduced state. Py4.1 cells were subsequently found to be also responsive to Cytochalasin B, albeit inconsistently and to a much lower extent than bEND5 cells (data not shown).

3.2.3 Actin microfilaments under the light microscope

In parallel to the SEM analysis, bEND5 cells subjected to Cytochalasin B and Latrunculin A time-courses were stained with fluorescently-labeled phalloidin to determine the state of actin microfilaments (Figures 3.10 and 3.11). Untreated cells

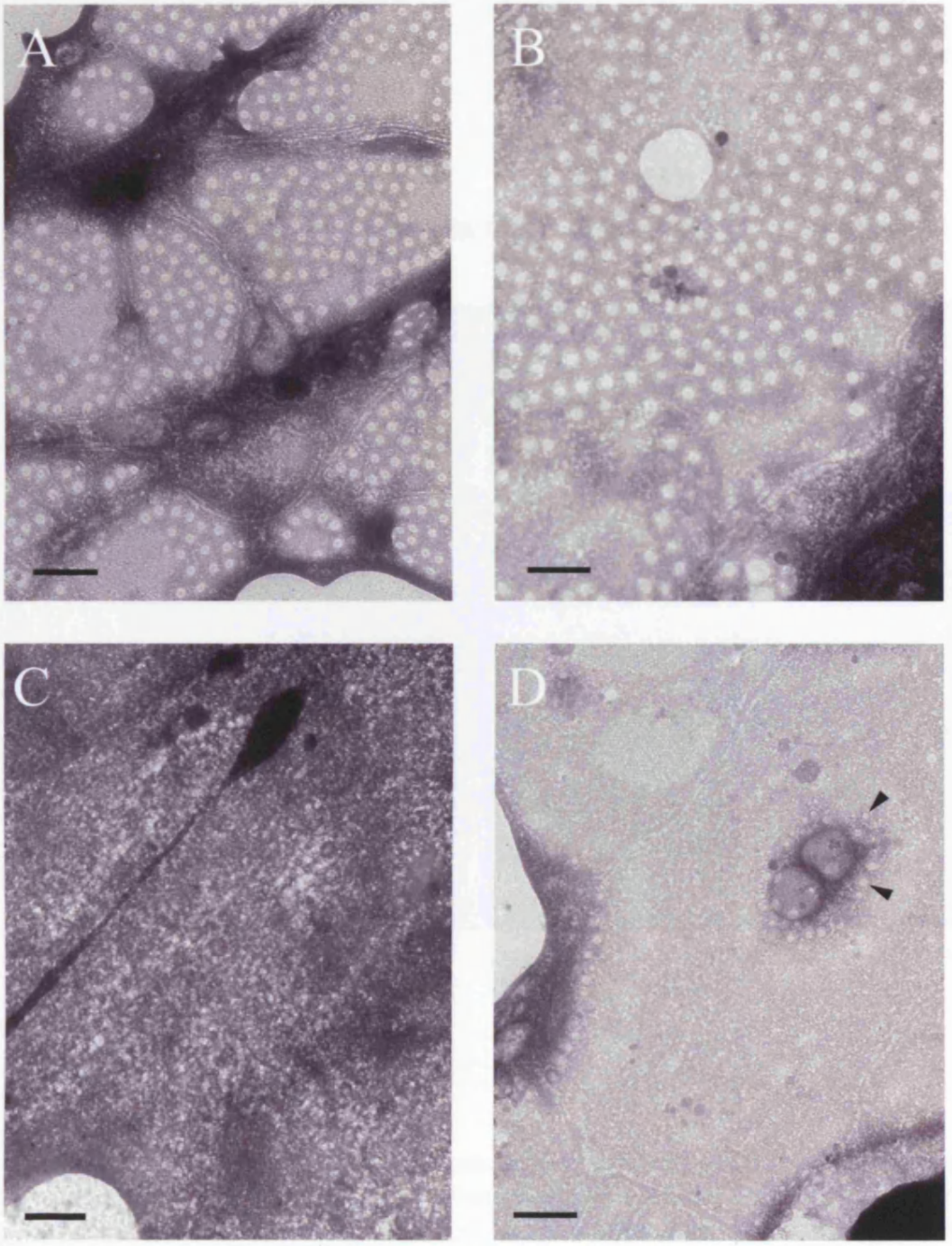

Figure 3.8 Comparison of fenestrae formation in different endothelial cell subtypes using wholemount TEM. bEND5, Py4.1, SVE and HUVE cells were treated with 2.5 μM Latrunculin A for 3 hours. Abundant fenestrae are present in bEND5 (A) and Py4.1 (B) treated cells. No fenestrae are present in SVE cells (C), while rare fenestrae (arrowheads) are detected in HUVECs (D). (Bar = 1μm)

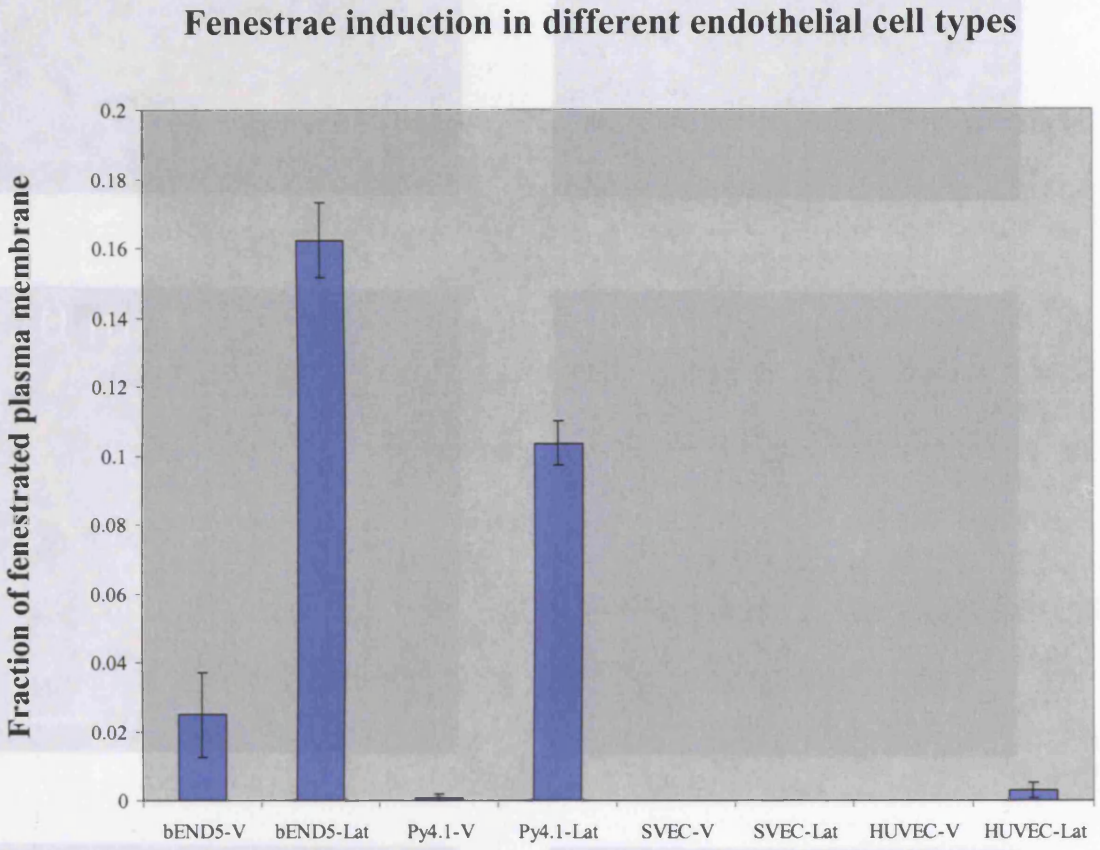

Figure 3.9 Quantitation of fenestrae induction in different endothelial cell subtypes. bEND5, Py4.1, SVE, and HUVE cells were treated for 3 hours with vehicle (V) or 2.5 μM Latrunculin A (Lat), and assessed using wholemount TEM. The number of fenestrae was estimated as a fraction of the plasma membrane area occupied by sieve plates. HUVECs were only treated for 2.5 hours as they displayed reduced viability with prolonged exposure. Data points represent the average of two experiments, with 36 images captured per sample in each experiment. Error bars represent standard deviation between the two experiments.

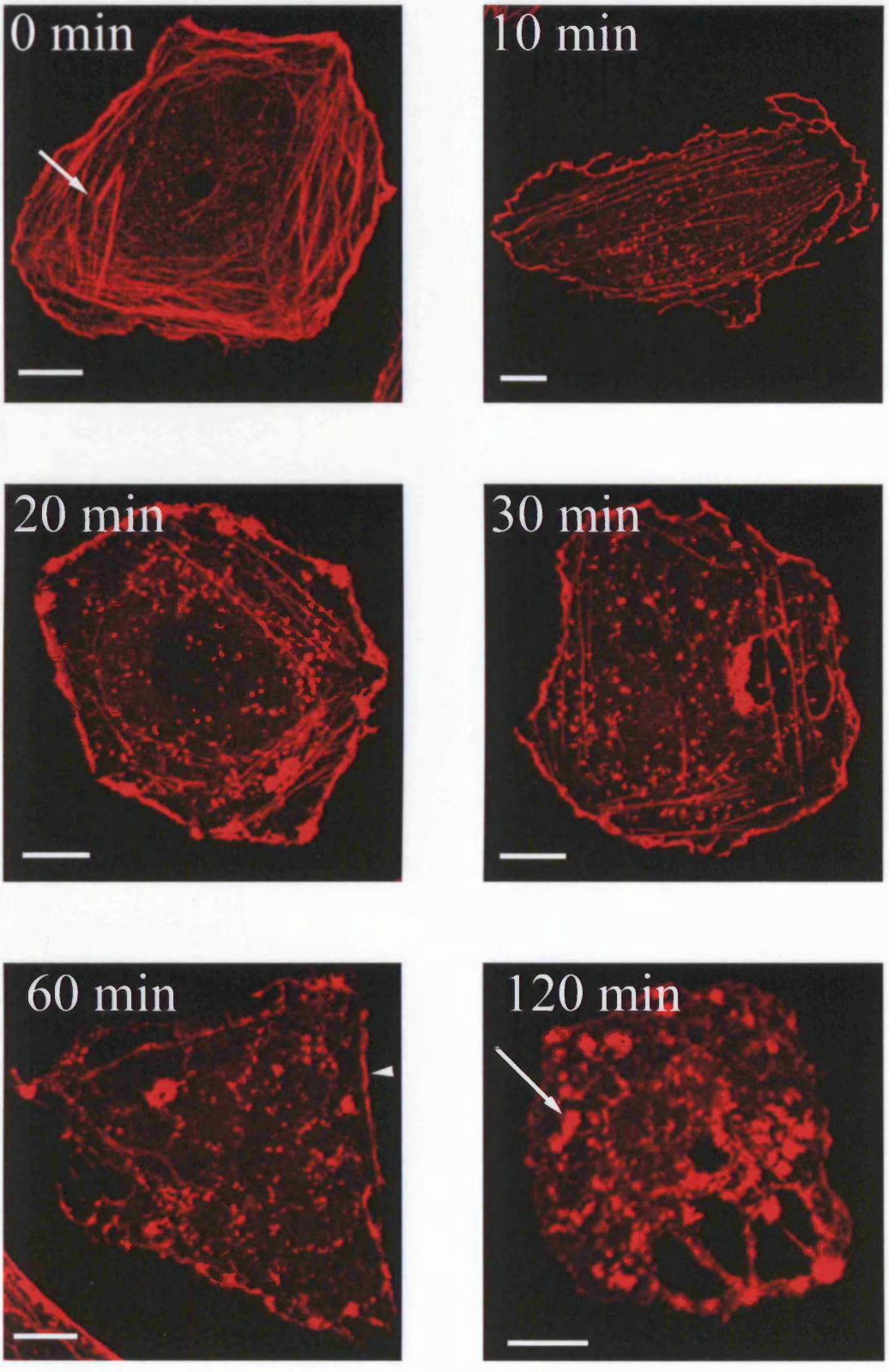

Figure 3.10 Actin microfilaments in bEND5 cells treated with 10 μM Cytochalasin B. Cells were fixed after different times of treatment and actin microfilaments were visualised using Alexa546-conjugated phalloidin. Confocal sections at the level of stress fibers (short arrow) revealed a reduction in stress fiber content within the first 20 minutes, and a persistence of cortical actin (arrowhead) until about 60 minutes of treatment. At 120 minutes, individual actin bundles (long arrow) were spread around the cytoplasm. (Bar = 8 μm)

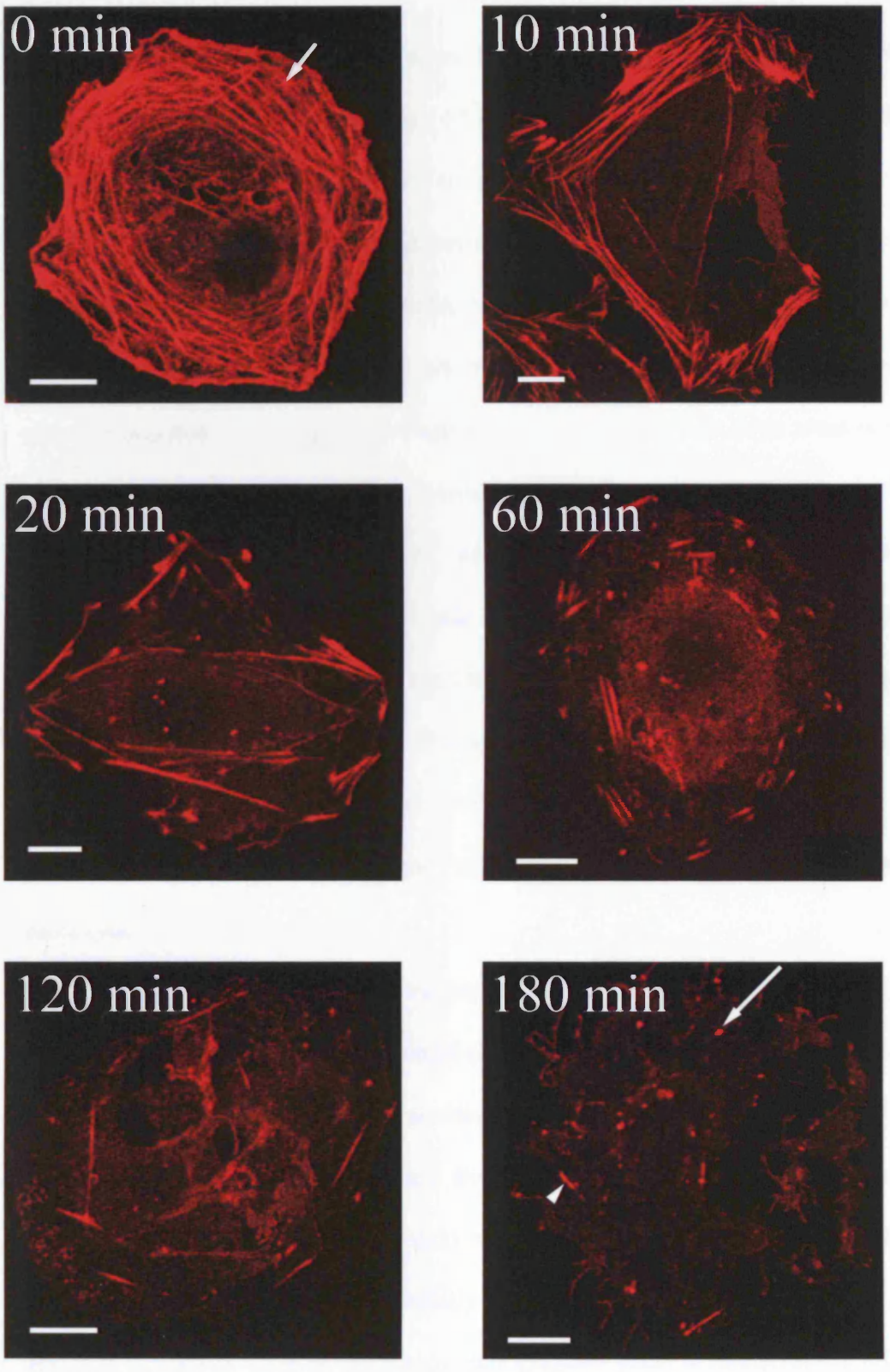

Figure 3.11 Actin microfilaments in bEND5 cells treated with 2.5 μM Latrunculin A. Cells were fixed after different times of treatment, and actin microfilaments were visualised using Alexa 546-conjugated phalloidin. Confocal sections at the level of stress fibers (short arrow) revealed a reduction in stress fiber content within the first 20 minutes, with complete disruption of the network at 60-120 minutes. Individual actin foci (long arrow) and small filaments (arrowhead), were present after 120-180 minutes of treatment. (Bar = 8 μm)

contained an extensive network of stress fibers spanning their cytoplasm. However, dramatic changes in the organisation of filamentous actin were observed within as early as 10 minutes of treatment with either agent. Cells treated with Cytochalasin B (Figure 3.10) exhibited a gradual decrease in the amount of stress fibers between the time points of 10, 20, and 30 minutes, with cortical actin remaining in place until about 60 minutes of treatment. At 120 minutes, the disassembled filamentous actin was concentrated in aggregates throughout the cytoplasm, while large areas remained microfilament-deficient. In cells treated with Latrunculin A (Figure 3.11) the disruption of stress fibers was faster, and the cortical cytoskeleton was dismantled within the first 20 minutes. Overall cells had more and larger microfilament-depleted areas, and the majority of actin remnants appeared irregularly arranged in short filaments within the cytoplasm. The appearance of microfilament-depleted areas under light microscopy, correlated well with the emergence of fenestrae under scanning electron microscopy, and suggested a relationship between the two processes.

In an attempt to explain the differential induction of endothelial cell subtypes by Latrunculin A, the actin cytoskeleton of all four cell types was stained with phalloidin (Figure 3.12). In all cases, the cytoskeleton was highly disrupted, confirming the non-discriminatory effect of the drug, and showing that actin microfilament disassembly alone is not sufficient for fenestrae induction. Close observation, however, of bEND5 and Py4.1 cells, highlighted a potentially significant difference: the latter had greater amounts of cortical actin in the steady state (Figures 3.12, A and 3.12, C). Notably, this correlated with their decreased susceptibility to fenestrae formation compared to bEND5 cells, a discrepancy particularly apparent during induction with Cytochalasin B, the less potent of the two cytoskeletal disruption agents.

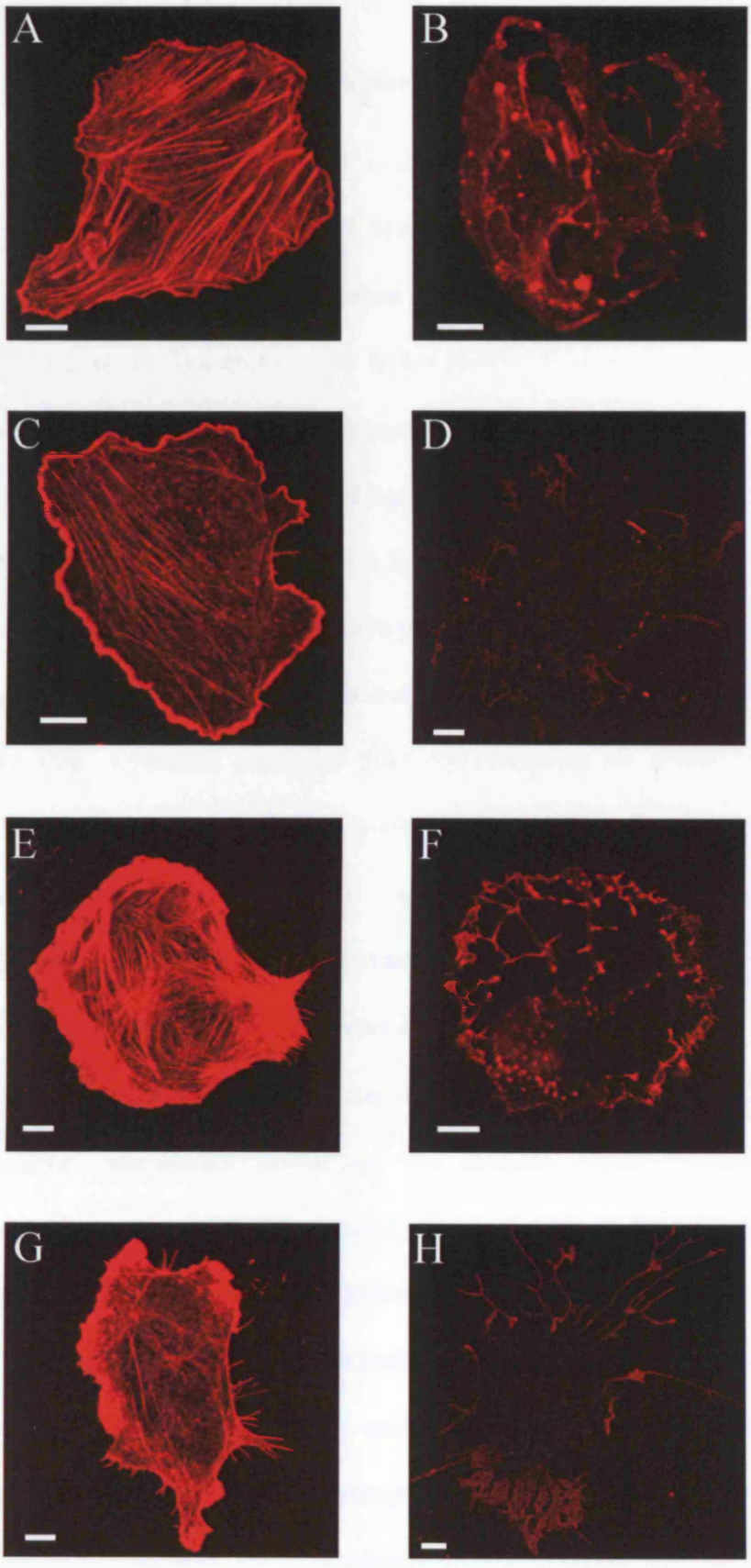

Figure 3.12 Actin microfilaments in different endothelial cell subtypes. bEND5 (A, B), Py4.1 (C, D), SVE (E, F), and HUVE (G, H) cells were untreated (A,C,E,G) or induced for 3 hours with 2.5 μM Latrunculin A (B,D,F,H). Epifluorescent images of Alexa 546-conjugated phalloidin, showed microfilament disruption in all treated cell types. (Bar = 8 μm)

3.2.4 Immunolabelling for the diaphragm marker PV-1

Fenestrae induced in bEND5 or Py4.1 cells appeared morphologically similar to fenestrae described *in vivo*. Observed under high power, they had a consistent circular diameter of about 70 nm and were usually spanned by a diaphragm. One feature of diaphragmed fenestrae *in vivo* is the protein PV-1, a shared component of the diaphragms of fenestrae and caveolae, and the only known constituent of fenestrae to date [16, 54]. Immunogold labelling using an antibody against PV-1 was performed on bEND5 cells induced for 3 hours with 2.5 μM Latrunculin A. PV-1 labelling was found to concentrate on sieve plates, and specifically on the diaphragms of fenestrae (Figure 3.13, A, C-D). In contrast, immunogold labelling for Platelet Endothelial Cell Adhesion Molecule (PECAM) showed no preference for any particular region of the cell, and was distributed in fenestrated and non-fenestrated areas alike (Figure 3.13, B). The poor morphology of the imaged cells reflected a compromise reached to satisfy the distinct and conflicting requirements of cell immunolabelling and ultrastructural preservation.

Previous studies had described fenestrated endothelia as extremely attenuated cells, with a central prominence containing the nucleus [100]. Microtubule-rich cytoplasmic areas were seen to extend from the nuclear area to the cell periphery, and between them encircle fenestrae sieve plates [61]. Given the extreme attenuation of the endothelium, the existence of intracellular organelles in areas other than the central prominence was deemed highly unlikely. These observations coupled to the immunoreactivity for PV-1 within diaphragmed fenestrae, formed the basis of a light microscopy assay, developed by K. Deinhardt in the laboratory (see Appendix I). By indirect immunofluorescence, she showed that in induced cells, PV-1-positive areas could be readily distinguished from the remainder of the cell, as they were negative

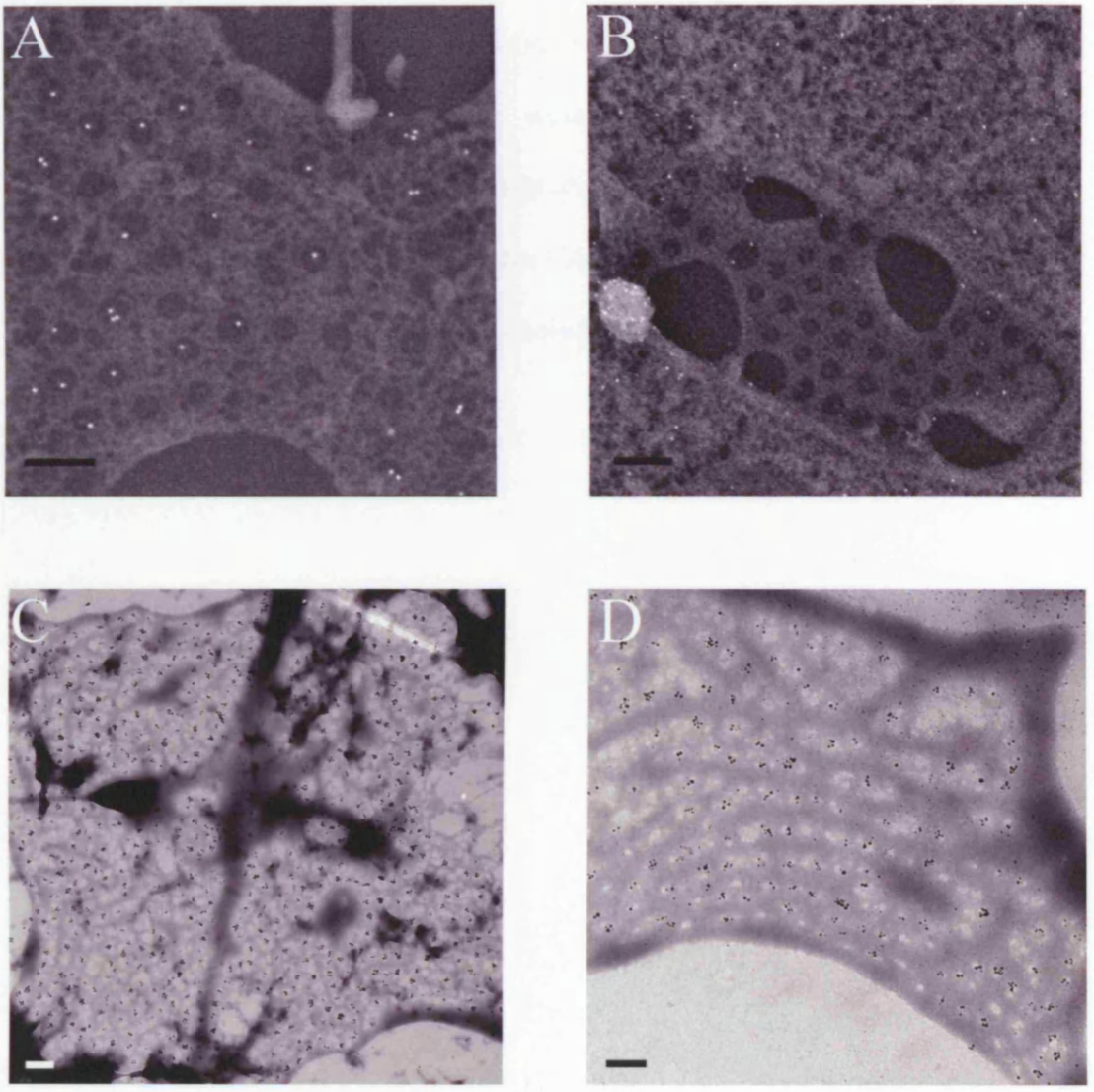

Figure 3.13 SEM and wholemount TEM Immunolabelling. bEND5 cells, induced with 2.5 μM Latrunculin A for 3 hours, were labeled for PV-1(A) and PECAM (B), and visualised using 10 nm and 5 nm gold conjugated secondary antibodies, respectively, under SEM backscatter mode. PV-1 is seen to localise specifically on the diaphragm of fenestrae (A), while PECAM is distributed throughout the surface of the cell (B). Latrunculin-induced bEND5 cells were labeled for PV-1 and visualised using a fluoronanogold-conjugated secondary antibody by means of wholemount TEM (C,D). A low magnification view shows labelling concentrated in fenestrae sieve plates (C) and a high magnification view shows multiple gold particles within the region of the fenestral diaphragm (D). (Bar = 200 nm)

for any organelle or cytoskeletal marker. Moreover, microtubules and organelles were confined to areas between PV-1-positive areas, while PECAM was present throughout the plasma membrane, consistent with ultrastructural observations. The observations from light microscopy were further validated by a correlative microscopy study (Amy Snodgrass, unpublished observations), whereby the same PV-1 positive fenestrae patches imaged under the light microscope could be identified as fenestrae sieve plates with nanogold-labeled diaphragms using wholemount TEM.

3.3 Discussion

3.3.1 A versatile model to study fenestrae biogenesis

Traditionally, cell biologists have used experimental model systems to further their understanding of organelles. Ultrastructural observations on alterations to the golgi apparatus during mitosis laid the foundations for establishing an *in vitro* model of golgi disassembly and reassembly in Hela cells [189, 190]. Initial morphological observations within the model were strengthened by thorough quantitative analyses and immunoelectron microscopy studies that validated a marker for mitotic golgi membranes. This gave rise to the successful isolation of golgi membranes, which coupled to the ability to mimic the processes of disassembly and reassembly in a cell-free assay, paved the way for the identification of membrane intermediates and important components in the pathway.

Akin to understanding other membranous organelles, my approach on the study of fenestrae was centered on establishing a model system that would mimic, as closely as possible, the situation observed in capillary beds *in vivo*. By means of combining different endothelial cell types and induction stimuli, an *in vitro* culture system for fenestrae formation was developed, conferring a number of advantages over previous approaches: 1) Fenestrae were formed in an endothelial cell line that could be maintained for tens of passages; 2) The induction protocol was fast and easy; 3) A relatively high-throughput stereological approach could be applied to its ultrastructural characterisation; 4) High levels of fenestrae were sustained; 5) A great induction over the uninduced state of the cell was achieved; 6) In combination with immunoreactivity for PV-1, it could be used as a light microscopy assay for fenestrae formation.

In the most efficient combination, that of bEND5 cells treated with Latrunculin A, fenestrae were induced 100-fold at levels of up to 5.3 fenestrae per μm^2. This favorably compared to previous reports of *in vitro* studies where adrenal cortex endothelial cells or HUVECs, induced with VEGF, phorbol esters, or retinoic acid, attained maximal levels of only 0.187 fenestrae per μm^2 [86, 88-90, 94]. Studies using primary liver endothelial cells with existing fenestrae and the cytoskeleton disruption agent swinholide A had reported fenestrae levels of up to 9.1 per μm^2, however, this represented a less than 3-fold induction, as the untreated control contained over 3 fenestrae per μm^2 [96]. Moreover, this enhancement of a phenotype was only possible in freshly-isolated endothelial cells from the liver sinusoids as attempts to immortalise them rendered them no longer susceptible to fenestrae formation [179]. Comparisons to the numbers of fenestrae observed *in vivo* are more complicated, as reported levels of fenestrae vary between as low as 0.58 per μm^2 [191] and as high as 60 per μm^2 [100], depending on the capillary bed investigated and even more on the methods of detection and quantitation employed.

3.3.2 Actin remodeling as a driving force for fenestrae formation

The role for actin remodeling in sustaining or increasing the number of fenestrae had been highlighted in studies involving fenestrated endothelial cells from the liver sinusoids [61, 95, 96, 178] and isolated kidney glomeruli [192], and was exploited in our system for the formation of *de novo* fenestrae. The most widely used drugs, Cytochalasin B and Latrunculin A, both target the actin cytoskeleton, but achieve disruption through different mechanisms. In agreement with the studies on liver sinusoidal endothelial cells [95], Latrunculin A was more potent at inducing fenestrae than Cytochalasin B. As previously suggested [95], the fact that two drugs with

different mechanisms of action, both led to the induction of fenestrae, supports the notion of fenestrae formation being linked to microfilament disassembly and not some secondary effect of the drug. Moreover, in our culture model, the different extent to which microfilament disassembly was achieved with either agent, correlated with the magnitude of the response in terms of fenestrae formation: treatment with latrunculin A resulted in greater disruption and also in more fenestrae.

The kinetics of fenestrae induction through cytoskeleton disruption were rapid, with fenestrae being visible within the first 20 minutes of treatment. The rapid fenestrae formation suggested that in this particular system, protein synthesis is unlikely to play a role. The components required for fenestrae formation most likely are already present in the cell and merely rearranged to form pores. The increase in fenestrae formation observed over time can be explained by a progression in the levels of actin disruption, resulting in the enlargement of small fenestrae patches within given cells and in a greater number of cells responding within the population. Further support for the notion that certain tissue endothelia are equipped for rapid fenestrae formation comes from *in vivo* studies showing that VEGF can induce fenestrations in certain normally non-fenestrated anatomical sites, within 10 minutes of topical application or intradermal injection [69].

The mechanism by which actin remodeling drives fenestrae formation is unclear. One hypothesis to explain our observations is consistent with the view of actin as a structural barrier for fusion. According to such a model, disruption of the cytoskeleton would be required to bring the apical and basal plasma membranes of the cell in close proximity to one another so as to allow the necessary steps of membrane fusion to take place. Actin removal has been implicated in exocytosis and yeast vacuole membrane fusion from *in vitro* studies showing that persistence of an actin coat surrounding the organelle in question acts as a physical impediment for the

recruitment of tethering factors and in turn for the close apposition of membranes [102, 193-196]. However, high concentrations of actin depolymerising agents have been shown to inhibit all phases of exocytosis [194, 195], while actin remodeling in yeast has been divided into an actin depolymerisation phase during docking, followed by a repolymerisation phase at the terminal stage of membrane fusion [193]. To explain the latter, actin has been postulated to contribute to the trafficking and aggregation of organelles and to coordinate the spatial restriction of particular fusogenic proteins to fusion sites [103, 193, 197, 198]. Whether the cytoskeleton is not just a physical barrier but also plays an active role in the process of fenestrae formation, remains to be established.

3.3.3 The role of signaling cascades

VEGF and PMA were less efficient than cytoskeleton disruption agents in fenestrae induction. Moreover, a comparison of different growth factors of the VEGF family, along with fibroblast growth factor (FGF), showed significant, though low fenestrae induction compared to the untreated control, with a trend towards FGF being the most potent inducer (data not shown). The observation that VEGF, a mediator of fenestrae formation *in vivo* [69, 92] and *in vitro* [94], was modestly effective in our system is interesting. A potential explanation for the lack of a response to VEGF, is the view of endothelioma cells producing their own complement of the growth factor [199] and thus being self-sufficient and saturated. Alternatively, a component in the VEGF signaling pathway downstream of the VEGF receptor could be activated in these cells, obviating the need for an exogenous growth factor.

A connection between the physiological inducer of fenestrae and the cytoskeleton has been suggested in a recent study which showed that a dominant negative version of

the small GTP-binding protein Rac could block VEGF-induced fenestrae formation in a corneal pocket angiogenesis assay [97]. Although direct evidence was absent, this was interpreted as a consequence of preventing the reorganisation of the cytoskeleton [97]. Futhermore, studies conducted in our laboratory established that the observed VEGF-driven induction of fenestrae could be abolished by pretreatment of cells with the actin filament stabilizing drug phalloidin (K.Deinhardt, unpublished observation).

3.3.4 Cellular predisposition guides fenestrae formation

Actin remodeling appears to be necessary for fenestrae formation, however it is not sufficient. Only a subpopulation of endothelial cells tested was able to respond to Latrunculin A by forming fenestrae, although microfilaments were disrupted in all cases. Thus, it would seem prudent to search for common features among induction competent endothelial cells.

One possible feature is the existence of a primed cytoskeleton in the responding cell lines. Interestingly, this notion is supported by evidence that jasplakinolide, a marine sponge peptide that induces actin polymerisation in a variety of cell types [200-203], resulted in actin disruption and fenestrae formation in bEND5 cells (data not shown), an effect previously observed only in liver sinusoid endothelial cells [96].

Another common feature could be related to the origins of the responding cell lines, as both bEND5 and Py4.1 cells, were derived through transformation with polyoma virus [180, 187]. Polyoma middle T antigen has been shown to associate with cellular membranes [204] and target a variety of cellular effectors including *src* tyrosine kinases (reviewed in [205]). Pathways downstream of activated tyrosine kinases may account for some of the resulting susceptibility through intersecting with the cytoskeleton. The importance of oncogene specificity in the response is underlined by

the inability of SVECs, endotheliomas derived from transformation with the virus SV40 [188], to form fenestrae upon the same stimulation. Furthermore, Polyoma middle T endotheliomas injected into mice or chick embryos, have been shown to produce hemangiomas consisting of discontinuous endothelial cells and accompanied by extesive hemorraging, though the presence of fenestrae has not been directly addressed [187, 206] [207].

It is noteworthy that not all endotheliomas derived from polyoma middle T infection are capable of forming fenestrae, as eEND or sEND cells are very weakly responsive (data not shown). In addition, within the positively predisposed endotheliomas, bEND5 cells have an increased susceptibility in comparison to Py4.1 cells. Tissue-specific differences related to the origin of endotheliomas and different genetic alterations during the establishment of the cell lines, could contribute to the observed variation. bEND5 cells were derived by Polyoma middle T infection of endothelial cell cultures from the brain microvasculature [180], one of the tissues rarely associated with fenestrae formation. Py4.1 cells, were obtained from neonatal hemangiomas of Polyoma middle T transgenic mice [187, 208], while the weakly responsive eEND and sEND lines were derived from hemangiomas of chimeric embryos, that had been generated using Polyoma middle T infected ES cells [209].

Another contributor to the endothelial cell predisposition to form fenestrae could involve the protein PV-1 [16, 54, 71]. PV-1 has been recognised as a structural component of the diaphragms of fenestrae and caveolae, and was recently deemed to be necessary and sufficient for diaphragm formation [210]. Nonetheless, PV-1 does not appear to be necessary and sufficient for fenestrae formation. Our data suggests that PV-1 is certainly not sufficient, as both bEND5 and Py 4.1 cells harbor high levels of PV-1 in steady state conditions with no fenestrae. Moreover transfection of PV-1 in HUVECs does not result in fenestrae formation [210].

Regarding the necessity of PV-1, there are scattered, contradictory reports. Stan et al. reported a correlation between the number of fenestrae and the levels of PV-1, in untreated or PMA-induced, endothelial cells [210]. A similar correlation was seen in our system, where bEND5 had higher amounts of PV-1 than Py 4.1 cells, while no PV-1 was detectable in SVE cells (data not shown). The level of PV-1 in HUVE cells could not be determined as the antibodies used did not recognize the human version of the protein, while wholemount TEM did not provide the desired resolution to assess the presence of diaphragms in the few fenestrae that were formed. Indirect support for a role of PV-1 in fenestrae formation comes from observations during the development of fenestrated vasculature i*n vivo*: The non-diaphragmed fenestrated capillaries of the liver sinusoids and the kidney glomerulus contain a diaphragm during organ development, before 17 days of gestation [101] and transiently during the first two postnatal weeks [85], respectively. In addition, neovasculature stemming from liver sinusoids after transplantation of pseudoislets contained diaphragmed fenestrae [211]. On the other hand, no diaphragms were reported during novel fenestrae formation in liver sinusoid endothelial cells *in vitro* [95, 96], arguing against a necessary role for PV-1.

An attempt to directly test this hypothesis was shown through the use of PV-1 siRNA to suppress PMA-induced fenestrae formation in HUVECs [210]. No fenestrae were observed upon silencing, however, the fact that cells were examined after at least 3 days of treatment, combined with the low level of fenestrae induction achieved by PMA (0.000079 per μm^2) prevented drawing accurate conclusions. Our system may provide a means for manipulating PV-1 expression in the future, so as to obtain a definitive answer to this question.

3.3.5 Dissecting the complex membrane dynamics that lead to fenestrae formation

In the course of optimizing the induction protocol, a number of membrane structures were encountered, many of which could represent intermediates in the process of fenestrae formation. Although the 'fenestrae forming centre' reported in liver sinusoidal endothelial cells [96] was never observed, I frequently came across areas of cytoplasmic depression (Figure 3.7, B) with structures reminiscent of partially fused fenestrae (Figure 3.7, C).

One model of membrane fusion that could fit these observations is the stalk hypothesis [212-215]. According to the stalk hypothesis an ordered series of events take place, starting with close apposition of two bilayers and mixing of their proximal monolayers, followed by stalk formation and hemifusion intermediates, and terminating with fusion pore formation [212-215]. Areas of visible cytoplasmic depression are likely to be sites of future sieve plate occupancy, with cortical actin potentially disrupted, and the distance between apical and basal plasma membranes reduced. When the two bilayers are found in sufficient proximity, mixing of components can result in hemifusion intermediates, potentially resembling the incomplete perforations of Figure 3.7. The arrangement of such invaginations is characterised by the order and symmetry present in sieve plates; however, the putative fenestrae predecessors appear devoid of fully-formed pores. Fenestral pore formation could start with the appearance of a narrow fusion pore that subsequently dilates, and opens to the correct diameter of a fenestra.

Membrane fusion according to the stalk hypothesis would require the presence of fusion co-factors such as Rab GTPases and SNAREs [215, 216]. Whether ubiquitous components of the fusion machinery are present on or around fenestrae, as in the case

of caveolae [217, 218], remains to be established. Interestingly, Ca^{2+} pump-ATPase and $Ca^{2+}Mg^{2+}$ ATPase have been reported to localise on hepatic sinusoidal endothelial fenestrae [75, 76] and have been implicated in the regulation of fenestrae contraction and dilatation [98, 219, 220]. Transient calcium fluxes are postulated to trigger fusion by activation of target proteins [216, 221, 222], therefore such calcium pumps could also participate in membrane fusion during fenestrae formation, by regulating intracellular and extracellular calcium levels. Consistent with such a role for local calcium gradients, the assembly of the nuclear pore complex, a structure that shares remarkable similarity to fenestrae, can be inhibited by the calcium chelator BAPTA [223].

An alternative mechanism for membrane fusion could involve an endocytic process whereby a vesicle forms as an invagination at the site of future fenestrae on the cell surface, and eventually fuses its membrane with the apposing plasma membrane once close proximity between the two has been reached. Future studies aimed at arresting the process at various stages, and examination of the intermediates by TEM, should help distinguish among the numerous possibilities.

This chapter presented the establishment of the first *in vitro* culture model for *de novo* fenestrae induction in quantities sufficient for cell biological and biochemical studies. This has enabled me to systematically dissect and attack different aspects of the biological problem, starting with the isolation of fenestrated plasma membranes and the characterisation of their molecular components, which will be described in the next chapter.

Chapter 4: Molecular characterisation of fenestrae

4.1 Background

The molecular composition of fenestrae is for the most part a mystery. The only known constituent of a subset of fenestrae to date is the protein PV-1, a shared feature of the diaphragms of fenestrae and caveolae [54]. Fenestrae of the liver sinusoids and the kidney glomerulus are devoid of diaphragms [60, 85], therefore remain without a single known molecular component. Attempts to characterise the structure so far have focused on the diaphragm itself, and showed it consists of multiple PV-1 dimers in close proximity to each other [71]. Cross-linking studies in cells rich in caveolae were unable to identify new proteins associated with PV-1 [71], and detergent extraction studies showed PV-1 to partition separately from other caveolae components [224], underlining the need for alternative approaches. Accordingly, to gain insight into the molecules that may constitute the rim of the pore, or the fenestrae sieve plate, I took advantage of the *in vitro* induction system and pursued a sub-cellular proteomic analysis.

The choice of a proteomic comparison as a suitable method to identify fenestrae-specific components was made on the following assumption: Fenestrae induction, albeit independent of protein synthesis in our system, involves a recruitment of novel components to the plasma membrane. To eliminate the non-specific effects of the induction, to minimize the protein complexity of the mixture to be analysed, and above all to focus on the subcellular fraction where the relevant changes occur, the first step was to isolate plasma membranes from other parts of the cell.

The prime difficulty in isolating plasma membranes on the basis of their physical properties lies in the similarity of their density to that of other subcellular fractions [225]. Furthermore, conventional methods for cell disruption lead to the vesicularisation of the membrane, and the remodeling of many surface microdomains

[225]. The challenges above demanded a rapid approach that would purify fenestrated plasma membranes and at the same time preserve their structural integrity. An unbiased affinity purification method based on the physico-chemical properties of the plasma membrane as a whole, rather than on the presence of particular antigens, was selected as the most appropriate. The method relies on the high affinity of cationic colloidal silica for negatively charged plasma membranes [226-230]; upon binding of silica, plasma membranes acquire a unique density that can be used to separate them from the remainder of the cell. The prediction was that silica would be attracted to fenestrated areas of the membrane due to their particularly high concentrations of negative charge [63], but also would stabilise the membrane substructure by firmly holding the negative charges in place. Silica-coating is reported to prevent vesicularisation of the fragmented plasma membrane, and to maintain spatiotemporal protein and lipid relationships without modifying any of the components as silica is chemically inert [218, 227, 231, 232].

This chapter describes how non-fenestrated and fenestrated states of the endothelial plasma membranes were captured, isolated and subjected to a biochemical analysis using 2D-gel electrophoresis and mass spectrometry. A subtractive analysis of non-fenestrated versus fenestrated plasma membrane proteomes highlighted differences that are expected to shed light on the molecular architecture of fenestrae.

4.2 Results

4.2.1 Isolation of plasma membranes

In order to purify plasma membranes from the remainder of the cell, a modification of the cationic colloidal silica plasma membrane isolation (Figure 4.1) was applied to bEND5 and Py 4.1 cells that had been untreated, or induced with 2.5 μM Latrunculin A for 3 hours.

4.2.1.1 Biochemical analysis

To ensure enrichment for plasma membrane components, the progress of the isolation procedure was followed biochemically, by retaining samples from various steps in the procedure. Equal amounts of protein from each fraction were separated by SDS-PAGE electrophoresis and assessed for the presence of particular organelle markers by western blotting (Figure 4.2). A comparison of equal protein amounts between whole cell, plasma membrane and nuclei, and plasma membrane fractions showed a progressive enrichment for plasma membrane markers such as VE-cadherin and PV-1. Densitometric analysis of bands corresponding to VE-cadherin and PV-1 revealed enrichment between 5 and 40 fold in the plasma membrane fraction versus whole cells, in a number of independent assays. Golgi markers such as GM130 showed depletion between 2 and 20 fold. In addition, no signal for plasma membrane markers was detected in the internal membrane fraction, suggesting that there is no or minimal loss of plasma membranes in the supernatant of the first low-speed centrifugation step. Plasma membranes co-sedimented with nuclei as predicted, according to their unique new density. It should be noted that the procedure does not result in the isolation of pure plasma membranes, but rather of a fraction that is enriched in plasma

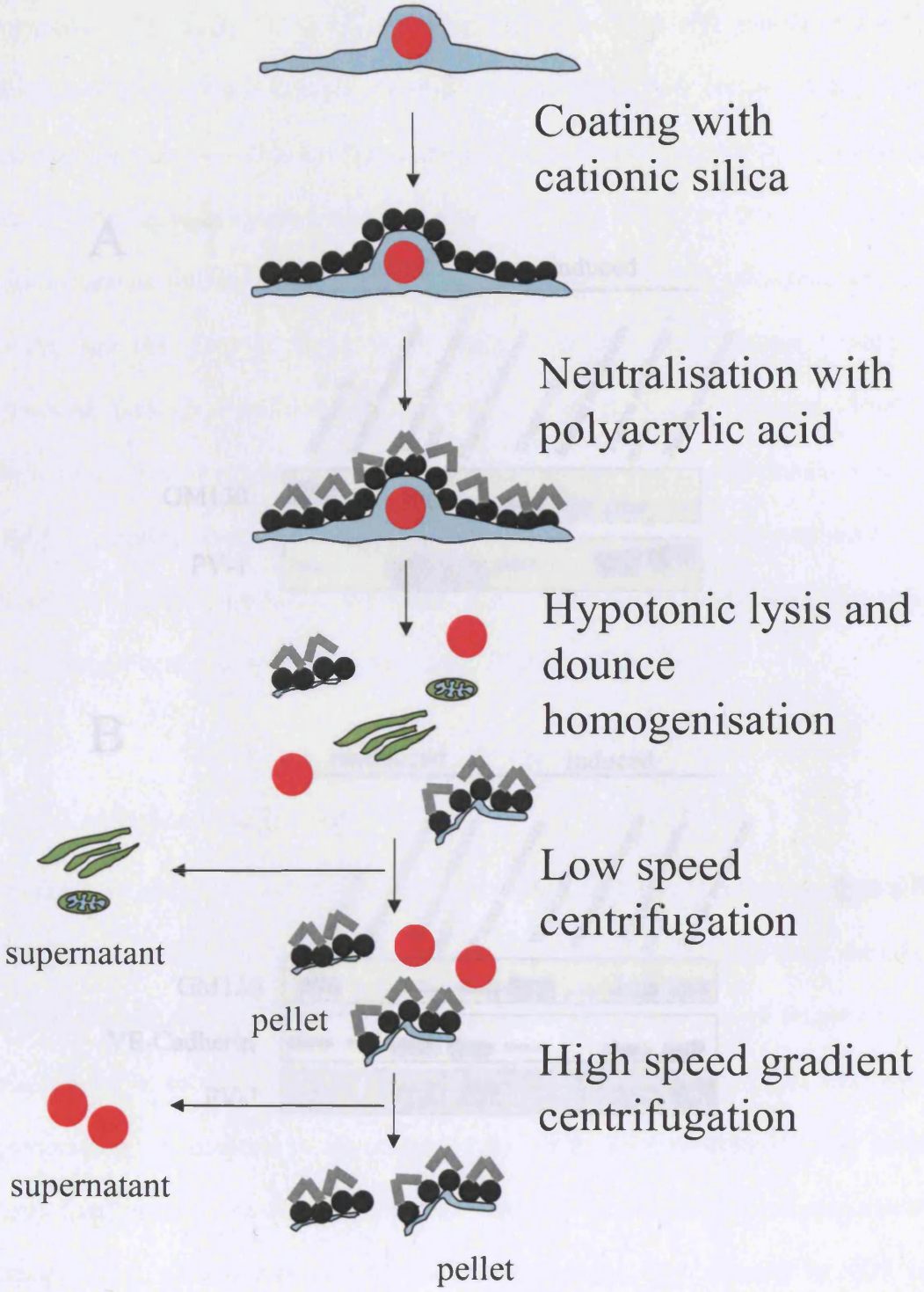

Figure 4.1 Schematic of the cationic colloidal silica isolation protocol. Cells are coated on the dish with a solution of cationic colloidal silica, which is neutralised by a subsequent coating with sodium polyacrylate. Cells are then lysed in a hypotonic buffer using a dounce homogeniser, and the various subcellular components are separated by centrifugation. A low-speed pellet containing nuclei and silica-coated plasma membranes is further fractionated by an ultracentrifugation step through a Nycodenz gradient to obtain a pellet of silica-coated plasma membranes.

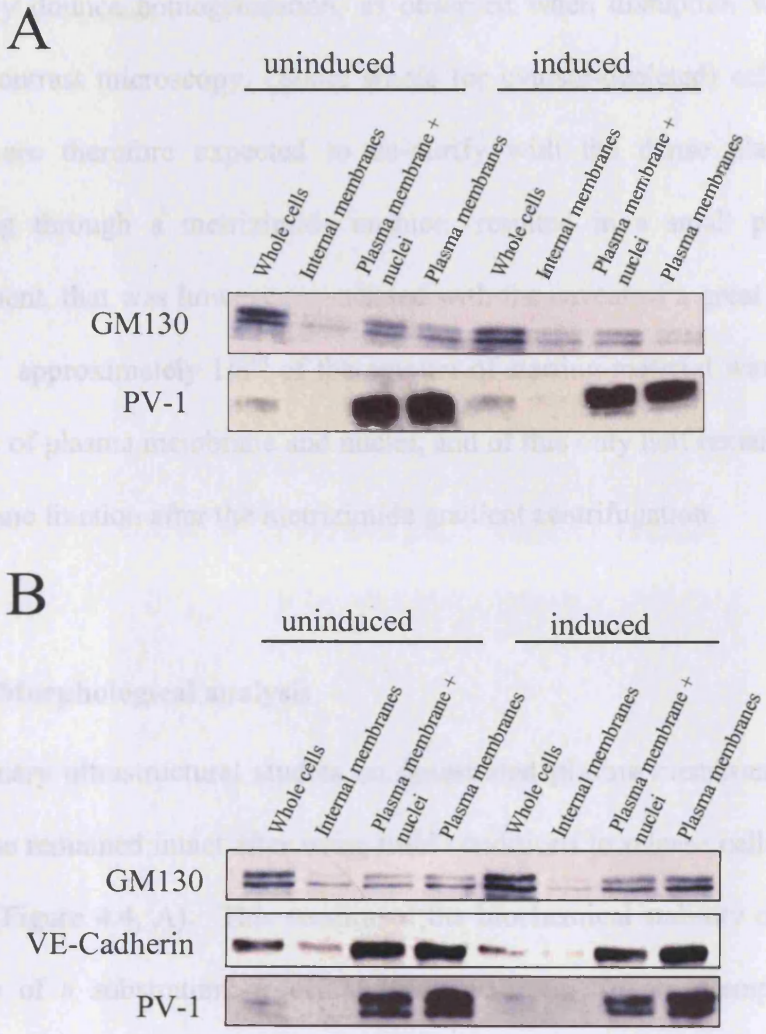

Figure 4.2 Biochemical analysis of cationic colloidal silica plasma membrane isolation. 10µg of protein from each subcellular fraction of bEND5 (A) and Py4.1 (B) cells was subjected to SDS-PAGE electrophoresis and Western Blotting using antibodies to the indicated proteins. Enrichment for the plasma membrane markers PV-1 and VE-cadherin, and depletion for the Golgi marker GM130 is seen in the plasma membrane fractions of bEND5 and Py4.1 cells, under uninduced or Latrunculin A-induced conditions.

membranes. Markers for Golgi and other organelles were still present in the final fraction (Figure 4.2 and data not shown), albeit at much lower concentrations than in the starting material. This can be accounted for by the incomplete cell lysis brought about by dounce homogenisation, as observed when disruption was monitored by phase-contrast microscopy. Some whole (or cytosol-depleted) cells that are silica-coated are therefore expected to co-purify with the dense plasma membranes. Spinning through a metrizimide cushion, resulted in a small plasma membrane enrichment, that was however associated with the caveat of a great reduction in total yield: approximately $1/8^{th}$ of the amount of starting material was recovered in the fraction of plasma membrane and nuclei, and of this only half remained in the plasma membrane fraction after the metrizimide gradient centrifugation.

4.2.1.2 Morphological analysis

Preliminary ultrastructural studies on fenestrated plasma membranes suggested that fenestrae remained intact after using mild conditions to release cells from the culture vessel (Figure 4.4, A). This confirmed the biochemical stability of fenestrae in the absence of a substratum or cell culture medium. In an attempt to validate the preservation of fenestrae in the course of the silica isolation protocol, thin sections from fixed plasma membrane pellets were examined under TEM. Low magnification images from plasma membrane pellets of uninduced and induced bEND5 cells showed that silica-coated plasma membrane sheets, appearing as 'beads on a string', were the predominant element in the fractions (Figure 4.3). Occasionally whole cells were encountered in the pellets (Figure 4.4, B), consistent with the biochemical data and the phase-contrast microscopy observations. High magnification images of plasma membranes from uninduced cells revealed the presence of caveolae attached

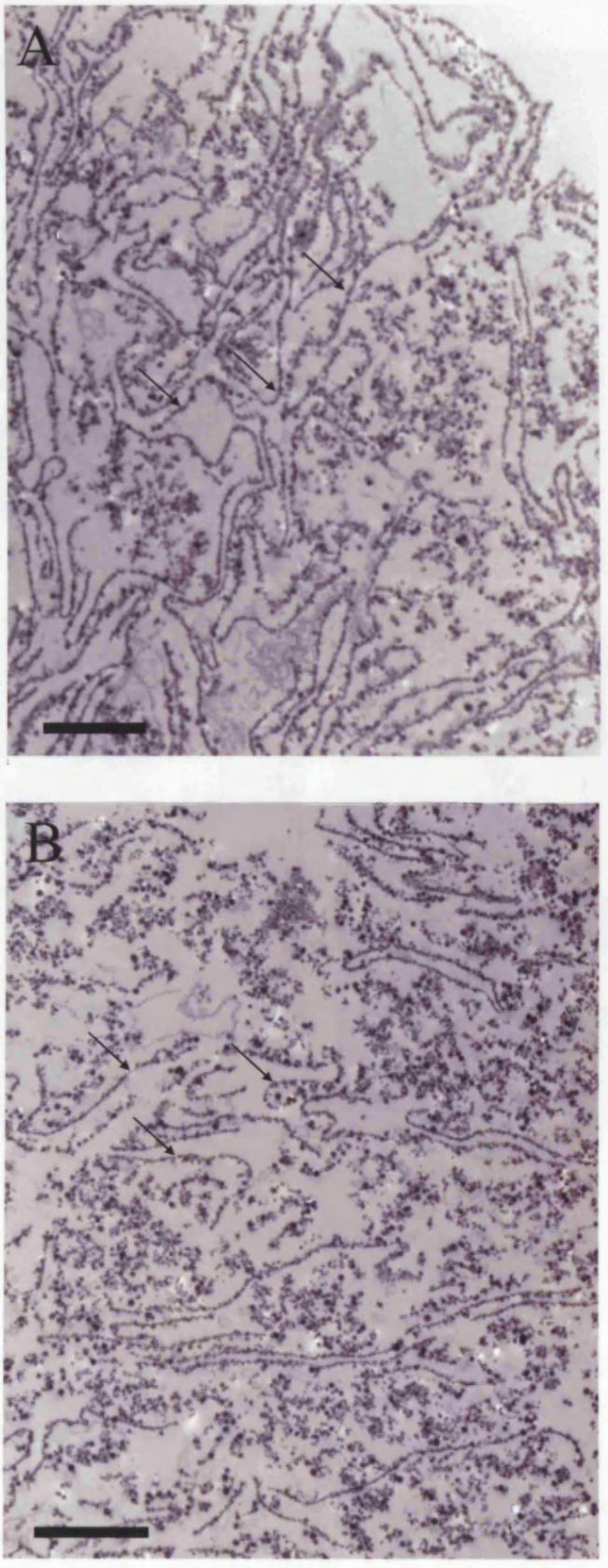

Figure 4.3 Ultrastructural examination of plasma membrane pellets. Silica coated plasma membrane sheets (arrows) are the predominant structure in pellets from untreated (A) and Latrunculin A-treated (B) endothelial cells. (Bar = 2 μm)

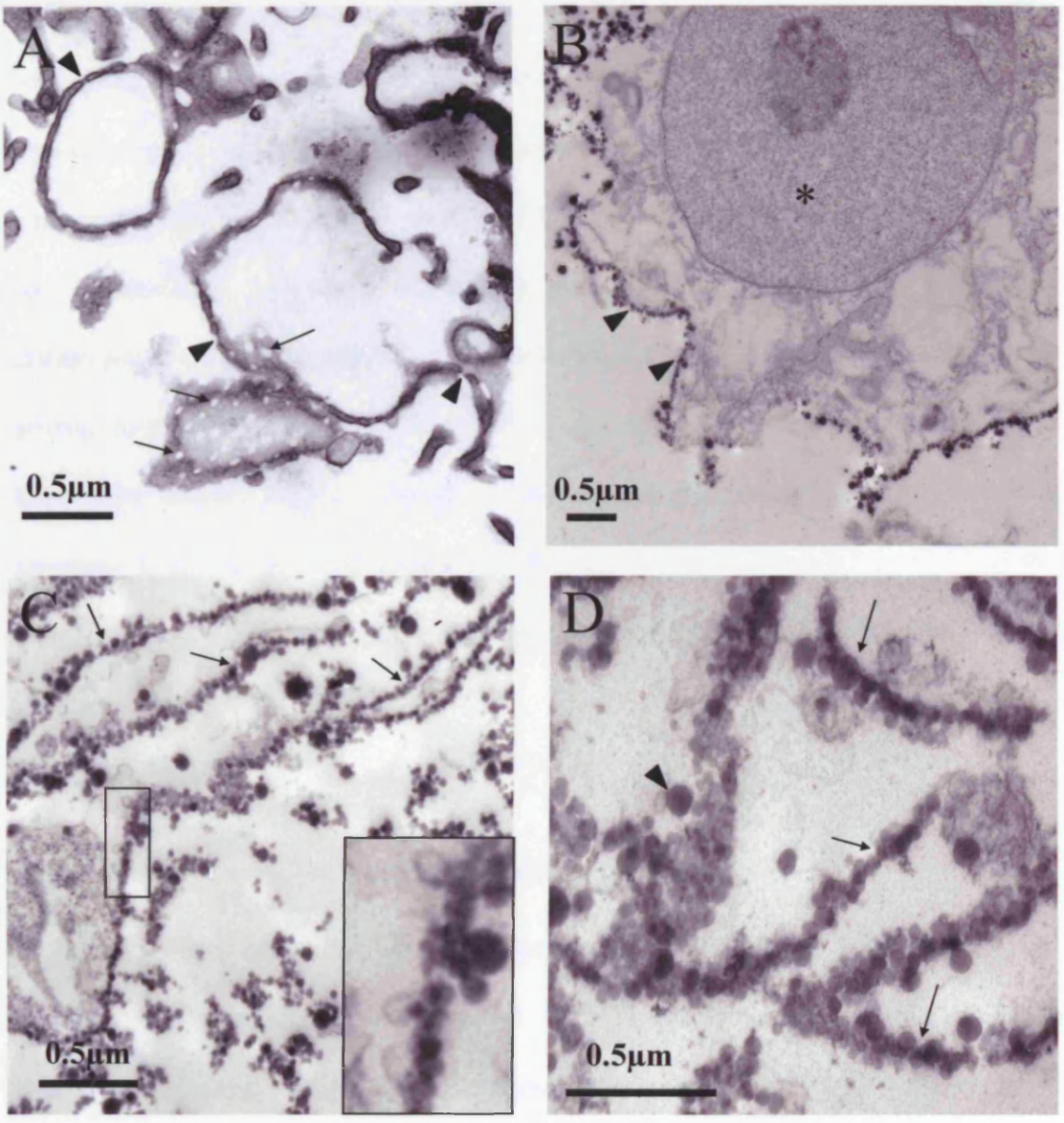

Figure 4.4 Ultrastructural examination of subcellular structures. Fenestrae in Latrunculin A-induced bEND5 cells can be maintained biochemically after release from the substratum (A). Fenestrae *en face* denoted by arrows, and fenestrae in cross-section denoted by arrowheads (A) Examples encountered in fractions of the silica isolation protocol are shown in B, C, and D. Whole cell contaminant of the plasma membrane pellet (B). The nucleus is denoted by a star, and the plasma membrane by arrowheads. Plasma membrane sheets (arrows) of untreated cells (C), and Latrunculin A-induced cells (D). Caveolae are isolated intact along with the plasma membranes of untreated cells (C, inset). The size of the silica pellicle (arrowhead) masks any underlying membrane ultrastructure and precludes visualisation of fenestrae in plasma membranes of induced cells (D).

to the cytoplasmic aspect of the isolated membrane sheets (Figure 4.4, C, inset), confirming previous reports in the literature [231, 232]. Both caveolae, and intracellular organelles in whole cells appeared morphologically intact, and the silica was confined to the exterior of the cell. Unfortunately, the size of the silica pellicle had an average diameter of 20-50 nm and therefore masked any underlying ultrastructure of the membrane itself, including fenestrae (Figures 4.4, D). In an attempt to visualise fenestrae in the pellets of induced cells, sub-saturating amounts of silica were employed so as to enable plasma membrane isolation without complete coverage of the surface. Dilutions of the amount of silica even down to $1/10^{th}$ of the concentration used in the standard isolation procedure failed to unmask the underlying ultrastructure (data not shown).

4.2.1.3 Quality control of starting material for proteomics

To identify differences between fenestrated and non-fenestrated cells, the highest possible levels of induction were required. bEND5 and Py4.1 cells, the two cell types that were susceptible to Latrunculin-mediated fenestrae induction were both subjected to subcellular proteomics. Each conferred unique advantages to the analysis: The highest numbers of fenestrae were attained with bEND5 cells, with the drawback of some background fenestrae present in the uninduced state. Py4.1 cells on the other hand had no background fenestrae, and although never displayed the high absolute values of induction seen in bEND5 cells, showed a better relative induction of fenestrae (see chapter 3, Figure 3.9)

To ensure the quality of the material processed for a proteomic comparison, fenestrae induction was verified by light microscopy and plasma membrane purification was followed biochemically. Coverslips included in the culture dishes were fixed at the

start of the isolation protocol and immunostained for the diaphragm marker PV-1 and tubulin. Consistent with observations from light microscopy (see Appendix I), the characteristic PV-1-positive sieve plates, delineated by microtubules, were easily distinguishable in all bEND5 and Py4.1 induction attempts (Figure 4.5, A).

For each cell type, plasma membranes of Latrunculin-induced and vehicle-induced material were isolated for comparison. For bEND5 cells, an additional control referred to as C1 was prepared. This represented cells that were entirely untreated, and processed for plasma membrane isolation at the start of the induction (time 0), which served to pinpoint exactly any differences due to the vehicle. Aliquots of the various subcellular fractions were retained throughout the progress of the purification protocol and examined for the enrichment of PV-1 and the depletion of intracellular components such as the golgi marker GS28 (Figure 4.5, B).

4.2.2 Fenestrae proteomics

4.2.2.1 Preliminary 2D-gel electrophoresis analysis

To assess the efficacy of 2D-gel electrophoresis in revealing differences between fenestrated and non-fenestrated plasma membranes, a small-scale analysis was conducted using silica-isolated material from untreated and induced bEND5 cells. Proteins were eluted from the silica-isolated membranes, precipitated, and resuspended in an appropriate buffer for isoelectric focusing, the first dimension of 2D-gel electrophoresis. After a first-round of separation on the basis of their charge, proteins were further separated in a second dimension, on the basis of their molecular weight, by SDS-PAGE electrophoresis. Results showed that the technique provided adequate resolution for identifying single protein spots in the given mixture, while no adverse effects of precipitation or streaking were encountered. Moreover,

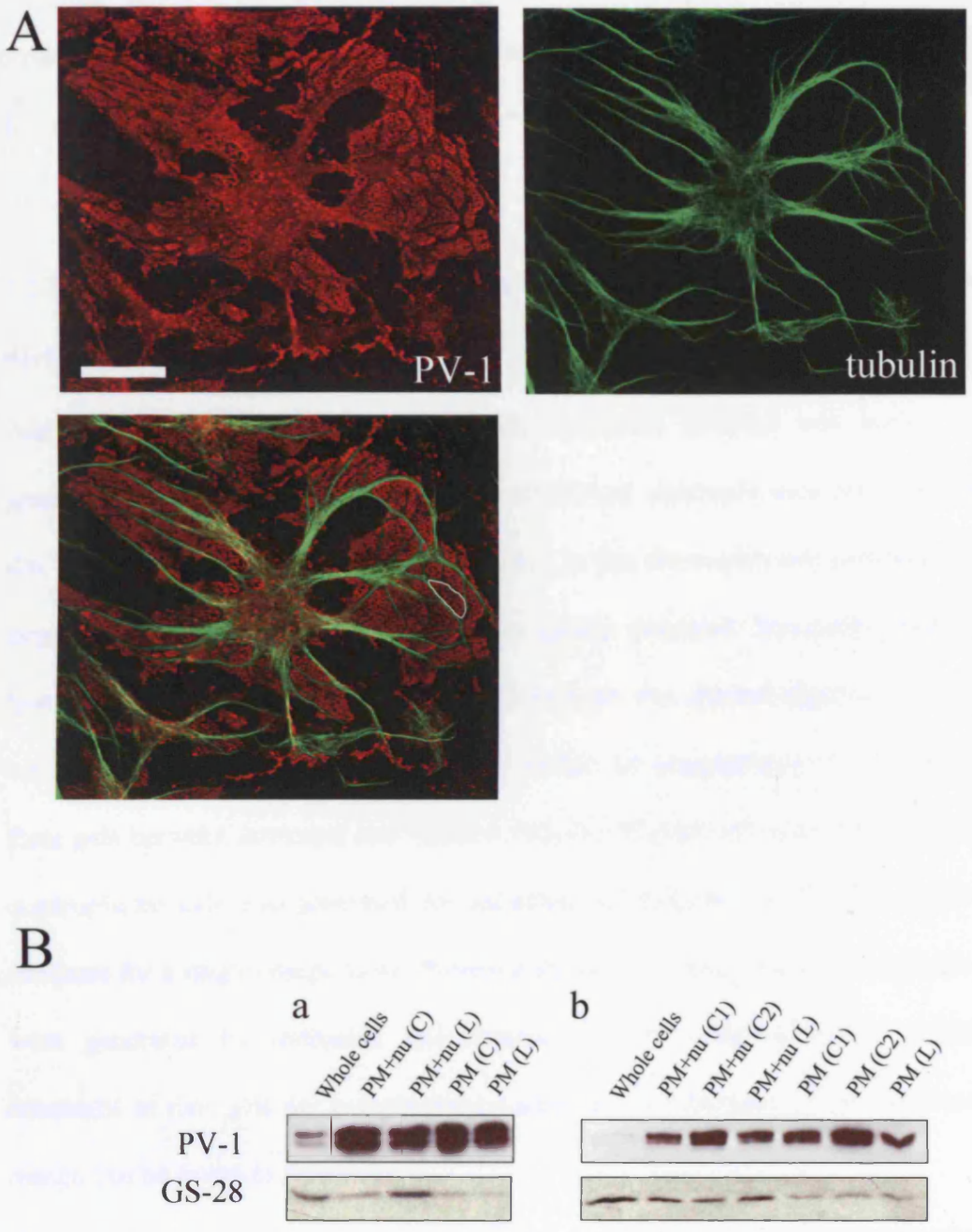

Figure 4.5 Quality control of isolated plasma membranes. (A) The success of fenestrae induction was monitored by the characteristic staining of PV-1 for fenestrae patches in areas that exclude microtubules. PV-1 labeling, tubulin labeling, and the overlay are shown for a bEND5 cell induced with 2.5 μM Latrunculin A for 3 hours. An example of a fenestrae patch is encircled by a white line in the overlay. (Bar = 20 μm) (B) The success of the isolation protocol was assessed by monitoring enrichment for PV-1 and de-enrichment for GS-28 in plasma membrane and nuclei (PM + nu), and plasma membrane (PM) fractions versus whole cell homogenates of control (C) and Latrunculin A-induced (L) Py4.1 (a) and bEND5 (b) cells. In bEND5 cells the additional control sampled at time 0 (C1) can be distinguished from the vehicle-induced sample (C2).

preliminary differences between the two experimental groups were observed (Figure 4.6, A-B).

4.2.2.2 Large-scale 2D-gel electrophoresis analysis (Collaboration with Charles River Proteomics)

Following the preliminary study, the silica-isolation protocol was scaled up to generate plasma membranes for a large-scale 2D-gel electrophoresis analysis (Figure 4.6, C-F). Some modifications were included in the electrophoresis protocol for the large-scale study, but the flow of the procedure remained essentially unchanged. Material from different silica-isolation experiments was pooled together in different batches, to provide sufficient amounts of protein for comparisons of a minimum of three gels between untreated and induced samples. Protein sufficient for one batch of quadruplicate gels was generated for untreated and induced Py4.1 cells, which was adequate for a single comparison. Protein sufficient for three batches of triplicate gels were generated for untreated and induced bEND5 samples, which combined, amounted to nine gels per experimental condition. A schematic of the experimental design can be found in Appendix II.

Comparisons between gels of induced and uninduced samples were performed separately for each cell type using Progenesis software. The program measured fold differences between the average staining intensities of spots in gels of induced and untreated samples (Figure 4.7). In addition, p-values for those differences were calculated using the Students t-test. A number of spots were observed to significantly decrease or increase in intensity; however, with an aim of identifying proteins involved in fenestrae biogenesis, only those increasing in the induced samples were considered for further study. In the first round of analysis, spots that qualified for one

Figure 4.6 Representative 2D-gels from the preliminary and large-scale proteomic studies. Preliminary comparison of plasma membrane proteins from untreated (A) and Latrunculin A-induced (B) bEND5 cells showed that 2D-gel electrophoresis provided adequate resolution while no streaking was encounterd. Examples of large-scale 2D-gel electrophoresis of plasma membrane proteins from untreated (C,E) and induced (D,F) bEND5 (C, D) and Py4.1 (E,F) cells.

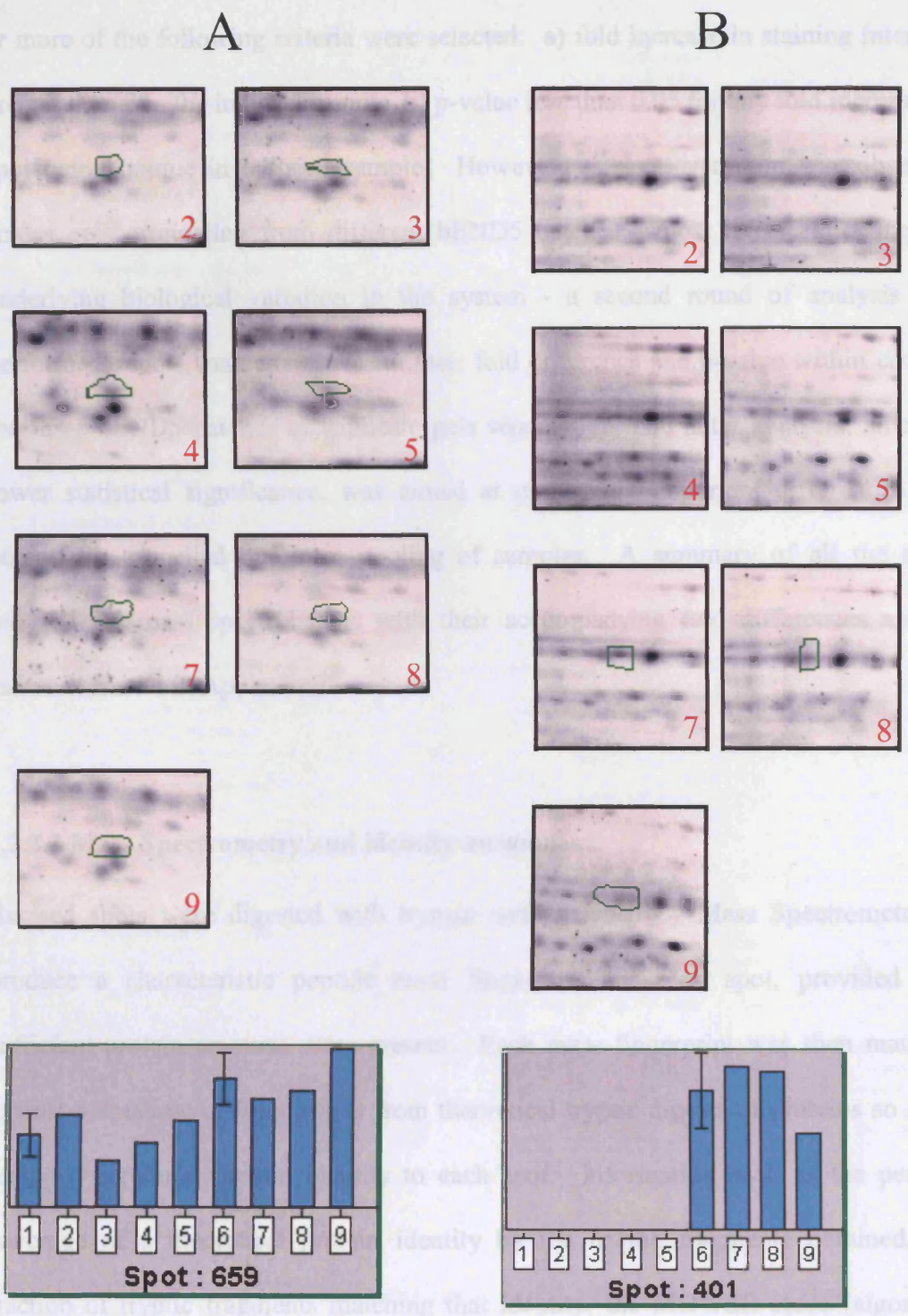

Figure 4.7 Spot intensity calculation using Progenesis Software. (A) shows spot 659 from the Py4.1 cell analysis, recognized as being 1.772 fold higher in the average (6) of the Latrunculin A-induced samples (7,8,9) compared to the average (1) of the control samples (2,3,4,5). Possible identities for spot 659 are alpha enolase, paralemmin, and kinesin light chain. (B) shows spot 401 from the Py4.1 cell analysis, which although recognized as being 3.8 fold higher in the average of the Latrunculin A-induced samples (6) compared to that of control samples (1), is actually part of a train of spots characteristic of different phosphorylation states of the same protein. Possible identities for spot 401 are radixin and moesin.

or more of the following criteria were selected: a) fold increase in staining intensity greater than 2 in the induced sample, b) p-value less than 0.05 for any fold increase, c) spot being unique in induced sample. However, as great variation was observed across gels originating from different bEND5 batches - most likely reflecting the underlying biological variation in the system - a second round of analysis was performed: spots were examined for their fold difference and p-value within each of the three bEND5 batches of triplicate gels separately. The latter analysis, albeit of lower statistical significance, was aimed at unmasking important differences that potentially cancelled out from pooling of samples. A summary of all the spots selected for mass spectrometry, with their accompanying fold differences and p-values is shown in Appendix II.

4.2.2.3 Mass Spectrometry and identity assignment

Excised spots were digested with trypsin and analysed by Mass Spectrometry to produce a characteristic peptide mass fingerprint for each spot, provided that sufficient protein amounts were present. Each mass fingerprint was then matched against a database of fingerprints from theoretical tryptic digests of proteins so as to assign a particular protein identity to each spot. Information such as the percent coverage of a theoretical protein identity by the tryptic fragments obtained, the fraction of tryptic fragments matching that identity, the MOWSE score (algorithm evaluating the statistical significance of a match), and the relationship between the isoelectric point (pI) and molecular weight of the excised spot and that of the theoretical identity, were all considered prior to assigning a particular identity. Often, more than one identity was assigned, which could be explained by similarities in sequence between potential identities, by coincident patterns of tryptic fragments, or

	Protein Name	Total Change	p-value	L vs C2 -1	p-value	L vs C2 -2	p-value	L vs C2 -3	p-value	cell type spot no.
Cytoskeletal association	Cofilin, non-muscle isoform	unique spot	N/A	19.635	Unknown	unique spot	N/A	unique spot	N/A	bENDs 486
	Myosin light chain alkali, smooth-muscle isoform (MLC3SM)	1.689 / 1.548	0.00018 /0.00263	-1.274 / 1.265	unknown/ 0.2492	1.503 / 1.423	0.0327 / 0.0111	2.373 / 2.269	0.0124 / 0.0222	bENDs 526/527
	Myosin regulatory light chain 2-A, smooth muscle isoform (Myosin RLC-A)	1.488	0.001198	1.345	0.09975	1.517	0.1585	1.842	0.122	bENDs 478
	Myosin regulatory light chain 2-B, smooth muscle isoform (Myosin RLC-B)									
	Actin monomer-binding protein twinfilin-1	1.671	0.02125	-1.064	0.8038	2.148	0.1855	3.067	0.01115	bENDs 304
	Protein tyrosine kinase 9	2.258	0.004779	N/A	N/A	N/A	N/A	N/A	N/A	Py4.1 793
	Transgelin 2	-	Unknown	3.99	0.008421	-	Unknown	-	Unknown	bENDs 473
	Kinesin light chain KLCt	1.772	0.02662	N/A	N/A	N/A	N/A	N/A	N/A	Py4.1 659
Membrane remodeling / endocytosis	Radixin	3.811	0.003184	N/A	N/A	N/A	N/A	N/A	N/A	Py 4.1 401
	Moesin									
	Nucleoside diphosphate kinase B (nm23-M2)	1.251 / 1.16	0.03035 / 0.945	1.611 / 4.502	0.003646 / Unknown	-	Unknown	1.334 / 1.373	0.03847 / 0.02015	bENDs 517/521
	Nucleoside diphosphate kinase A (nm23-M1)									
	Nucleoside diphosphate kinase B (nm23-H2)									
	Paralemmin	1.772	0.02662	N/A	N/A	N/A	N/A	N/A	N/A	Py 4.1 659
	Annexin II (Lipocortin II)	1.193	0.3104	1.052	0.7728	-	Unknown	1.396	0.01084	bENDs 334
Transcription/translation	Putative RNA-binding protein 3	1.251	0.03035	1.611	0.003646	-	Unknown	1.334	0.03847	bENDs 517
	Heterogeneous nuclear ribonucleoprotein K (hnRNP K)	1.883 / 1.71	0.1927 / 0.1852	9.224 / 3.28	0.03162 / 0.1096	-1.392 / 1.199	0.6478 / 0.571	1.495 / 1.381	0.1227 / 1.381	bENDs 138/146
	Eukaryotic translation initiation factor 4H	-1.012	0.9481	1.03	0.353	-1.394	0.1313	1.416	0.01322	bENDs 400
	Musculin (Myogenic repressor)									
Housekeeping	60 kDa heat shock protein, mitochondrial precursor	-1.176	0.3662	-	Unknown	-1.381	0.3138	1.266	0.157	bENDs 153
	ATP synthase, H+ transporting mitochondrial F1 complex, beta subunit	1.358	0.377	1.074	0.543	-1.24	0.02935	1.641	0.0105	bENDs 215
	ATP synthase beta chain, mitochondrial precursor									
Metabolism	Alpha enolase (Non-neural enolase)	1.826	0.02507	2.103	0.001633	2.447	0.1313	1.58	0.08104	bENDs 233
		2.038 / 1.772	0.002161 / 0.02662	N/A	N/A	N/A	N/A	N/A	N/A	Py 4.1 658 / 659

Table 4.1 Summary of candidate proteins grouped according to their function. For proteins with more than one function, only the best-characterised one is indicated. Fold change and accompanying p-value are shown for all the different types of analysis performed. Total change refers to the fold change in spot intensity in Latrunculin A-induced versus control cells across all gels from the bEND5-cell or the Py4.1-cell comparison. Columns L vs C2 (1), L vs C2 (2), and L vs C2 (3) refer to fold change in spot intensity in individual batch analyses performed for bEND5 cells. Note that more than one protein identity can be assigned to one spot (e.g. bEND5 400), and the same protein identity can be encountered in multiple spots (e.g. bEND5 526 and 527). The fold changes that determined the selection of the particular spot for excision and subsequent protein content identification are highlighted in yellow.

A

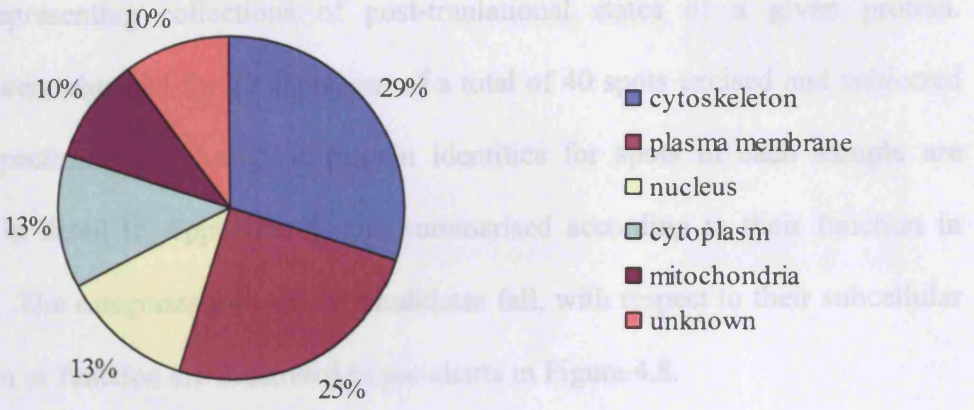

B

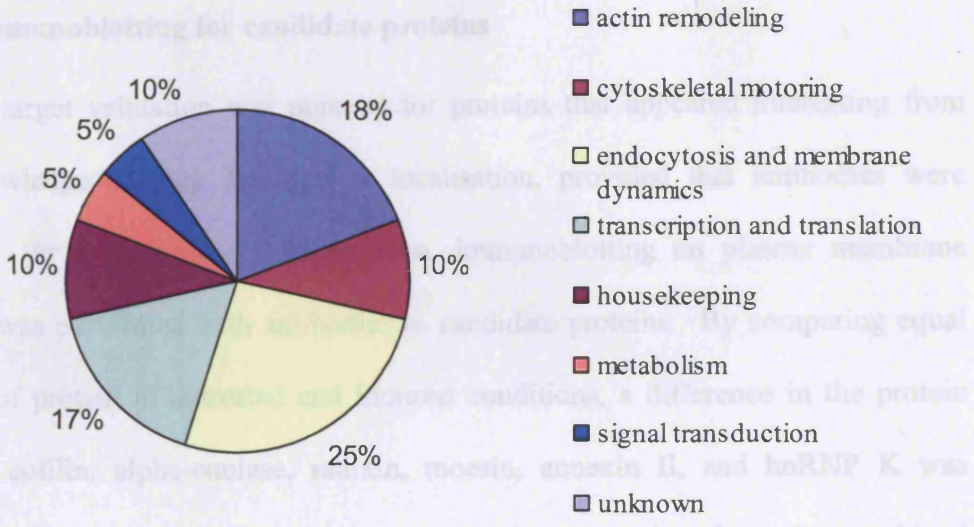

Figure 4.8 Categorisation of candidate proteins with respect to their subcellular localisation (A) and function (B). For a protein falling into more than one category, its value was split between categories. Where multiple isoforms or polypeptide chains for the same protein were identified, the protein was counted only once.

by the presence of more than one protein within a single spot on the gel. In addition, separate spots frequently corresponded to the same protein, especially when found in clusters representing collections of post-tranlational states of a given protein. Identities were obtained for 22 spots, out of a total of 40 spots excised and subjected to mass spectrometry. Assigned protein identities for spots in each sample are presented in detail in Appendix II, and summarised according to their function in Table 4.1. The categories into which candidates fall, with respect to their subcellular localisation or function are illustrated in pie-charts in Figure 4.8.

4.2.3 Target validation

4.2.3.1 Immunoblotting for candidate proteins

Selective target validation was pursued for proteins that appeared interesting from prior knowledge of their function or localisation, provided that antibodies were available. In a first round of validation, immunoblotting on plasma membrane fractions was performed with antibodies to candidate proteins. By comparing equal amounts of protein in untreated and induced conditions, a difference in the protein levels of cofilin, alpha-enolase, radixin, moesin, annexin II, and hnRNP K was confirmed (Figure 4.9, A-B). Cofilin, a candidate emerging from the combined comparison of all three batches of bEND5 samples, was upregulated in all induced plasma membrane fractions examined. On the other hand, Annexin II, a candidate from the analysis of the 3rd batch only, was not consistently upregulated. Alpha-enolase and hnRNP K appeared both to be upregulated, but were only detected when high amounts of protein were loaded on the gel. Interestingly, although no upregulation in the induced fraction was seen for the related proteins moesin and radixin, probing with an antibody that primarily recognizes the phosphorylated

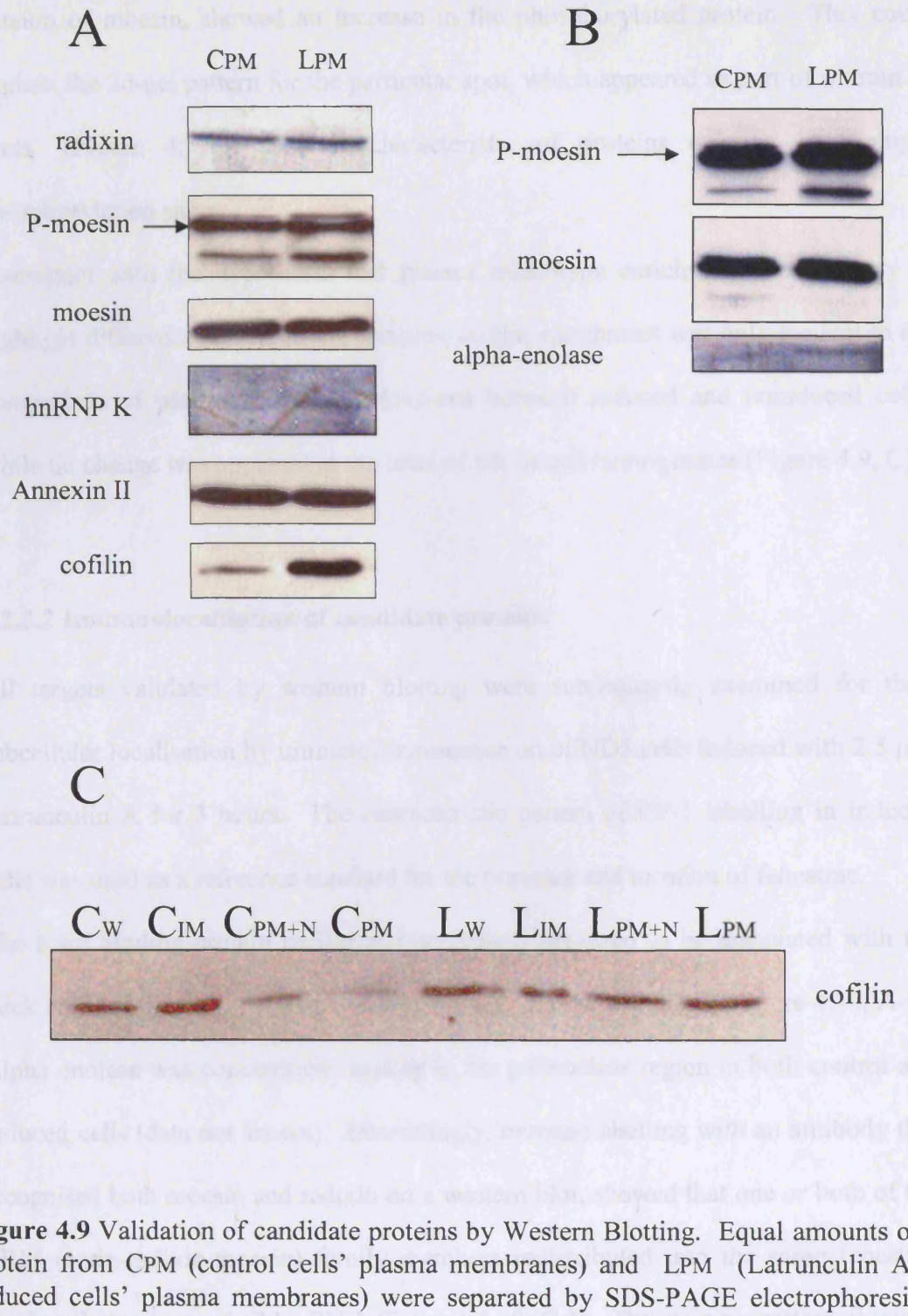

Figure 4.9 Validation of candidate proteins by Western Blotting. Equal amounts of protein from CPM (control cells' plasma membranes) and LPM (Latrunculin A-induced cells' plasma membranes) were separated by SDS-PAGE electrophoresis and probed for the indicated proteins by Western Blotting. Targets from the bEND5 cell analysis are shown in (A) and from the Py4.1 cell analysis in (B). Enrichment in induced cells is confirmed for phosphorylated moesin, hnRNP K, cofilin, and alpha-enolase. A comparison of the enrichment in cofilin between the membrane fractions of control and induced cells (CPM, LPM) versus that between the whole cell – homogenates of control and induced cells (CW, LW) is shown in (C). Cofilin enrichment is only evident at the level of the plasma membrane. The bands for internal membranes (CIM, LIM), and for plasma membrane and nuclei (CPM+N, LPM+N) are also indicated.

version of moesin, showed an increase in the phosphorylated protein. This could explain the 2d-gel pattern for the particular spot, which appeared as part of a 'train of spots' (Figure 4.7, B) and is characteristic of proteins existing in multiple phosphorylation states.

Consistent with the hypothesis that plasma membrane enrichment is necessary to highlight differences between the samples, cofilin enrichment was only evident in the comparison of plasma membrane fractions between induced and uninduced cells, while no change was apparent at the level of whole cell homogenates (Figure 4.9, C).

4.2.3.2 Immunolocalisation of candidate proteins

All targets validated by western blotting were subsequently examined for their subcellular localisation by immunofluorescence on bEND5 cells induced with 2.5 μM Latrunculin A for 3 hours. The characteristic pattern of PV-1 labelling in induced cells was used as a reference standard for the presence and location of fenestrae.

The actin binding protein cofilin and annexin II appeared to be associated with the thick areas of the cell that act as spacers between fenestrae patches (Figure 4.10, A-F). Alpha enolase was concentrated mainly in the perinuclear region in both control and induced cells (data not shown). Interestingly, immunolabelling with an antibody that recognised both moesin and radixin on a western blot, showed that one or both of the ERM (ezrin-radixin-moesin) family members redistributed into the same fenestrae patches that were marked by PV-1 (Figures 4.10, G-I). The staining pattern obtained with the cross-reactive goat polyclonal anti-moesin antibody was confirmed for moesin using a mouse monoclonal anti-moesin antibody. Further confirmation for the specificity of the moesin staining was obtained by a peptide competition experiment: The labelling for moesin obtained with either antibody could be competed by pre-

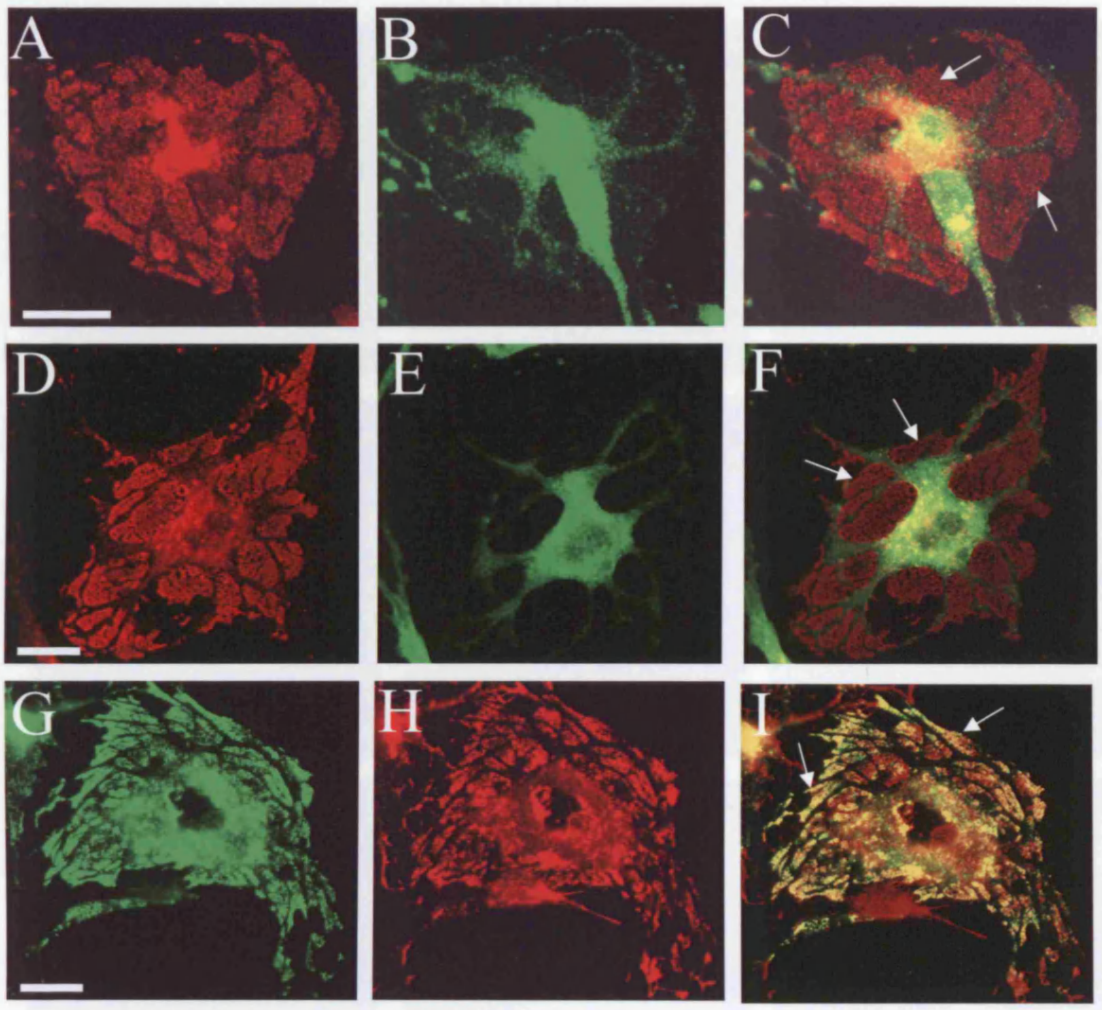

Figure 4.10 Validation of candidate proteins by Immunofluorescence. bEND5 cells, induced with 2.5μM Latrunculin A for 3 hours, were stained for PV-1 (A, D, G) and the following candidate proteins: cofilin (B), annexin (E), radixin/moesin (H). The corresponding overlays (C), (F), (I) show that radixin and/or moesin localise on the same fenestrae patches (arrows) that are labeled by PV-1, whereas cofilin and annexin are excluded from those regions. Images were obtained using epifluorescence microscopy. (Bar = 20 μm)

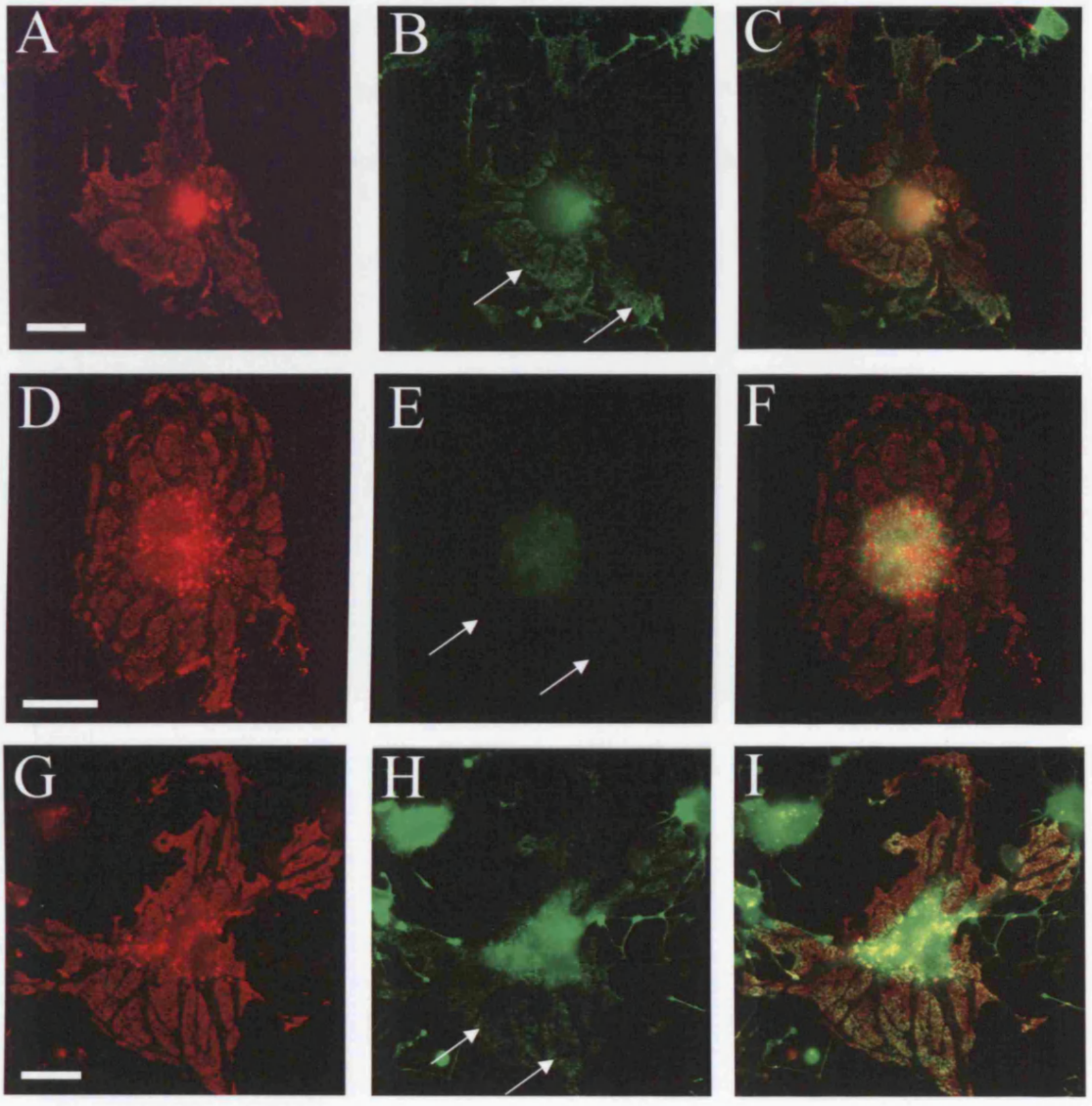

Figure 4.11 Competition study for anti-moesin mAb. Specificity for the labeling of the anti-moesin mAb (B) is seen by the disappearance of the signal (arrows) after preadsorption of the antibody with the peptide against which it was raised (E). Pre-adsorption with an irrelevant peptide has no effect on the labeling (H). The corresponding PV-1 labeling (A,D,G) and overlay of the two signals (C,F,I) are shown. Images were obtained using epifluorescence microscopy. (Bar = 20 μm)

incubating each antibody with the peptide against which it had been raised (Figure 4.11, A-C and data not shown).

Variable success with the remainder of antibodies in immunofluorescence prevented reaching a conclusion for the localisation of all targets. Candidates of interest will be pursued in the future, by means of alternative approaches such as cDNA tagging to assist visualisation.

4.3 Discussion

4.3.1 Overview of proteomic results

Despite the recent revolution in the field of genomics, when it comes to the characterisation of cell structures, proteomics remains the method of choice. Proteomic approaches directly look at the components of a structure, rather than the genes that encode them, and can be combined with fractionation techniques to specifically focus on the subcellular fraction in question. Success stories in the history of 'subcellular proteomics' include the proteome characterisations of nuclear pore complexes [233] phagosomes [234], mitochondria [235], centrosomes [236], chloroplasts [237], nucleoli [238], and others [239-241].

Using the above rationale, this study sought to characterise the components of fenestrae from cultured cells in which they are present in high abundance. Since the lack of a specific molecular marker hindered the isolation of pure fenestrae for characterisation, the approach taken was that of enriching for fenestrated plasma membranes and performing a subtractive proteomic analysis against plasma membranes from cells without fenestrae. A key element was the use of the cationic colloidal silica isolation technique that resulted in significant plasma membrane enrichment over the whole cell homogenate. A caveat inherent in the method was the masking of any ultrastructure associated with the extracellular leaflet of the plasma membrane due to the size of the silica pellicle [228], thus preventing the visualisation of presumably enriched fenestrae for quality control purposes. Nevertheless, given that in induced cells the majority of the plasma membrane is fenestrated, and that a combination of biochemical and ultrastructural evidence indicated that plasma membranes were isolated with comparable yields from induced and uninduced cells,

suggested that the procedure was effective in the isolation of fenestrae. Furthemore, the potential loss of fenestrae in the course of the isolation protocol should be circumvented, as silica coating reportedly prevents the lateral mobility of proteins to which it binds, preserving the spatial and temporal characteristics of membrane domains [229, 231, 232]. The compatibility of the silica isolation method with proteomics was recently shown in two papers concerned with lung endothelial surface heterogeneity [242, 243]. Validation for its effectiveness in this study came with the identification of candidate proteins, such as cofilin, whose levels were only altered at the level of the plasma membrane, and ultimately with the discovery of fenestrae sieve plate components.

In general, subtractive proteomic approaches yield a smaller and more manageable set of candidate proteins than high-resolution whole proteome analyses. In such a differential expression approach, the size of the candidate set can vary depending on the level of differences between the samples under comparison, and the stringency criteria set by the investigator. In this comparison plasma membranes of identical cell types differing in their treatment with an actin-disrupting agent, only spots that were either unique, greater than 2-fold upregulated in the treated sample, or increased in the treated sample with a confidence interval of $p<0.05$ were considered, resulting in a set of 26 unique protein identities. Often, the same spot yielded more than one protein identity. This can be attributed to the non-absolute method of identity assignment used that is based on matching mass fingerprints rather than amino acid sequences against protein databases. When the ambiguity between two or more identities could not be resolved, they were all deemed possible, taking into account the limitations in the identity assignment method and the resolving capabilities of the 2d-gel itself.

Overall, out of 26 protein identities, 23 were characterised gene products, 2 had been previously identified in functional screens (Ras suppressor protein 1, interferon-

activatable protein 205), and one was partially characterised on the basis of structural similarity to known proteins (putative RNA-binding protein 3).

4.4.2 Categories of candidate proteins

Categorisation of proteins on the basis of their reported, or in some cases putative, subcellular localisation indicated that a total of 60% was associated with the plasma membrane and the co-purifying cytoskeleton, and another 32% with various other cytoplasmic structures. Within the set of plasma membrane associated proteins, none of the proteins had membrane spanning regions, and instead were peripherally attached or lipid anchored to the bilayer. Categorisation of proteins with respect to their function, indicated that the majority of candidates were involved in membrane remodeling or endocytic processes, while a great proportion was also occupied by actin binding proteins, cytoskeletal motors, and proteins with roles in transcription or translation. Validation of candidates by immunoblotting or immunofluorescence was pursued for proteins with interesting function or localisation, but was not always possible due to lack of antibody availability or suitability in particular techniques. Where validation was possible, all protein changes were confirmed by either or both methods, apart from that of annexin II whose upregulation remains questionable. When viewed in the context of fenestrae, candidate proteins, validated or not, can be split into two categories: those of structural components and those involved in some stage of fenestrae biogenesis.

The role of cytoskeletal remodeling in fenestrae formation has been well documented by us and others [95, 97, 178, 244, 245], thus the abundance of cytoskeleton associated proteins within the candidate list was expected. Cofilin binds to both monomeric and filamentous actin and is reported to increase actin filament

disassembly by depolymerising filaments from their pointed ends and by inhibiting spontaneous nucleotide exchange on monomeric GDP-bound actin [246, 247]. Twinfilin (or protein tyrosine kinase 9) has a less clear role in actin dynamics, though its ability to sequester actin monomers and prevent their nucleotide exchange is believed to inhibit monomer assembly [247, 248]. Transgelin is the least characterised of the actin binding protein candidates, but reportedly plays a role in cross-linking actin filaments into aggregates [249, 250], seemingly opposite to the functions of cofilin and twinfilin. These endogenous actin binding proteins could have roles in the actin-filament disassembly that is required for fenestrae formation as aids to the exogenously added latrunculin A, which presumably drives the process. It is unlikely that any of them would be structural components of fenestrae, as exemplified by the validation of cofilin as an upregulated candidate in the membrane/cytoskeleton fraction, but not in the specific structure of interest.

Myosins and kinesins are molecular motor proteins that move on actin-filaments or microtubules, respectively, performing work in a cell [251-253]. Both are found as oligomers of heavy and light chains, with heavy chains serving as motor domains and light chains having either regulatory roles, in the case of myosins, or determining subcellular localisation and cargo selection in kinesins [251-253]. Although only light chains were identified in this screen, the entire protein functional unit will be considered. In a model of fenestrae biogenesis consistent with a large re-organisation in the architecture of a cell, one can foresee the need for organelle movement and re-localisation. Myosins and kinesins could catalyse this process by driving vesicles and organelles to or away from the area that is about to become fenestrated. Latrunculin A is reported to induce the internalisation of caveolae and their movement along microtubules [254], and whether or not related to fenestrae formation, this could be driven by kinesin. Interestingly, the presence of myosin near fenestrae has been

previously described as part of an actin cytoskeleton ring that surrounds and regulates the size of the pore [98].

Apart from cytoskeletal disassembly and organelle movement, an obvious part of fenestrae biogenesis is the remodeling of the membrane itself, from a continuous structure to that of a discontinuous one, intermitted by numerous pores. Endocytosis, as a means of membrane cycling from the plasma membrane to some internal organelle is a plausible mechanism for such membrane remodeling, and in this context, the tumor promoter Nm23, has been shown to be necessary for dynamin-mediated endocytosis of adherens junctions [145]. Paralemmin is another protein implicated in plasma membrane dynamics, through its association with the cytoplasmic face of membranes at sites of plasma membrane activity and its ability to induce cell expansion and process formation [255]. Annexin II, a protein found both in the cytoplasm and bound to membranes, is implicated in membrane sorting and trafficking through its essential role in the dettachment of multivesicular bodies from early endosomes [256]. Interestingly, annexin II was found upregulated in bEND5 versus Py4.1 cells, in a transcriptional profiling comparison (data not shown). Annexin had been identified as a major component of fusogenic membranes [257], and in this context could provide an explanation for the increased susceptibility of bEND5 cells for fenestrae formation.

Finally, radixin and moesin, representing the ERM family of proteins, can link the fundamental processes of actin disassembly and plasma membrane remodeling through their role as membrane-cytoskeleton adaptors [258]. Interestingly, upregulation for the phosphorylated version of moesin was validated by western blotting, and localisation of one or both proteins in fenestrae sieve plates was confirmed by immunofluorescence using an antibody of dual specificity. Their specific role in fenestrae biogenesis will be further addressed in the following chapter.

Candidate proteins with seemingly irrelevant functions and localisations could be contaminants due to the nature of the isolation protocol. The particularly high proportion of nuclear proteins can be explained by the inefficient gradient centrifugation step employed to separate silica-coated membranes from nuclei. Also, polycationic proteins such as RNA binding proteins, could non-specifically adsorb to the polyanionic polyacrilic acid crosslinker of the silica after tissue disruption, and co-purify with the membrane pellet. No protein should be completely disregarded, however, as it is not unusual for proteins thought of as residents of particular organelles, to be later discovered in secondary subcellular compartments. In relevance to this analysis, alpha-enolase, a glycolytic enzyme residing in the cytosol, has been subsequently found to associate with the plasma membrane and act as a receptor for plasminogen [259, 260]. Furthermore, in a recent mass-spectrometry study, RNA binding proteins such as hnRNPs were unexpectedly identified as components of focal adhesion complexes [261]. In the same study, validation of these candidate proteins by immunofluorescence, highlighted a novel function for RNA binding proteins as components of spreading initiation centers at the initial stages of focal adhesion assembly [261]. One can envision that in the course of fenestrae biogenesis, attachments to the substratum undergo remodeling too. The absence of the typical vinculin staining that is characteristic of focal adhesions from fenestrated cells (data not shown) suggests that focal adhesions need to be disassembled. The candidate protein hnRNP K could participate in such a process that would essentially be the reverse of its newly reported function.

4.4.3 Integral versus peripheral membrane proteins in fenestrae

The fact that none of the identified proteins had transmembrane domains was unexpected, but can be attributed to one or more of the following reasons: (1) technical problems associated with 2d-gel electrophoresis of membrane proteins, (2) integral membrane proteins being present in the 18 spots that were not identified by mass spectrometry, (3) no novel protein components being inserted in the membrane upon fenestrae formation. Although 2D-gel electrophoresis provides the highest resolution among protein separation techniques, a number of limitations are encountered when the technique is applied to membrane proteins [262] . The major impediments are the poor solubility of hydrophobic proteins in the chaotrope-detergent mixtures of the isoelectric focusing, and the precipitation of some solubilised proteins out of solution when they migrate to their isoelectric point. This is reflected in published protocols that aim to improve the solubilisation of membrane protocols using organic solvents [263, 264] and new detergent mixtures [265-267]. Alternatively, the need for solubilisation is often obviated altogether by coupling 1D-gel electrophoresis, and occasionally liquid chromatography for increased resolution, to mass spectrometry [268-271]. It should be stressed that the most difficult part in the solubilisation process of a membrane protein is its dissociation from the hydrophobic environment of the lipid bilayer. In the case of silica-coated membranes, the proteins are already released from the bilayer upon removal of the silica with 2% SDS. Thus, the resolubilisation of the proteins in the isoelectric focusing buffer after acetone precipitation should be less of an obstacle. A pellet was obtained after resolubilisation, suggesting the presence of some insoluble components, however no bands were visible when it was subjected to 1D SDS-PAGE analysis (data not shown).

The presence of transmembrane proteins among the 18 unidentified spots is another plausible explanation for their absence from the list of candidate proteins. This seems less likely from a statistical point of view, as there were no transmembrane proteins in 22 out of a total of 40 spots, and also none at all in the Py4.1 set, where identities were obtained for all spots. Failure to obtain a peptide mass fingerprint is commonly due to insufficient protein amounts, therefore scaling up the procedure would be required to obtain a definitive answer.

A much more conceivable explanation is the absence altogether of any novel protein insertion in the lipid bilayer during fenestrae biogenesis. In the case of a mere lateral rearrangement of existing proteins, there would be no differences in protein content between the plasma membranes of an induced and an uninduced cell. The high membrane curvature at the rim of fenestrae could be due to the recruitment of proteins from different parts of the same membrane into a structure that overcomes the resistance of mechanically bending the membrane. Alternatively, the observed membrane deformation could be due entirely to lipids or the presence of peripheral proteins. Different lipid species reportedly favour low or high membrane curvature, depending on their geometries or physico-chemical properties [272], and may have a heterogeneous distribution to favour budding or fusion [273, 274]. Similarly, peripheral membrane proteins can drive membrane curvature, as seen with coat proteins on vesicles [275, 276] and dynamin assembly into rings and spirals that drive tubule formation [277].

There are many ways in which the current molecular characterisation approach can be improved to yield more information. Given the lack of a unique molecular marker for the specific purification of fenestrae, the silica isolation approach would still be the preferred method for enrichment of the structure. Unfortunately, unlike the isolation of caveolae [231, 232], the lack of distinct ultrastructure upon silica binding also

prevents the selective purification of the structure from the remainder of the membrane. Nonetheless, the membrane subfraction can be further fractionated non-specifically to enrich for proteins with particular physico-chemical proteins. Peripheral proteins are known to be released by sodium carbonate at pH11.5 [278], while organic solvents [279, 280], detergents [239], or chaotropes [239] can enrich for subsets of proteins depending on their hydrophobicity. Silica-isolated membranes have been previously shown to fractionate into caveolae, other detergent resistant membranes, and an insoluble membrane pellet attached to silica, using a combination of sonication, potassium phosphate, and detergents [231]. Applied to this system, different fractions of the membrane subfraction could be isolated and compared separately in 2D-gels that would be less complex and enriched for particular protein types. Complexity in such a 2D-gel could be reduced even further, by focusing on a narrow pI and molecular weight range. Finally, the most hydrophobic proteins that are resistant to solubilisation in the 2D-gel buffer could then be analysed separately on a 1d-gel.

A variation to the classical subtractive proteomic approach of comparing normal to disease states is that of differentially analysing cross-contaminated cellular subfractions, to highlight proteins unique to particular structures. A recent study on the nuclear envelope proteome, showed the purification and proteomic analysis of nuclear envelopes in addition to organelles known to co-fractionate with them [281]. Unique nuclear envelope proteins were subsequently identified by subtracting the organelle-specific proteins from the nuclear envelope data set [281]. An analogous comparison of silica-isolated plasma membranes contaminated with nuclei against purified nuclei would pinpoint proteins that are specific to the membrane. To further simplify this subset of proteins they could be the focus of yet another round of subtractive proteomics between untreated and induced samples. As there is no single

approach for the optimal protein characterisation of fenestrae, it seems that a combination of strategies should be pursued in order to exhaust their proteome.

This study was the first to use a subtractive proteomic comparison of organelle – rich to organelle - deficient states of the same cell type, in order to define such an organelle's protein complement. It was also the first successful attempt to discover and validate proteins of the fenestrae sieve plate. In a similar fashion to PV-1 however, moesin and radixin are not unique to fenestrae, and may form part of other cell structures. Deciphering the relationship of more candidates to fenestrae will be a challenge, and may require functional tests in addition to expression validation. In the next chapter, the characterisation of moesin and radixin within fenestrae sieve plates will be presented, and the biological significance of this novel relationship will be addressed.

Chapter 5: Moesin as a component of the fenestrae sieve plate

5.1 Background

Moesin and radixin, two newly identified components of the fenestrae sieve plate, are members of the ERM (ezrin-radixin-moesin) family of proteins, which are known to act as adaptors between the cortical cytoskeleton and the plasma membrane [282]. The three closely related proteins ezrin [283], radixin [284], and moesin [285], that make up the ERM family, along with the related protein merlin [286, 287], belong to the larger 4.1 superfamily of proteins, the members of which are characterised by a FERM (four-point one, ezrin, radixin, moesin) domain at their amino terminus [286, 288-290]. The N-terminal domains of ERM proteins are highly conserved with approximately 85% homology, and are responsible for interacting directly or indirectly with integral membrane proteins [258, 291]. Following the ~300 residue N-terminal domain is an extended alpha-helical domain and finally an ~80 residue C-terminal filamentous actin (F-actin) binding domain, which represent the less conserved regions within the ERM proteins [258, 291]. Merlin, the product of the *Neurofibromatosis 2* tumor suppressor gene [286, 287], contains an N-terminal FERM domain, shares some binding partners with ERM proteins at the plasma membrane but lacks an F-actin binding domain at its C-terminus[258]. Nevertheless, it too has been reported to interact with F-actin, through actin binding regions within the FERM domain [292, 293].

Consistent with the high degree of structural similarity between ERM proteins is their reported functional redundancy. Although they show a wide distribution that appears to be regulated in a tissue-specific manner [294, 295], a moesin knockout mouse is viable with no obvious abnormalities [296], while a radixin deficiency is partially complemented by the upregulation of ezrin in a radixin null mouse [297]. To further complicate matters, it appears that all ERM proteins are co-expressed in cultured cells

[282, 291, 294, 298], putting an obstacle to manipulations destined towards understanding their function. The use of constitutively active [299-301] or dominant negative [302-304] versions of the proteins, however, have shed light onto their crucial roles in cell polarity and morphogenesis. ERM proteins have been implicated in functions ranging from the determination of cell shape, adhesion, motility, cytokinesis, phagocytosis, to integration of membrane transport with signaling cascades [258]. The related protein merlin shares a number of the aforementioned functions [305].

Regulation of the ERM protein function is thought to occur at the level of their conformation, which then translates to a particular subcellular localisation. An inhibitory interaction between the FERM domain and the C-terminal domain maintains ERM proteins as monomers, and confines them to the cytoplasm [306, 307]. Interaction with phosphatidylinositol 4,5-bisphosphate (PIP_2) through the FERM domain followed by phosphorylation at a conserved threonine residue in the C-terminal domain, are thought to unmask both membrane and actin binding sites [308-310]. Inhibitory interactions can occur intermolecularly as well as intramolecularly, however the significance of the oligomeric states is currently unclear [300, 306, 311]. ERM phosphorylation and phospholipid binding have been proposed to lie downstream of the Rho signaling cascade [308, 312-314], while an ERM function downstream of Rac has also been reported [315]. ERM proteins have also been shown to function upstream of Rho, either as positive [316], or as negative [317] regulators, suggesting the presence of a feedback mechanism.

My aim in this study was to characterize these novel components of fenestrae sieve plates. *In vitro* and *in vivo* evidence was accumulated to support the presence of the ERM protein moesin within fenestrae. The subcellular distribution, phosphorylation state, and detergent solubility of the protein were assessed in the bEND5 cell line.

Furthermore, the potential role of moesin in fenestrae biogenesis was addressed through a time-course of fenestrae formation and immunoprecipitation experiments.

5.2 Results

5.2.1 Specificity for sieve plate localisation within the ERM family

The presence of all ERM family members in most cultured cells, and specifically their co-existence in the cell lines susceptible to fenestrae formation, prompted an investigation into the subcellular distribution of each member (Figure 5.1). Latrunculin-induced bEND5 cells were immunostained for ezrin, radixin, moesin, or the related protein merlin. To ascertain for fenestrae localisation, anti-PV-1 (MECA-32) was used as a counterstain that marks fenestrae sieve plates. Interestingly, and despite the reported functional redundancies, the only two ERM members that localised to sieve plates were the ones identified in the proteomic study, moesin (Figure 5.1, A-C) and radixin (Figure 5.1, J-L). In contrast, ezrin (Figure 5.1, D-F) and merlin (Figure 5.1, G-I), appeared to be excluded from the sieve plates, and instead were confined to the cytoplasmic spacers between them.

A frequent problem encountered in the study of individual ERM family members is the cross-reactivity of the antibodies with different ERM proteins. A combination of antibodies that were first assessed by western blotting on bEND5 cell lysates (data not shown) was thus employed to draw definitive conclusions for particular ERM members. The subcellular localisation of moesin was determined using a rabbit polyclonal antibody that recognised both moesin and radixin on a western blot, and also a mouse monoclonal antibody that recognised only moesin on a western blot. Two independent antibodies were also used in the case of ezrin; a mouse monoclonal antibody and a rabbit polyclonal antibody. Both antibodies appeared specific for ezrin by western blotting, however slight immunoreactivity with fenestrae sieve plates was observed in the case of the mouse monoclonal antibody, especially at high antibody

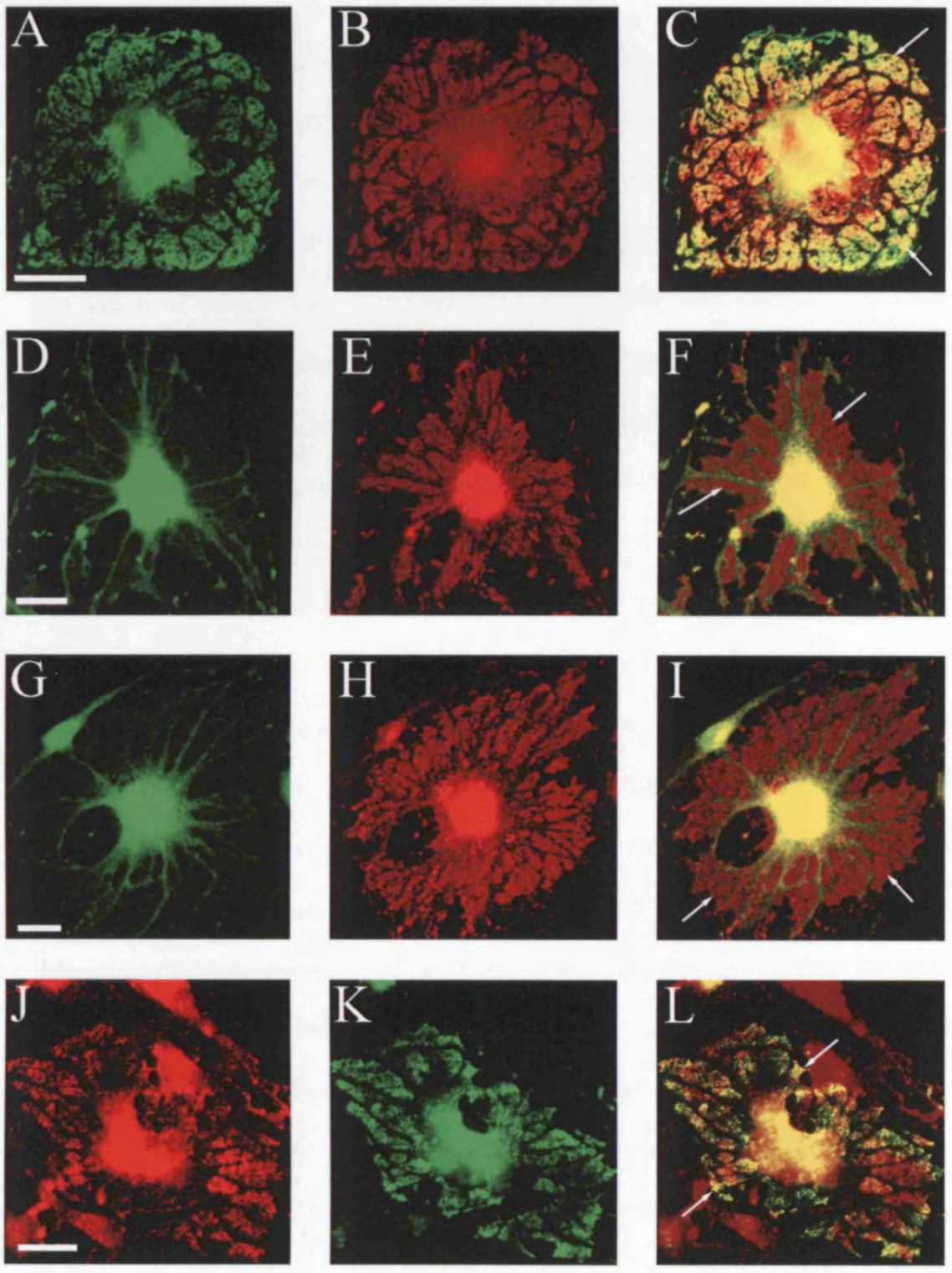

Figure 5.1 ERM family distribution within fenestrae patches. bEND5 cells, induced with 2.5 μM Latrunculin A for 3 hours, were immunostained for moesin (A), ezrin (D), merlin (G), and radixin (J) and counterstained for PV-1 (B,E,H,K), to mark the location of fenestrae. Overlays of the antibody combinations are shown in C,F,I, and L. Moesin (A) and radixin (J) appear to colocalise with the PV-1 staining on fenestrae (B,C) and (K,L), respectively, while ezrin (D) and merlin (G) appear excluded from the PV-1 positive regions of the cell (E,F) and (H,I), respectively. Epifluorescent images are shown, and representative fenestrae patches are marked by arrows. (Bar = 20 μm)

concentrations. Since the majority of ezrin was confined to the cytoplasmic arms around sieve plates, and immunostaining with the rabbit polyclonal antibody showed no reactivity with fenestrae, the low labelling obtained with the mouse antibody was attributed to cross-reactivity rather than true localisation of ezrin. The subcellular localisation of radixin was determined using a goat polyclonal antibody that only recognised radixin by western blotting. Finally, an unambiguous classification could be performed for merlin, as it is less homologous to the ERM proteins than family members are between them, and the rabbit polyclonal antibody against it appeared specific for the protein by western blotting.

The specificity displayed by ERM family members and merlin for fenestrae in cultured endothelial cells was mirrored in an analysis of a fenestrated capillary bed *in vivo*. The choriocapillaris of the eye was chosen as a suitable tissue for analysis, as it contains fenestrae with diaphragms [318, 319] that can be visualised by immunostaining for the diaphragm protein PV-1 (Stephen Poor, unpublished observation). In triple stainings of eye sections (Figure 5.2), two distinct tissues were immediately visible: the retinal pigment epithelium, with immunoreactivity for ezrin (Figure 5.2 B,F), as previously reported [320, 321], and the fenestrated choriocapillaris, with immunoreactivity for both moesin [321] and PV-1 (Figure 5.2, A,C,E,G). A differential interference contrast (DIC) image of an eye section is included in Appendix III for orientation purposes. The overlay of all three channels, at both low (Figure 5.2, D) and high (Figure 5.2, H) magnifications, showed colocalisation of moesin and PV-1 within the same cell type, and exclusion of ezrin. Very weak immunoreactivity for moesin was detected for some parts of the retinal pigment epithelium, probably due to cross-reactivity of the rabbit polyclonal antibody used in the staining. It is noteworthy that the antibody used for the localisation of moesin displayed cross-reactivity for radixin on a western blot, however the absence

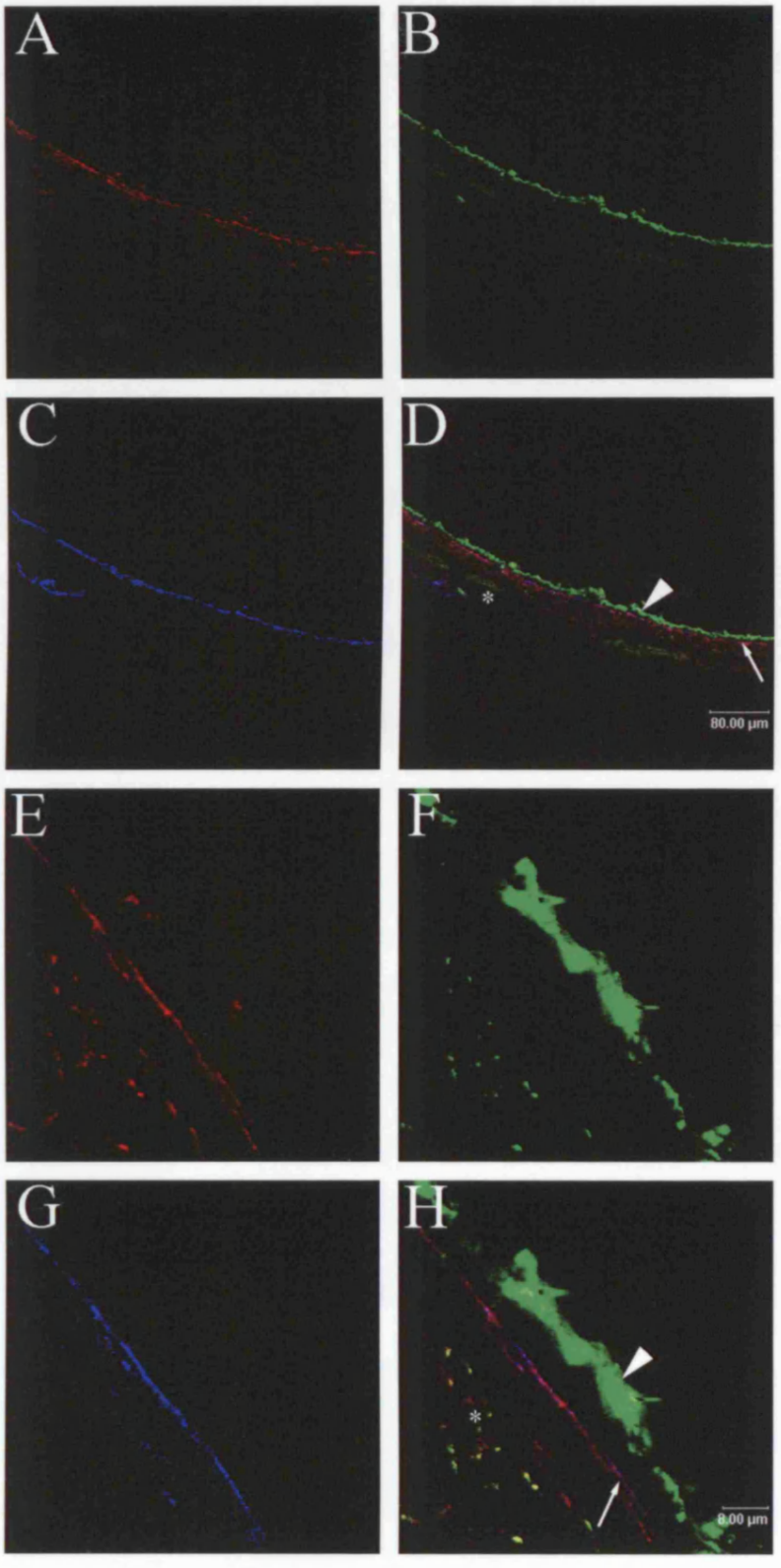

Figure 5.2 Distribution of ERM family members *in vivo*. Confocal analysis of mouse eye sections triply labeled for moesin (A), ezrin (B), and PV-1 (C). Moesin colocalises with PV-1 in the endothelium of the choriocapillaris (arrow), while ezrin is confined to the retinal pigment epithelium layer (arrowhead), as seen in the overlay (D). High magnification images of the same specimen labeled for moesin (E), ezrin (F), and PV-1 (G) are shown, along with the overlay (H). Some coincident staining between moesin and ezrin is seen in the sclera (asterisk), below the choriocapillaris.

of any immunoreactivity for radixin in the eye using the radixin – specific antibody, suggested that among the two, moesin was the most likely component of the choriocapillaris.

5.2.2 Characterisation of moesin in fenestrae sieve plates

5.2.2.1 Colocalisation studies of moesin with PV-1 and caveolin-1

In light of the distribution of moesin in fenestrated bEND5 cells and the choriocapillaris, its reported preferential expression in endothelium *in vivo* [294, 295], and the availability of better antibody reagents for assessing its distribution than in the case of radixin, moesin became the focus of further studies.

The first question concerned the specificity of the association between moesin and fenestrae sieve plates. High resolution confocal sections through the plane of PV-1 - positive sieve plates showed almost complete colocalisation of moesin with PV-1 (Figure 5.3, A-F). As seen more clearly in the magnified images (Figure 5.3, D-F), moesin was confined to the thin cell areas marked by PV-1, while it was absent from the cytoplasmic spacers that separated the sieve plates. In addition, moesin was present in filopodia, in agreement with studies in other cell types [298, 302], which were not stained by the anti-PV-1 antibody.

Given that PV-1 is a marker for the diaphragms of both fenestrae and caveolae, the next question was whether moesin also resided in caveolae. Untreated bEND5 cells were used to address this, as they display a characteristic and recognisable pattern of caveolae accumulated at the cell edges. In optical sections at the level of caveolae, moesin appeared to be evenly dispersed around the cytoplasm (Figure 5.3, G), with no specific enrichment in areas of PV-1–labeled caveolae (Figure 5.3, H-I). At higher magnification, moesin seemed slightly enriched in the region adjacent to caveolae

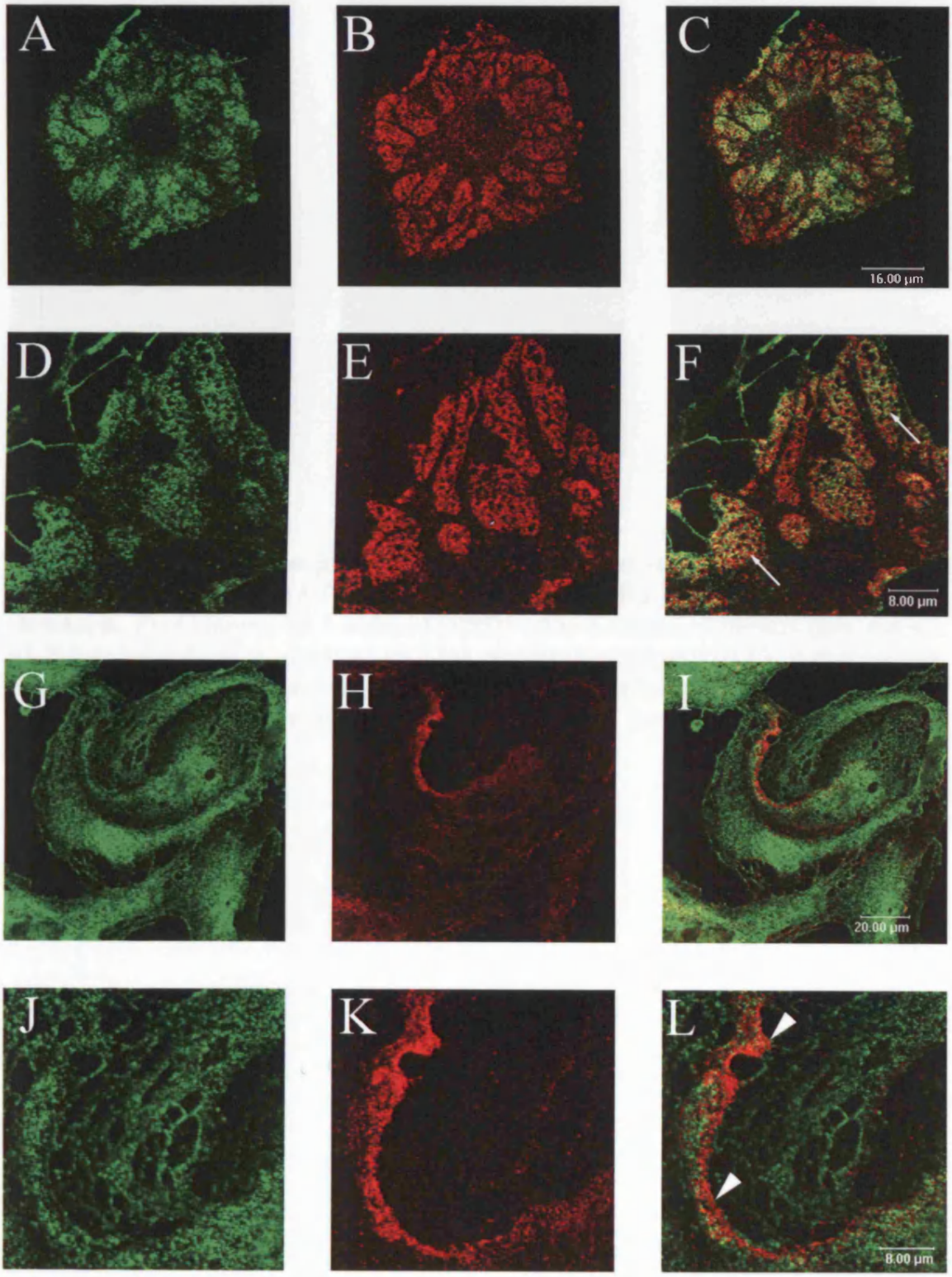
A
B
C
16.00 µm
D
E
F
8.00 µm
G
H
I
20.00 µm
J
K
L
8.00 µm

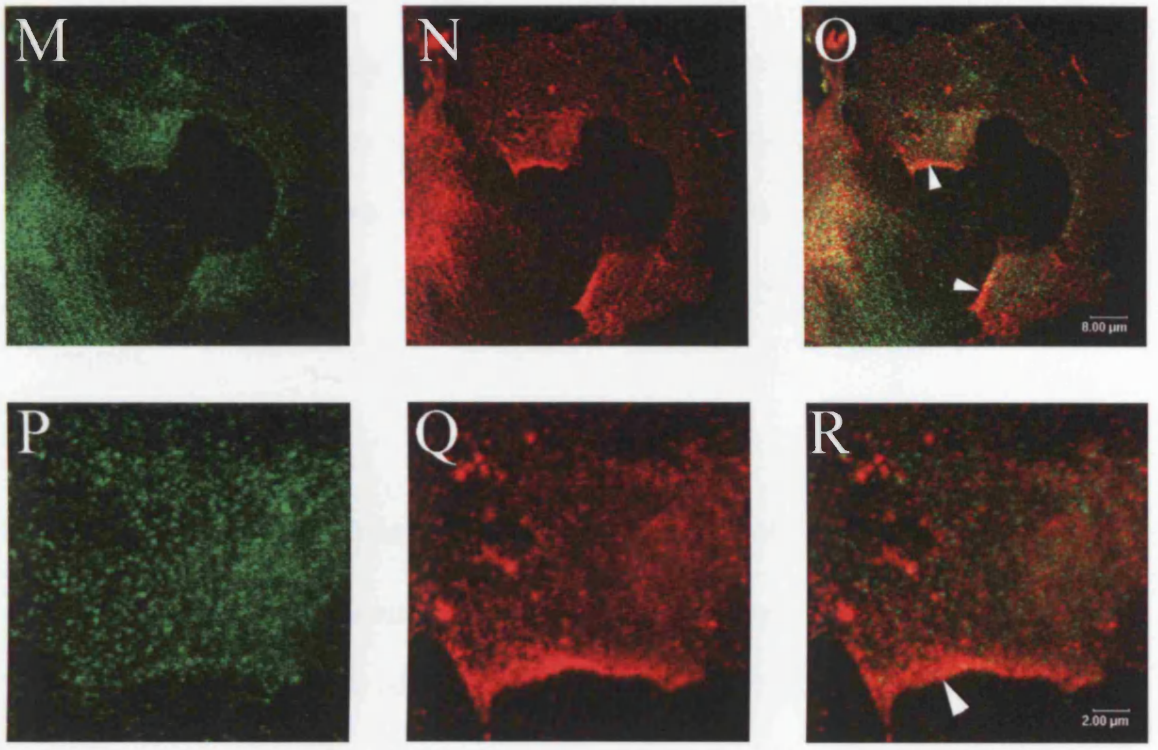

Figure 5.3 (continued from previous page) Colocalisation studies of moesin with PV-1 and caveolin-1. Moesin (A,D) colocalises with PV-1 (B,E) in fenestrae sieve plates (arrows) (C,F) of Latrunculin A-induced bEND5 cells. In untreated bEND5 cells, moesin (G,J) does not colocalize with PV-1 (H,K) in caveolae (arrowheads) (I,L). Labeling with caveolin-1 (N,Q) confirms that moesin (M,P) is not enriched in caveolae (arrowheads) (O, R). Confocal sections were obtained either at the level of fenestrae (A-F) or at the level of caveolae (G-R).

(Figure 5.3, J-L). Further confirmation for the absence of an association between moesin and caveolae came from a double immunostaining for moesin and the integral membrane caveolar protein caveolin-1 (Figure 5.3, M-R). The same diffuse staining of moesin was observed, with no coincidence of fluorescence between the two antigens.

5.2.2.2 Post-translational modification and solubility of moesin

The localisation and function of ERM proteins is reportedly dependent on their conformation, with active ERM proteins existing in an 'open' state, and inactive ones existing in a 'closed' state. Since binding to PIP_2 followed by threonine phosphorylation are the hallmarks of such an active form, the phosphorylation state of moesin was assessed by immunofluorescence using an antibody specific for the phosphorylated version of the protein (Figure 5.4). Moesin appeared phosphorylated in filopodia of untreated bEND5 cells, but not at its residence in the cell cortex (Figure 5.4, A-D). Coincidence of fluorescence between moesin and its phosphorylated version was also observed in fenestrae sieve plates of induced cells (Figure 5.4, E-H), suggesting that the protein is phosphorylated in that particular subcellular location.

According to the same hypothesis of phosphorylation – dependent regulation, phosphorylated ERMs associate with the actin cytoskeleton and have been shown to resist extraction by the detergent Triton X-100. This seemed puzzling, considering that fenestrae appeared in the areas of actin disruption, so a differential extraction of untreated or induced bEND5 cells was performed, using varying amounts of Triton X-100. Equal amounts of detergent soluble and detergent insoluble fractions were separated by SDS-PAGE gel electrophoresis, and western blotting was performed

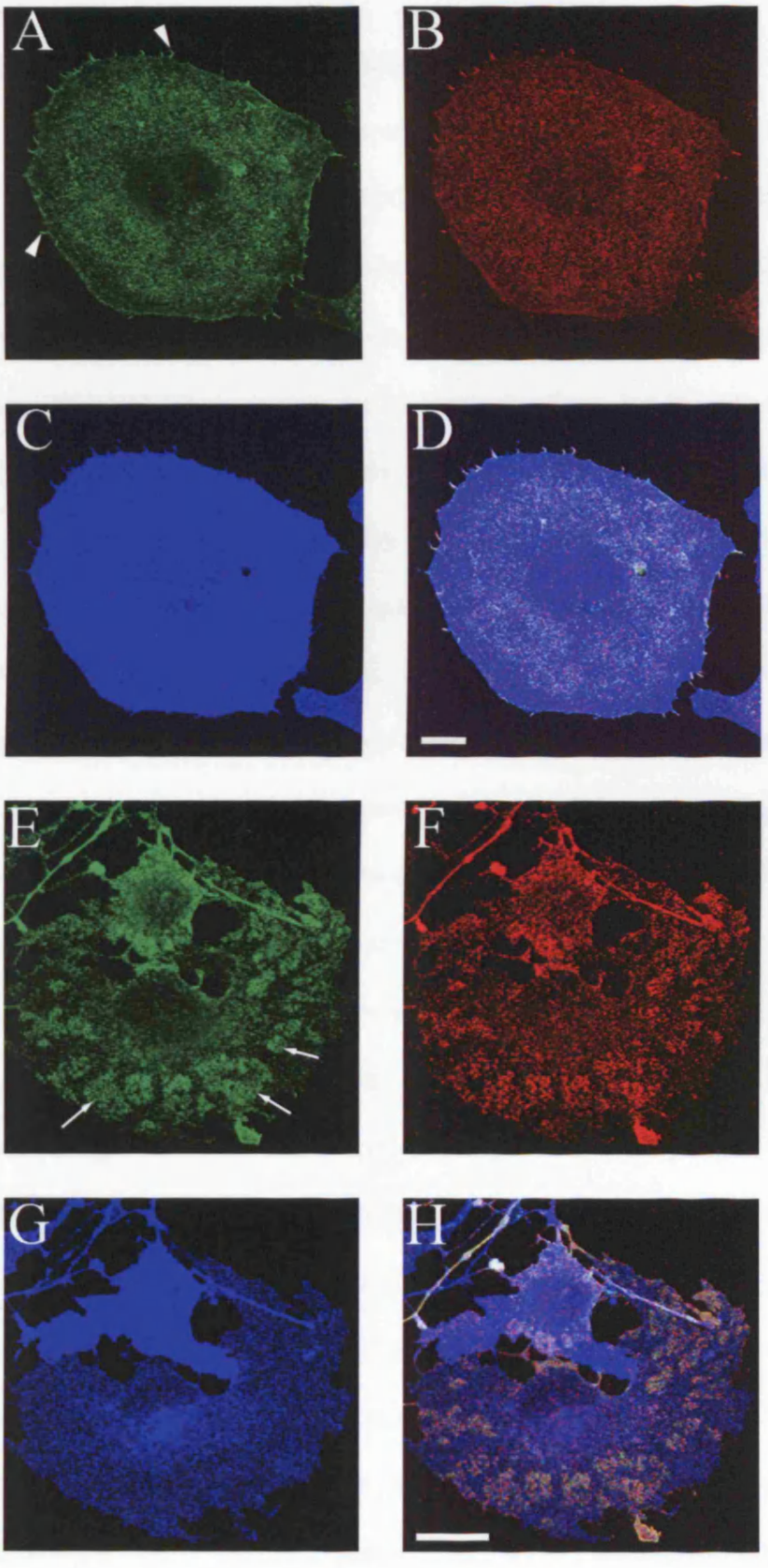

Figure 5.4 Analysis of moesin phosphorylation in untreated and induced bEND5 cells. Untreated (A-D) and Latrunculin A-induced (E-H) bEND5 cells were triple labelled for moesin (A,E), phosphorylated moesin (B,F), and PECAM (C,G), with the overlay shown in (D,H). Confocal sections were obtained at the level of filopodia (arrowheads) (A-D) and fenestrae sieve plates (arrows) (E-F). Moesin appeared phosphorylated in both structures. (Bar = 20 μm)

with antibodies against PV-1, moesin, phosphorylated moesin, and caveolin-1 (Figure 5.5). The diaphragm protein PV-1 appeared almost entirely detergent soluble, in untreated or induced cells, with Triton X-100 concentrations as low as 0.1%. Using the rabbit polyclonal anti-moesin antibody, which recognised both radixin and moesin, the two ERM proteins were shown to be mainly soluble in Triton X-100 detergent. A small amount remained in the insoluble fractions, but the low signal-to-noise ratio obtained with the antibody precluded the drawing of any meaningful conclusions. Detergent solubility did not vary as a function of detergent concentration, and in a similar fashion to PV-1, was independent of the induction state of the cell. When the phosphorylated version of moesin was probed using the specific antibody against it, again, the majority of the protein was present in the soluble fraction, an amount that did not alter in relation to the detergent concentration. Interestingly, when phosphorylated moesin was compared between untreated and induced cells, it was immediately apparent that a higher proportion of the protein resisted detergent solubilisation after induction. As a negative control, membranes were also probed for caveolin-1, an integral membrane protein which typically resists Triton X-100 solubilisation. In these cells caveolin-1 appeared to partition mainly in the detergent insoluble fractions, independently of the induction state of the cell, though some was rendered soluble with concentrations as low as 0.1% Triton X-100.

To examine the subcellular localisation of the insoluble portion of moesin and its phosphorylated counterpart, induced bEND5 cells were extracted with 0.1% Triton X-100 prior to fixation, using the same buffers as above, and processed for immunofluorescence. Cells extracted post–fixation were included for comparison. Consistent with the biochemical results of the extraction studies, PV-1 was completely extracted from the sieve plates where it resides in induced cells (Figure 5.6, A-B). Interestingly, the majority of moesin was extracted, but some insoluble

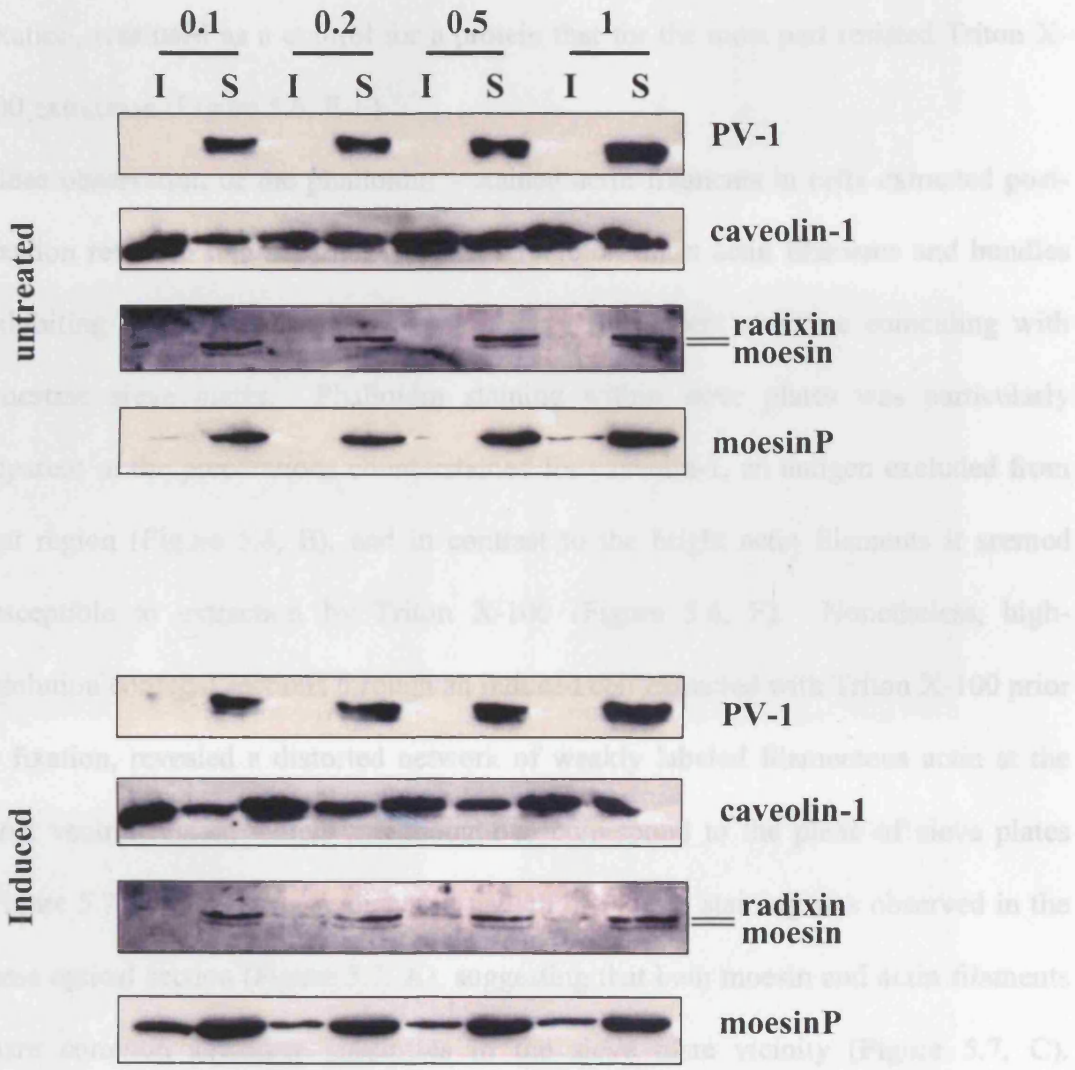

Figure 5.5 Detergent extraction of untreated and induced cells. Untreated or Latrunculin A-induced bEND5 cells were extracted with various concentrations of Triton X-100 (0.1, 0.2, 0.5, and 1%). Insoluble material was resuspended in the same volume as the soluble fraction, and equal volumes were separated by SDS-PAGE electrophoresis. Western blotting, using antibodies against PV-1, caveolin-1, moesin, and phosphorylated moesin, highlighted differences in the levels of insoluble phosphorylated moesin between induced and untreated cells.

material was left behind (Figure 5.6, C-D). Such detergent-resistant regions culminated to one or more of the short F-actin filaments that remained after latrunculin treatment. The localisation of caveolin-1, in cells fixed prior to and post fixation, was used as a control for a protein that for the most part resisted Triton X-100 extraction (Figure 5.6, E-F).

Close observation of the phalloidin – stained actin filaments in cells extracted post-fixation revealed two separate types of structure: short actin filaments and bundles exhibiting bright fluorescence, and a weakly fluorescent structure coinciding with fenestrae sieve plates. Phalloidin staining within sieve plates was particularly apparent in the preparations counterstained for caveolin-1, an antigen excluded from that region (Figure 5.6, E), and in contrast to the bright actin filaments it seemed susceptible to extraction by Triton X-100 (Figure 5.6, F). Nonetheless, high-resolution confocal sections through an induced cell extracted with Triton X-100 prior to fixation, revealed a distorted network of weakly labeled filamentous actin at the most ventral region, which was thought to correspond to the plane of sieve plates (Figure 5.7, B). A similarly distorted pattern of moesin staining was observed in the same optical section (Figure 5.7, A), suggesting that both moesin and actin filaments share common solubility properties in the sieve plate vicinity (Figure 5.7, C). Colocalisation attempts were inconclusive, as a result of the particularly weak signal for the sieve-plate-associated actin, and the likely alteration of the original structure by the detergent.

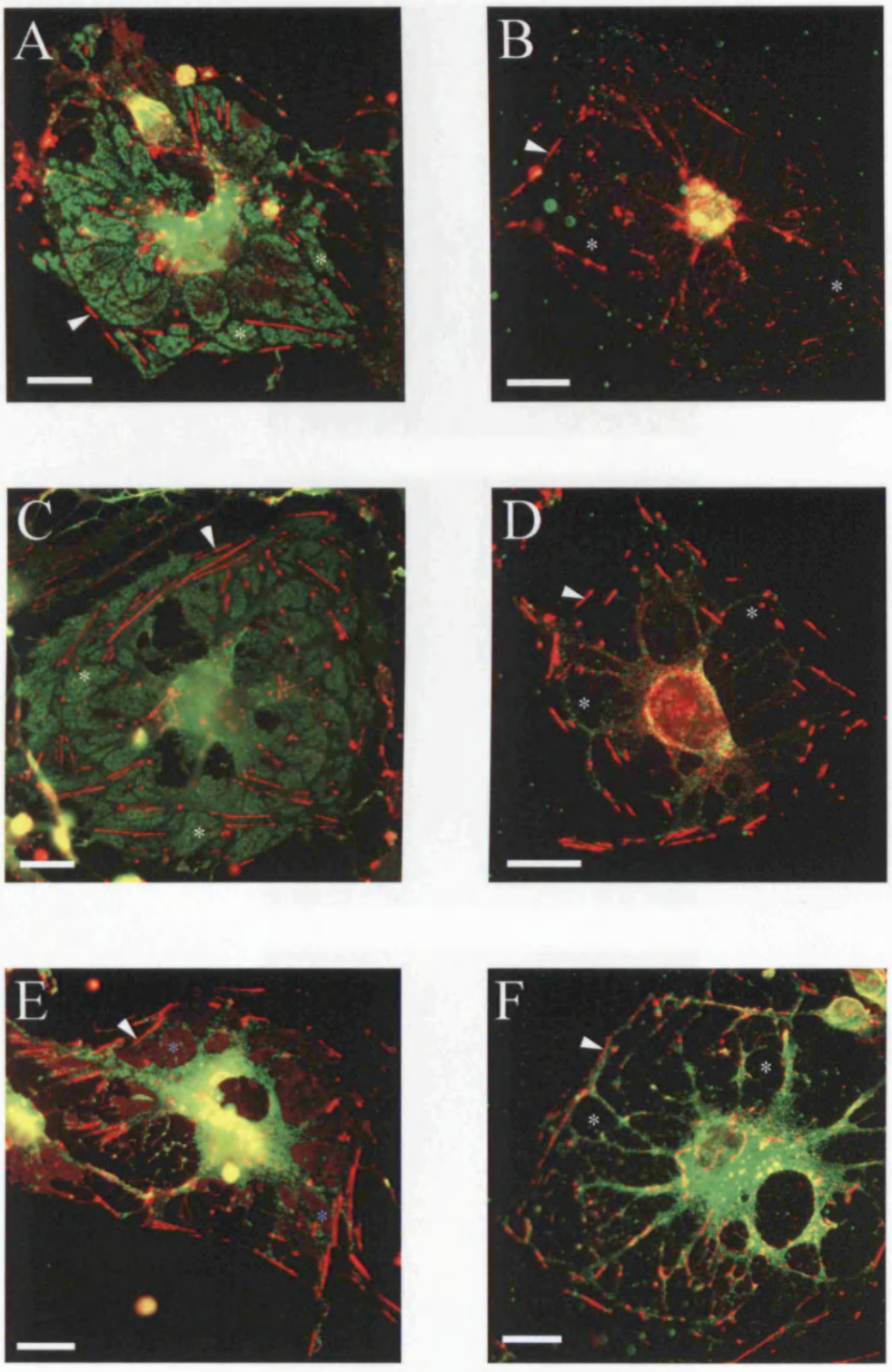

Figure 5.6 Epifluorescence microscopy on sieve plates after detergent extraction. Latrunculin A-induced bEND5 cells were detergent-extracted with 0.1% Triton X-100, after (A,C,E) or before (B,D,F) paraformaldehyde fixation. Cells were labelled for PV-1 (A,B), moesin (C,D), and caveolin-1 (E,F), with Alexa 488-conjugated secondary antibodies. F-actin was stained with Alexa 546-conjugated phalloidin (A-F). Short actin filaments resisting extraction are denoted by arrowheads. PV-1 along with moesin in sieve plates (asterisks) are extractable at this detergent concentration, while caveolin-1, in the cytoplasmic spacers between sieve plates, resists extraction. Light blue asterisks (E) mark sieve plates exhibiting weak phalloidin staining (Bar = 20 μm)

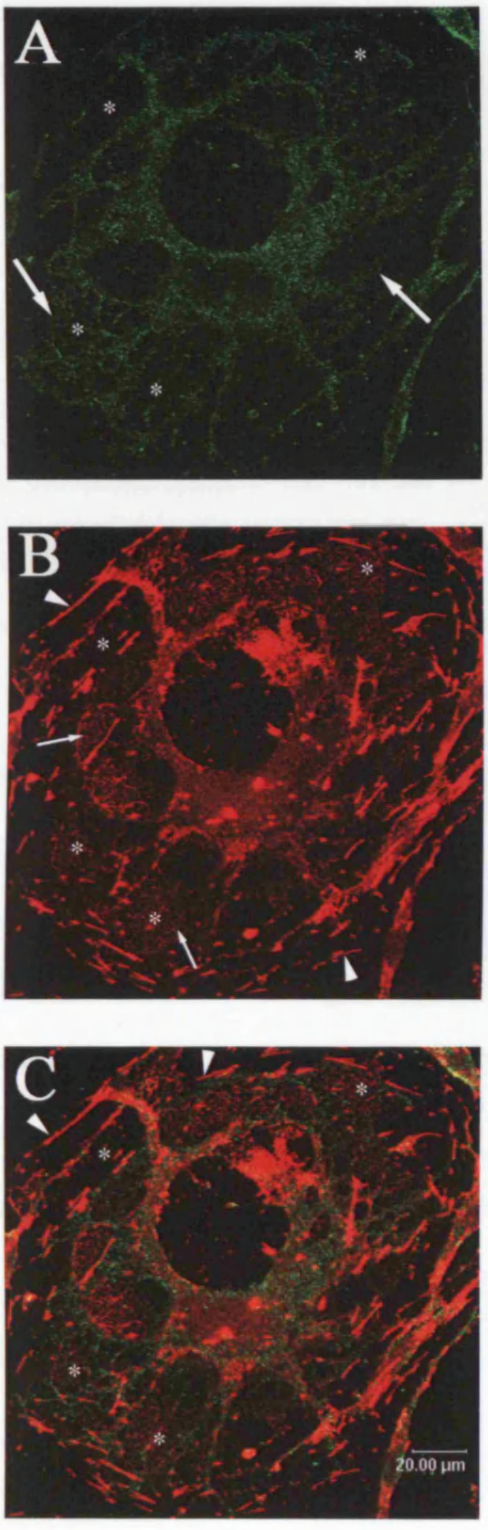

Figure 5.7 Confocal microscopy on detergent-extracted sieve plates. bEND5 cells, induced with Latrunculin A, were immunostained for moesin (A), using Alexa 546-conjugated phalloidin as a counterstain (B). Confocal sections obtained at the level of fenestrae sieve plates (asterisks) reveal the partial extraction of both moesin (A) and filamentous actin (B). Stress fibre remnants (arrowheads) were completelely resistant to detergent extraction, whereas the weakly fluorescent actin filaments within sieve plates were extracted in part, with their remnants (thin arrows) exhibiting a distorted filamentous pattern (B). A similar pattern was observed in the moesin remnants (thick arrows) (A), though colocalisation was difficult to ascertain with the given signal intensities (C).

5.2.3 Investigation into the role of moesin in fenestrae sieve plates

5.2.3.1 Actin distribution revisited

The unexpected finding of filamentous actin within fenestrae sieve plates provoked an examination of the actin content of untreated and induced bEND5 cells, using a variety of probes for actin and different fixation methods (Figure 5.8). Untreated cells fixed with methanol or paraformaldehyde, and probed for filamentous actin with Alexa 488–conjugated phalloidin, showed a similar pattern of bright stress fiber and cortical actin staining, with slightly better structural preservation when paraformaldehyde was used (Figure 5.8, A and C). Induced cells stained with phalloidin appeared different depending on the fixation conditions: only short microfilaments were apparent in the cytoplasm of cells fixed with methanol (Figure 5.8, B), while in addition to such microfilament remnants, a less intense signal emanating from sieve plates was visible in the case of paraformaldehyde – fixed cells (Figure 5.8, D). Moreover, the signal was specific for sieve plates, versus their cytoplasmic spacers, and for filopodia, and it was absent in induced cells that were fixed in methanol and probed with a monoclonal antibody that recognised all forms of actin (Figure 5.8, F). Furthermore, probing for globular actin, in paraformaldehyde fixed induced cells, using Alexa 488–conjugated Dnase I, confirmed that globular actin was absent from sieve plates, and was instead concentrated in the cytoplasmic arms surrounding them (Figure 5.8, H).

Taken together, these results suggested that some form of filamentous, and not globular, actin resides within sieve plates. The extraction of these filaments entirely by methanol fixation, and partially by Triton X-100 treatment before paraformaldehyde fixation, highlighted their different nature compared to the insoluble stress fibers, cortical actin, or short filaments after latrunculin treatment.

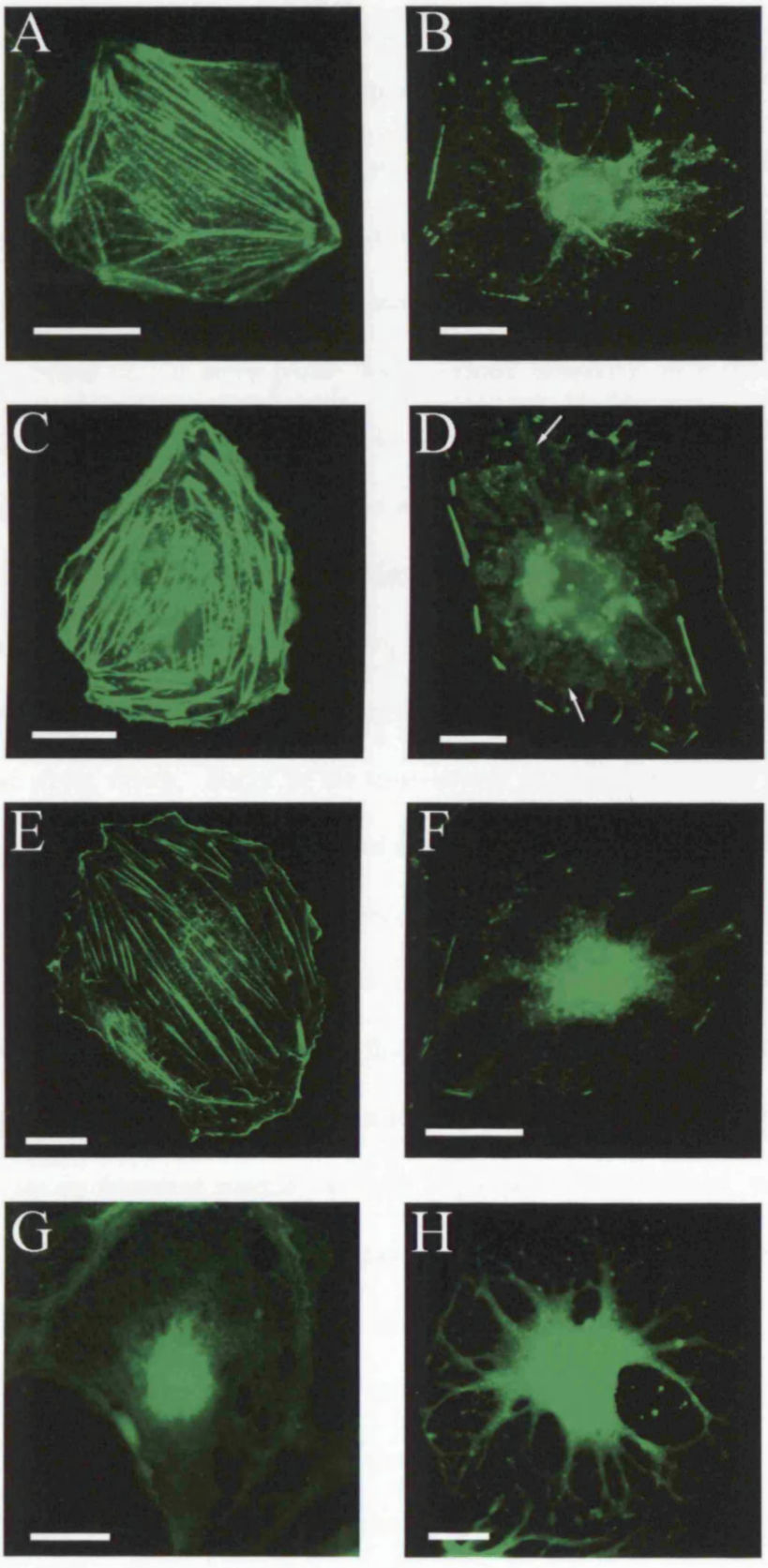

Figure 5.8 Visualisation of the actin cytoskeleton in untreated (A,C,E,G) and Latrunculin A-induced (B,D,F,H) bEND5 cells. Phalloidin stains filamentous actin in cells fixed with methanol (A,B) or paraformaldehyde (C,D), with more detail (arrows) revealed in the latter. Anti-actin AC15 mAb recognizes both globular and filamentous actin in methanol fixed cells (E,F). Dnase I stains globular actin in paraformaldehyde-fixed cells (G,H). Epifluorescent images are shown. (Bar = 20 μm)

5.2.3.2 Moesin in a time-course of fenestrae induction

The identification of F-actin elements together with moesin in fenestrae sieve plates, along with their common solubility properties, suggested a functional interplay between them. The potential role of moesin in linking the F-actin elements with the plasma membrane of the sieve plates was assessed indirectly, in a time-course of fenestrae induction with latrunculin A. Cells were triply labeled for PV-1, moesin, and filamentous actin (Figure 5.9). Under steady state conditions, PV-1 was confined to regions associated with caveolae, moesin was distributed throughout the cell with a preference for cell edges, while the cytoplasm of cells was spanned by numerous stress fibers. No significant colocalisation was observed between PV-1 and moesin or moesin and stress fibers. Early in the time-course of induction, stress fibers were reduced in number and size. PV-1 moved out of caveolae and migrated to the centre and the periphery of the cell, while moesin didn't appear to significantly alter in distribution. When stress fibers were reduced even further, and the cytoplasmic areas between them appeared devoid of actin, the first small fenestrae sieve plates began to appear, marked by the presence of both moesin and PV-1. The colocalisation became more obvious as fenestrae patches became larger and better defined, whilst at the same time the presence of a discrete network of actin filaments was apparent in the patches. Moesin and F-actin were also colocalised in filopodia emanating from the edges of the cell. When the induction stimulus was washed out after a three-hour induction, and the cells were re-incubated in normal culture medium for another fifteen minutes, a striking pattern was evident: PV-1 moved away from the cell periphery, and back towards the centre of the cell; moesin and actin formed a ring at the cell cortex, essentially surrounding the PV-1-positive area. When the re-incubation time following stimulus removal was extended to thirty minutes, the

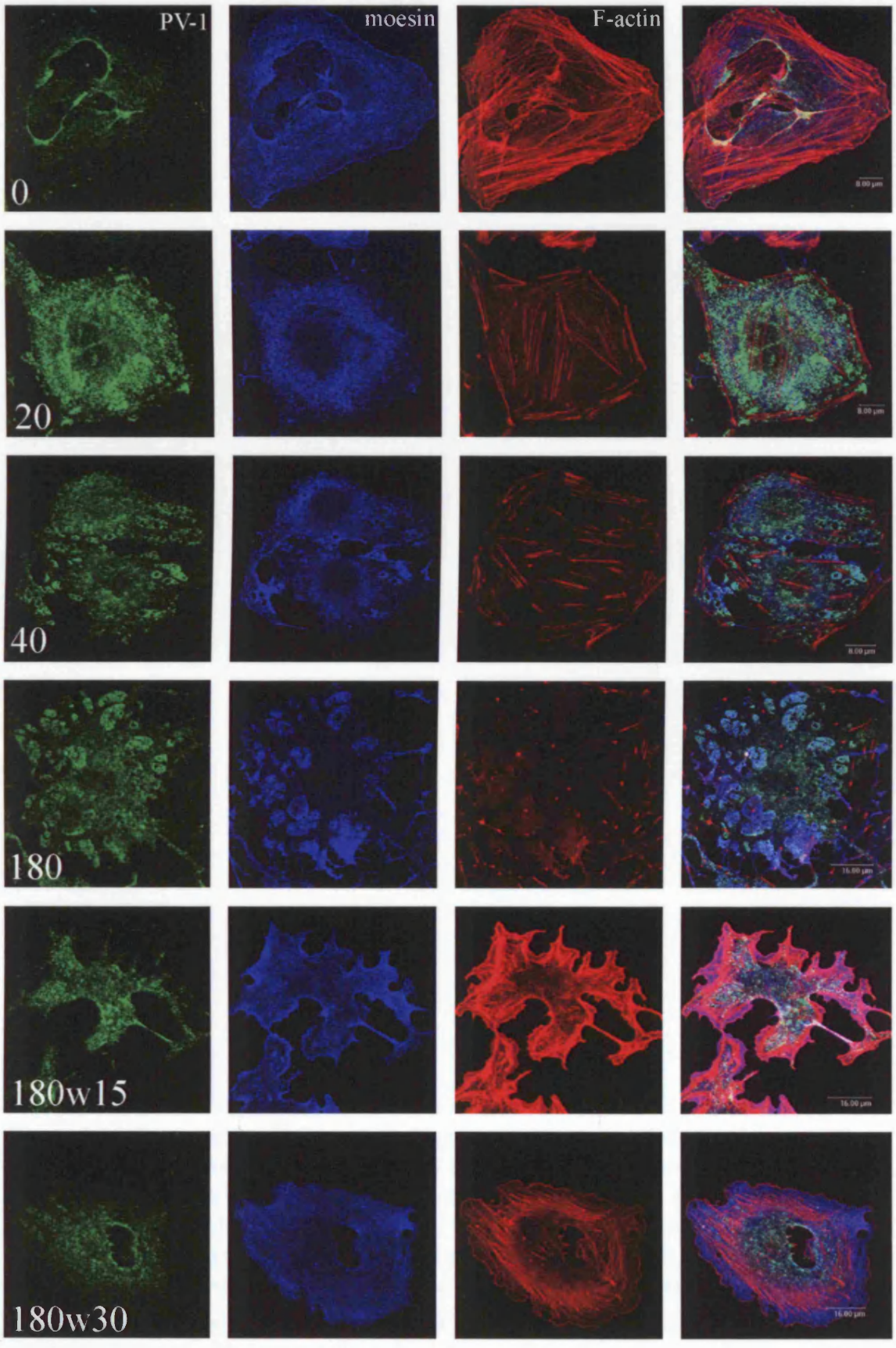
PV-1
moesin
F-actin
0
20
40
180
180w15
180w30

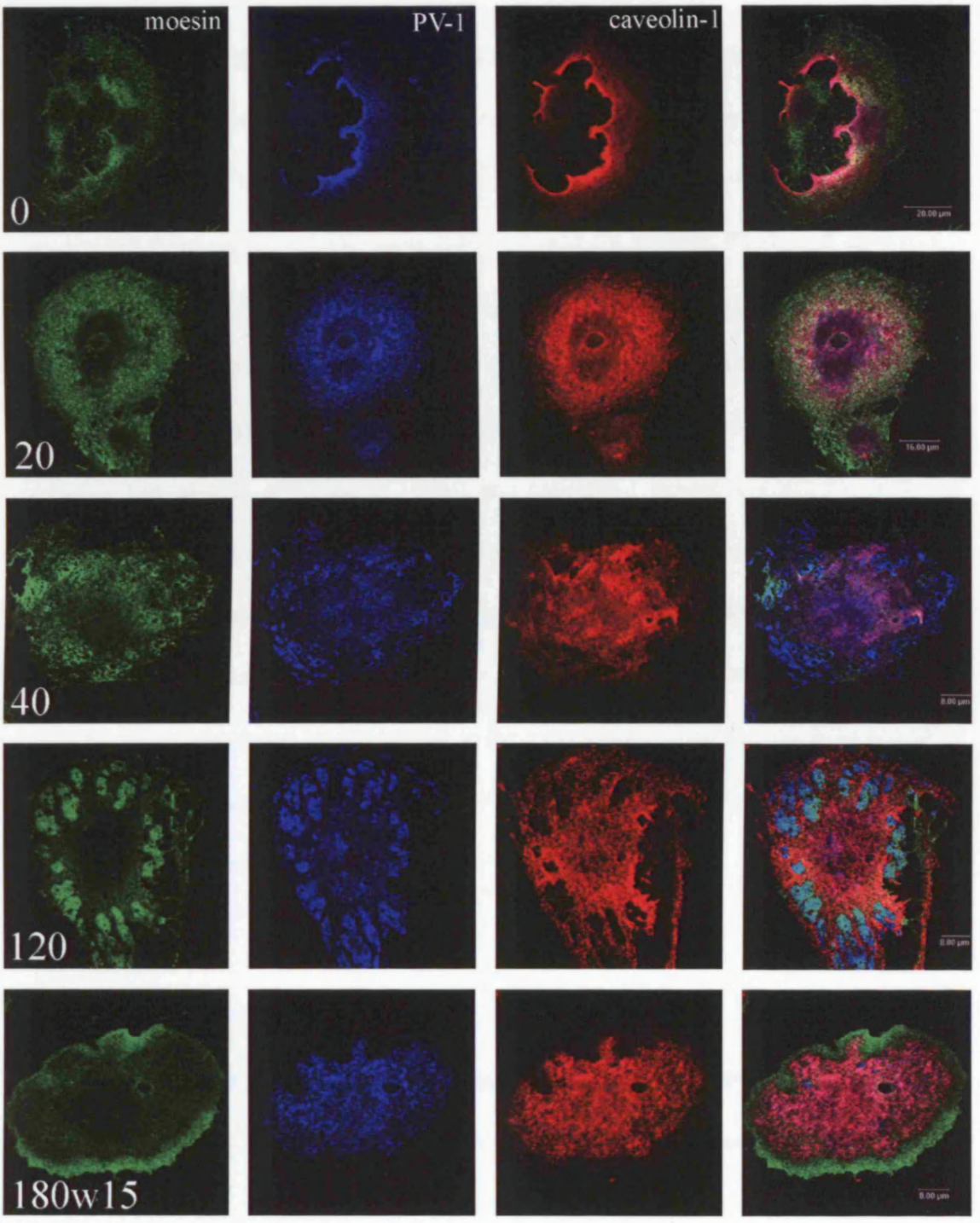

Figure 5.10 Time-course of induction by Light Microscopy II. bEND5 cells were induced with Latrunculin A for 3 hours, after which the stimulus was removed for 1 hour. Cells were fixed at various time-points and immunostained for moesin, PV-1, and caveolin-1, with secondary antibodies conjugated to Alexa 488, Alexa 633, and Alexa 546 respectively. Representative confocal sections are shown for 0, 20, 40, and 120 minutes of induction, along with 15 minutes of washing out the stimulus post-induction (180w15).

Figure 5.9 (previous page) Time-course of induction by Light Microscopy I. bEND5 cells were induced with Latrunculin A for 3 hours, after which the stimulus was removed for 1 hour. Cells were fixed at various time-points, immunostained for PV-1, and moesin, with secondary antibodies conjugated to Alexa 488 and Alexa 633, respectively, and counterstained with Alexa 546-conjugated phalloidin . Representative confocal sections are shown for 0, 20, 40, and 180 minutes of induction, along with 15 and 30 minutes of washing out the stimulus after 180 minutes of induction (180w15 and 180w30).

distribution of all three markers resembled steady state conditions. PV-1 became concentrated in caveolae, moesin was distributed throughout the cell, and a network of stress fibers was beginning to assemble.

In a parallel time-course, cells were triply labeled for moesin, PV-1, and caveolin-1 (Figure 5.10). In this case, at the steady state, PV-1 was found colocalised with caveolin-1 in caveolae, with moesin in the region immediately adjacent to them. When induction was initiated, the characteristic pattern of caveolae at the thick edges of cells disappeared, and instead PV-1 and caveolin-1 moved towards the centre of the cell. PV-1 was also targeted to the periphery of the cell, exhibiting the first signs of segregation from caveolin-1. The first patches of fenestrae that appeared in the cell periphery saw moesin and PV-1 colocalizing, and caveolin-1 excluded, while mature patches were surrounded by caveolin-1 in the cytoplasmic arms that lay between sieve plates. Interestingly, within fifteen minutes of washing out the stimulus, PV-1 had segregated from moesin, to coincide again with caveolin-1.

5.2.3.3 Immunoprecipitation studies

In view of the intimate spatial and temporal correlation between the presence of moesin and PV-1 in sieve plates, a physical association between the two was examined through immunoprecipitation experiments. Immunoprecipitations were carried out in lysates from untreated and induced bEND5 cells in an attempt to highlight differences between a state of potential interaction (fenestrae) and a state of definite non-association (caveolae). In addition, immunoprecipitation reactions were performed in lysates prepared in a variety of buffers (see Chapter 2), which had been previously used successfully in the isolation of ERM complexes [322-324] or were effective in solubilizing PV-1 and the majority of the moesin content of sieve plates in

the detergent extraction studies described earlier. Using the monoclonal anti-MECA-32 antibody, PV-1 was immunoprecipitated in untreated and induced conditions, in all buffers tested (Figure 5.11). Moesin, however, was not present in the immunoprecipitated complex in neither untreated nor induced conditions.

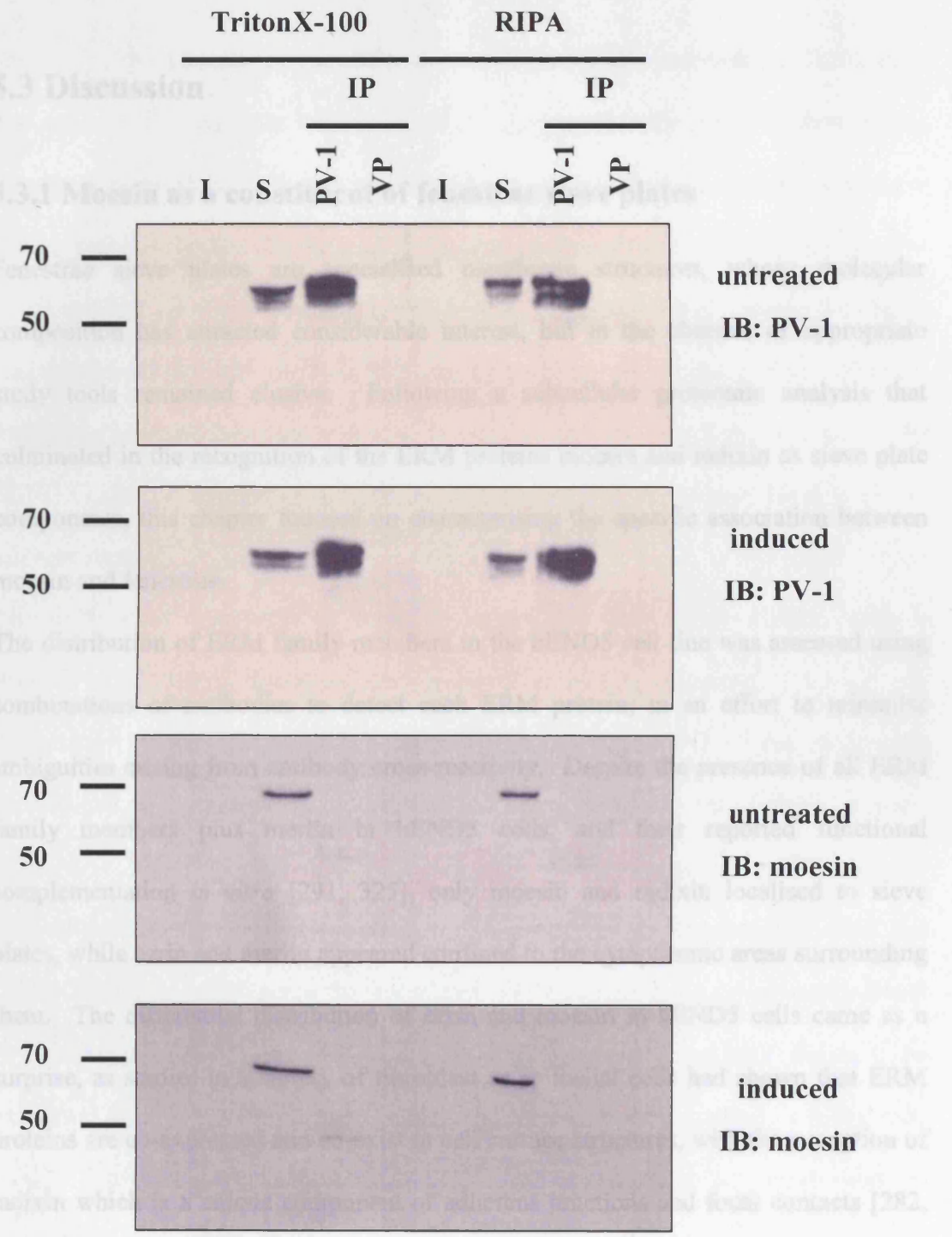

Figure 5.11 Immunoprecipitation of PV-1 from bEND5 cell lysates. Untreated or Latrunculin A-induced bEND5 cells were extracted with 0.1% Triton X-100 or RIPA buffer. Extracts were subjected to immunoprecipitation for PV-1 using anti-MECA-32 or an irrelevant antibody, anti-VE-PTP (VP). Immunoprecipitates were separated by SDS-PAGE electrophoresis, next to equal volumes of insoluble and soluble material generated after extraction with the specific buffer. Western blotting for PV-1 showed an enrichment of PV-1 in the immunoprecipitate, while no enrichment was observed for moesin after stripping and reprobing the same membrane. No difference was observed between untreated and induced cells.

5.3 Discussion

5.3.1 Moesin as a constituent of fenestrae sieve plates

Fenestrae sieve plates are specialised membrane structures, whose molecular composition has attracted considerable interest, but in the absence of appropriate study tools remained elusive. Following a subcellular proteomic analysis that culminated in the recognition of the ERM proteins moesin and radixin as sieve plate components, this chapter focused on characterising the specific association between moesin and fenestrae.

The distribution of ERM family members in the bEND5 cell line was assessed using combinations of antibodies to detect each ERM protein, in an effort to minimise ambiguities arising from antibody cross-reactivity. Despite the presence of all ERM family members plus merlin in bEND5 cells, and their reported functional complementation *in vitro* [291, 325], only moesin and radixin localised to sieve plates, while ezrin and merlin appeared confined to the cytoplasmic areas surrounding them. The differential distribution of ezrin and moesin in bEND5 cells came as a surprise, as studies in a variety of fibroblast or epithelial cells had shown that ERM proteins are co-expressed and co-exist in cell surface structures, with the exception of radixin which is a unique component of adherens junctions and focal contacts [282, 284, 298, 325]. The cell surface structures where ERMs have been previously localised include microvilli, filopodia, uropods, ruffling membranes, retraction fibers [282, 298, 325, 326], all of which, like fenestrae, are membrane specialisations arising from cytoskeletal remodeling. Interestingly, moesin in bEND5 cells appeared specifically enriched in fenestrae and not in the related structure of caveolae, consistent with the absence of such an association in previous ERM localisation

studies [327]. The subcellular distribution of ERM family members in Py4.1 cells was somewhat puzzling, as although moesin was present in the fenestrae sieve plates, it was not restricted to that area, also residing in the cytoplasmic arms between sieve plates (data not shown). Differences in the endogenous complement of ERM proteins could account for this discrepancy, with moesin compensating for some other ERM function associated with the area between the patches. As the sieve plate definition using immunocytochemistry was not as clear in the Py4.1 cells compared to the bEND5 cells, investigations on this cell line at the light microscopy level were not pursued further.

The differential specificity of family members for fenestrae in bEND5 cells is suggestive of distinct functions, and is likely to be physiologically relevant. In sections of mouse eyes, moesin was co-expressed with PV-1 in the fenestrated choriocapillaris, whereas ezrin expression was limited to the retinal pigment epithelium [320, 321]. Previous analyses on the tissue distribution of ERM proteins showed that all family members had a wide pattern of expression, but ezrin and radixin displayed a preference for epithelium, while moesin was predominantly found in endothelium [294, 295]. Within the endothelium, moesin had been shown to be expressed in both small and large vessels, radixin had been described as being only weakly expressed in vessels, and ezrin as being absent from the endothelium of arterioles, venules, or capillaries [295]. Moreover, the case for moesin was strengthened as its expression had been documented in tissues where fenestrated capillary beds are known to exist, such as liver, pancreatic, intestinal, and kidney endothelia [294, 328]. All of these tissues excluded ezrin, which reportedly is confined to tissues immediately adjacent to moesin-positive fenestrated endothelia: the retinal pigment epithelium [320, 321] adjacent to the choriocapillaris, and the glomerular podocytes [329-331] adjacent to the glomerular endothelial cells [332].

Findings in the *in vitro* induction system, combined with previously published data, indicate that moesin and ezrin are expressed in morphologically similar, yet distinct structures. Integrated within the same organ, such structures may act in a co-operative and complementary fashion to promote physiological functions.

5.3.2 Moesin modification and interactions

In light of the well-recognised role of ERM proteins as adaptors between the plasma membrane and the cytoskeleton in cell-surface structures [282, 333], it was plausible to consider a similar role for moesin within the context of fenestrae. Consistent with such a role, moesin in sieve plates is part of a specialised structure of the plasma membrane. On the other hand, this structure was thought to lack any underlying cytoskeleton as its formation has been intimately linked to microfilament disassembly. The recent observation of weak phalloidin reactivity for fenestrae sieve plates, however, not only highlighted an unexpected structure and localisation for F-actin, but also reconciled the paradox of moesin localisation in a cytoskeleton deficient region. Moreover, phosphorylated moesin is reportedly found predominantly in cell-surface structures [312, 334], and investigations into the phosphorylation state of moesin by immunocytochemistry suggest that the protein is phosphorylated within the context of fenestrae. According to the conformational regulation hypothesis an intramolecular association maintains ERM proteins in a 'closed' and inactive state [335, 336], and phosphorylation at a conserved threonine residue is required to relieve this inhibition [308, 309]. Phosphorylated moesin is therefore expected to be in an 'open' state, and interacting with both the membrane and the cytoskeleton of fenestrae sieve plates. Further evidence for increased moesin phosphorylation in the membrane and cytoskeleton subcellular fractions, upon fenestrae formation, came from 2D-gel

electrophoresis (see Chapter 4) and detergent extraction studies, respectively. In agreement with the biochemical data, immunofluorescence on detergent extracted cells revealed a partially resistant loose network of actin filaments and a similar network of moesin, in areas expected to accommodate sieve plates. However, Co-localisation was difficult to ascertain, given the distortion of the structures by the extraction, and their partial susceptibility to detergent solubilisation. Collectively, these data point towards an active involvement of moesin in fenestrae microdomains, rather than a random distribution of dormant, 'closed', moesin in a cell area that acts as a sink for proteins with aberrant distribution under the conditions created by Latrunculin induction.

The N-terminal FERM domain of ERM proteins has been recognised as responsible for membrane binding through direct or indirect interactions with membrane components. A direct association has been observed between ERM proteins and integral membrane proteins such as CD44 [323, 337], the ICAM family of adhesion molecules [326, 338, 339], the sodium-hydrogen exchanger isoform 1 [340], the T-cell mucin CD43[341], the podocyte sialomucin podocalyxin [330, 342], and others [258], through interactions with their cytoplasmic domains [339]. Indirect associations with membrane proteins are mediated by cytoplasmic scaffolding proteins consisting of multiple substrate-interaction domains, such as the ERM-binding phosphoprotein 50/regulatory co-factor of the sodium-hydrogen exchanger isoform 3 [343] and others [258]. The obvious candidate for moesin's binding partner on the membrane was the only published component of diaphragmed fenestrae to date, the protein PV-1. Immunoprecipitation studies were carried out using a panel of buffers that had been shown to successfully preserve the interaction between ERM proteins and CD43 [322], CD44 [323], Dbl [324], or were effective in solubilizing PV-1, entirely, and moesin, partially, from the fenestrae sieve plates. Moesin was

absent from PV-1 immunoprecipitates, in all conditions tested, suggesting either the failure to preserve the interaction with the detergents in question or the absence of such an interaction altogether. A recent attempt to cross-link PV-1 with other proteins *in situ,* similarly failed to identify any protein that could associate with PV-1 [71]. It is of interest to note that the presence of moesin has been documented in non-diaphragmed fenestrated capillary beds such as the glomerular endothelium [295], where it would be expected to exist independently of PV-1. Whether PV-1 is necessary only for the targeting of moesin to fenestrae sieve plates, in agreement with a speculative role for the diaphragm in the development of glomerular endothelial fenestrae, or whether PV-1 and moesin merely coincide in the same structure with no physical interaction are open questions. Moreover, given the differential specificity of moesin for fenestrae and not caveolae, if a physical association indeed exists, it is expected to be dependent on phosphorylation or other post-translational modifications, which could favour or inhibit particular conformations and molecular interactions.

Finally, ERM proteins bind membrane lipids, and specifically PIP_2 [344], an association deemed essential for membrane localisation of ERMs [345] as well as for their conformational activation [310, 346, 347]. PIP_2 would be a valid candidate for attracting moesin to the membrane of fenestrae sieve plates, alone, or in co-operation with a yet unidentified protein.

5.3.3 Actin filaments within fenestrae patches

The observation of filamentous actin in fenestrae sieve plates was validated in a study using different actin probes and fixation methods. Actin was confirmed to be in a polymerised state, through its interaction with the F-actin binding protein phalloidin

but not the G-actin binding protein Dnase I. Methanol fixation or 0.1% Triton X-100 detergent extraction prior to paraformaldehyde fixation, however, solubilised or distorted the filamentous actin in sieve plates, suggesting a different nature to that of short stress fiber remnants, which remained intact.

The precise structural arrangement of the filamentous actin component in fenestrae sieve plates remains a mystery. Based on the reported sieve plate dimensions *in vivo*, quoting a cytoplasm thickness of 40 nm and a distance between individual fenestrae of 60 nm [59], only some actin filament networks or intermediate filaments, among cytoskeletal polymers, could be accommodated. Within the family of actin filament networks, actin filaments can be found in long, unbranched parallel bundles, as occur in filopodia, or in branched structures typical of lamellipodia [348]. The two possibilities could be distinguished by ultrastructural methods, or by probing for actin binding proteins that would be specific for each structure, such as α-actinin or filamin [348].

Initially this filamentous actin structure and localisation was surprising, considering the prerequisite of cytoskeletal disruption for fenestrae formation in our system. Moreover, the continual presence of Latrunculin is expected to inhibit actin polymerisation by sequestering actin monomers [185, 186]. Nonetheless, as this assay does not provide information on the developmental stages a fenestrae patch goes through before it reaches maturity, one cannot unambiguously determine the timing of actin's appearance within sieve plates. ERM proteins have been implicated in actin polymerisation [315, 349] and recently also in *de novo* actin assembly on the surface of isolated phagosomes [350]. One explanation could therefore involve moesin in promoting actin nucleation on the cytoplasmic surface of the membranes in fenestrae sieve plates. The effect of moesin could perhaps override the function of latrunculin, resulting in the polymerisation of actin both within fenestrae patches and

cell-surface filopodia. On the other hand, in view of the actin-binding properties of ERM proteins, the reverse could be true, and this type of actin filaments could act to recruit moesin.

Finally, whether filamentous actin plays a role in propelling membrane fusion during fenestrae formation, as reported for the terminal phases of exocytosis and some intracellular fusion events [103, 193, 197, 198], or merely provides accessory structural support is an open question. Irrespective of whether it plays a structural or a functional role, the physiological relevance of filamentous actin within fenestrae sieve plates awaits validation. Cytoskeleton rings, composed of actin and myosin [98], and maintained after cytochalasin B or latrunculin A treatement [95], have been documented to surround fenestrae in sieve plates of liver endothelial cells *ex vivo*, but remain poorly defined. No report has addressed the cytoskeletal content of fenestrae capillary beds *in vivo* to date.

5.3.4 Moesin's putative role in fenestrae biogenesis

The triple stainings for PV-1/moesin/actin and moesin/PV-1/caveolin-1 in a time-course of induction were useful in drawing correlative relationships between putative partners in fenestrae formation. With the onset of actin remodeling, a spatial and temporal correlation between PV-1 and moesin was observed along the periphery of the cell, which culminated in their complete coincidence upon formation of well-defined fenestrae patches. In the same time-frame, PV-1 was seen to gradually segregate from the caveolar protein caveolin-1, until they became completely separate, in fenestrae patches and cytoplasmic arms between sieve plates, respectively. The situation was rapidly reversed following the removal of the stimulus: within the first fifteen minutes, PV-1 had segregated from moesin, and

colocalised again with caveolin-1. At this stage, moesin appeared as a ring at the cell cortex, surrounding a thick filamentous actin structure. Consistent with its aformementioned role in actin nucleation [315, 350], it could promote the development of stress fibers, that were observed in abundance during the next stage, thirty minutes after stimulus removal. The characteristic pattern of sieve plates was sometimes associated with immunoreactivity for either PV-1 or moesin. This observation, together with the strict colocalisation of moesin and PV-1 in fenestrae, and not caveolae or any other undefined intermediate, rules out a tentative role for moesin as the carrier of PV-1 from one cell structure to the other. On the other hand, at time-points preceding clear fenestrae assembly or disassembly, caveolin-1 and PV-1 do appear to colocalise at the centre of the cell, in a different structure than that of characteristic pattern of caveolae at the edges of cells. These could represent cell-surface peri-nuclear caveolae, or alternatively an intermediate structure between the two extremes of fenestrae and caveolae, occuring at the cell-surface or internally. Caveolae are known to move towards the centrosomal region of the cell upon Latrunculin A treatment [254], and once internalised they could join the endocytic pathway, whereupon segregation of PV-1 from caveolin-1 would be achieved. As to the path of moesin towards and away from fenestrae, perhaps more insight could be gained through following its activation state by probing for its phosphorylation or its localisation relative to PIP_2.

Ultimately, to draw causative relationships between moesin and fenestrae, perturbation of its function is required. To overcome the functional redundancy stemming from the presence of all ERM members in mammalian cells, a number of studies have made use of constitutively active or dominant negative ERM constructs. Site-directed mutagenesis at a conserved threonine residue, in both ezrin and moesin, have produced pseudophosphorylated variants of the proteins that lead to the

formation of lamellipodia, membrane ruffles, and microvilli-like structures in epithelial or COS7 cells [299-301]. Alternatively, the expression of the N-terminal FERM domain of either ezrin or moesin alone, lead to the mislocalisation of all endogenous ERM proteins and to altered responses upon growth factor stimulation in epithelial cells [302-304]. Efforts to use such constructs to promote or inhibit fenestrae formation in our *in vitro* model have been hampered by technical difficulties at the level of DNA introduction into cells: cells transfected with any plasmid, are altered in shape, and preclude fenestrae formation. Alternative approaches for the expression of proteins that perturb ERM function in bEND5 cells should help clarify whether moesin plays a role in fenestrae biogenesis.

At present, speculations on moesin's role can be made from looking at the reported functions of ERM proteins in model organisms. Due to functional redundancies among family members, specific roles have been assigned in the cases of organisms containing only one ortholog of the ERM family or tissues exhibiting specific expression of only one ERM protein. An *in vivo* role as modulators of signaling pathways has been suggested from studies of the drosophila ERM ortholog *Dmoesin* [317], but the majority of observations point towards structural roles in tissue integrity and polarity [297, 351-353]. Mouse ezrin and the *c.elegans* ERM ortholog erm-1 have been deemed essential for epithelial tubulogenesis through their actions as scaffolds with static and/or dynamic effects on the apical membranes that are facing lumina [352, 353]. Radixin has been deemed essential for the maintenance of cochlear sterocilia in mice [297], and *Dmoesin* as essential for the assembly of the photoreceptor rhabdomere in drosophila [351].

Considering its dual binding properties, moesin could act as a coordinator within fenestrae biogenesis, translating the modulation of the cytoskeleton to a remodeling of the plasma membrane. Alternatively, an architectural contribution of moesin in

fenestrae sieve plates could involve a role in restricting particular proteins to specialised membrane microdomains, as occurs in the T cell synapse [322] and the podocyte foot processes [330]. Finally, moesin could play a scaffolding role in providing the cytoskeletal support of the fenestrated area, or in maintaining the close apposition between the apical and basal plasma membranes through its oligomerisation properties. Interestingly, the overwhelming majority of specialised cell-surface structures that are associated with ERM proteins share the common property of negative membrane curvature. Intestinal microvilli, stereocilia, podocyte foot processes, and the membrane lining fenestrae, all bear a sharp negative curvature. In contrast, caveolae or clathrin-coated pits, specialised membrane domains with positive curvature, have never been found associated with ERM proteins, despite their connection with cytoskeletal elements. Furthering our knowledge into the relationship between such curvature and ERM function could potentially highlight yet unappreciated roles for moesin in the context of fenestrae.

Lastly, if moesin is indeed found to play a role in fenestrae biogenesis, determining whether such a role is indispensable will be important. Clues from a moesin knockout mouse suggest that loss of moesin does not result in any abnormality, without the compensatory up-regulation of ezrin or radixin [296]. Nonetheless, precise phenotypic analysis is required before reaching definitive conclusions, as evidenced by a recent study on the radixin deficient mouse showing that radixin was only essential in the maintenance of stereocilia, whose development could be rescued by the compensatory up-regulation of ezrin [297].

In the first cell biological approach to understanding fenestrae, a novel component of fenestrae sieve plates has been characterised. The connection between the membrane-

cytoskeleton adaptor moesin and fenestrae establishes a conceptual framework that unifies actin filaments, actin binding proteins, and membrane proteins of the sieve plate, within the context of a highly specialised feature of endothelial cells. This bears significant functional implications, and opens new avenues in the study of this organelle's biogenesis. A number of questions that require ultrastructural or functional approaches to be definitively addressed remain open, however an important step towards the visualisation of fenestrae by light microscopy has been accomplished: The classification of fenestrae on the basis of immunoreactivity for PV-1, a marker with dual specificity for caveolae and fenestrae, can be made less ambiguous in combination with anti-moesin labelling, which is specific for the latter. Moreover, moesin immunoreactivity could be useful in probing for non-diaphragmed capillary beds, which as suggested in the literature, lack PV-1, but contain moesin.

Chapter 6: Conditional overexpression of VE-PTP in mice

6.1 Background

Vascular permeability, similar to blood vessel growth, is thought to be governed by the co-ordinated and competing actions of Receptor Tyrosine Kinases (RTKs) and Receptor Protein Tyrosine Phosphatases (RPTPs) [28, 354, 355]. Extensive experimental evidence has implicated the VEGF-A and Angiopoietin (Ang) signaling cascades in the regulation of permeability, through the activation of the endothelial cell-specific RTKs, VEGFR-2 and Tie-2 respectively [28].

Among the tyrosine phosphatases present in endothelial cells [28], the recently characterised Vascular Endothelial Protein Tyrosine Phosphatase (VE-PTP) is specifically expressed in this tissue [159]. VE-PTP has been detected in the vasculature of embryos, as early as embryonic day E9.5. *In situ* hybridisation analysis revealed restricted expression of VE-PTP to endothelial cells lining larger, smooth muscle cell invested vessels [159]. In the adult, strong expression for VE-PTP has been reported in the brain, lung, and kidney, by Northern blotting [159].

A role for VE-PTP in the control of paracellular permeability has been supported by evidence of an interaction with the junctional protein VE-Cadherin [161]. VEGF-driven tyrosine phosphorylation of the adherens junction components is known to destabilise the integrity of endothelial cell contacts, leading to an increase in paracellular permeability [114, 158]. VE-PTP has been shown to reverse VEGFR-2-mediated tyrosine phosphorylation of VE-cadherin, and to increase the integrity of the endothelial monolayer in a cell-based assay [161].

An association between VE-PTP and the seemingly opposing Tie-2 pathway of endothelial barrier regulation has also been suggested. Although its mechanism of action remains poorly defined, the angiopoietin/Tie-2 signalling cascade has been implicated in the regulation of vascular integrity, and in blocking the vascular

permeability induced by VEGF [28, 356, 357]. Modulation of Tie-2 by VE-PTP was suggested from co-precipitation experiments, however, no functional effect stemming from the interaction has been shown [159].

Early embryonic lethality in mice with targeted disruption of many components in VEGF and Ang signaling cascades [112, 358-362] has hampered the analysis of the precise physiological function of these pathways during later stages of vascular development and adulthood. To circumvent these problems I opted for a conditional overexpression system to perturb the function of VE-PTP in a tightly controlled spatial and temporal manner. Such qualities are fulfilled by the tetracycline-responsive binary expression system, which is based on the *E.coli* tetracycline resistance operon (Figure 6.1) [176, 363-365]. The system relies on two parts; a driver transgene harbouring a recombinant tetracycline transactivator (tTA), and a responder transgene harbouring the gene of interest under the control of the tetracycline operon (tetO). When a driver line of mice is crossed to a responder line of mice, induction of expression of the gene of interest is achieved as a result of the high affinity of the tTA transcription factor for the tetO response element. Spatial control of gene expression is ensured by placing the tTA gene cassette downstream of tissue-specific promoters [366-371]. Temporal control of gene expression is achieved through the use of the antibiotic doxycycline, which can reversibly suppress the binding of tTA to the tetO element, thereby preventing induction of the gene of interest [176, 364, 365].

In an attempt to analyse the role of VE-PTP in regulating paracellular permeability *in vivo*, I sought to create responder mouse lines that would be crossed to an existing endothelial-specific driver line. This chapter describes the generation and characterisation of TetO-VE-PTP responder lines, using transgenes that are likely to promote gain or loss of VE-PTP function. A number of responder founder lines were

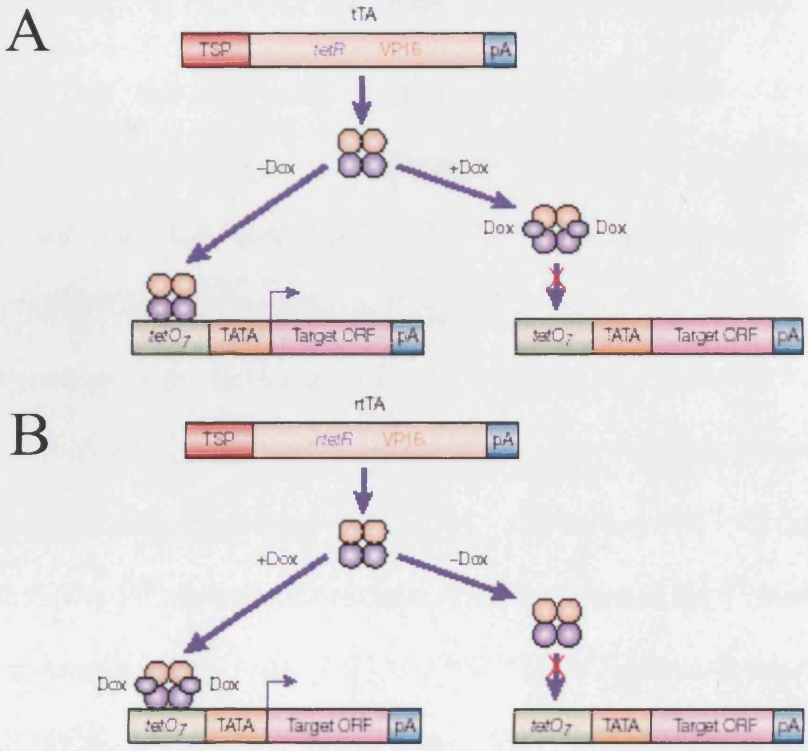

Figure 6.1 The tetracycline-responsive regulatory system for transcriptional transactivation. (A) The tetracycline transactivator of transcription (tTA) is encoded by a chimeric construct of the *E.coli* Tn10*tetR* gene (purple) and the VP16 transactivation domain (orange). In the absence of Doxycycline (Dox), tTA dimers bind to the tetracycline operon, consisting of seven tandemly repeated 19-bp *tetO* sequences (*tetO*7), and activate transcription of the gene of interest (target ORF) from a minimal promoter (TATA). When bound to Dox, tTA undergoes a conformational change that prevents it from binding *tetO*7. (B) In the reverse tTA (rtTA) system, the *tetR* gene has been mutated so that tTA binds to *tetO*7 only in the presence of Dox. Only upon binding of Dox, does tTA undergo the necessary conformational change that allows it to bind to *tetO*7 to activate transcription. (ORF, open reading frame; pA, polyadenylation site; TSP, tissue specific promoter). (Reproduced from Ref. 377)

screened by means of an approach centred on measuring RNA transcript levels for the TetO-VE-PTP transgene. Two founder lines were identified as potential models to further explore the effects of modulating VE-PTP function

6.2 Results

6.2.1 Subcloning of TetO-VE-PTP transgenic constructs

Responder line constructs were designed to produce wildtype or dominant negative versions of the VE-PTP protein. Three separate versions of the VE-PTP cDNA were used: 1) wildtype, full-length cDNA, 2) VE-PTP extracellular (EC) domain mutant, and 3) VE-PTP catalytic domain trapping mutant (R/A).

Overexpression of the full-length VE-PTP transgene is expected to increase the levels of VE-PTP protein in endothelial cells, and as shown for other phosphatases, amplify an already existing phenotype [372, 373]. Given that VE-PTP and VE-Cadherin interact via the 17th membrane proximal FNIII domain and the 5th membrane proximal cadherin domain respectively [161], the VE-PTP EC mutant is expected to interfere with the extracellular domain interactions of VE-PTP and possibly obstruct binding of the wildtype phosphatase to VE-cadherin [374]. The R/A trapping mutant can bind to the substrate and, whilst unable to perform catalysis, does not release it, potentially preventing the recruitment of the wildtype phosphatase or other signaling molecules downstream [159]. cDNAs for full-length or mutant VE-PTP were subcloned downstream of a tetracycline response element linked to a cytomegalovirus (CMV) minimal promoter [176]. An artificial intron and a polyadenylation signal were added to the 3' end of the cDNA for optimal expression (Figure 6.2, A).

Before injecting the constructs into fertilised oocytes it was critical to ensure that VE-PTP protein could be expressed. To determine protein expression, a commercially available MEF 3T3 Tet-Off cell line, expressing the tTA, was transfected with the constructs for VE-PTP full-length, and VE-PTP R/A, and expression of the protein was assessed by immunofluorescence using a rabbit anti-serum (Figure 6.3). A

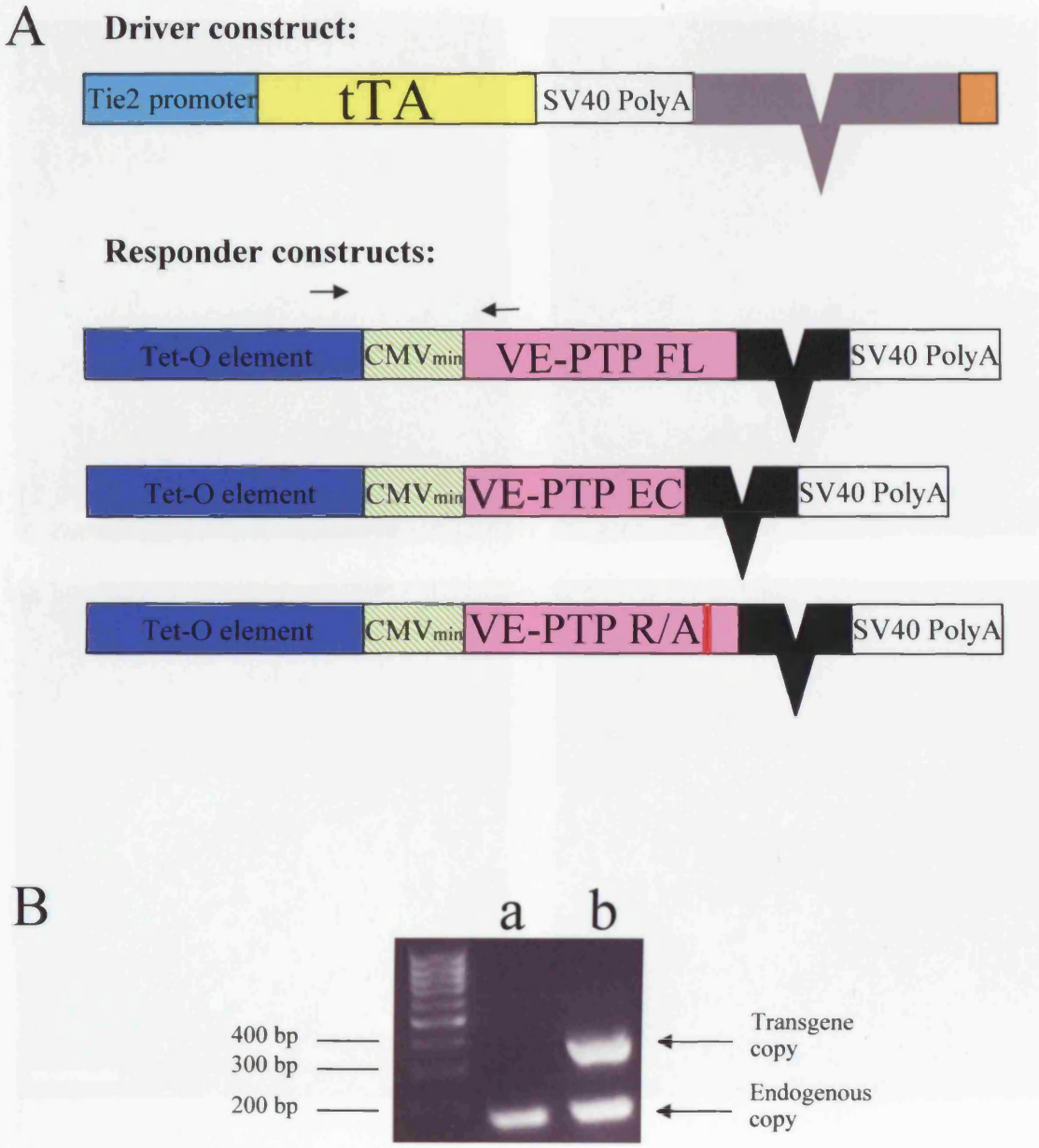

Figure 6.2 Generation and genotyping of TetO-VE-PTP responder mice (A) Schematic of driver and responder transgenes. Grey and orange regions in the driver transgene denote the Tie2 first intron and an enhancer element, respectively. Responder transgenes for VE-PTP full-length (FL), extracellular domain only (EC), and trapping mutant (R/A) are depicted. The black region in responder transgenes represents a chimaeric intron. Arrows denote PCR primers used to genotype transgenic animals. (B) Genotyping results for a wildtype (a) and a responder transgenic (b) mouse, using a dual PCR to amplify the transgene (340bp), and the endogenous (200bp) copies of VE-PTP. The two amplifications share the same reverse primer, but differ in their forward primers. The transgene-specific primer is shown in (A), while the endogenous-specific primer anneals in a 5'untranslated region present only in the endogenous copy.

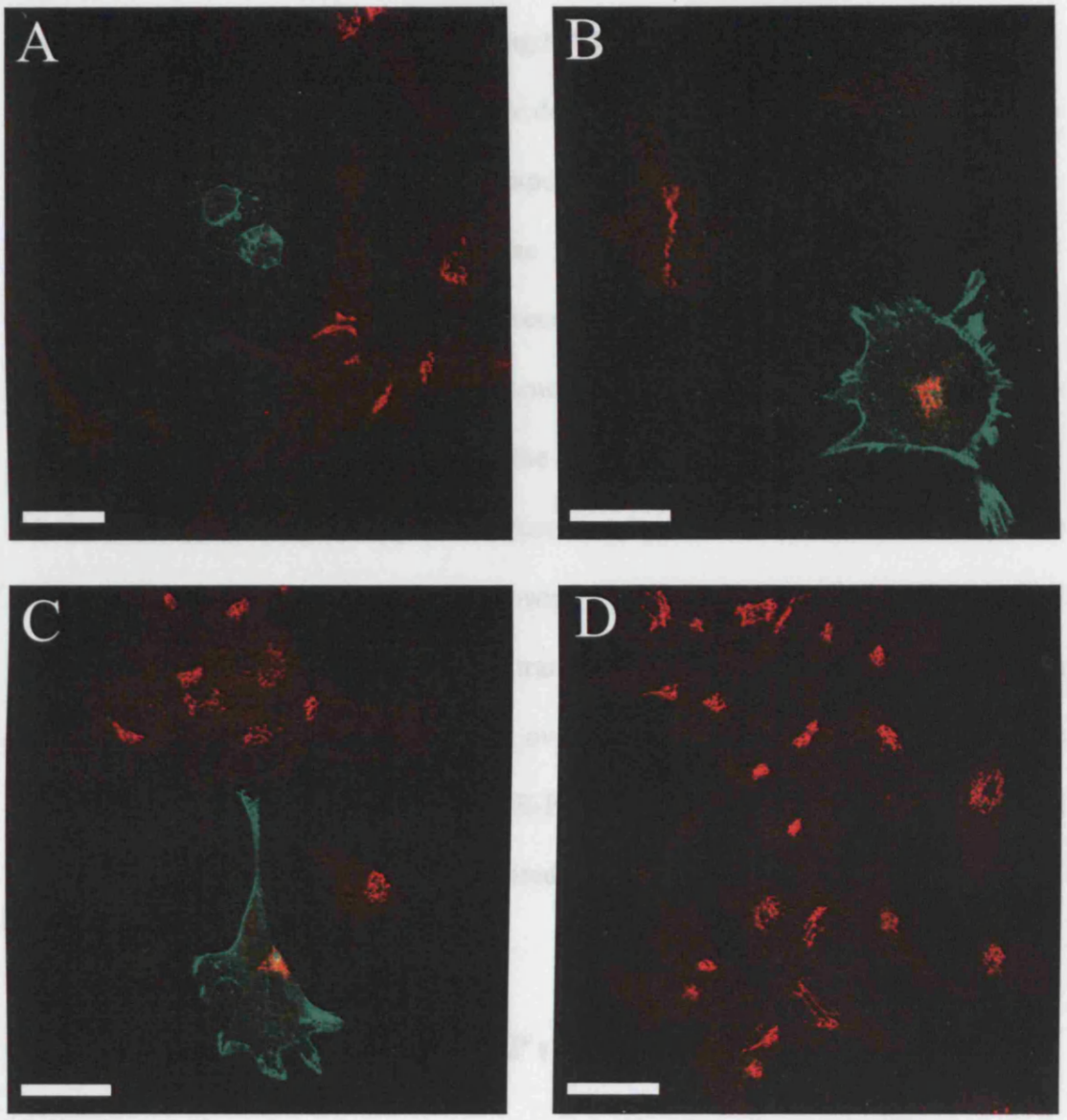

Figure 6.3 VE-PTP induction *in vitro*. MEF 3T3 cells expressing the tTA transactivator were transfected with plasmids containing CMV-VE-PTP (A) TetO-VE-PTP (B,D), and TetO-VE-PTP R/A (C). Doxycycline (2 μg/ml) was included in the culture medium in (D) to suppress the tTA-driven transcription. Immunolabeling for VE-PTP (green), and the golgi marker GM130 (red) showed that VE-PTP is constitutively expressed in (A), induced in (B) and (C), and repressed in (D). Confocal sections were obtained at the level of the golgi. (Bar = 20 μm)

plasmid harbouring CMV-driven full-length VE-PTP was used as a positive control for VE-PTP expression, and the antibiotic doxycycline was omitted or included in the culture medium to allow or suppress, respectively, the tTA-driven induction of VE-PTP. The VE-PTP EC construct was not included in the experiment as its presumptive nature of a soluble protein, secreted into the medium, would be expected to preclude detection by immunofluorescence. The expression of both VE-PTP full-length and VE-PTP R/A was induced in the absence of doxycycline (Figure 6.3, B-C). Moreover, expression was suppressed when doxycycline was included in the culture medium (Figure 6.3, D and data not shown). Considerable cell death was observed among the population of MEF 3T3 transfected cells, consistent with previous observations during full-length VE-PTP overexpression in CHO or COS cells. The surviving transfected cells expressed VE-PTP on their plasma membrane, but had altered morphology and sometimes appeared retracted from the substratum.

6.2.2 Generation of TetO-VE-PTP responder mice

Following confirmation of transgene expression, the three TetO-VE-PTP transgenic cassettes were excised from their respective cloning vectors and injected into pronuclei of mice from two different backgrounds, namely C57BL6/J and B6CBAF1 x F1 hybrid. 'Responder' founders were obtained for all transgenes, as assessed by PCR (Figure 6.2, B), and all but one of the identified founder animals transmitted the transgene to their progeny. The total of 16 founder animals that were capable of transmitting the transgene, once bred to C57BL6/J or B6CBAF1 x F1 hybrid mice, produced normal litter sizes of about 8 pups, with the exception of founder line 3650B2. This line was very difficult to breed, and its litters consisted of 3-5 animals on average. Overall, the presence of the responder transgene alone did not appear to

have a negative impact on mouse development. The problems encountered within founder line 3650B2 could be due to a disruption of a normal cellular function caused by transgene insertion or to uncontrolled expression of the transgene itself, but were not investigated further.

6.2.3 Screening responder founder lines for VE-PTP expression

6.2.3.1 Screening for inducibility *ex vivo*

The first attempt to screen between the different founder lines was based on selecting for VE-PTP inducibility without breeding to the driver lines. This entailed isolating mouse embryonic fibroblasts (MEFs) from E14.5 mice and transfecting them with an rtTA expressing construct (pTetOn). rtTA, the reverse tetracycline transactivator, differs from tTA by only four amino acids, and in contrast to the latter, drives expression of the target gene upon addition of doxycycline to the medium (Figure 6.1) [364]. As a positive control, MEFs were co-transfected with the plasmid containing the TetO-VE-PTP transgene in addition to the rtTA plasmid. Immunofluorescence analysis using rabbit anti-VE-PTP antiserum revealed that stably integrated transgenes could be induced to express VE-PTP *ex vivo* in the presence of an exogenous transactivator element (Figure 6.4, B). Moreover, this expression was contingent upon the presence of doxycycline (Figure 6.4, B), as no expression was observed in the absence of the antibiotic (Figure 6.4,A). As expected, co-transfected cells exhibited higher levels of protein expression due to the presence of multiple copies of the transgene following transient transfection, compared to stable integration in the genome as occurs in the transgenic MEFs (Figure 6.4, C-D).

A number of responder lines were found to sustain the induction of VE-PTP *ex vivo*. Nevertheless, given that considerable cell death was observed, induction was weak in

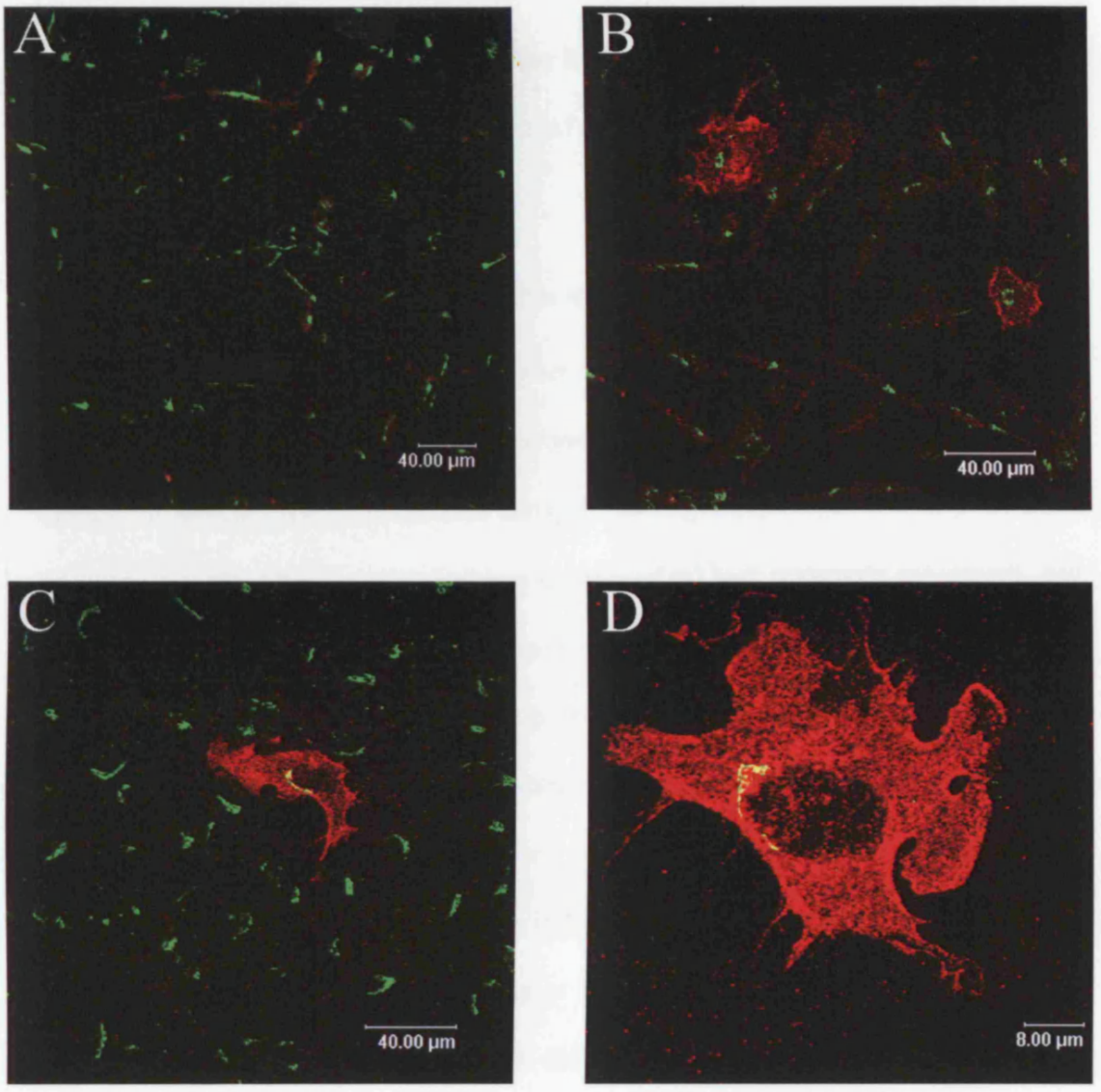

Figure 6.4 VE-PTP induction *ex vivo*. Mouse embryonic fibroblasts (MEFs) isolated from responder TetO-VE-PTP founder lines were transfected with a plasmid expressing the reverse tetracycline transactivator (rtTA) (A,B), and cultured in the absence (A) or in the presence (B) of doxycycline (2 µg/ml). Immunolabelling for VE-PTP (red channel) and GM130 (green channel) demonstrated that VE-PTP is expressed only when doxycycline is included in the medium (A,B). MEFs co-transfected with the rtTA plasmid plus the plasmid used in the generation of the TetO-VE-PTP lines, and cultured with doxycycline, were used as a positive control (C,D). Confocal sections were captured at the level of the golgi (A-C), or the plasma membrane (D). VE-PTP labeling throughout the plasma membrane is observed, with an enrichment in peripheral areas.

surviving cells, and the response was often inconsistent even within the same founder line, the strategy was abandoned in favour of *in vivo* screening for induction.

6.2.3.2 Screening for induction in double transgenic embryos

Screening for induction *in vivo* was deemed to be the ultimate selection method as it assesses the capability of transgene induction from a given integration site, within the context of relevant levels of the tTA driver in the organism. The screening rationale was aimed at identifying responder lines capable of (a) high transgene expression, and (b) regulated transgene expression by the tTA.

Unsuccessful attempts to detect the endogenous VE-PTP protein in tissues, using the available antibody tools, precluded a screening approach based on assessing protein levels. An RNA-based screening method was deemed preferable as it conferred the additional advantage of monitoring the induction of all three transgenes: full-length, VE-PTP EC, and VE-PTP R/A transcript levels in the cell could all be measured, avoiding complications associated with the detection of secreted VE-PTP EC by an antibody. Moreover, unique elements in the untranslated regions of the endogenous and transgenic VE-PTP transcripts provided a means of differentiating between the two versions.

A Tie2-tTa driver line of mice (provided by Dr. Urban Deutsch, Theodor Kocher Institute, Bern, Switzerland), capable of driving uniform vascular endothelial-specific tTA expression in embryos [375], was crossed to each of the responder founder lines, and embryos were harvested at E11.5. At this embryonic stage the Tie2 promoter is highly active [375, 376], and Lac Z staining of E11.5 embryos which were double transgenic for the Tie2-tTA transgene and a TetO-Lac Z responder transgene exhibited strong Lac Z expression throughout the vasculature (Figure 6.5, A).

A

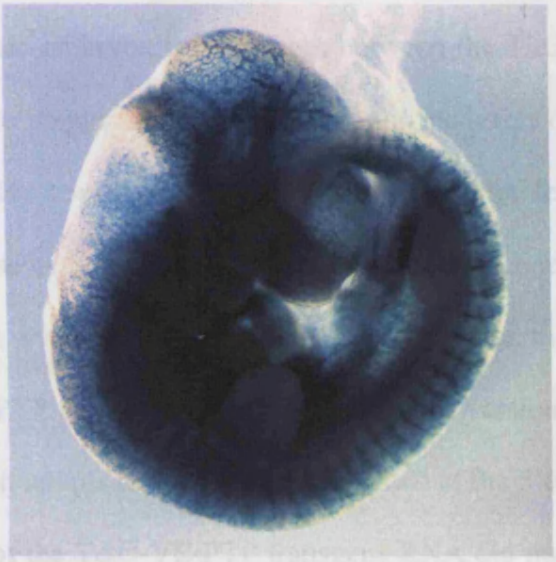

B

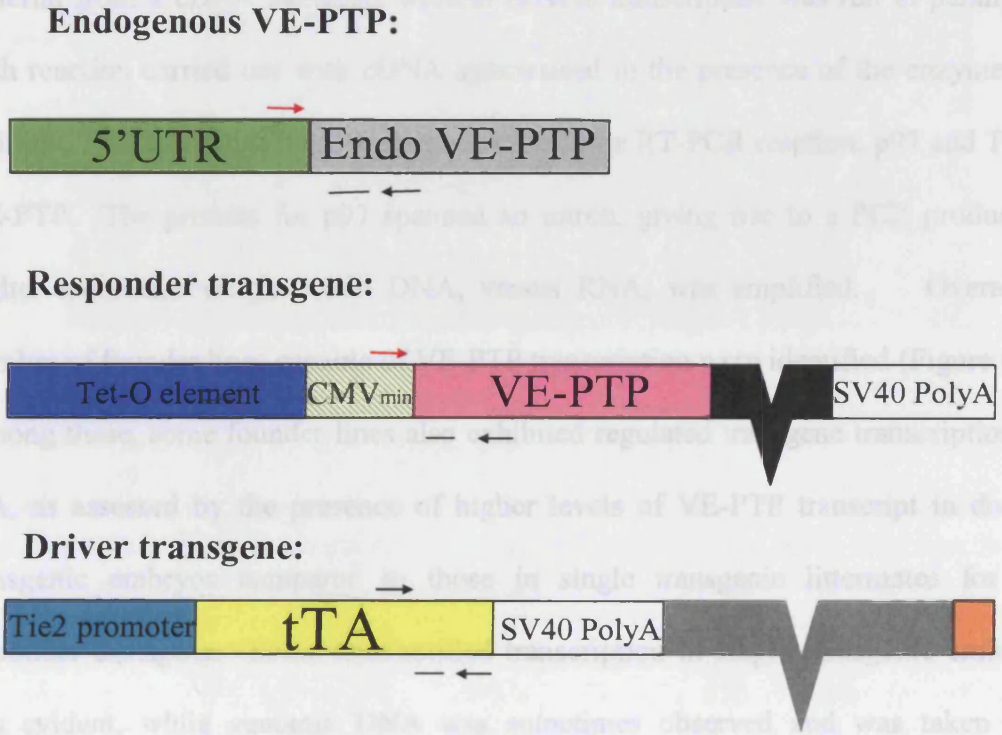

Figure 6.5 Strategy for VE-PTP transcript analysis *in vivo*. Tie2-tTA drivers are confirmed as capable of driving transcription of a LacZ reporter gene in the endothelium at E11.5 (A). Schematic of Real-time PCR primer and probe set positions (B). Primers are denoted by black or red arrows, and probes by grey lines. Probes and reverse primers are common for endogenous and transgene VE-PTP transcripts, but forward primers (red arrows) are unique to each construct. RT-PCR primers for transgene VE-PTP were designed in the same region as for Real-time PCR. For simplicity, only one version of the three transgene constructs is shown, and introns are omitted from the endogenous copy.

Double transgenic embryos from crosses between the Tie2-tTA driver line and each TetO-VE-PTP responder line were assessed for the levels of TetO-VE-PTP transcript by RT-PCR. By comparing TetO-VE-PTP transcript levels of double transgenic embryos to those of littermates carrying only the responder transgene, the regulation of transcription by tTA was also assessed. In order to distinguish the transgene version of VE-PTP transcript from the endogenous version, primers were designed to amplify a region unique to the transgene, located at the 5'end (Figure 6.5, B). Given that the 5'end of the TetO-VE-PTP transgene RNA did not differ from the DNA that encoded it, a number of controls were included to ensure that the observed signal was attributable to the presence of an mRNA transcript. An RT-PCR reaction using material from a cDNA synthesis without reverse transcriptase was run in parallel to each reaction carried out with cDNA synthesised in the presence of the enzyme. In addition, two transcripts were amplified in the same RT-PCR reaction: p97 and TetO-VE-PTP. The primers for p97 spanned an intron, giving rise to a PCR product of higher molecular weight when DNA, versus RNA, was amplified. Overall, a number of founder lines capable of VE-PTP transcription were identified (Figure 6.6). Among these, some founder lines also exhibited regulated transgene transcription by tTA, as assessed by the presence of higher levels of VE-PTP transcript in double transgenic embryos compared to those in single transgenic littermates for the responder transgene. Some uncontrolled transcription in single transgenic embryos was evident, while genomic DNA was sometimes observed and was taken into account in the interpretation of each signal.

To confirm and also obtain a quantitative estimate of the observations from RT-PCR, the analysis was validated by Real-time quantitative PCR (TaqMan). This method ensures increased accuracy, as two primers and one probe must specifically anneal to each cDNA for detection. Moreover it adds quantitative value, as relative product

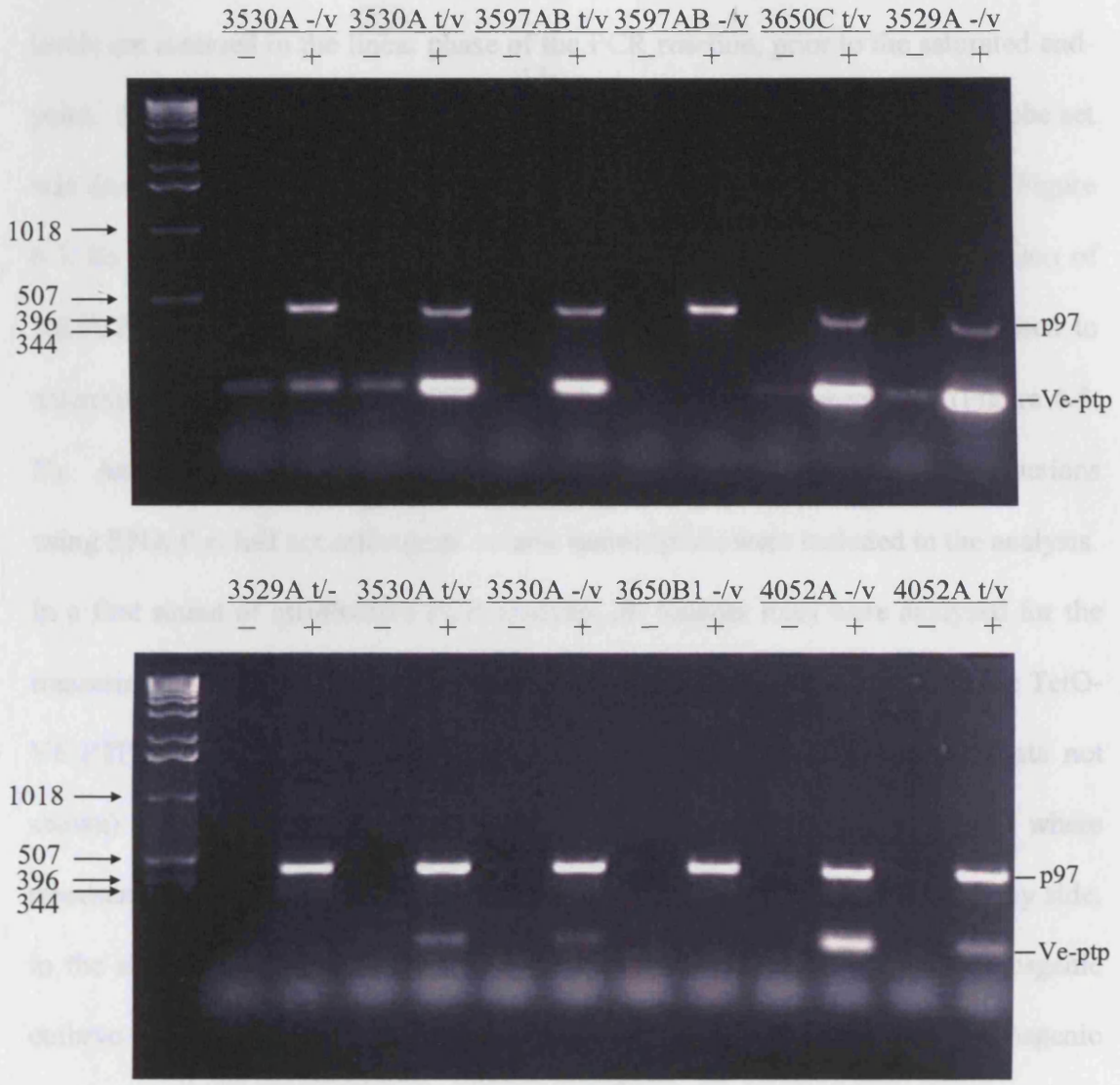

Figure 6.6 Screening through TetO-VE-PTP founder lines by RT-PCR. TetO-VE-PTP and p97 transcripts were amplified in the same reaction, from RNA that was reverse transcribed with the inclusion (+) or the omission (-) of reverse transcriptase. A 153 bp fragment was amplified in samples containing the TetO-VE-PTP transcript, while a 470 bp fragment from the constitutively expressed p97 gene was amplified in all samples. The presence of a 153 bp band for TetO-VE-PTP or a 670 bp band for p97 (after inclusion of an intron) in the (-) lane was indicative of a contribution by genomic DNA. The founder lines and genotypes are indicated on top of each gel picture. The nomenclature used for each founder line consists of a four-digit number plus one or two letters, collectively indicating each event of oocyte transfer into a pseudopregnant female. Numbers following letters in the nomenclature distinguish different founders stemming from the same oocyte transfer event. The genotype of the animals is abbreviated using the following scheme: t = Tie2-tTA transgene, v = TetO-VE-PTP transgene. Accordingly, double transgenic animals are denoted as t/v, while single transgenic animals for the driver transgene or the responder transgene are denoted as t/- and -/v, respectively. Molecular weight markers and the identity of the obtained bands are indicated.

levels are assessed in the linear phase of the PCR reaction, prior to the saturated end-point. Following the same rational to the RT-PCR screening, a primer and probe set was designed to amplify a region unique to the transgenic version of VE-PTP (Figure 6.5, B). In addition, a primer and probe set specific for the endogenous version of VE-PTP, as well as another set specific for the Tie2-tTA transcript, were used to determine the endogenous VE-PTP and driver tTA levels, respectively (Figure 6.5, B). As a control for the presence of genomic DNA contamination, PCR reactions using RNA that had not undergone reverse transcription were included in the analysis. In a first round of quantitative PCR analysis, all founder lines were analysed for the transcription of VE-PTP, and lines with no or insignificant amplification of the TetO-VE-PTP transcript (namely 3598C, 4052A, and 3664B) were eliminated (data not shown). Subsequently, a second round of analysis was carried out, where representative samples from all remaining founder lines were compared side by side, in the same Taqman run (Figure 6.7). For each founder line, a double transgenic embryo was assessed, and where possible, its TetO-VE-PTP single transgenic littermate was included for comparison. This allowed ranking the founder lines according to their levels of TetO-VE-PTP transcript, and also quantitatively assessing how much of the observed levels were due to uncontrolled transcription, even in the absence of the driver transgene. It was immediately apparent that the founder lines harbouring the highest levels of VE-PTP transcript (3529A and 3650C) were not inducible, as samples displayed similar levels in the presence or the absence of the tTA driver (Figures 6.7, A and data not shown).

Founder lines displaying the highest levels of regulated transgene VE-PTP transcription were selected for each of the three types of TetO-VE-PTP transgene, to undergo yet a third-round of transgene expression evaluation (Figure 6.8). Given that an over-expression approach depends on flooding the system with a protein that will

A

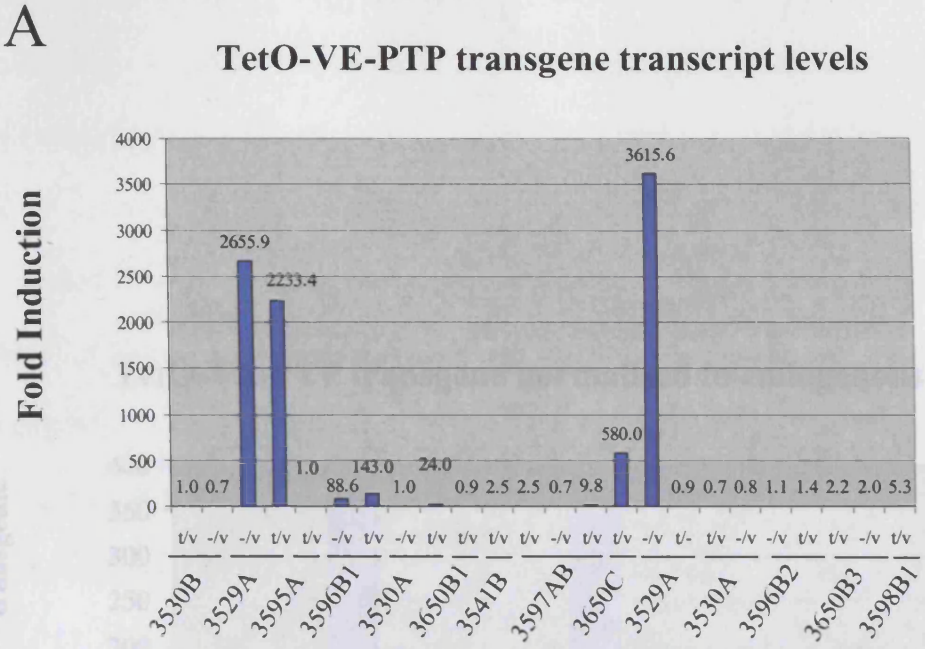

B

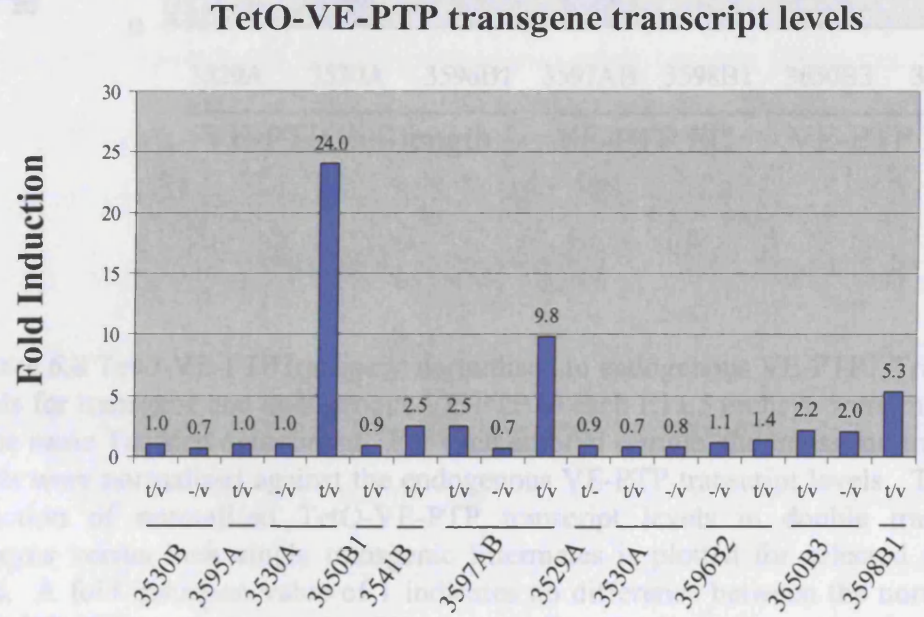

Figure 6.7 Screening through TetO-VE-PTP founder lines by Real-time PCR (TaqMan). TetO-VE-PTP transcript levels in representative E11.5 embryos from different founder lines were measured in a single Taqman experiment. Transcript levels are expressed as a fold induction over a sample with very low amounts of transcript, namely 3530B t/v. (A) differs from (B) in lacking the samples with the highest 6 scores, to highlight differences at low transcript levels. The genotypes and founder lines of the animals are denoted beneath the graph, according to the scheme described in Figure 6.6.

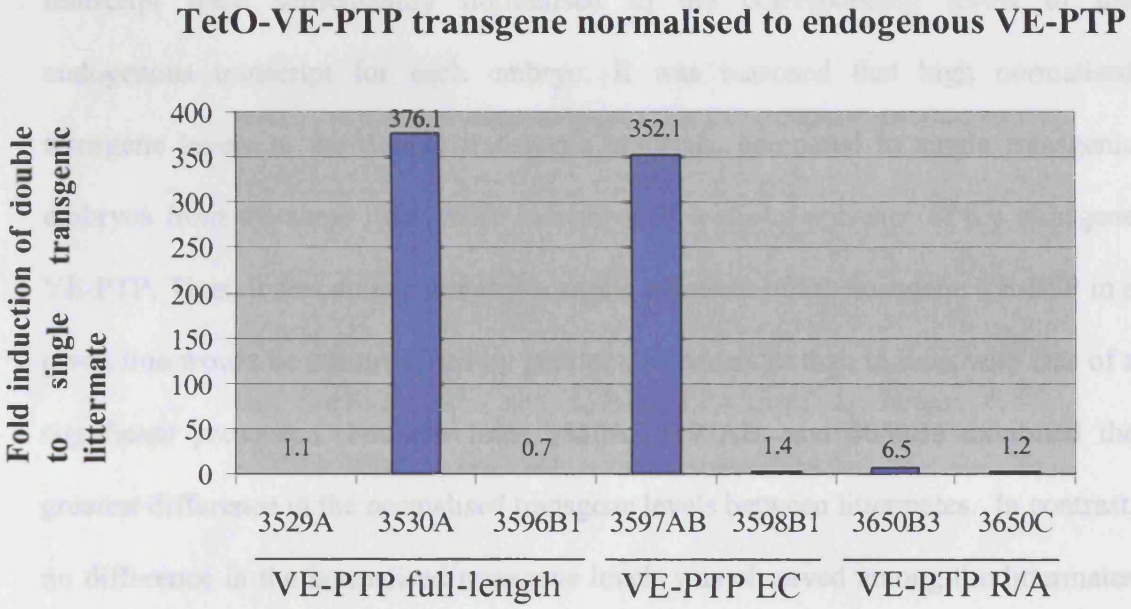

Figure 6.8 TetO-VE-PTP transgene normalised to endogenous VE-PTP. Transcript levels for transgene and endogenous VE-PTP in each E11.5 embryo were measured in the same TaqMan experiment. For each embryo sample, the transgene transcript levels were normalised against the endogenous VE-PTP transcript levels. The fold induction of normalised TetO-VE-PTP transcript levels in double transgenic embryos versus their single transgenic littermates is plotted for selected founder lines. A fold induction value of 1 indicates no difference between the normalised TetO-VE-PTP transcript levels of littermates. Founder lines along with the type of TetO-VE-PTP construct they harbour are denoted.

enhance or override the normal cellular counterpart, an attempt to predict in which founder line it would be more likely for the transgene to have an impact was initiated by comparing the levels of transgene VE-PTP transcript to those of endogenous VE-PTP. To this end, transcript levels for transgene and endogenous VE-PTP were measured in double and single transgenic littermates. Levels of transgene VE-PTP transcript were subsequently normalised to the corresponding levels of the endogenous transcript for each embryo. It was reasoned that high normalised transgene levels in the double transgenic embryos, compared to single transgenic embryos from the same litter, were indicative of a strong presence of the transgene VE-PTP. Thus, it was anticipated that a strong presence of the transgene VE-PTP in a given line would be accompanied by greater consequences than in lines with less of a significant presence. Founder lines 3530A, 3597AB, and 3650B3 exhibited the greatest difference in the normalised transgene levels between littermates. In contrast, no difference in the normalised transgene levels was observed among the littermates of line 3596B1 or within the non-inducible lines 3529A and 3650C.

Finally, levels of the tTA transcript were measured between littermates of different founder lines. As expected, the tTA driver was expressed in all animals of the appropriate genotype (Figure 6.9). Some differences in tTA transcript levels between founder lines and within littermates were noted, however, no correlation between the driver transcript levels and the attained responder transcript levels was observed.

Collectively, the above observations (summarised in Table 6.1) suggested that founder lines 3530A, 3597AB, and 3650B3, for TetO-VE-PTP full length, EC only, and R/A mutant, respectively, were the most promising for further study.

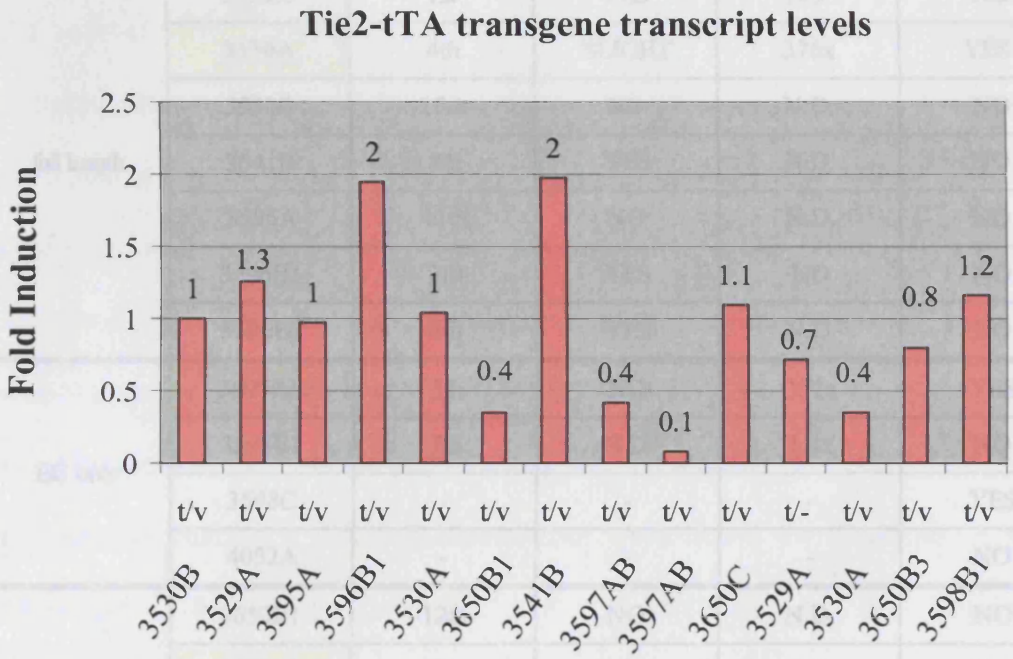

Figure 6.9 Tie2-tTA transcript levels. Driver transgene transcript levels in representative E11.5 embryos from different founder lines were measured in a single Taqman experiment. Transcript levels were expressed as a fold induction over sample 3530B. The genotypes and founder lines of the animals are denoted beneath the graph according to the scheme described in Figure 6.6.

TetO-VE-PTP construct	Founder line	Rank according to transgene transcript levels	comparison within founder lines:		Phenotype trends
			uncontrolled transcription in -/v	normalized transgene induction in t/v over -/v	
full length	3529A	1st	YES	NO	NO
	3530A	4th	SLIGHT	376x	YES
	3530B	10th	NO	N.D.	NO
	3541B	8th	YES	N.D.	NO
	3595A	11th	NO	N.D.	NO
	3596B1	3rd	YES	NO	NO
	3596B2	6th	YES	N.D.	NO
EC only	3597AB	5th	NO	352x	YES
	3598B1	7th	N.D.	1.4x	NO
	3598C	-	-	-	YES
	4052A	-	-	-	NO
R/A mutant	3650B1	12th	NO	N.D.	NO
	3650B3	9th	YES	6.5x	NO
	3650C	2nd	YES	NO	NO
	3664B	-	-	-	NO

Table 6.1 Summary of Real-time PCR and morphological observations. TetO-VE-PTP founder lines are ranked according to their transgene transcript levels measured in a parallel comparison within a single TaqMan experiment. Uncontrolled expression in -/v refers to transgene transcription in a single transgenic animal for the responder transgene, in the absence of the tTA transactivator. Normalised transgene induction in double transgenic (t/v) versus their single transgenic (-/v) littermate refers to an empirical estimate of the increase in transgene levels, described in Figure 6.8. Phenotypic trends observed in E11.5 embryos are indicated for the appropriate founder lines. The most promising founder line for each different TetO-VE-PTP construct is highlighted in yellow. The nomenclature for founder lines and genotypes follows the scheme described in Figure 6.6. N.D. stands for not determined.

6.2.4 Further analysis of selected founder lines

In order to validate the induction at the protein level, double transgenic embryos from inducible and non-regulatable lines were processed for western blotting and wholemount immunostaining using a monoclonal anti-VE-PTP antibody. Although the antibody readily recognised VE-PTP in immunoblotting from cell extracts and immunocytochemistry [161], previous attempts to detect endogenous VE-PTP protein in tissues had been met with little or no success (personal communication; Dr. Urban Deutsch). In an attempt to detect potentially increased levels of total VE-PTP protein, that would fall within the range of sensitivity for the particular antibody, inducible as well as non-regulatable lines were processed. Nonetheless, no protein was apparent in any experimental sample (data not shown), suggesting that VE-PTP protein levels in wildtype, inducible, or non-regulatable lines were below the threshold of protein recognition by the antibody, in immunoblotting or wholemount immunohistochemistry assays alike.

Despite the inability to assess VE-PTP protein induction, phenotypic trends observed in founder lines capable of high and regulated VE-PTP transgene transcription, were suggestive of a perturbation at the protein level. Double transgenic animals in lines 3530A and 3597AB were often developmentally delayed, compared to their littermates, and exhibited enlarged pericardia with haemorrhage (Figure 6.10). Moreover, the sub-Mendelian ratios of double transgenic offspring in a litter from either line (Table 6.2) were indicative of embryonic lethality. Observed defects ranged from subtle to very dramatic, suggesting a dose-dependency on VE-PTP in the severity of the phenotype exhibited.

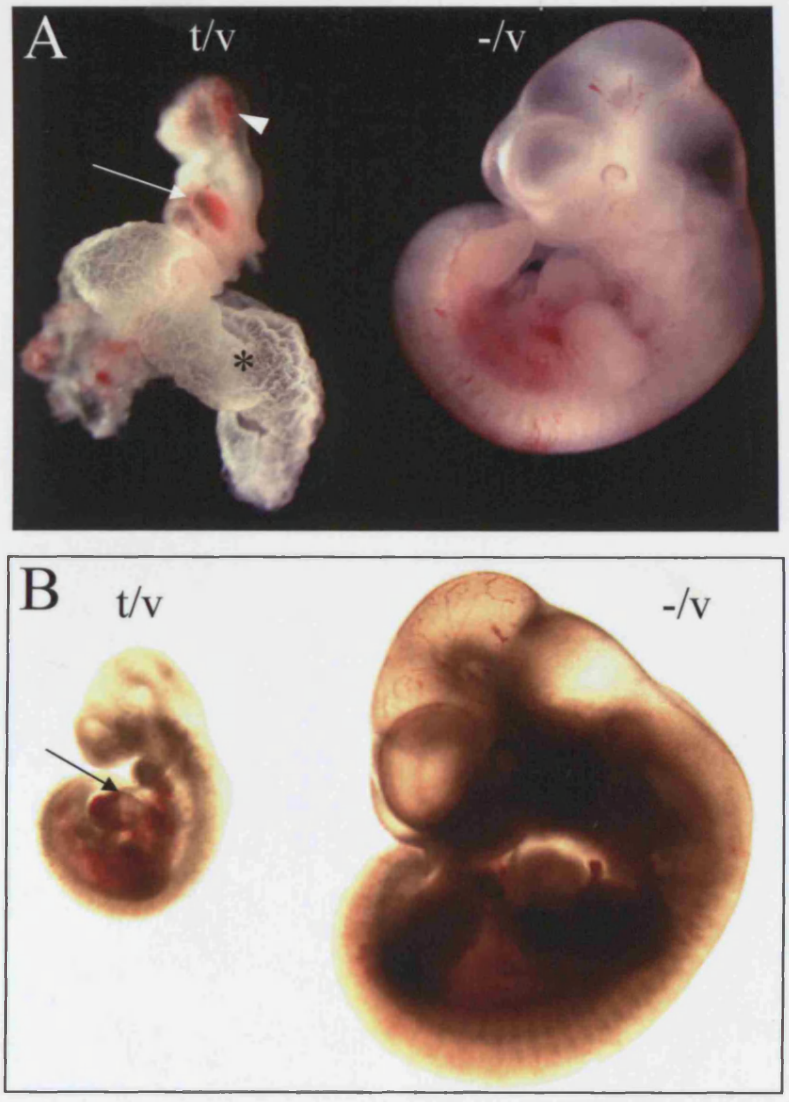

Figure 6.10 Abnormalities in double transgenic embryos. E11.5 double transgenic (t/v) and single transgenic (-/v) littermates from 2 different litters (A and B) of a cross between Tie2-tTA driver and TetO-VE-PTP 3597AB responder lines. The double transgenic embryos in both litters were developmentally retarded in comparison to their littermates, displayed haemorrhages (arrowhead) and enlarged pericardia (arrows). The partially dissected yolksac of the double transgenic embryo in (A) is marked by an asterisk.

Founder line	E10.5	E11.5	P7
3530A	11.1% (n=9)	17.9% (n=28)	11.1% (n=18)
3597AB	33% (n=6)	20%(n=25)	7.7% (n=13)

Table 6.2 Genotype records for crosses between the Tie2-tTA driver line and the 3530A or 3597AB responder lines. 10.5-11.5 old embryos, and 7-day old pups were genotyped for the presence of both transgenes. The percentage of double transgenic animals in a litter, and the total number of animals assessed (n) are indicated.

6.3 Discussion

6.3.1 System overview

Conditional gene expression in mice is a popular tool for dissecting the precise roles of genes in complex physiological processes [377]. Among binary overexpression systems based on transcriptional transactivation [363, 378, 379], the tetracycline-resistance system has seen the widest use in the study of spatially- and temporally-specific gene function [366, 370, 371, 380-385].

A conditional and endothelial cell-specific overexpression system in the analysis of VE-PTP function was thought to confer a number of advantages. First of all, tight control of the onset and location of gene expression should provide a means for studying the VEGF and Ang signalling cascades *in vivo*. Conventional knockout or transgenic approaches, aimed at elucidating the precise physiological functions of components in these pathways, have been limited due to early embryonic lethality [112, 358-362]. In addition to obviating lethality, the ability to switch expression on or off, should allow one to specifically focus on multiple stages of vascular development or disease. Finally, using one system, but varying the transgenic construct, should enable the study of both gain and loss of function of VE-PTP.

6.3.2 Selection of responder founder lines

In consideration of the above, the ideal responder line should be silent for the transgene it harbours, until crossed to the driver line, whereupon it should sustain high levels of expression upon induction. Given that inducible lines are often a minority among responder lines [386], a number of oocytes are typically injected, generating a

number of potential founder lines. Among the resulting 16 responder founder lines, the 15 responder lines that were capable of efficient germline transmission of the transgene, were sorted according to their mRNA transcript levels for TetO-VE-PTP. The different responses observed can be used to classify responder mice into three broad categories: 1) Founder lines that did not show expression of the TetO-VE-PTP transgene, 2) Founder lines that displayed non-regulatable TetO-VE-PTP transgene expression even in the absence of the transactivator, and 3) Founder lines that expressed no, or very little, TetO-VE-PTP transgene in the absence of the transactivator, but could support an induction in its presence.

A critical determinant in the ability of a promoter-less transgene to remain silent, induced only in the presence of a transcriptional transactivator, is the site of chromosomal integration [363, 365, 387]. Transgenes can integrate into the genome near endogenous promoters leading to their constitutive transcription in the absence of the tTA transactivator. Alternatively, integration sites can be surrounded by silencer elements that preclude transcription, even in the presence of the tTA transactivator. Stimulatory or suppressive signals in the genome have also been attributed to factors affecting the three-dimensional structure of chromatin, such as acetylation or methylation [388]. Non-regulatable expression, or absence of expression altogether have been previously reported for other responder lines [367, 371, 381, 385].

The two founder lines that displayed the best induction properties (3530A, 3597AB), showed minimal transgene expression in the absence of a tTA transactivator, and an increase in transgene expression on the order of 10-25 fold upon transcriptional activation. They also exhibited the greatest difference between normalised transgene transcripts of double transgenic embryos and their single transgenic littermates, an empirical measurement devised to predict the effectiveness of transgene induction. Normalizing the relative transgene levels to those of endogenous VE-PTP was

deemed more relevant than measuring total (transgene and endogenous) levels, as the latter could be misleading in the case of high endogenous levels in a non-transgenic animal. Normalised transgene levels were increased on the order of 300-400 fold in the presence of a transactivator. In agreement with the observations at the RNA level, founder lines 3530A and 3597AB were accompanied by trends of a phenotype in double transgenic embryos.

The two non-regulatable VE-PTP responder lines (3529A, 3650C) displayed the highest levels of TetO-VE-PTP transcript among founder lines, without exhibiting any obvious morphological or behavioural defect. A number of interpretations could account for the above observation. One explanation is consistent with the specificity of VE-PTP expression for the vasculature [159]. Substrate specificity for vascular targets could preclude an adverse phenotype in a situation of ectopic expression. Another explanation could be the inability of the particular transcripts to be translated into protein. Lastly, the possibility of full-length (line 3529A), or R/A mutant (line 3650C), VE-PTP overexpression not leading to an overt phenotype should be considered. However, in view of the toxicity associated with VE-PTP overexpression *in vitro* and the observed phenotype trends in the founder lines displaying inducible VE-PTP expression, the last interpretation seems the least likely of all.

6.3.3 Preliminary phenotypic analysis

The phenotypic trends associated with overexpression at the RNA level, coupled to the ability of protein translation *ex vivo*, constitute indirect evidence for the expression of VE-PTP protein in tissues. For future reference, one way to have circumvented the problem of VE-PTP protein detection *in vivo* could be the inclusion of a tag in the transgene cassette to aid visualisation by either means.

Defects observed in the embryos of lines 3530A and 3597AB were associated with a decrease in embryo size, enlarged pericardia, and haemorrhages. Embryonic lethality was inferred from sub-Mendelian ratios of double transgenic offspring. It should be stressed that phenotypes were not exhibited in all double transgenic embryos of the selected lines, and phenotype manifestation varied in severity. The variability could reflect differences in the levels of VE-PTP overexpression attained between, or even within, litters of the same founder line. Variations in the expression of responder transgenes between littermates has been previously noted [363]. However, in contrast to reports linking variation in responder gene expression to the levels of the transactivator [387, 389], no correlation was observed among the tTA and TetO-VE-PTP transcript levels among littermates with identical genotype (Figures 6.9).

Heart phenotypes are a common occurence in many mutants of components of the vasculature [112, 358-360, 362]. Further studies are necessary to distinguish true endothelial defects from secondary myocardial defects in a dying embryo. If the phenotypes are indeed related to the perturbation of VE-PTP in the vasculature, they could be conceptually linked to the dual functions of its substrate VE-cadherin in permeability and endothelial cell assembly during angiogenesis [17, 112, 120, 165]. Alternatively, or in conjunction with effects on VE-cadherin, modulation of the Tie-2 pathway could result in defects in vascular remodelling and permeability [28, 390]. Detailed analysis, however, is required to define the onset and nature of the observed phenotypes, as well as the differences between the effects of full-length or mutant overexpression. Finally, the ultimate assessment for the suitability of the selected responder lines as components of a binary overexpression system will be the suppression of transgene expression and associated phenotypes, upon administration of doxycycline.

In conclusion, I have generated tools to perturb VE-PTP function *in vivo*. These consist of two responder transgenic lines for full-length and extracellular domain VE-PTP, which sustain transgene induction, and exhibit defects associated with overexpression. Combined with a driver line that restricts expression to the vasculature, the significance of VE-PTP function perturbation can be assessed within the context of endothelial barrier assembly, maintenance, and breakdown.

Concluding remarks and future outlook

As is the case for most research endeavours, this scientific study has opened more questions than it has answered. Nonetheless, the novel tools generated, and the new concepts formulated should help guide future research in the area of vascular permeability. A number of possible directions are discussed below.

With this work, one of the major obstacles to studying fenestrae was surmounted, as a method was developed to reproduce fenestrae in abundance, *in vitro*, using a combination of predisposed cell lines and microfilament disruption agents. This *in vitro* culture system can serve as a platform to address questions concerning the biogenesis, composition, regulation, and function of fenestrae. Future studies may benefit from rendering the culture system conditions more close to the situation in the organism, as the physiological relevance of the extreme phenotype displayed by induced endothelioma cells is currently unknown. Triggering fenestrae induction through the use of growth factors or extracellular matrix components, should allow drawing more accurate parallels between capillary beds *in vivo* and the *in vitro* model. The first successful use of the *in vitro* model towards understanding fenestrae biology was in the subcellular, subtractive proteomics study. A number of components involved in membrane and cytoskeletal remodelling were identified, which can be accommodated within a unifying conceptual framework for the biogenesis of specialised membrane structures. Evidence presented in this thesis favours a model in which actin remodelling, PV-1 relocalisation, and the cross-linking actions of ERM proteins collaborate in orchestrating the biological response of fenestrae formation. Future studies aimed at perturbing the function of ERM proteins and altering the

reorganisation properties of microfilaments, should shed light on their precise contributions and help transform a speculative model into a substantiated theory.

The identification of a novel fenestrae sieve plate component may be of future practical use in the fields of diagnosis and treatment of vascular disease. Preliminary evidence from the physiological tissue distribution of moesin and PV-1 suggests that the two antigens, together, are promising as a composite biomarker for identifying fenestrae. Further efforts are required to establish the presence of moesin and PV-1 in fenestrae of the neovasculature, and to assess their suitability as indicators of structures contributing to leakage. Furthermore, recognition of a functional interaction between moesin and the fenestrae sieve plate would provide a new target for therapies aimed at controlling aberrant permeability.

The creation of a mouse model for VE-PTP function modulation in the endothelium constitutes the first step in an effort to understand phosphatase regulation of paracellular permeability *in vivo*. An assessment of paracellular permeability, by measuring leakage of dyes or tracers, in the new models of VE-PTP gain or loss of function should help define the physiological role of VE-PTP within the endothelial barrier. Finally, combining the TetO-VE-PTP transgenic mice with experimental conditions of endothelial barrier dysfunction such as the retinopathy of prematurity (ROP) model or tumor models could highlight roles for VE-PTP within pathological paracellular permeability.

Appendices

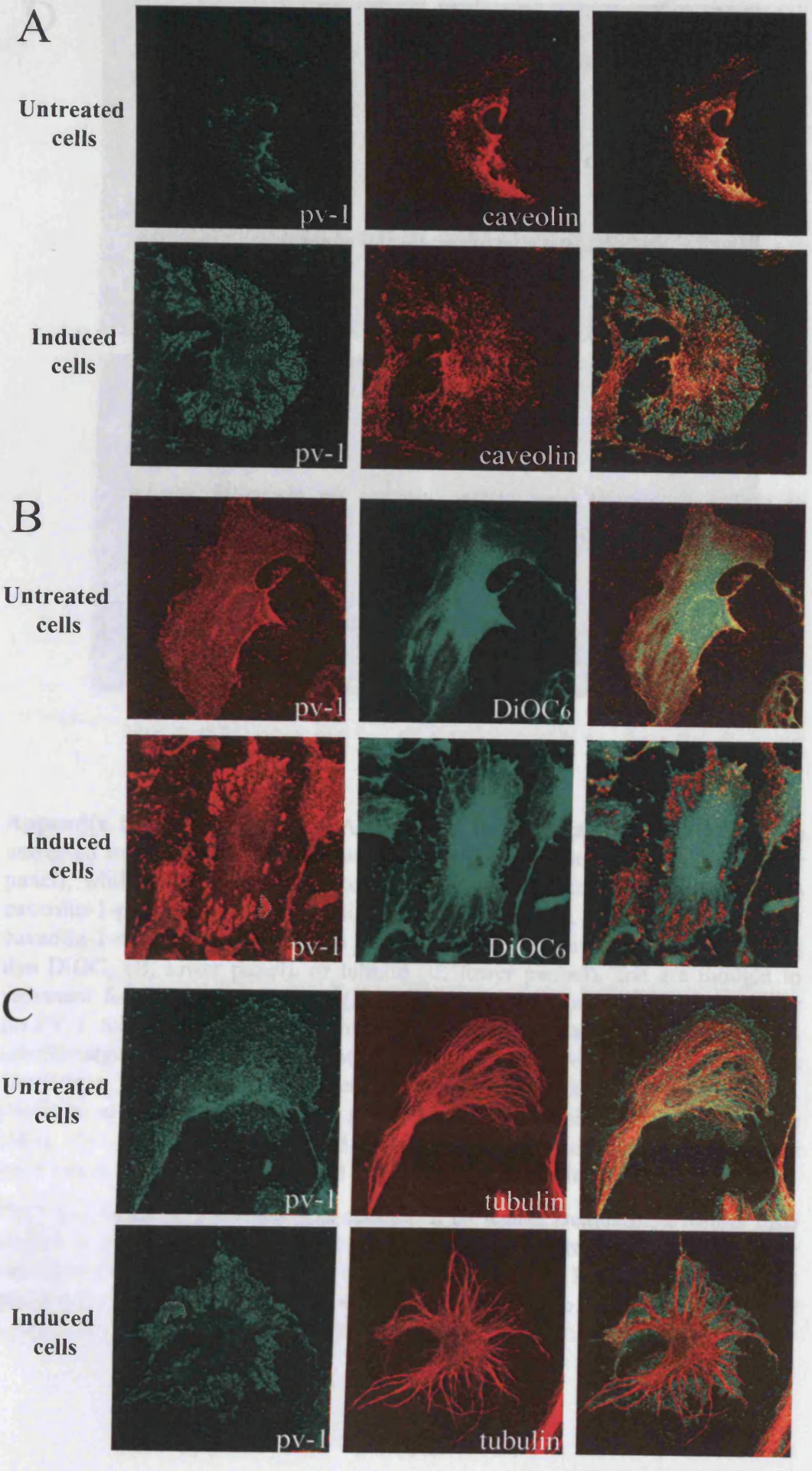
A
Untreated cells
pv-1
caveolin
Induced cells
pv-1
caveolin
B
Untreated cells
pv-1
DiOC6
Induced cells
pv-1
DiOC6
C
Untreated cells
pv-1
tubulin
Induced cells
pv-1
tubulin

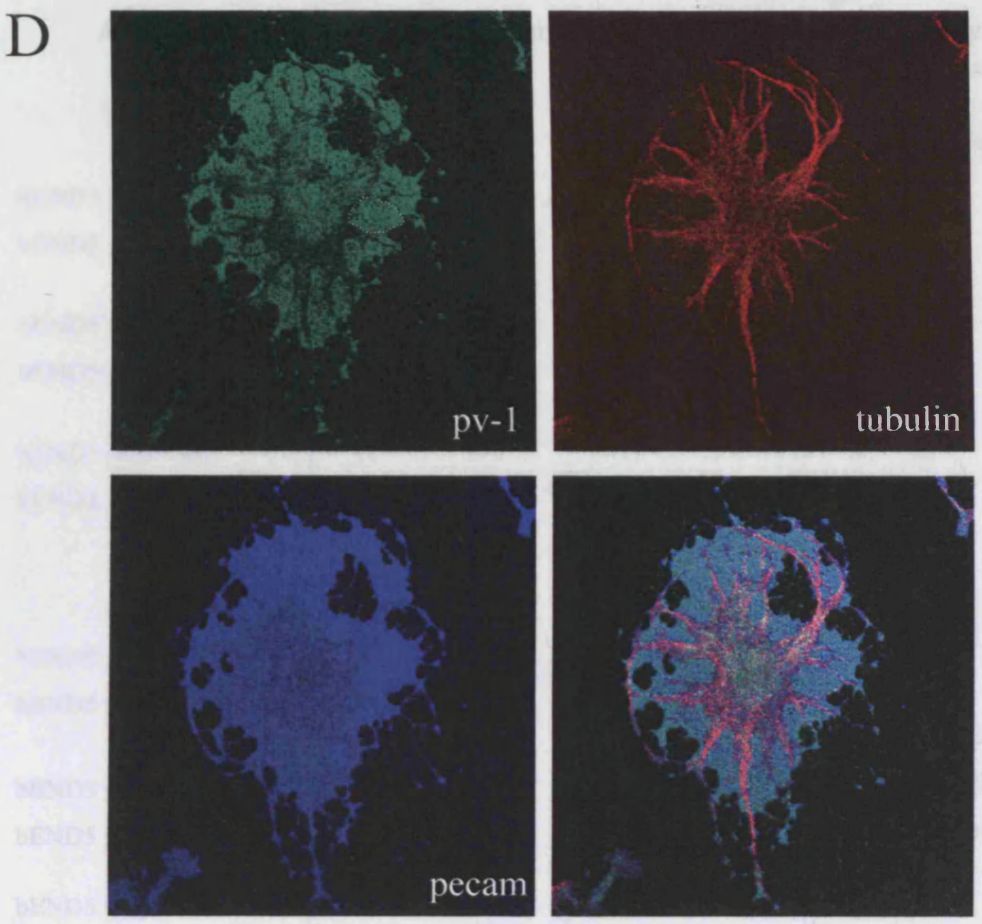

Appendix I Light Microscopy Assay using the diaphragm marker PV-1. In untreated cells PV-1 colocalises with the caveolar marker caveolin-1 (A,upper panel), while upon fenestrae induction, it distributes into two distinct areas: a caveolin-1-positive and a caveolin-1-negative area (A, lower panel). Such caveolin-1-negative areas are also devoid of labelling for the organelle-binding dye $DiOC_6$ (B, lower panel), or tubulin (C, lower pannel), and are thought to represent fenestrae sieve plates. (D) A triple immunostaining of induced cells for PV-1, tubulin, and PECAM shows that the distinct areas of PV-1-positive and tubulin-negative labelling are not a generalised phenomenon of the plasma membrane, which can be labelled throughout its surface area for PECAM. Confocal sections were obtained at the level of organelles or fenestrae sieve plates, for untreated and induced cells respectively. Representative fenestrae sieve plates are encircled by dotted lines in each panel of induced cells.

The Light Microscopy Assay was developed by Katrin Deinhardt, a former PhD student at the Endothelial Cell Biology Laboratory, currently at the Molecular Neuropathobiology Laboratory, Cancer Research UK. Part of this work was presented as a poster at the 42nd Annual Meeting of The American Society for Cell Biology, held in December 2002.

Appendix II (i) Experimental design for large-scale proteomic study

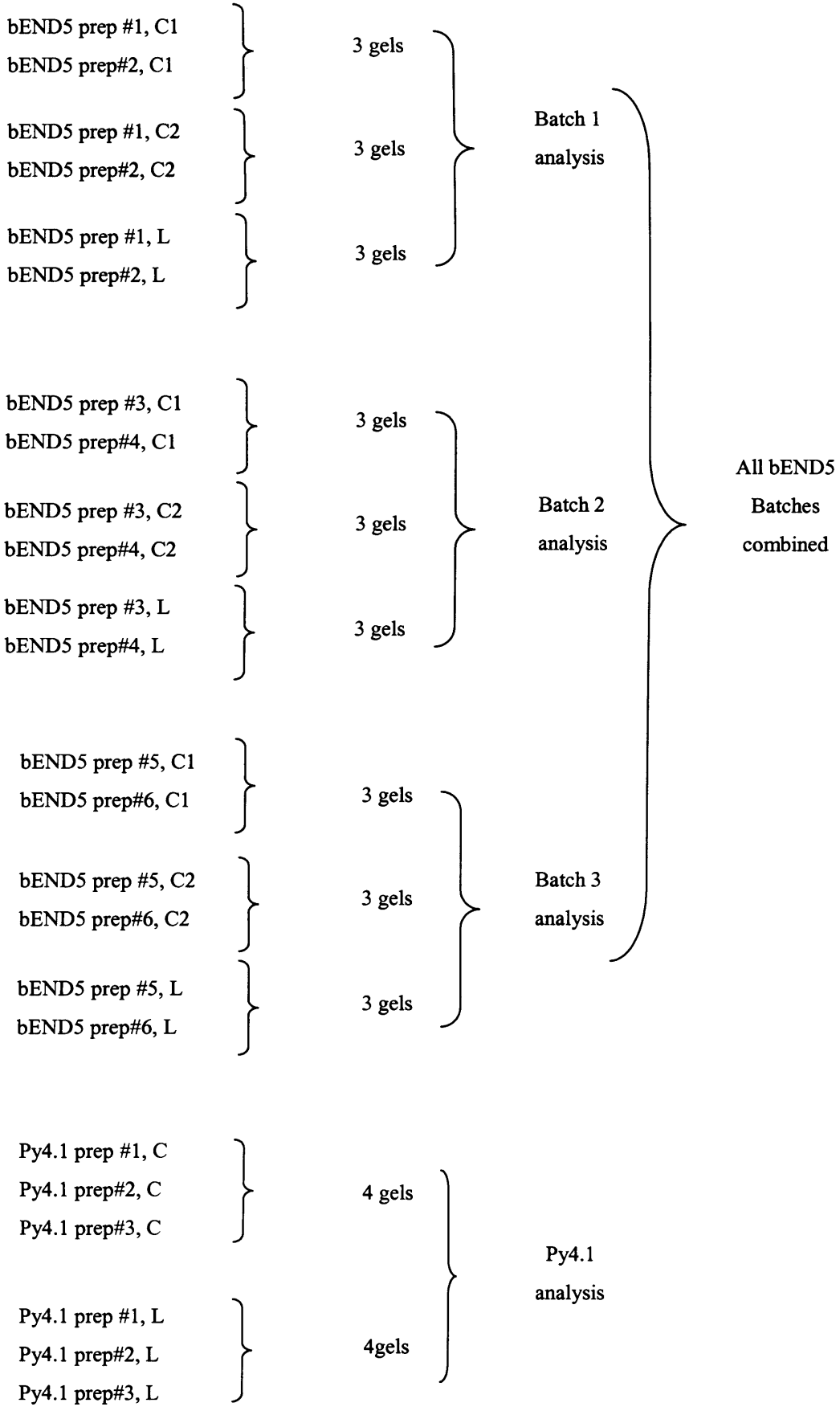

Appendix II (ii) Intensities of spots excised for mass spectrometry

	Spot no	total LvsC2	p-value	L vs C2 (1)	p-value	L vs C2 (2)	p-value	L vs C2 (3)	p-value
spots with protein identities	138	1.883	0.1927	9.224	0.03162	-1.392	0.6478	1.495	0.1227
	146	1.71	0.1852	3.28	0.1096	1.199	0.571	1.381	0.004115
	153	-1.176	0.3662	-	Unknown	-1.381	0.3138	1.266	0.157
	215	1.358	0.377	1.074	0.543	-1.24	0.02935	1.641	0.0105
	233	1.826	0.02507	2.103	0.001633	2.447	0.1313	1.58	0.08104
	237	1.364	0.1417	1.595	0.02001	1.445	0.3797	1.273	0.4535
	304	1.671	0.02125	-1.064	0.8038	2.148	0.1855	3.067	0.01115
	334	1.193	0.3104	1.052	0.7728	-	Unknown	1.396	0.01084
	400	-1.012	0.9481	1.03	0.353	-1.394	0.1313	1.416	0.01322
	406	1.229	0.2688	1.52	0.00371	1.042	0.7731	1.372	0.1275
	414	1.927	0.007195	3.415	0.1368	1.135	0.4678	2.675	0.009798
	473	-	Unknown	3.99	0.008421	-	Unknown	-	Unknown
	478	1.488	0.001198	1.345	0.09975	1.517	0.1585	1.842	0.122
	486	-	Unknown	19.635	Unknown	-	Unknown	-	Unknown
	517	1.251	0.03035	1.611	0.003646	-	Unknown	1.334	0.03847
	521	1.16	0.945	4.502	Unknown	-	Unknown	1.373	0.02015
	526	1.689	0.0001765	-1.274	Unknown	1.503	0.03269	2.373	0.01236
	527	1.548	0.002631	1.265	0.2492	1.423	0.01114	2.269	0.02215
spots without protein identities	65	1.247	0.4155	-1.846	0.05807	1.494	0.0008652	1.052	0.001266
	125	1.928	0.1568	1.332	0.05748	1.255	0.04611	1.669	0.6696
	155	-1.264	0.7714	-	Unknown	-1.264	0.3465	1.463	0.0003429
	188	1.315	0.5625	1.397	0.01912	-	Unknown	-	Unknown
	200	1.448	0.001263	1.36	0.1691	1.492	0.1217	1.509	0.1035
	239	1.256	0.2898	-1.771	Unknown	1.293	0.7221	1.462	0.02508
	271	-	Unknown	-	Unknown	only in L		-	Unknown
	292	1.145	0.3585	-1.08	0.5231	1.025	0.8736	1.404	0.01543
	366	2.973	0.1192	-	Unknown	1.442	0.000735	-	Unknown
	399	-1.008	0.08448	1.484	0.01762	-	Unknown	1.766	0.1215
	402	1.348	0.06779	1.847	0.008672	1.172	0.1845	1.146	0.7076
	410	1.144	0.3432	1.357	0.04608	-1.227	0.5891	1.395	0.1706
	411	1.385	0.1231	1.071	0.5587	1.049	0.4479	2.401	0.02249
	443	1.426	0.07064	2.311	0.01659	-1.116	0.7321	1.404	0.4977
	450	1.164	0.1214	2.12	0.02537	-1.857	0.5471	2.524	0.2858
	479	1.875	0.02106	2.043	0.3201	-1.007	0.1216	-	Unknown
	488	3.264	0.00418	3.019	0.0222	1.839	0.1587	-	Unknown
	491	1.475	0.5093	-	Unknown	-	Unknown	2.205	0.01431

	Fold changes for excised spots from Py4.1 cell analysis		
	Spot no	total LvsC	p-value
spots with protein identities	401	3.811	0.003184
	658	2.038	0.002161
	659	1.772	0.02662
	793	2.258	0.004779

Appendix II (iii) Protein identity assignment

bEND5 cells upregulated spots:									
Gel #	**Spot # (Gel)**	**Protein Name**	**Accession #**	**Species**	**MW (Kda)**	**pI**	**# peptides matched**	**MOWSE Score**	**% sequence covered by matching**
373	235	Alpha enolase	P17182.40	*Mus musculus*	46.9	6.4	6	60	22.4
373	257	Eukaryotic initiation factor 4A-like	Q8BVY3.23	*Mus musculus*	46.7	6.64	9	102	28.95
		Probable ATP-dependent helicase	Q91VC3.42	*Mus musculus*	46.8	6.33	9	102	28.95
373	233	Alpha enolase	P17182.40	*Mus musculus*	46.9	6.4	10	124	34.64
552	486	Cofilin, non-muscle isoform	P18760.16	*Mus musculus*	18.5	8.25	5	47	45.78
552	527	Myosin light chain alkali, smooth-muscle	Q64119.35	*Mus musculus*	16.8	4.46	6	61	45.33
552	304	Actin monomer-binding protein	Q80X09.24	*Mus musculus*	40.1	6.35	6	57	24.86
552	414	14-3-3 protein zeta/delta	P35215.28	*Mus musculus*	27.7	4.73	5	41	28.16
552	526	Myosin light chain alkali(MLC3 SM)	Q64119.35	*Mus musculus*	16.8	4.46	5	42	34.67
473	478	Myosin regulatory light chain 2-A	P13832.13	*Rattus Norvegicus*	19.7	4.65	11	152	63.16
		Myosin regulatory light chain 2-B	P18666.32	*Rattus Norvegicus*	19.6	4.76	8	91	40.94
BATCH ANALYSIS -1									
406	237	Interferon-activatable protein 205 (IFI-205)	Q08619.35	*Mus musculus*	47	8.4	4	12	8.94

470	406	Ras suppressor protein 1 (Rsu-1)	Q01730.29	*Mus musculus*	31.5	8.86	5	31	19.49
406	473	Similar to transgelin 2	Q91VU2.19	*Mus musculus*	22.3	8.43	5	35	31.16
406	517	Putative RNA-binding protein 3	Q89086.38	*Mus musculus*	16.5	7.04	3	11	28.76
BATCH ANALYSIS -3									
470	138	Heterogeneous nuclear ribonucleoprotein K	Q8BGQ8.23	*Mus musculus*	48.4	5.69	5	33	14.35
557	138	Heterogeneous nuclear ribonucleoprotein K	Q8BGQ8.23	*Mus musculus*	48.4	5.69	14	180	35.76
		Heterogeneous nuclear ribonucleoprotein K	Q60577.40	*Homo Sapiens, Rattus Norvegicus,*	50.9	5.25	13	163	30.6
541	146	Heterogeneous nuclear ribonucleoprotein K	Q60577.40	*Mus musculus*	50.9	5.25	5	27	11.64
557	146	Heterogeneous nuclear ribonucleoprotein K	Q60577.40	*Mus musculus*	50.9	5.25	13	165	31.25
		Heterogeneous nuclear ribonucleoprotein K	Q8BGQ8.23	*Mus musculus*	48.4	5.69	14	182	36.45
541	153	60 kDa heat shock protein, mitochondria	P19226.36	*Mus musculus, Rattus Norvegicus*	60.9	5.92	7	68	15.71
541	215	ATP synthase beta subunit	Q9CWA2.17	*Mus musculus*	56.9	5.44	8	89	22.85
557	215	ATP synthase beta chain	P56480.41	*Mus musculus*	56.2	5.19	13	175	34.78
541	334	Annexin II (Lipocortin II)	P07356.07	*Mus musculus*	38.5	7.69	4	18	11.24

557	334	Annexin II (Lipocortin II)	P07356.07	*Mus musculus*	38.5	7.69	4	19	14.5
557	400	Eukaryotic translation initiation factor 4H	O9WUK2.40	*Mus musculus*	27.3	6.95	10	96	35.08
		Musculin (Myogenic repressor)	O88940.40	*Mus musculus*	21.5	9.45	6	44	28.36
541	517	Putative RNA-binding protein 3	O89086.38	*Mus musculus*	16.5	7.04	4	31	30.07
470	517	Putative RNA-binding protein 3	O89086.38	*Mus musculus*	16.5	7.04	6	67	53.59
		Putative RNA-binding protein 3	O89086.38	*Mus musculus*	16.5	7.04	5	37	39.22
		Nucleoside diphosphate kinase B	Q01768.25	*Mus musculus*	17.3	7.21	5	38	40.79
557	517	Putative RNA-binding protein 3	O89086.38	*Mus musculus*	16.5	7.04	5	41	33.99
		Nucleoside diphosphate kinase A	P15532.14	*Mus musculus*	17.1	7.1	5	36	38.16
		Nucleoside diphosphate kinase B	P22392.19	*Homo Sapiens*	17.2	8.56	4	21	31.58
557	521	Nucleoside diphosphate kinase A	P15532.14	*Mus musculus*	17.1	7.1	7	58	37.5
		Nucleoside diphosphate kinase B	Q01768.25	*Mus musculus*	17.3	7.21	11	125	69.74
541	521	Nucleoside diphosphate kinase B	Q01768.25	*Mus musculus*	17.3	7.21	3	5	23.68

Py4.1 cells: upregulated spots									
Gel #	**Spot # (Gel)**	**Protein Name**	**Accession #**	**Species**	**MW (Kda)**	**pI**	**# peptides matched**	**MOWSE Score**	**% Coverage**
561	401	Radixin	P26043.22	*Mus musculus*	68.4	5.82	11	120	21.78
		Moesin	P26041.28	*Mus musculus*	67.5	6.23	19	246	31.6
561	658	Elongation factor 1-gamma	Q9D8N0.40	*Mus musculus*	50	6.33	13	151	27
		Alpha enolase	P17182.40	*Mus musculus*	46.9	6.4	18	240	46.42
561	793	Protein tyrosine kinase 9	O91YR1.19	*Mus musculus*	40	6.26	8	90	32.29
561	659	Alpha enolase	P04764.05	*Mus musculus*	46.9	6.18	7	80	27.71
		Paralemmin	Q9Z0P4.10	*Mus musculus*	41.5	4.79	5	42	21.41
		Kinesin light chain KLCt	Q9ESH7	*Rattus norvegicus*	55.8	6.16	5	46	19.01

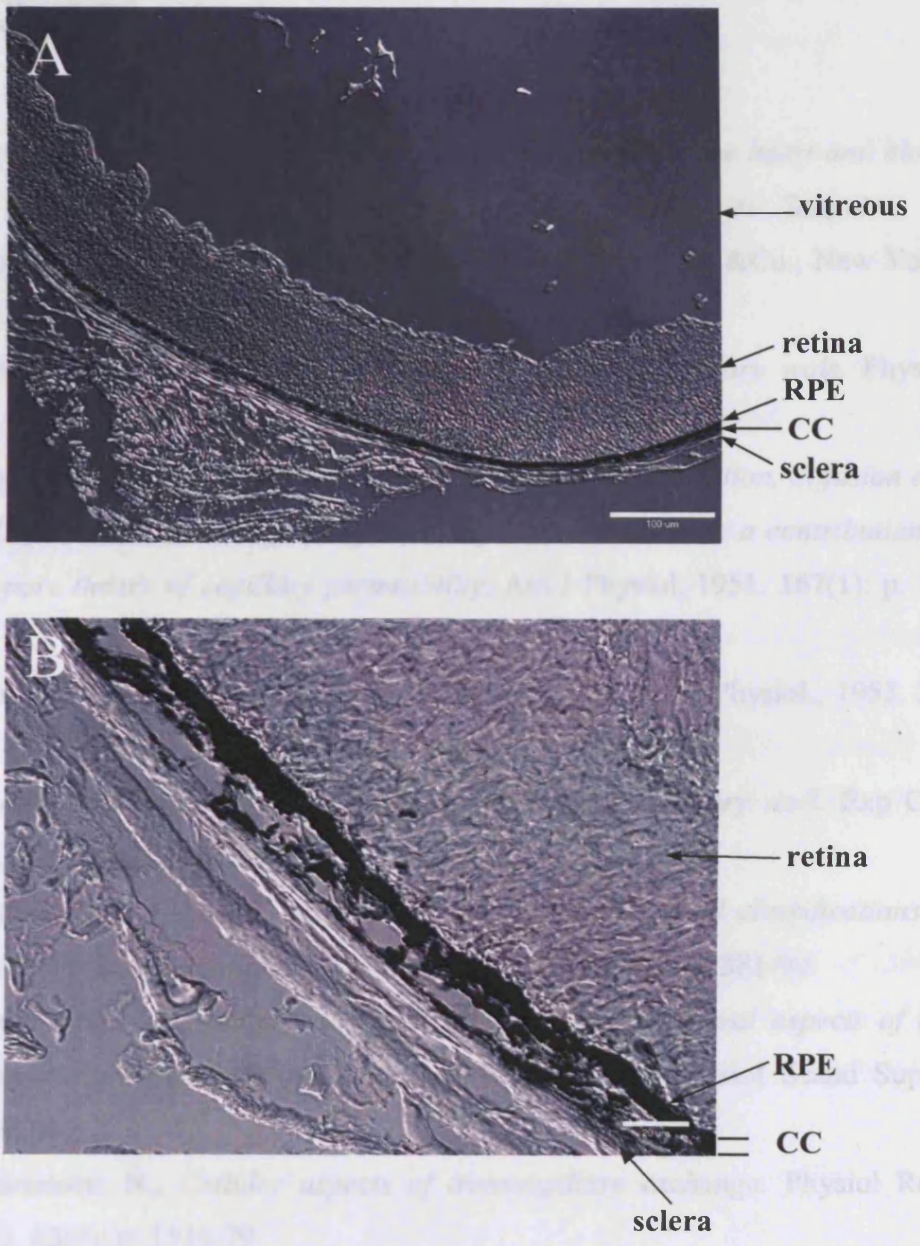

Appendix III Differential interference contrast (DIC) microscopy on eye sections. Low (A) and high (B) magnification images show the topology of the sections and the different layers included: retina, retinal pigment epithelium (RPE), choriocapillaris (CC), sclera. (Bars = 100 μm and 20 μm, respectively)

References

1. Harvey, W., *An anatomical discuisition on the motion of the heart and blood in animals (Exercitatio Anatomica de Motu Cordis et Sanguinis in Animalibus)*. Everyman's library. 1908: London, J.M. Dent &Co.; New York, E.P. Dutton &Co.
2. Pappenheimer, J.R., *Passage of molecules through capillary wals.* Physiol Rev, 1953. **33**(3): p. 387-423.
3. Pappenheimer, J.R., E.M. Renkin, and L.M. Borrero, *Filtration, diffusion and molecular sieving through peripheral capillary membranes; a contribution to the pore theory of capillary permeability.* Am J Physiol, 1951. **167**(1): p. 13-46.
4. Palade, G.E., *Fine structure of blood capillaries.* J. Appl. Physiol., 1953. **24**: p. 1424.
5. Rhodin, J., *Electron microscopy of the glomerular capillary wall.* Exp Cell Res, 1955. **8**(3): p. 572-4.
6. Bennett, H.S., J.H. Luft, and J.C. Hampton, *Morphological classifications of vertebrate blood capillaries.* Am J Physiol, 1959. **196**(2): p. 381-90.
7. Palade, G.E., M. Simionescu, and N. Simionescu, *Structural aspects of the permeability of the microvascular endothelium.* Acta Physiol Scand Suppl, 1979. **463**: p. 11-32.
8. Simionescu, N., *Cellular aspects of transcapillary exchange.* Physiol Rev, 1983. **63**(4): p. 1536-79.
9. Farquhar, M.G. and G.E. Palade, *Junctional complexes in various epithelia.* J Cell Biol, 1963. **17**: p. 375-412.
10. Staehelin, L.A., *Further observations on the fine structure of freeze-cleaved tight junctions.* J Cell Sci, 1973. **13**(3): p. 763-86.
11. Bearer, E.L. and L. Orci, *Endothelial fenestral diaphragms: a quick-freeze, deep-etch study.* J Cell Biol, 1985. **100**(2): p. 418-28.
12. Furuse, M., et al., *Occludin: a novel integral membrane protein localizing at tight junctions.* J Cell Biol, 1993. **123**(6 Pt 2): p. 1777-88.

13. Furuse, M., et al., *Claudin-1 and -2: novel integral membrane proteins localizing at tight junctions with no sequence similarity to occludin.* J Cell Biol, 1998. **141**(7): p. 1539-50.
14. Lampugnani, M.G., et al., *A novel endothelial-specific membrane protein is a marker of cell-cell contacts.* J Cell Biol, 1992. **118**(6): p. 1511-22.
15. Rothberg, K.G., et al., *Caveolin, a protein component of caveolae membrane coats.* Cell, 1992. **68**(4): p. 673-82.
16. Stan, R.V., et al., *Isolation, cloning, and localization of rat PV-1, a novel endothelial caveolar protein.* J Cell Biol, 1999. **145**(6): p. 1189-98.
17. Cattelino, A., et al., *The conditional inactivation of the beta-catenin gene in endothelial cells causes a defective vascular pattern and increased vascular fragility.* J Cell Biol, 2003. **162**(6): p. 1111-22.
18. Nitta, T., et al., *Size-selective loosening of the blood-brain barrier in claudin-5-deficient mice.* J Cell Biol, 2003. **161**(3): p. 653-60.
19. Razani, B., et al., *Caveolin-1 null mice are viable but show evidence of hyperproliferative and vascular abnormalities.* J Biol Chem, 2001. **276**(41): p. 38121-38.
20. Drab, M., et al., *Loss of caveolae, vascular dysfunction, and pulmonary defects in caveolin-1 gene-disrupted mice.* Science, 2001. **293**(5539): p. 2449-52.
21. Rubin, L.L. and J.M. Staddon, *The cell biology of the blood-brain barrier.* Annu Rev Neurosci, 1999. **22**: p. 11-28.
22. Engelhardt, B., *Development of the blood-brain barrier.* Cell Tissue Res, 2003. **314**(1): p. 119-29.
23. Cunha-Vaz, J.G., *The blood-retinal barriers system. Basic concepts and clinical evaluation.* Exp Eye Res, 2004. **78**(3): p. 715-21.
24. Pardridge, W.M., R.J. Boado, and C.R. Farrell, *Brain-type glucose transporter (GLUT-1) is selectively localized to the blood-brain barrier. Studies with quantitative western blotting and in situ hybridization.* J Biol Chem, 1990. **265**(29): p. 18035-40.
25. Risau, W., *Induction of blood-brain barrier endothelial cell differentiation.* Ann N Y Acad Sci, 1991. **633**: p. 405-19.

26. Mann, G.E., D.L. Yudilevich, and L. Sobrevia, *Regulation of amino acid and glucose transporters in endothelial and smooth muscle cells.* Physiol Rev, 2003. **83**(1): p. 183-252.
27. Oliver, G., *Lymphatic vasculature development.* Nat Rev Immunol, 2004. **4**(1): p. 35-45.
28. Jones, N., et al., *Tie receptors: new modulators of angiogenic and lymphangiogenic responses.* Nat Rev Mol Cell Biol, 2001. **2**(4): p. 257-67.
29. Simionescu, M., *Structural, Biochemical and Functional differentiation of the Vascular Endothelium*, in *Morphogenesis of Endothelium*, W.a.R. Risau, G.M., Editor. 2000, Harwood Academic: Amsterdam. p. 1-21.
30. Dejana, E., M. Corada, and M.G. Lampugnani, *Endothelial cell-to-cell junctions.* Faseb J, 1995. **9**(10): p. 910-8.
31. Casley-Smith, J.R., *The phylogeny of the fine structure of blood vessels and lymphatics: similarities and differences.* Lymphology, 1987. **20**(4): p. 182-8.
32. Kuhn, K., H. Stolte, and E. Reale, *The fine structure of the kidney of the hagfish (Myxine glutinosa L.): A thin section and freeze-fracture study.* Cell Tissue Res, 1975. **164**(2): p. 201-13.
33. Bazzoni, G. and E. Dejana, *Endothelial cell-to-cell junctions: molecular organization and role in vascular homeostasis.* Physiol Rev, 2004. **84**(3): p. 869-901.
34. Tsukita, S., M. Furuse, and M. Itoh, *Multifunctional strands in tight junctions.* Nat Rev Mol Cell Biol, 2001. **2**(4): p. 285-93.
35. Bundgaard, M., *The three-dimensional organization of tight junctions in a capillary endothelium revealed by serial-section electron microscopy.* J Ultrastruct Res, 1984. **88**(1): p. 1-17.
36. Tsukita, S. and M. Furuse, *Pores in the wall: claudins constitute tight junction strands containing aqueous pores.* J Cell Biol, 2000. **149**(1): p. 13-6.
37. Tang, V.W. and D.A. Goodenough, *Paracellular ion channel at the tight junction.* Biophys J, 2003. **84**(3): p. 1660-73.
38. Yamada, E., *The fine structure of the gall bladder epithelium of the mouse.* J Biophys Biochem Cytol, 1955. **1**(5): p. 445-58.
39. Razani, B., S.E. Woodman, and M.P. Lisanti, *Caveolae: from cell biology to animal physiology.* Pharmacol Rev, 2002. **54**(3): p. 431-67.

40. Palade, G.E., *Transport in quanta across the endothelium of blood capillaries.* Anat Rec, 1960. **136**: p. 254.

41. Clementi, F. and G.E. Palade, *Intestinal capillaries. I. Permeability to peroxidase and ferritin.* J Cell Biol, 1969. **41**(1): p. 33-58.

42. Ghitescu, L., et al., *Specific binding sites for albumin restricted to plasmalemmal vesicles of continuous capillary endothelium: receptor-mediated transcytosis.* J Cell Biol, 1986. **102**(4): p. 1304-11.

43. Schubert, W., et al., *Caveolae-deficient endothelial cells show defects in the uptake and transport of albumin in vivo.* J Biol Chem, 2001. **276**(52): p. 48619-22.

44. Vasile, E., M. Simionescu, and N. Simionescu, *Visualization of the binding, endocytosis, and transcytosis of low-density lipoprotein in the arterial endothelium in situ.* J Cell Biol, 1983. **96**(6): p. 1677-89.

45. Williams, T.M. and M.P. Lisanti, *The caveolin proteins.* Genome Biol, 2004. **5**(3): p. 214.

46. Palade, G.E. and R.R. Bruns, *Structural modulations of plasmalemmal vesicles.* J Cell Biol, 1968. **37**(3): p. 633-49.

47. Kohn, S., et al., *Pathways of macromolecular tracer transport across venules and small veins. Structural basis for the hyperpermeability of tumor blood vessels.* Lab Invest, 1992. **67**(5): p. 596-607.

48. Dvorak, A.M., et al., *The vesiculo-vacuolar organelle (VVO): a distinct endothelial cell structure that provides a transcellular pathway for macromolecular extravasation.* J Leukoc Biol, 1996. **59**(1): p. 100-15.

49. Vasile, E., et al., *Caveolae and vesiculo-vacuolar organelles in bovine capillary endothelial cells cultured with VPF/VEGF on floating Matrigel-collagen gels.* J Histochem Cytochem, 1999. **47**(2): p. 159-67.

50. Feng, D., et al., *Pathways of macromolecular extravasation across microvascular endothelium in response to VPF/VEGF and other vasoactive mediators.* Microcirculation, 1999. **6**(1): p. 23-44.

51. Dvorak, A.M. and D. Feng, *The vesiculo-vacuolar organelle (VVO). A new endothelial cell permeability organelle.* J Histochem Cytochem, 2001. **49**(4): p. 419-32.

52. Simionescu, N., M. Siminoescu, and G.E. Palade, *Permeability of muscle capillaries to small heme-peptides. Evidence for the existence of patent transendothelial channels.* J Cell Biol, 1975. **64**(3): p. 586-607.

53. Dvorak, H.F., et al., *Vascular permeability factor/vascular endothelial growth factor and the significance of microvascular hyperpermeability in angiogenesis.* Curr Top Microbiol Immunol, 1999. **237**: p. 97-132.

54. Stan, R.V., M. Kubitza, and G.E. Palade, *PV-1 is a component of the fenestral and stomatal diaphragms in fenestrated endothelia.* Proc Natl Acad Sci U S A, 1999. **96**(23): p. 13203-7.

55. Gautier, A., W. Bernhard, and C. Oberling, *[The existence of a pericapillary lacunar apparatus in the malpighian glomeruli revealed by electronic microscopy].* C R Seances Soc Biol Fil, 1950. **144**(23-24): p. 1605-7.

56. Yamada, E., *The fine structure of the renal glomerulus of the mouse.* J Histochem Cytochem, 1955. **3**(4): p. 309.

57. Pease, D.C., *Electron microscopy of the vascular bed of the kidney cortex.* Anat Rec, 1955. **121**(4): p. 701-21.

58. Trier, J.S., *The fine structure of the parathyroid gland.* J Biophys Biochem Cytol, 1958. **4**(1): p. 13-22.

59. Rhodin, J.A., *The diaphragm of capillary endothelial fenestrations.* J Ultrastruct Res, 1962. **6**: p. 171-85.

60. Braet, F. and E. Wisse, *Structural and functional aspects of liver sinusoidal endothelial cell fenestrae: a review.* Comp Hepatol, 2002. **1**(1): p. 1.

61. Braet, F., et al., *Comparative scanning, transmission and atomic force microscopy of the microtubular cytoskeleton in fenestrated liver endothelial cells.* Scanning Microsc Suppl, 1996. **10**: p. 225-35; discussion 235-6.

62. Simionescu, M., N. Simionescu, and G.E. Palade, *Morphometric data on the endothelium of blood capillaries.* J Cell Biol, 1974. **60**(1): p. 128-52.

63. Simionescu, N., M. Simionescu, and G.E. Palade, *Differentiated microdomains on the luminal surface of the capillary endothelium. I. Preferential distribution of anionic sites.* J Cell Biol, 1981. **90**(3): p. 605-13.

64. Simionescu, M., et al., *Differentiated microdomains on the luminal surface of the capillary endothelium. II. Partial characterization of their anionic sites.* J Cell Biol, 1981. **90**(3): p. 614-21.

65. Simionescu, M., N. Simionescu, and G.E. Palade, *Differentiated microdomains on the luminal surface of capillary endothelium: distribution of lectin receptors.* J Cell Biol, 1982. **94**(2): p. 406-13.

66. Pino, R.M., *Binding and endocytosis of heparin-gold conjugates by the fenestrated endothelium of the rat choriocapillaris.* Cell Tissue Res, 1987. **250**(2): p. 257-66.

67. Pino, R.M., *The cell surface of a restrictive fenestrated endothelium. I. Distribution of lectin-receptor monosaccharides on the choriocapillaris.* Cell Tissue Res, 1986. **243**(1): p. 145-55.

68. Bankston, P.W. and A.J. Milici, *A survey of the binding of polycationic ferritin in several fenestrated capillary beds: indication of heterogeneity in the luminal glycocalyx of fenestral diaphragms.* Microvasc Res, 1983. **26**(1): p. 36-48.

69. Roberts, W.G. and G.E. Palade, *Neovasculature induced by vascular endothelial growth factor is fenestrated.* Cancer Res, 1997. **57**(4): p. 765-72.

70. Simionescu, M., N. Simionescu, and G.E. Palade, *Preferential distribution of anionic sites on the basement membrane and the abluminal aspect of the endothelium in fenestrated capillaries.* J Cell Biol, 1982. **95**(2 Pt 1): p. 425-34.

71. Stan, R.V., *Multiple PV1 dimers reside in the same stomatal or fenestral diaphragm.* Am J Physiol Heart Circ Physiol, 2004. **286**(4): p. H1347-53.

72. Levick, J.R. and L.H. Smaje, *An analysis of the permeability of a fenestra.* Microvasc Res, 1987. **33**(2): p. 233-56.

73. Simionescu, N., F. Lupu, and M. Simionescu, *Rings of membrane sterols surround the openings of vesicles and fenestrae, in capillary endothelium.* J Cell Biol, 1983. **97**(5 Pt 1): p. 1592-600.

74. Mayer, G., G. Boileau, and M. Bendayan, *Furin interacts with proMT1-MMP and integrin alphaV at specialized domains of renal cell plasma membrane.* J Cell Sci, 2003. **116**(Pt 9): p. 1763-73.

75. Yokomori, H., et al., *Hepatic sinusoidal endothelial fenestrae express plasma membrane Ca++pump and Ca++Mg++-ATPase.* Liver, 2000. **20**(6): p. 458-64.

76. Ogi, M., et al., *Expression of plasma membrane Ca2+-ATPase on hepatic sinusoidal endothelial fenestrae: modification of the one-step method.* Med Electron Microsc, 2000. **33**(3): p. 143-50.

77. Hart, T.K. and R.M. Pino, *Capillary permeability in the pancreas and colon: restriction of exogenous and endogenous molecules by fenestrated endothelia.* Am J Anat, 1986. **175**(1): p. 49-58.

78. Pino, R.M. and E. Essner, *Permeability of rat choriocapillaris to hemeproteins. Restriction of tracers by a fenestrated endothelium.* J Histochem Cytochem, 1981. **29**(2): p. 281-90.

79. Simionescu, N. and G.E. Palade, *Dextrans and glycogens as particulate tracers for studying capillary permeability.* J Cell Biol, 1971. **50**(3): p. 616-24.

80. Fahrenkrog, B., J. Koser, and U. Aebi, *The nuclear pore complex: a jack of all trades?* Trends Biochem Sci, 2004. **29**(4): p. 175-82.

81. Granger, D.N., et al., *Analysis of the permeability characteristics of cat intestinal capillaries.* Circ Res, 1979. **44**(3): p. 335-44.

82. Engelhardt, B., K. Wolburg-Buchholz, and H. Wolburg, *Involvement of the choroid plexus in central nervous system inflammation.* Microsc Res Tech, 2001. **52**(1): p. 112-29.

83. Ryan, U.S., et al., *Fenestrated endothelium of the adrenal gland: freeze-fracture studies.* Tissue Cell, 1975. **7**(1): p. 181-90.

84. Pino, R.M. and E. Essner, *Structure and permeability to ferritin of the choriocapillary endothelium of the rat eye.* Cell Tissue Res, 1980. **208**(1): p. 21-7.

85. Reeves, W.H., Y.S. Kanwar, and M.G. Farquhar, *Assembly of the glomerular filtration surface. Differentiation of anionic sites in glomerular capillaries of newborn rat kidney.* J Cell Biol, 1980. **85**(3): p. 735-53.

86. Milici, A.J., M.B. Furie, and W.W. Carley, *The formation of fenestrations and channels by capillary endothelium in vitro.* Proc Natl Acad Sci U S A, 1985. **82**(18): p. 6181-5.

87. Carley, W.W., A.J. Milici, and J.A. Madri, *Extracellular matrix specificity for the differentiation of capillary endothelial cells.* Exp Cell Res, 1988. **178**(2): p. 426-34.

88. Lombardi, T., et al., *Endothelial diaphragmed fenestrae: in vitro modulation by phorbol myristate acetate.* J Cell Biol, 1986. **102**(5): p. 1965-70.

89. Lombardi, T., R. Montesano, and L. Orci, *Phorbol ester induces diaphragmed fenestrae in large vessel endothelium in vitro.* Eur J Cell Biol, 1987. **44**(1): p. 86-9.

90. Lombardi, T., et al., *In vitro modulation of endothelial fenestrae: opposing effects of retinoic acid and transforming growth factor beta.* J Cell Sci, 1988. **91 (Pt 2)**: p. 313-8.

91. Ruhrberg, C., *Growing and shaping the vascular tree: multiple roles for VEGF.* Bioessays, 2003. **25**(11): p. 1052-60.

92. Breier, G., et al., *Expression of vascular endothelial growth factor during embryonic angiogenesis and endothelial cell differentiation.* Development, 1992. **114**(2): p. 521-32.

93. Wallow, I.H. and P.S. Geldner, *Endothelial fenestrae in proliferative diabetic retinopathy.* Invest Ophthalmol Vis Sci, 1980. **19**(10): p. 1176-83.

94. Esser, S., et al., *Vascular endothelial growth factor induces endothelial fenestrations in vitro.* J Cell Biol, 1998. **140**(4): p. 947-59.

95. Braet, F., et al., *Microfilament-disrupting agent latrunculin A induces and increased number of fenestrae in rat liver sinusoidal endothelial cells: comparison with cytochalasin B.* Hepatology, 1996. **24**(3): p. 627-35.

96. Braet, F., et al., *A novel structure involved in the formation of liver endothelial cell fenestrae revealed by using the actin inhibitor misakinolide.* Proc Natl Acad Sci U S A, 1998. **95**(23): p. 13635-40.

97. Eriksson, A., et al., *Small GTP-binding protein Rac is an essential mediator of vascular endothelial growth factor-induced endothelial fenestrations and vascular permeability.* Circulation, 2003. **107**(11): p. 1532-8.

98. Gatmaitan, Z., et al., *Studies on fenestral contraction in rat liver endothelial cells in culture.* Am J Pathol, 1996. **148**(6): p. 2027-41.

99. Sorensson, J., et al., *Glomerular endothelial fenestrae in vivo are not formed from caveolae.* J Am Soc Nephrol, 2002. **13**(11): p. 2639-47.

100. Friederici, H.H., *The tridimensional ultrastructure of fenestrated capillaries.* J Ultrastruct Res, 1968. **23**(5): p. 444-56.

101. Bankston, P.W. and R.M. Pino, *The development of the sinusoids of fetal rat liver: morphology of endothelial cells, Kupffer cells, and the transmural migration of blood cells into the sinusoids.* Am J Anat, 1980. **159**(1): p. 1-15.

102. Burgoyne, R. and T. Cheek, *Reorganization of peripheral actin filaments as a prelude to exocytosis.* Biosci. Rep., 1987. **7**: p. 281-288.

103. Eitzen, G., *Actin remodeling to facilitate membrane fusion.* Biochim Biophys Acta, 2003. **1641**(2-3): p. 175-81.

104. Bruns, R.R. and G.E. Palade, *Studies on blood capillaries. I. General organization of blood capillaries in muscle.* J Cell Biol, 1968. **37**(2): p. 244-76.

105. Wheelock, M.J. and K.R. Johnson, *Cadherins as modulators of cellular phenotype.* Annu Rev Cell Dev Biol, 2003. **19**: p. 207-35.

106. Gory, S., et al., *The vascular endothelial-cadherin promoter directs endothelial-specific expression in transgenic mice.* Blood, 1999. **93**(1): p. 184-92.

107. Corada, M., et al., *Vascular endothelial-cadherin is an important determinant of microvascular integrity in vivo.* Proc Natl Acad Sci U S A, 1999. **96**(17): p. 9815-20.

108. Iyer, S., et al., *VE-cadherin-p120 interaction is required for maintenance of endothelial barrier function.* Am J Physiol Lung Cell Mol Physiol, 2004. **286**(6): p. L1143-53.

109. Vincent, P.A., et al., *VE-cadherin: adhesion at arm's length.* Am J Physiol Cell Physiol, 2004. **286**(5): p. C987-97.

110. Schmelz, M. and W.W. Franke, *Complexus adhaerentes, a new group of desmoplakin-containing junctions in endothelial cells: the syndesmos connecting retothelial cells of lymph nodes.* Eur J Cell Biol, 1993. **61**(2): p. 274-89.

111. Breier, G., et al., *Molecular cloning and expression of murine vascular endothelial-cadherin in early stage development of cardiovascular system.* Blood, 1996. **87**(2): p. 630-41.

112. Carmeliet, P., et al., *Targeted deficiency or cytosolic truncation of the VE-cadherin gene in mice impairs VEGF-mediated endothelial survival and angiogenesis.* Cell, 1999. **98**(2): p. 147-57.

113. Rabiet, M.J., et al., *Thrombin-induced increase in endothelial permeability is associated with changes in cell-to-cell junction organization.* Arterioscler Thromb Vasc Biol, 1996. **16**(3): p. 488-96.

114. Esser, S., et al., *Vascular endothelial growth factor induces VE-cadherin tyrosine phosphorylation in endothelial cells.* J Cell Sci, 1998. **111 (Pt 13)**: p. 1853-65.

115. Kevil, C.G., et al., *Vascular permeability factor/vascular endothelial cell growth factor-mediated permeability occurs through disorganization of endothelial junctional proteins.* J Biol Chem, 1998. **273**(24): p. 15099-103.

116. Andriopoulou, P., et al., *Histamine induces tyrosine phosphorylation of endothelial cell-to-cell adherens junctions.* Arterioscler Thromb Vasc Biol, 1999. **19**(10): p. 2286-97.

117. Vestweber, D., *Regulation of endothelial cell contacts during leukocyte extravasation.* Curr Opin Cell Biol, 2002. **14**(5): p. 587-93.

118. Adamson, P., et al., *Lymphocyte migration through brain endothelial cell monolayers involves signaling through endothelial ICAM-1 via a rho-dependent pathway.* J Immunol, 1999. **162**(5): p. 2964-73.

119. Allport, J.R., W.A. Muller, and F.W. Luscinskas, *Monocytes induce reversible focal changes in vascular endothelial cadherin complex during transendothelial migration under flow.* J Cell Biol, 2000. **148**(1): p. 203-16.

120. Dejana, E., G. Bazzoni, and M.G. Lampugnani, *Vascular endothelial (VE)-cadherin: only an intercellular glue?* Exp Cell Res, 1999. **252**(1): p. 13-9.

121. Dejana, E., *Endothelial cell-cell junctions: happy together.* Nat Rev Mol Cell Biol, 2004. **5**(4): p. 261-70.

122. Gumbiner, B.M., *Regulation of cadherin adhesive activity.* J Cell Biol, 2000. **148**(3): p. 399-404.

123. Timmerman, L.A., et al., *Notch promotes epithelial-mesenchymal transition during cardiac development and oncogenic transformation.* Genes Dev, 2004. **18**(1): p. 99-115.

124. Kondapalli, J., A.S. Flozak, and M.L. Albuquerque, *Laminar shear stress differentially modulates gene expression of p120 catenin, Kaiso transcription factor, and vascular endothelial cadherin in human coronary artery endothelial cells.* J Biol Chem, 2004. **279**(12): p. 11417-24.

125. Gory, S., et al., *Requirement of a GT box (Sp1 site) and two Ets binding sites for vascular endothelial cadherin gene transcription.* J Biol Chem, 1998. **273**(12): p. 6750-5.

126. Kobielak, A. and E. Fuchs, *Alpha-catenin: at the junction of intercellular adhesion and actin dynamics.* Nat Rev Mol Cell Biol, 2004. **5**(8): p. 614-25.

127. Perez-Moreno, M., C. Jamora, and E. Fuchs, *Sticky business: orchestrating cellular signals at adherens junctions.* Cell, 2003. **112**(4): p. 535-48.

128. Vasioukhin, V., et al., *Directed actin polymerization is the driving force for epithelial cell-cell adhesion.* Cell, 2000. **100**(2): p. 209-19.

129. Fukata, M. and K. Kaibuchi, *Rho-family GTPases in cadherin-mediated cell-cell adhesion.* Nat Rev Mol Cell Biol, 2001. **2**(12): p. 887-97.

130. Lampugnani, M.G., et al., *Cell confluence regulates tyrosine phosphorylation of adherens junction components in endothelial cells.* J Cell Sci, 1997. **110 (Pt 17)**: p. 2065-77.

131. Chen, Y.T., D.B. Stewart, and W.J. Nelson, *Coupling assembly of the E-cadherin/beta-catenin complex to efficient endoplasmic reticulum exit and basal-lateral membrane targeting of E-cadherin in polarized MDCK cells.* J Cell Biol, 1999. **144**(4): p. 687-99.

132. Le, T.L., et al., *Protein kinase C regulates endocytosis and recycling of E-cadherin.* Am J Physiol Cell Physiol, 2002. **283**(2): p. C489-99.

133. Le, T.L., A.S. Yap, and J.L. Stow, *Recycling of E-cadherin: a potential mechanism for regulating cadherin dynamics.* J Cell Biol, 1999. **146**(1): p. 219-32.

134. Otero, K., et al., *Albumin-derived advanced glycation end-products trigger the disruption of the vascular endothelial cadherin complex in cultured human and murine endothelial cells.* Biochem J, 2001. **359**(Pt 3): p. 567-74.

135. Alexander, J.S., et al., *The role of cadherin endocytosis in endothelial barrier regulation: involvement of protein kinase C and actin-cadherin interactions.* Inflammation, 1998. **22**(4): p. 419-33.

136. Kevil, C.G., N. Okayama, and J.S. Alexander, *H(2)O(2)-mediated permeability II: importance of tyrosine phosphatase and kinase activity.* Am J Physiol Cell Physiol, 2001. **281**(6): p. C1940-7.

137. Ireton, R.C., et al., *A novel role for p120 catenin in E-cadherin function.* J Cell Biol, 2002. **159**(3): p. 465-76.

138. Xiao, K., et al., *Cellular levels of p120 catenin function as a set point for cadherin expression levels in microvascular endothelial cells.* J Cell Biol, 2003. **163**(3): p. 535-45.

139. Davis, M.A., R.C. Ireton, and A.B. Reynolds, *A core function for p120-catenin in cadherin turnover.* J Cell Biol, 2003. **163**(3): p. 525-34.

140. Xiao, K., et al., *Mechanisms of VE-cadherin processing and degradation in microvascular endothelial cells.* J Biol Chem, 2003. **278**(21): p. 19199-208.

141. Fujita, Y., et al., *Hakai, a c-Cbl-like protein, ubiquitinates and induces endocytosis of the E-cadherin complex.* Nat Cell Biol, 2002. **4**(3): p. 222-31.

142. Chen, X., et al., *p120 catenin associates with kinesin and facilitates the transport of cadherin-catenin complexes to intercellular junctions.* J Cell Biol, 2003. **163**(3): p. 547-57.

143. Peifer, M. and A.S. Yap, *Traffic control: p120-catenin acts as a gatekeeper to control the fate of classical cadherins in mammalian cells.* J Cell Biol, 2003. **163**(3): p. 437-40.

144. Izumi, G., et al., *Endocytosis of E-cadherin regulated by Rac and Cdc42 small G proteins through IQGAP1 and actin filaments.* J Cell Biol, 2004. **166**(2): p. 237-48.

145. Palacios, F., et al., *ARF6-GTP recruits Nm23-H1 to facilitate dynamin-mediated endocytosis during adherens junctions disassembly.* Nat Cell Biol, 2002. **4**(12): p. 929-36.

146. Paterson, A.D., et al., *Characterization of E-cadherin endocytosis in isolated MCF-7 and chinese hamster ovary cells: the initial fate of unbound E-cadherin.* J Biol Chem, 2003. **278**(23): p. 21050-7.

147. Noe, V., et al., *Release of an invasion promoter E-cadherin fragment by matrilysin and stromelysin-1.* J Cell Sci, 2001. **114**(Pt 1): p. 111-118.

148. Marambaud, P., et al., *A presenilin-1/gamma-secretase cleavage releases the E-cadherin intracellular domain and regulates disassembly of adherens junctions.* Embo J, 2002. **21**(8): p. 1948-56.

149. Wu, W.B. and T.F. Huang, *Activation of MMP-2, cleavage of matrix proteins, and adherens junctions during a snake venom metalloproteinase-induced endothelial cell apoptosis.* Exp Cell Res, 2003. **288**(1): p. 143-57.

150. Hermant, B., et al., *Identification of proteases involved in the proteolysis of vascular endothelium cadherin during neutrophil transmigration.* J Biol Chem, 2003. **278**(16): p. 14002-12.

151. Matsuyoshi, N., et al., *Cadherin-mediated cell-cell adhesion is perturbed by v-src tyrosine phosphorylation in metastatic fibroblasts.* J Cell Biol, 1992. **118**(3): p. 703-14.

152. Lickert, H., et al., *Casein kinase II phosphorylation of E-cadherin increases E-cadherin/beta-catenin interaction and strengthens cell-cell adhesion.* J Biol Chem, 2000. **275**(7): p. 5090-5.

153. Ohkubo, T. and M. Ozawa, *p120(ctn) binds to the membrane-proximal region of the E-cadherin cytoplasmic domain and is involved in modulation of adhesion activity.* J Biol Chem, 1999. **274**(30): p. 21409-15.

154. Eliceiri, B.P., et al., *Selective requirement for Src kinases during VEGF-induced angiogenesis and vascular permeability.* Mol Cell, 1999. **4**(6): p. 915-24.

155. Weis, S., et al., *Endothelial barrier disruption by VEGF-mediated Src activity potentiates tumor cell extravasation and metastasis.* J Cell Biol, 2004. **167**(2): p. 223-9.

156. Tsukita, S., et al., *Specific proto-oncogenic tyrosine kinases of src family are enriched in cell-to-cell adherens junctions where the level of tyrosine phosphorylation is elevated.* J Cell Biol, 1991. **113**(4): p. 867-79.

157. Ukropec, J.A., et al., *SHP2 association with VE-cadherin complexes in human endothelial cells is regulated by thrombin.* J Biol Chem, 2000. **275**(8): p. 5983-6.

158. Wright, T.J., et al., *Dynamics of vascular endothelial-cadherin and beta-catenin localization by vascular endothelial growth factor-induced angiogenesis in human umbilical vein cells.* Exp Cell Res, 2002. **280**(2): p. 159-68.

159. Fachinger, G., U. Deutsch, and W. Risau, *Functional interaction of vascular endothelial-protein-tyrosine phosphatase with the angiopoietin receptor Tie-2.* Oncogene, 1999. **18**(43): p. 5948-53.

160. Brady-Kalnay, S.M. and N.K. Tonks, *Protein tyrosine phosphatases as adhesion receptors.* Curr Opin Cell Biol, 1995. **7**(5): p. 650-7.

161. Nawroth, R., et al., *VE-PTP and VE-cadherin ectodomains interact to facilitate regulation of phosphorylation and cell contacts.* Embo J, 2002. **21**(18): p. 4885-95.

162. Gaits, F., et al., *Increase in receptor-like protein tyrosine phosphatase activity and expression level on density-dependent growth arrest of endothelial cells.* Biochem J, 1995. **311 (Pt 1)**: p. 97-103.

163. Takahashi, T., et al., *Endothelial localization of receptor tyrosine phosphatase, ECRTP/DEP-1, in developing and mature renal vasculature.* J Am Soc Nephrol, 1999. **10**(10): p. 2135-45.

164. Grazia Lampugnani, M., et al., *Contact inhibition of VEGF-induced proliferation requires vascular endothelial cadherin, beta-catenin, and the phosphatase DEP-1/CD148.* J Cell Biol, 2003. **161**(4): p. 793-804.

165. Takahashi, T., et al., *A mutant receptor tyrosine phosphatase, CD148, causes defects in vascular development.* Mol Cell Biol, 2003. **23**(5): p. 1817-31.

166. Hashizume, H., et al., *Openings between defective endothelial cells explain tumor vessel leakiness.* Am J Pathol, 2000. **156**(4): p. 1363-80.

167. Jin, E., et al., *Angiogenesis and phenotypic alteration of alveolar capillary endothelium in areas of neoplastic cell spread in primary lung adenocarcinoma.* Pathol Int, 2001. **51**(9): p. 691-700.

168. Madigan, M.C. and P.L. Penfold, *Human retinoblastoma: a morphological study of apoptotic, leukocytic, and vascular elements.* Ultrastruct Pathol, 1997. **21**(2): p. 95-107.

169. Paleolog, E.M., *Angiogenesis in rheumatoid arthritis.* Arthritis Res, 2002. **4 Suppl 3**: p. S81-90.

170. Arbiser, J.L., *Angiogenesis and the skin: a primer.* J Am Acad Dermatol, 1996. **34**(3): p. 486-97.

171. Braverman, I.M. and A. Yen, *Ultrastructure of the capillary loops in the dermal papillae of psoriasis.* J Invest Dermatol, 1977. **68**(1): p. 53-60.

172. Barber, A.J. and D.A. Antonetti, *Mapping the blood vessels with paracellular permeability in the retinas of diabetic rats.* Invest Ophthalmol Vis Sci, 2003. **44**(12): p. 5410-6.

173. Roberts, W.G. and G.E. Palade, *Increased microvascular permeability and endothelial fenestration induced by vascular endothelial growth factor.* J Cell Sci, 1995. **108 (Pt 6)**: p. 2369-79.

174. Inai, T., et al., *Inhibition of vascular endothelial growth factor (VEGF) signaling in cancer causes loss of endothelial fenestrations, regression of tumor vessels, and appearance of basement membrane ghosts.* Am J Pathol, 2004. **165**(1): p. 35-52.

175. Ishida, S., et al., *VEGF164 is proinflammatory in the diabetic retina.* Invest Ophthalmol Vis Sci, 2003. **44**(5): p. 2155-62.

176. Gossen, M. and H. Bujard, *Tight control of gene expression in mammalian cells by tetracycline-responsive promoters.* Proc Natl Acad Sci U S A, 1992. **89**(12): p. 5547-51.

177. Folkman, J. and C. Haudenschild, *Angiogenesis in vitro.* Nature, 1980. **288**(5791): p. 551-6.

178. Steffan, A.M., J.L. Gendrault, and A. Kirn, *Increase in the number of fenestrae in mouse endothelial liver cells by altering the cytoskeleton with cytochalasin B.* Hepatology, 1987. **7**(6): p. 1230-8.

179. Steffan, A.M., et al., *Mouse hepatitis virus type 3 infection provokes a decrease in the number of sinusoidal endothelial cell fenestrae both in vivo and in vitro.* Hepatology, 1995. **22**(2): p. 395-401.

180. Wagner, E.F. and W. Risau, *Oncogenes in the study of endothelial cell growth and differentiation.* Semin Cancer Biol, 1994. **5**(2): p. 137-45.

181. MacLean-Fletcher, S. and T.D. Pollard, *Mechanism of action of cytochalasin B on actin.* Cell, 1980. **20**(2): p. 329-41.

182. Cooper, J.A., *Effects of cytochalasin and phalloidin on actin.* J Cell Biol, 1987. **105**(4): p. 1473-8.

183. Yahara, I., et al., *Correlation between effects of 24 different cytochalasins on cellular structures and cellular events and those on actin in vitro.* J Cell Biol, 1982. **92**(1): p. 69-78.

184. Coue, M., et al., *Inhibition of actin polymerization by latrunculin A.* FEBS Lett, 1987. **213**(2): p. 316-8.

185. Morton, W.M., K.R. Ayscough, and P.J. McLaughlin, *Latrunculin alters the actin-monomer subunit interface to prevent polymerization.* Nat Cell Biol, 2000. **2**(6): p. 376-8.

186. Spector, I., et al., *Latrunculins: novel marine toxins that disrupt microfilament organization in cultured cells.* Science, 1983. **219**(4584): p. 493-5.

187. Dubois, N.A., et al., *Isolation and characterization of an established endothelial cell line from transgenic mouse hemangiomas.* Exp Cell Res, 1991. **196**(2): p. 302-13.

188. O'Connell, K.A. and M. Edidin, *A mouse lymphoid endothelial cell line immortalized by simian virus 40 binds lymphocytes and retains functional characteristics of normal endothelial cells.* J Immunol, 1990. **144**(2): p. 521-5.

189. Warren, G., *Cell biology: mitosis and membranes.* Nature, 1989. **342**(6252): p. 857-8.

190. Cabrera-Poch, N., R. Pepperkok, and D.T. Shima, *Inheritance of the mammalian Golgi apparatus during the cell cycle.* Biochim Biophys Acta, 1998. **1404**(1-2): p. 139-51.

191. Milici, A.J., N. L'Hernault, and G.E. Palade, *Surface densities of diaphragmed fenestrae and transendothelial channels in different murine capillary beds.* Circ Res, 1985. **56**(5): p. 709-17.

192. Andrews, P.M., *Investigations of cytoplasmic contractile and cytoskeletal elements in the kidney glomerulus.* Kidney Int, 1981. **20**(5): p. 549-62.

193. Eitzen, G., et al., *Remodeling of organelle-bound actin is required for yeast vacuole fusion.* J Cell Biol, 2002. **158**(4): p. 669-79.

194. Orci, L., K.H. Gabbay, and W.J. Malaisse, *Pancreatic beta-cell web: its possible role in insulin secretion.* Science, 1972. **175**(26): p. 1128-30.

195. Muallem, S., et al., *Actin filament disassembly is a sufficient final trigger for exocytosis in nonexcitable cells.* J Cell Biol, 1995. **128**(4): p. 589-98.

196. Morales, M., M.A. Colicos, and Y. Goda, *Actin-dependent regulation of neurotransmitter release at central synapses.* Neuron, 2000. **27**(3): p. 539-50.

197. Jahraus, A., et al., *ATP-dependent membrane assembly of F-actin facilitates membrane fusion.* Mol Biol Cell, 2001. **12**(1): p. 155-70.

198. Kjeken, R., et al., *Fusion between phagosomes, early and late endosomes: a role for actin in fusion between late, but not early endocytic organelles.* Mol Biol Cell, 2004. **15**(1): p. 345-58.

199. Muhlner, U., et al., *Formation of transformed endothelial cells in the absence of VEGFR- 2/Flk-1 by Polyoma middle T oncogene.* Oncogene, 1999. **18**(29): p. 4200-10.

200. Crews, P., *Jasplakinolide, a cyclodepsipeptide from the marine sponge Jaspis sp.* Tetr Hedrn Lett, 1986. **27**: p. 2797-2800.

201. Bubb, M.R., et al., *Jasplakinolide, a cytotoxic natural product, induces actin polymerization and competitively inhibits the binding of phalloidin to F-actin.* J Biol Chem, 1994. **269**(21): p. 14869-71.

202. Senderowicz, A.M., et al., *Jasplakinolide's inhibition of the growth of prostate carcinoma cells in vitro with disruption of the actin cytoskeleton.* J Natl Cancer Inst, 1995. **87**(1): p. 46-51.

203. Cramer, L.P., *Role of actin-filament disassembly in lamellipodium protrusion in motile cells revealed using the drug jasplakinolide.* Curr Biol, 1999. **9**(19): p. 1095-105.

204. Carmichael, G.G., et al., *Carboxy terminus of polyoma middle-sized tumor antigen is required for attachment to membranes, associated protein kinase activities, and cell transformation.* Proc Natl Acad Sci U S A, 1982. **79**(11): p. 3579-83.

205. Dilworth, S.M., *Polyoma virus middle T antigen and its role in identifying cancer-related molecules.* Nat Rev Cancer, 2002. **2**(12): p. 951-6.

206. Primo, L., et al., *Human endothelial cells expressing polyoma middle T induce tumors.* Oncogene, 2000. **19**(32): p. 3632-41.

207. Williams, R.L., et al., *Endothelioma cells expressing the polyoma middle T oncogene induce hemangiomas by host cell recruitment.* Cell, 1989. **57**(6): p. 1053-63.

208. Wang, R. and V.L. Bautch, *The polyomavirus early region gene in transgenic mice causes vascular and bone tumors.* J Virol, 1991. **65**(10): p. 5174-83.

209. Williams, R.L., S.A. Courtneidge, and E.F. Wagner, *Embryonic lethalities and endothelial tumors in chimeric mice expressing polyoma virus middle T oncogene.* Cell, 1988. **52**(1): p. 121-31.

210. Stan, R.V., E. Tkachenko, and I.R. Niesman, *PV1 is a key structural component for the formation of the stomatal and fenestral diaphragms.* Mol Biol Cell, 2004. **15**(8): p. 3615-30.

211. Hart, T.K. and R.M. Pino, *Pseudoislet vascularization. Induction of diaphragm-fenestrated endothelia from the hepatic sinusoids.* Lab Invest, 1986. **54**(3): p. 304-13.

212. Kozlov, M.M. and V.S. Markin, *[Possible mechanism of membrane fusion].* Biofizika, 1983. **28**(2): p. 242-7.

213. Chernomordik, L.V., G.B. Melikyan, and Y.A. Chizmadzhev, *Biomembrane fusion: a new concept derived from model studies using two interacting planar lipid bilayers.* Biochim Biophys Acta, 1987. **906**(3): p. 309-52.

214. Chernomordik, L.V. and M.M. Kozlov, *Protein-lipid interplay in fusion and fission of biological membranes.* Annu Rev Biochem, 2003. **72**: p. 175-207.

215. Jahn, R., T. Lang, and T.C. Sudhof, *Membrane fusion.* Cell, 2003. **112**(4): p. 519-33.

216. Wickner, W., *Yeast vacuoles and membrane fusion pathways.* Embo J, 2002. **21**(6): p. 1241-7.

217. Predescu, S.A., D.N. Predescu, and G.E. Palade, *Endothelial transcytotic machinery involves supramolecular protein-lipid complexes.* Mol Biol Cell, 2001. **12**(4): p. 1019-33.

218. Schnitzer, J.E., J. Liu, and P. Oh, *Endothelial caveolae have the molecular transport machinery for vesicle budding, docking, and fusion including VAMP, NSF, SNAP, annexins, and GTPases.* J Biol Chem, 1995. **270**(24): p. 14399-404.

219. Yokomori, H., et al., *Endothelin-1 suppresses plasma membrane Ca++-ATPase, concomitant with contraction of hepatic sinusoidal endothelial fenestrae.* Am J Pathol, 2003. **162**(2): p. 557-66.

220. Brauneis, U., Z. Gatmaitan, and I.M. Arias, *Serotonin stimulates a Ca2+ permeant nonspecific cation channel in hepatic endothelial cells.* Biochem Biophys Res Commun, 1992. **186**(3): p. 1560-6.

221. Lindau, M. and W. Almers, *Structure and function of fusion pores in exocytosis and ectoplasmic membrane fusion.* Curr Opin Cell Biol, 1995. **7**(4): p. 509-17.

222. Burgoyne, R.D. and A. Morgan, *Calcium sensors in regulated exocytosis.* Cell Calcium, 1998. **24**(5-6): p. 367-76.

223. Macaulay, C. and D.J. Forbes, *Assembly of the nuclear pore: biochemically distinct steps revealed with NEM, GTP gamma S, and BAPTA.* J Cell Biol, 1996. **132**(1-2): p. 5-20.

224. Ghitescu, L.D., P. Crine, and B.S. Jacobson, *Antibodies specific to the plasma membrane of rat lung microvascular endothelium.* Exp Cell Res, 1997. **232**(1): p. 47-55.

225. *Subcellular Fractionation*, in *Cells A Laboratory manual.* 1998, Cold Spring Harbor Laboratory Press. p. 34.1-34.9.

226. Jacobson, B.S. and D. Branton, *Plasma membrane: rapid isolation and exposure of the cytoplasmic surface by use of positively charged beads.* Science, 1977. **195**(4275): p. 302-4.

227. Chaney, L.K. and B.S. Jacobson, *Coating cells with colloidal silica for high yield isolation of plasma membrane sheets and identification of transmembrane proteins.* J Biol Chem, 1983. **258**(16): p. 10062-72.

228. Stolz, D.B. and B.S. Jacobson, *Examination of transcellular membrane protein polarity of bovine aortic endothelial cells in vitro using the cationic colloidal silica microbead membrane-isolation procedure.* J Cell Sci, 1992. **103 (Pt 1)**: p. 39-51.

229. Stolz, D.B., G. Bannish, and B.S. Jacobson, *The role of the cytoskeleton and intercellular junctions in the transcellular membrane protein polarity of bovine aortic endothelial cells in vitro.* J Cell Sci, 1992. **103 (Pt 1)**: p. 53-68.

230. Mason, P.W. and B.S. Jacobson, *Isolation of the dorsal, ventral and intracellular domains of HeLa cell plasma membranes following adhesion to a gelatin substrate.* Biochim Biophys Acta, 1985. **821**(2): p. 264-76.

231. Schnitzer, J.E., et al., *Separation of caveolae from associated microdomains of GPI-anchored proteins.* Science, 1995. **269**(5229): p. 1435-9.

232. Schnitzer, J.E., et al., *Caveolae from luminal plasmalemma of rat lung endothelium: microdomains enriched in caveolin, Ca(2+)-ATPase, and inositol trisphosphate receptor.* Proc Natl Acad Sci U S A, 1995. **92**(5): p. 1759-63.

233. Rout, M.P., et al., *The yeast nuclear pore complex: composition, architecture, and transport mechanism.* J Cell Biol, 2000. **148**(4): p. 635-51.

234. Garin, J., et al., *The phagosome proteome: insight into phagosome functions.* J Cell Biol, 2001. **152**(1): p. 165-80.

235. Mootha, V.K., et al., *Integrated analysis of protein composition, tissue diversity, and gene regulation in mouse mitochondria.* Cell, 2003. **115**(5): p. 629-40.

236. Andersen, J.S., et al., *Proteomic characterization of the human centrosome by protein correlation profiling.* Nature, 2003. **426**(6966): p. 570-4.

237. Kleffmann, T., et al., *The Arabidopsis thaliana chloroplast proteome reveals pathway abundance and novel protein functions.* Curr Biol, 2004. **14**(5): p. 354-62.

238. Andersen, J.S., et al., *Directed proteomic analysis of the human nucleolus.* Curr Biol, 2002. **12**(1): p. 1-11.

239. Dreger, M., et al., *Nuclear envelope proteomics: novel integral membrane proteins of the inner nuclear membrane.* Proc Natl Acad Sci U S A, 2001. **98**(21): p. 11943-8.

240. Bell, A.W., et al., *Proteomics characterization of abundant Golgi membrane proteins.* J Biol Chem, 2001. **276**(7): p. 5152-65.

241. Fialka, I., et al., *Subcellular fractionation of polarized epithelial cells and identification of organelle-specific proteins by two-dimensional gel electrophoresis.* Electrophoresis, 1997. **18**(14): p. 2582-90.

242. Oh, P., et al., *Subtractive proteomic mapping of the endothelial surface in lung and solid tumours for tissue-specific therapy.* Nature, 2004. **429**(6992): p. 629-35.

243. Durr, E., et al., *Direct proteomic mapping of the lung microvascular endothelial cell surface in vivo and in cell culture.* Nat Biotechnol, 2004. **22**(8): p. 985-92.

244. Braet, F., et al., *Structure and dynamics of the fenestrae-associated cytoskeleton of rat liver sinusoidal endothelial cells.* Hepatology, 1995. **21**(1): p. 180-9.

245. Yokomori, H., et al., *Rho modulates hepatic sinusoidal endothelial fenestrae via regulation of the actin cytoskeleton in rat endothelial cells.* Lab Invest, 2004. **84**(8): p. 1079.

246. Bamburg, J.R., *Proteins of the ADF/cofilin family: essential regulators of actin dynamics.* Annu Rev Cell Dev Biol, 1999. **15**: p. 185-230.

247. Paavilainen, V.O., et al., *Regulation of cytoskeletal dynamics by actin-monomer-binding proteins.* Trends Cell Biol, 2004. **14**(7): p. 386-94.

248. Palmgren, S., M. Vartiainen, and P. Lappalainen, *Twinfilin, a molecular mailman for actin monomers.* J Cell Sci, 2002. **115**(Pt 5): p. 881-6.

249. Lawson, D., M. Harrison, and C. Shapland, *Fibroblast transgelin and smooth muscle SM22alpha are the same protein, the expression of which is down-regulated in many cell lines.* Cell Motil Cytoskeleton, 1997. **38**(3): p. 250-7.

250. Shapland, C., et al., *Purification and properties of transgelin: a transformation and shape change sensitive actin-gelling protein.* J Cell Biol, 1993. **121**(5): p. 1065-73.

251. Tuxworth, R.I. and M.A. Titus, *Unconventional myosins: anchors in the membrane traffic relay.* Traffic, 2000. **1**(1): p. 11-8.

252. Sellers, J.R., *Myosins: a diverse superfamily.* Biochim Biophys Acta, 2000. **1496**(1): p. 3-22.

266. Chevallet, M., et al., *New zwitterionic detergents improve the analysis of membrane proteins by two-dimensional electrophoresis.* Electrophoresis, 1998. **19**(11): p. 1901-9.

267. Pedersen, S.K., et al., *Unseen proteome: mining below the tip of the iceberg to find low abundance and membrane proteins.* J Proteome Res, 2003. **2**(3): p. 303-11.

268. Ferro, M., et al., *Integral membrane proteins of the chloroplast envelope: identification and subcellular localization of new transporters.* Proc Natl Acad Sci U S A, 2002. **99**(17): p. 11487-92.

269. Wasiak, S., et al., *Enthoprotin: a novel clathrin-associated protein identified through subcellular proteomics.* J Cell Biol, 2002. **158**(5): p. 855-62.

270. Simpson, R.J., et al., *Proteomic analysis of the human colon carcinoma cell line (LIM 1215): development of a membrane protein database.* Electrophoresis, 2000. **21**(9): p. 1707-32.

271. Galeva, N. and M. Altermann, *Comparison of one-dimensional and two-dimensional gel electrophoresis as a separation tool for proteomic analysis of rat liver microsomes: cytochromes P450 and other membrane proteins.* Proteomics, 2002. **2**(6): p. 713-22.

272. Farsad, K. and P. De Camilli, *Mechanisms of membrane deformation.* Curr Opin Cell Biol, 2003. **15**(4): p. 372-81.

273. Thiele, C., et al., *Cholesterol binds to synaptophysin and is required for biogenesis of synaptic vesicles.* Nat Cell Biol, 2000. **2**(1): p. 42-9.

274. Ostrowski, S.G., et al., *Mass spectrometric imaging of highly curved membranes during Tetrahymena mating.* Science, 2004. **305**(5680): p. 71-3.

275. Musacchio, A., et al., *Functional organization of clathrin in coats: combining electron cryomicroscopy and X-ray crystallography.* Mol Cell, 1999. **3**(6): p. 761-70.

276. Bi, X., R.A. Corpina, and J. Goldberg, *Structure of the Sec23/24-Sar1 pre-budding complex of the COPII vesicle coat.* Nature, 2002. **419**(6904): p. 271-7.

277. Takei, K., et al., *Tubular membrane invaginations coated by dynamin rings are induced by GTP-gamma S in nerve terminals.* Nature, 1995. **374**(6518): p. 186-90.

278. Lebel, S. and Y. Raymond, *Lamin B from rat liver nuclei exists both as a lamina protein and as an intrinsic membrane protein.* J Biol Chem, 1984. **259**(5): p. 2693-6.

279. Ferro, M., et al., *Proteomics of the chloroplast envelope membranes from Arabidopsis thaliana.* Mol Cell Proteomics, 2003.

280. Brugiere, S., et al., *The hydrophobic proteome of mitochondrial membranes from Arabidopsis cell suspensions.* Phytochemistry, 2004. **65**(12): p. 1693-707.

281. Schirmer, E.C., et al., *Nuclear membrane proteins with potential disease links found by subtractive proteomics.* Science, 2003. **301**(5638): p. 1380-2.

282. Sato, N., et al., *A gene family consisting of ezrin, radixin and moesin. Its specific localization at actin filament/plasma membrane association sites.* J Cell Sci, 1992. **103 (Pt 1)**: p. 131-43.

283. Bretscher, A., *Purification of an 80,000-dalton protein that is a component of the isolated microvillus cytoskeleton, and its localization in nonmuscle cells.* J Cell Biol, 1983. **97**(2): p. 425-32.

284. Tsukita, S. and Y. Hieda, *A new 82-kD barbed end-capping protein (radixin) localized in the cell-to-cell adherens junction: purification and characterization.* J Cell Biol, 1989. **108**(6): p. 2369-82.

285. Lankes, W., et al., *A heparin-binding protein involved in inhibition of smooth-muscle cell proliferation.* Biochem J, 1988. **251**(3): p. 831-42.

286. Trofatter, J.A., et al., *A novel moesin-, ezrin-, radixin-like gene is a candidate for the neurofibromatosis 2 tumor suppressor.* Cell, 1993. **72**(5): p. 791-800.

287. Rouleau, G.A., et al., *Alteration in a new gene encoding a putative membrane-organizing protein causes neuro-fibromatosis type 2.* Nature, 1993. **363**(6429): p. 515-21.

288. Gould, K.L., et al., *cDNA cloning and sequencing of the protein-tyrosine kinase substrate, ezrin, reveals homology to band 4.1.* Embo J, 1989. **8**(13): p. 4133-42.

289. Lankes, W.T. and H. Furthmayr, *Moesin: a member of the protein 4.1-talin-ezrin family of proteins.* Proc Natl Acad Sci U S A, 1991. **88**(19): p. 8297-301.

290. Funayama, N., et al., *Radixin is a novel member of the band 4.1 family.* J Cell Biol, 1991. **115**(4): p. 1039-48.

291. Tsukita, S. and S. Yonemura, *Cortical actin organization: lessons from ERM (ezrin/radixin/moesin) proteins.* J Biol Chem, 1999. **274**(49): p. 34507-10.

292. Xu, H.M. and D.H. Gutmann, *Merlin differentially associates with the microtubule and actin cytoskeleton.* J Neurosci Res, 1998. **51**(3): p. 403-15.

293. Brault, E., et al., *Normal membrane localization and actin association of the NF2 tumor suppressor protein are dependent on folding of its N-terminal domain.* J Cell Sci, 2001. **114**(Pt 10): p. 1901-12.

294. Berryman, M., Z. Franck, and A. Bretscher, *Ezrin is concentrated in the apical microvilli of a wide variety of epithelial cells whereas moesin is found primarily in endothelial cells.* J Cell Sci, 1993. **105 (Pt 4)**: p. 1025-43.

295. Schwartz-Albiez, R., et al., *Differential expression of the microspike-associated protein moesin in human tissues.* Eur J Cell Biol, 1995. **67**(3): p. 189-98.

296. Doi, Y., et al., *Normal development of mice and unimpaired cell adhesion/cell motility/actin-based cytoskeleton without compensatory up-regulation of ezrin or radixin in moesin gene knockout.* J Biol Chem, 1999. **274**(4): p. 2315-21.

297. Kitajiri, S., et al., *Radixin deficiency causes deafness associated with progressive degeneration of cochlear stereocilia.* J Cell Biol, 2004. **166**(4): p. 559-70.

298. Amieva, M.R. and H. Furthmayr, *Subcellular localization of moesin in dynamic filopodia, retraction fibers, and other structures involved in substrate exploration, attachment, and cell-cell contacts.* Exp Cell Res, 1995. **219**(1): p. 180-96.

299. Oshiro, N., Y. Fukata, and K. Kaibuchi, *Phosphorylation of moesin by rho-associated kinase (Rho-kinase) plays a crucial role in the formation of microvilli-like structures.* J Biol Chem, 1998. **273**(52): p. 34663-6.

300. Gautreau, A., D. Louvard, and M. Arpin, *Morphogenic effects of ezrin require a phosphorylation-induced transition from oligomers to monomers at the plasma membrane.* J Cell Biol, 2000. **150**(1): p. 193-203.

301. Pujuguet, P., et al., *Ezrin regulates E-cadherin-dependent adherens junction assembly through Rac1 activation.* Mol Biol Cell, 2003. **14**(5): p. 2181-91.

302. Amieva, M.R., et al., *Disruption of dynamic cell surface architecture of NIH3T3 fibroblasts by the N-terminal domains of moesin and ezrin: in vivo imaging with GFP fusion proteins.* J Cell Sci, 1999. **112 (Pt 1)**: p. 111-25.

303. Crepaldi, T., et al., *Ezrin is an effector of hepatocyte growth factor-mediated migration and morphogenesis in epithelial cells.* J Cell Biol, 1997. **138**(2): p. 423-34.

304. Allenspach, E.J., et al., *ERM-dependent movement of CD43 defines a novel protein complex distal to the immunological synapse.* Immunity, 2001. **15**(5): p. 739-50.

305. Bretscher, A., et al., *ERM-Merlin and EBP50 protein families in plasma membrane organization and function.* Annu Rev Cell Dev Biol, 2000. **16**: p. 113-43.

306. Berryman, M., R. Gary, and A. Bretscher, *Ezrin oligomers are major cytoskeletal components of placental microvilli: a proposal for their involvement in cortical morphogenesis.* J Cell Biol, 1995. **131**(5): p. 1231-42.

307. Bretscher, A., R. Gary, and M. Berryman, *Soluble ezrin purified from placenta exists as stable monomers and elongated dimers with masked C-terminal ezrin-radixin-moesin association domains.* Biochemistry, 1995. **34**(51): p. 16830-7.

308. Matsui, T., et al., *Rho-kinase phosphorylates COOH-terminal threonines of ezrin/radixin/moesin (ERM) proteins and regulates their head-to-tail association.* J Cell Biol, 1998. **140**(3): p. 647-57.

309. Simons, P.C., et al., *C-terminal threonine phosphorylation activates ERM proteins to link the cell's cortical lipid bilayer to the cytoskeleton.* Biochem Biophys Res Commun, 1998. **253**(3): p. 561-5.

310. Fievet, B.T., et al., *Phosphoinositide binding and phosphorylation act sequentially in the activation mechanism of ezrin.* J Cell Biol, 2004. **164**(5): p. 653-9.

311. Gary, R. and A. Bretscher, *Heterotypic and homotypic associations between ezrin and moesin, two putative membrane-cytoskeletal linking proteins.* Proc Natl Acad Sci U S A, 1993. **90**(22): p. 10846-50.

312. Fukata, Y., et al., *Association of the myosin-binding subunit of myosin phosphatase and moesin: dual regulation of moesin phosphorylation by Rho-associated kinase and myosin phosphatase.* J Cell Biol, 1998. **141**(2): p. 409-18.

313. Shaw, R.J., et al., *RhoA-dependent phosphorylation and relocalization of ERM proteins into apical membrane/actin protrusions in fibroblasts.* Mol Biol Cell, 1998. **9**(2): p. 403-19.

314. Kotani, H., et al., *Rho regulates association of both the ERM family and vinculin with the plasma membrane in MDCK cells.* Oncogene, 1997. **14**(14): p. 1705-13.

315. Mackay, D.J., et al., *Rho- and rac-dependent assembly of focal adhesion complexes and actin filaments in permeabilized fibroblasts: an essential role for ezrin/radixin/moesin proteins.* J Cell Biol, 1997. **138**(4): p. 927-38.

316. Takahashi, K., et al., *Direct interaction of the Rho GDP dissociation inhibitor with ezrin/radixin/moesin initiates the activation of the Rho small G protein.* J Biol Chem, 1997. **272**(37): p. 23371-5.

317. Speck, O., et al., *Moesin functions antagonistically to the Rho pathway to maintain epithelial integrity.* Nature, 2003. **421**(6918): p. 83-7.

318. Pino, R.M., *Restriction to endogenous plasma proteins by a fenestrated capillary endothelium: an ultrastructural immunocytochemical study of the choriocapillary endothelium.* Am J Anat, 1985. **172**(4): p. 279-89.

319. Guymer, R.H., A.C. Bird, and G.S. Hageman, *Cytoarchitecture of choroidal capillary endothelial cells.* Invest Ophthalmol Vis Sci, 2004. **45**(6): p. 1660-6.

320. Hofer, D. and D. Drenckhahn, *Molecular heterogeneity of the actin filament cytoskeleton associated with microvilli of photoreceptors, Muller's glial cells and pigment epithelial cells of the retina.* Histochemistry, 1993. **99**(1): p. 29-35.

321. Bonilha, V.L., S.C. Finnemann, and E. Rodriguez-Boulan, *Ezrin promotes morphogenesis of apical microvilli and basal infoldings in retinal pigment epithelium.* J Cell Biol, 1999. **147**(7): p. 1533-48.

322. Delon, J., K. Kaibuchi, and R.N. Germain, *Exclusion of CD43 from the immunological synapse is mediated by phosphorylation-regulated relocation of the cytoskeletal adaptor moesin.* Immunity, 2001. **15**(5): p. 691-701.

323. Tsukita, S., et al., *ERM family members as molecular linkers between the cell surface glycoprotein CD44 and actin-based cytoskeletons.* J Cell Biol, 1994. **126**(2): p. 391-401.

324. Vanni, C., et al., *Phosphorylation-independent membrane relocalization of ezrin following association with Dbl in vivo.* Oncogene, 2004. **23**(23): p. 4098-106.

325. Franck, Z., R. Gary, and A. Bretscher, *Moesin, like ezrin, colocalizes with actin in the cortical cytoskeleton in cultured cells, but its expression is more variable.* J Cell Sci, 1993. **105 (Pt 1)**: p. 219-31.

326. Serrador, J.M., et al., *Moesin interacts with the cytoplasmic region of intercellular adhesion molecule-3 and is redistributed to the uropod of T lymphocytes during cell polarization.* J Cell Biol, 1997. **138**(6): p. 1409-23.

327. Stickney, J.T., et al., *Activation of the tumor suppressor merlin modulates its interaction with lipid rafts.* Cancer Res, 2004. **64**(8): p. 2717-24.

328. Amieva, M.R., K.K. Wilgenbus, and H. Furthmayr, *Radixin is a component of hepatocyte microvilli in situ.* Exp Cell Res, 1994. **210**(1): p. 140-4.

329. Hugo, C., et al., *The plasma membrane-actin linking protein, ezrin, is a glomerular epithelial cell marker in glomerulogenesis, in the adult kidney and in glomerular injury.* Kidney Int, 1998. **54**(6): p. 1934-44.

330. Takeda, T., et al., *Loss of glomerular foot processes is associated with uncoupling of podocalyxin from the actin cytoskeleton.* J Clin Invest, 2001. **108**(2): p. 289-301.

331. Takeda, T., *Podocyte cytoskeleton is connected to the integral membrane protein podocalyxin through Na+/H+-exchanger regulatory factor 2 and ezrin.* Clin Exp Nephrol, 2003. **7**(4): p. 260-9.

332. Hugo, C., et al., *The cytoskeletal linking proteins, moesin and radixin, are upregulated by platelet-derived growth factor, but not basic fibroblast growth factor in experimental mesangial proliferative glomerulonephritis.* J Clin Invest, 1996. **97**(11): p. 2499-508.

333. Turunen, O., T. Wahlstrom, and A. Vaheri, *Ezrin has a COOH-terminal actin-binding site that is conserved in the ezrin protein family.* J Cell Biol, 1994. **126**(6): p. 1445-53.

334. Hayashi, K., et al., *Immunofluorescence detection of ezrin/radixin/moesin (ERM) proteins with their carboxyl-terminal threonine phosphorylated in cultured cells and tissues.* J Cell Sci, 1999. **112 (Pt 8)**: p. 1149-58.

335. Gary, R. and A. Bretscher, *Ezrin self-association involves binding of an N-terminal domain to a normally masked C-terminal domain that includes the F-actin binding site.* Mol Biol Cell, 1995. **6**(8): p. 1061-75.

336. Reczek, D. and A. Bretscher, *The carboxyl-terminal region of EBP50 binds to a site in the amino-terminal domain of ezrin that is masked in the dormant molecule.* J Biol Chem, 1998. **273**(29): p. 18452-8.

337. Legg, J.W. and C.M. Isacke, *Identification and functional analysis of the ezrin-binding site in the hyaluronan receptor, CD44.* Curr Biol, 1998. **8**(12): p. 705-8.

338. Heiska, L., et al., *Association of ezrin with intercellular adhesion molecule-1 and -2 (ICAM-1 and ICAM-2). Regulation by phosphatidylinositol 4, 5-bisphosphate.* J Biol Chem, 1998. **273**(34): p. 21893-900.

339. Yonemura, S., et al., *Ezrin/radixin/moesin (ERM) proteins bind to a positively charged amino acid cluster in the juxta-membrane cytoplasmic domain of CD44, CD43, and ICAM-2.* J Cell Biol, 1998. **140**(4): p. 885-95.

340. Denker, S.P., et al., *Direct binding of the Na--H exchanger NHE1 to ERM proteins regulates the cortical cytoskeleton and cell shape independently of H(+) translocation.* Mol Cell, 2000. **6**(6): p. 1425-36.

341. Serrador, J.M., et al., *CD43 interacts with moesin and ezrin and regulates its redistribution to the uropods of T lymphocytes at the cell-cell contacts.* Blood, 1998. **91**(12): p. 4632-44.

342. Orlando, R.A., et al., *The glomerular epithelial cell anti-adhesin podocalyxin associates with the actin cytoskeleton through interactions with ezrin.* J Am Soc Nephrol, 2001. **12**(8): p. 1589-98.

343. Reczek, D., M. Berryman, and A. Bretscher, *Identification of EBP50: A PDZ-containing phosphoprotein that associates with members of the ezrin-radixin-moesin family.* J Cell Biol, 1997. **139**(1): p. 169-79.

344. Niggli, V., et al., *Identification of a phosphatidylinositol-4,5-bisphosphate-binding domain in the N-terminal region of ezrin.* FEBS Lett, 1995. **376**(3): p. 172-6.

345. Barret, C., et al., *Mutagenesis of the phosphatidylinositol 4,5-bisphosphate (PIP(2)) binding site in the NH(2)-terminal domain of ezrin correlates with its altered cellular distribution.* J Cell Biol, 2000. **151**(5): p. 1067-80.

346. Nakamura, F., et al., *Regulation of F-actin binding to platelet moesin in vitro by both phosphorylation of threonine 558 and polyphosphatidylinositides.* Mol Biol Cell, 1999. **10**(8): p. 2669-85.

347. Yonemura, S., T. Matsui, and S. Tsukita, *Rho-dependent and -independent activation mechanisms of ezrin/radixin/moesin proteins: an essential role for polyphosphoinositides in vivo.* J Cell Sci, 2002. **115**(Pt 12): p. 2569-80.

348. Revenu, C., et al., *The co-workers of actin filaments: from cell structures to signals.* Nat Rev Mol Cell Biol, 2004. **5**(8): p. 635-46.

349. Yao, X., L. Cheng, and J.G. Forte, *Biochemical characterization of ezrin-actin interaction.* J Biol Chem, 1996. **271**(12): p. 7224-9.

350. Defacque, H., et al., *Involvement of ezrin/moesin in de novo actin assembly on phagosomal membranes.* Embo J, 2000. **19**(2): p. 199-212.

351. Karagiosis, S.A. and D.F. Ready, *Moesin contributes an essential structural role in Drosophila photoreceptor morphogenesis.* Development, 2004. **131**(4): p. 725-32.

352. Gobel, V., et al., *Lumen morphogenesis in C. elegans requires the membrane-cytoskeleton linker erm-1.* Dev Cell, 2004. **6**(6): p. 865-73.

353. Saotome, I., M. Curto, and A.I. McClatchey, *Ezrin is essential for epithelial organization and villus morphogenesis in the developing intestine.* Dev Cell, 2004. **6**(6): p. 855-64.

354. Hanahan, D., *Signaling vascular morphogenesis and maintenance.* Science, 1997. **277**(5322): p. 48-50.

355. Risau, W., *Mechanisms of angiogenesis.* Nature, 1997. **386**(6626): p. 671-4.

356. Thurston, G., et al., *Leakage-resistant blood vessels in mice transgenically overexpressing angiopoietin-1.* Science, 1999. **286**(5449): p. 2511-4.

357. Thurston, G., et al., *Angiopoietin-1 protects the adult vasculature against plasma leakage.* Nat Med, 2000. **6**(4): p. 460-3.

358. Dumont, D.J., et al., *Dominant-negative and targeted null mutations in the endothelial receptor tyrosine kinase, tek, reveal a critical role in vasculogenesis of the embryo.* Genes Dev, 1994. **8**(16): p. 1897-909.

359. Carmeliet, P., et al., *Abnormal blood vessel development and lethality in embryos lacking a single VEGF allele.* Nature, 1996. **380**(6573): p. 435-9.

360. Sato, T.N., et al., *Distinct roles of the receptor tyrosine kinases Tie-1 and Tie-2 in blood vessel formation.* Nature, 1995. **376**(6535): p. 70-4.

361. Shalaby, F., et al., *Failure of blood-island formation and vasculogenesis in Flk-1-deficient mice.* Nature, 1995. **376**(6535): p. 62-6.

362. Suri, C., et al., *Requisite role of angiopoietin-1, a ligand for the TIE2 receptor, during embryonic angiogenesis.* Cell, 1996. **87**(7): p. 1171-80.

363. Furth, P.A., et al., *Temporal control of gene expression in transgenic mice by a tetracycline-responsive promoter.* Proc Natl Acad Sci U S A, 1994. **91**(20): p. 9302-6.

364. Gossen, M., et al., *Transcriptional activation by tetracyclines in mammalian cells.* Science, 1995. **268**(5218): p. 1766-9.

365. Kistner, A., et al., *Doxycycline-mediated quantitative and tissue-specific control of gene expression in transgenic mice.* Proc Natl Acad Sci U S A, 1996. **93**(20): p. 10933-8.

366. Mayford, M., et al., *Control of memory formation through regulated expression of a CaMKII transgene.* Science, 1996. **274**(5293): p. 1678-83.

367. Sarao, R. and D.J. Dumont, *Conditional transgene expression in endothelial cells.* Transgenic Res, 1998. **7**(6): p. 421-7.

368. Yu, Z., C.S. Redfern, and G.I. Fishman, *Conditional transgene expression in the heart.* Circ Res, 1996. **79**(4): p. 691-7.

369. Jaubert, J., et al., *Tetracycline-regulated transactivators driven by the involucrin promoter to achieve epidermal conditional gene expression.* J Invest Dermatol, 2004. **123**(2): p. 313-8.

370. Ju, H., et al., *Conditional and targeted overexpression of vascular chymase causes hypertension in transgenic mice.* Proc Natl Acad Sci U S A, 2001. **98**(13): p. 7469-74.

371. Manickan, E., et al., *Conditional liver-specific expression of simian virus 40 T antigen leads to regulatable development of hepatic neoplasm in transgenic mice.* J Biol Chem, 2001. **276**(17): p. 13989-94.

372. Zabolotny, J.M., et al., *Overexpression of the LAR (leukocyte antigen-related) protein-tyrosine phosphatase in muscle causes insulin resistance.* Proc Natl Acad Sci U S A, 2001. **98**(9): p. 5187-92.

373. Zabolotny, J.M., et al., *Transgenic overexpression of protein-tyrosine phosphatase 1B in muscle causes insulin resistance, but overexpression with leukocyte antigen-related phosphatase does not additively impair insulin action.* J Biol Chem, 2004. **279**(23): p. 24844-51.

374. Maegawa, H., et al., *Expression of a dominant negative SHP-2 in transgenic mice induces insulin resistance.* J Biol Chem, 1999. **274**(42): p. 30236-43.

375. Schlaeger, T.M., et al., *Uniform vascular-endothelial-cell-specific gene expression in both embryonic and adult transgenic mice.* Proc Natl Acad Sci U S A, 1997. **94**(7): p. 3058-63.

376. Dumont, D.J., et al., *Vascularization of the mouse embryo: a study of flk-1, tek, tie, and vascular endothelial growth factor expression during development.* Dev Dyn, 1995. **203**(1): p. 80-92.

377. Lewandoski, M., *Conditional control of gene expression in the mouse.* Nat Rev Genet, 2001. **2**(10): p. 743-55.

378. Gossen, M., A.L. Bonin, and H. Bujard, *Control of gene activity in higher eukaryotic cells by prokaryotic regulatory elements.* Trends Biochem Sci, 1993. **18**(12): p. 471-5.

379. Cronin, C.A., W. Gluba, and H. Scrable, *The lac operator-repressor system is functional in the mouse.* Genes Dev, 2001. **15**(12): p. 1506-17.

380. Dor, Y., et al., *Conditional switching of VEGF provides new insights into adult neovascularization and pro-angiogenic therapy.* Embo J, 2002. **21**(8): p. 1939-47.

381. Tremblay, P., et al., *Doxycycline control of prion protein transgene expression modulates prion disease in mice.* Proc Natl Acad Sci U S A, 1998. **95**(21): p. 12580-5.

382. Gross, C., et al., *Serotonin1A receptor acts during development to establish normal anxiety-like behaviour in the adult.* Nature, 2002. **416**(6879): p. 396-400.

383. Yang, L.L., et al., *Conditional cardiac overexpression of endothelin-1 induces inflammation and dilated cardiomyopathy in mice.* Circulation, 2004. **109**(2): p. 255-61.

384. Suarez, J., et al., *Doxycycline inducible expression of SERCA2a improves calcium handling and reverts cardiac dysfunction in pressure overload-induced cardiac hypertrophy.* Am J Physiol Heart Circ Physiol, 2004. **287**(5): p. H2164-72.

385. You, X.M., et al., *Conditional expression of a dominant-negative c-Myb in vascular smooth muscle cells inhibits arterial remodeling after injury.* Circ Res, 2003. **92**(3): p. 314-21.

386. Corbel, S.Y. and F.M. Rossi, *Latest developments and in vivo use of the Tet system: ex vivo and in vivo delivery of tetracycline-regulated genes.* Curr Opin Biotechnol, 2002. **13**(5): p. 448-52.

387. Robertson, A., et al., *Effects of mouse strain, position of integration and tetracycline analogue on the tetracycline conditional system in transgenic mice.* Gene, 2002. **282**(1-2): p. 65-74.

388. Pikaart, M.J., F. Recillas-Targa, and G. Felsenfeld, *Loss of transcriptional activity of a transgene is accompanied by DNA methylation and histone deacetylation and is prevented by insulators.* Genes Dev, 1998. **12**(18): p. 2852-62.

389. Bogeroger, H. and P. Gruss, *Functional determinants for the tetracycline-dependent transactivator tTA in transgenic mouse embryos.* Mech Dev, 1999. **83**(1-2): p. 141-53.

390. Thurston, G., *Role of Angiopoietins and Tie receptor tyrosine kinases in angiogenesis and lymphangiogenesis.* Cell Tissue Res, 2003. **314**(1): p. 61-8.